UNIVERSIDAD DE SEVILLA

CONSEJO SUPERIOR DE INVESTIGACIONES CIENTÍFICAS

Departamento de Química Inorgánica

Instituto de Investigaciones Químicas

Synthesis, reactivity and computational studies of Ir complexes bearing terphenyl phosphine ligands

Juan José Moreno Díaz

Sevilla, 2018

Synthesis, reactivity and computational studies of Ir complexes bearing terphenyl phosphine ligands

por

Juan José Moreno Díaz

Trabajo presentado para aspirar
al Título de Doctor en Química
Sevilla, 2018

Juan José Moreno

Directores de Tesis

Jesús Campos Manzano
Científico Titular
(CSIC)

Joaquín López Serrano
Profesor Titular
(Universidad de Sevilla)

Ernesto Carmona Guzmán
Catedrático de Química Inorgánica
(Universidad de Sevilla)

TABLE OF CONTENTS

Consideraciones Generales 1

Abbreviations 5

Chapter 1. C−H Activation at Unsaturated Ir(III) Complexes

I.1 Introduction

I.1.1 Transition Metal Mediated C−H Activation 11

I.1.2 Iridium Complexes in C−H Activation 21

I.1.3 Non-innocent Behavior of Cyclopentadienyl and Phosphine Ligands 25

I.2 Results and Discussion

I.2.1 Synthesis of Cyclopentadienyl Terphenyl Phosphine Complexes 29

I.2.2. Dicationic Complexes as Intermediates in C−H Activation 39

I.2.2.1 Computational Studies on Electrophilic C−H Activation 47

I.2.2.2 Electrophilic C−H Activation: Alternative Pathways 52

I.2.3 Base-Promoted, C_5Me_5-Mediated C−H and C−C Bond Formation 59

I.2.3.1 Computational Investigation of the Rearrangement of $2(Dipp)^+$ into $4(Dipp)^+$ and $3(Dipp)^+$ 64

I.2.3.2 Localized Molecular Orbital (LMO) Analysis 69

I.2.3.3 C_5Me_5 Deprotonation 71

I.2.3.4 C−C Bond Formation 74

I.2.3.5 C−C Bond Formation at the Cationic Fulvene Complex B 76

I.2.3.6 C−C Bond Formation at the Neutral Fulvene Complex A 80

I.2.3.7 C−C Bond Formation: Alternative Pathway 82

I.2.3.8 Isomerization of 4(Dipp)$^+$ 83

I.2.3.9 Isomerization of 4(Dipp)$^+$: Alternative Pathways 87

I.2.4 Reactivity of 2(Xyl)$^+$ towards NEt_3 89

I.2.4.1 Computational Study of the Formation of 5(Xyl)$^+$ 95

I.2.4.2 Conversion of 4(Xyl)$^+$ to 5(Xyl)$^+$ 100

I.2.4.3 Computational Study of the Potential Formation of 5(Dipp)$^+$ 104

I.2.5 Reactivity of the Cationic Chloride Complex [(η5-C_5Me_5)Ir(Cl)($PMe_2Ar^{Dipp}_2$)]$^+$, 2(Dipp)$^+$, Towards LiMe, H_2 and $PhSiH_3$

I.2.5.1 Reactivity of 2(Dipp)$^+$ Towards LiMe 105

I.2.5.2 Computational Studies of the Reactivity of 2(Dipp)$^+$ Towards LiMe 110

I.2.5.3 Reactivity of 2(Dipp)$^+$ towards H_2 and $PhSiH_3$ 115

I.2.6 Transition Metal Only Frustrated Lewis Pair Reactivity 124

I.2.7 Summary and Conclusions 137

I.3 Experimental Section

I.3.I General Considerations 138

I.3.I Synthesis and Characterization of New Complexes 141

I.4 References 163

Chapter 2. Hemilabile Behavior of Dialkyl Terphenyl Phosphines

II.1 Introduction

II.1.1 Ligand Hemilability in Organometallic Chemistry 176

II.1.2 Hemilabile Phosphine Ligands 180

II.1.2.1 Phosphine-Borane Ligands 182

II.1.2.2 Phosphine-Containing Pincer-Type Ligands 184

II.1.2.3 Dialkylbiaryl Phosphines 186

II.2 Results and Discussion

II.2.1 Stereoelectronic properties of terphenyl phosphine ligands 188

II.2.2 Synthesis and Reactivity of Iridium(I) Neutral Complexes 204

II.2.2.1 Iridium(I) Methyl Complexes 209

II.2.2.2 C−H Activation at Iridium(I): Computational Studies 211

II.2.2.3 Alternative mechanisms 218

II.2.2.4 Neutral Carbonyl Complexes 224

II.2.3 Synthesis and Reactivity of Ir(I) Cationic Complexes 226

II.2.3.1 Cationic Carbonyl Complexes 227

II.2.3.2 Topological analysis of $5^{+}(CO)_2$ 231

II.2.3.3 Reactivity of $5^{+}(CO)_2$ *Complexes* 233

II.2.3.4 Kinetic and Computational Studies 242

II.2.3.5 Cationic Alkene Complexes 249

II.2.4 Summary and Conclusions 259

II.3 Experimental Section

II.3.I General Considerations 261

II.3.I Synthesis and Characterization of New Complexes 263

II.4 References 295

CONSIDERACIONES GENERALES

Los resultados que se presentan en esta Memoria se encuadran en una de las líneas de investigación que desarrolla el grupo de Química Organometálica y Catálisis Homogénea del Instituto de Investigaciones Químicas (Centro Mixto Universidad de Sevilla−CSIC), que tiene como objetivo el estudio de las reacciones de ruptura y formación de enlaces C−H, C−O, C−C y otros similares, inducidas de manera selectiva por complejos de los metales del grupo 9 (Rh e Ir).

Los experimentos que se describen en esta Tesis Doctoral incluyen, entre otros, la síntesis de compuestos organometálicos de Ir estabilizados por ligandos fosfina voluminosos de composición PMe_2Ar', donde Ar' es un sustituyente de tipo terfenilo. Los nuevos compuestos sintetizados se han caracterizado fundamentalmente mediante espectroscopía de Resonancia Magnética Nuclear y estudios de difracción de rayos X de monocristal. Estas determinaciones cristalográficas se llevaron a cabo de manera independiente por la Dra. María Fernández, el Dr. Jesús Campos, la Dra. Celia Maya y el Dr. Eleuterio Álvarez. Se describen además los pertinentes estudios de reactividad que, en casos de interés, se complementan con estudios computacionales. Todos los estudios computacionales son obra del autor de este trabajo.

La Tesis tiene una estructura clásica basada en: **Introducción**, **Resultados y Discusión** y **Parte Experimental**, para cada uno de los capítulos que la componen. Para facilitar su lectura, la bibliografía aparece tanto a pie de página como al final de cada capítulo y de forma independiente en cada uno de ellos. Esta distribución hace que algunas referencias puedan aparecer en

distintos capítulos. La numeración de los esquemas, figuras y compuestos es independiente en cada uno de ellos.

Como parte del programa de Formación de Profesorado Universitario del Plan Propio de la Universidad de Sevilla se ha realizado una estancia breve de tres meses en Heriot Watt University, en Edimburgo (Escocia), bajo la supervisión del Prof. Stuart A. Macgregor. Parte de los estudios computacionales llevados a cabo durante dicha estancia se han incluido en el primer capítulo de esta Tesis. Con el objeto de obtener la mención de Doctor Internacional (RD 99/2011; BOE 10-02-2011, Art. 15), la mayor parte de la Tesis se ha redactado en inglés, exceptuando las Consideraciones Generales del inicio, escritas exclusivamente en español, y las Conclusiones finales, redactadas tanto en inglés como en español. Una parte de los resultados obtenidos se ha publicado en forma preliminar o como trabajo completo, mientras que otras secciones son todavía inéditas.

El objetivo fundamental del primer capítulo de esta Tesis Doctoral es el estudio de la reactividad de complejos catiónicos y coordinativamente insaturados de Ir(III) estabilizados por ligandos ciclopentadienilo (C_5Me_5) y fosfinas voluminosas de terfenilo (PMe_2Ar', Ar' = 2,6-diarilfenil). Los estudios experimentales y computacionales realizados sobre la reactividad de algunos complejos catiónicos en reacciones de activación de enlaces C–H demuestran que estas transcurren a través de la participación de intermedios dicatiónicos. El carácter no inocente del ligando C_5Me_5 en estos complejos, que en la mayor parte de los casos se comporta como un espectador robusto, se puso de manifiesto en presencia de una base de Brönsted, participando así de manera activa en reacciones de rotura y formación de enlaces C–H y C–C. El estudio computacional de estos procesos demuestra que el centro metálico solo participa de manera indirecta a través de ciclos redox Ir(I)-

Ir(III). El ligando C_5Me_5 también muestra una notable electrofilia en la reacción de estos complejos insaturados con a LiMe. Por último, se explora la reactividad del complejo insaturado frente al dihidrógeno, H_2, incluyendo su potencial participación como ácido de Lewis voluminoso en pares de Lewis frustrados constituidos por complejos de metales de transición.

En el segundo capítulo de esta Tesis Doctoral se describen las diferentes metodologías empleadas para evaluar las propiedades estereoelectrónicas de los ligandos dimetil fosfina de terfenilo y la reactividad de diversos complejos de Ir(I) que contienen estos ligandos. El Parámetro Electrónico de Tolman, TEP, se compara con el valor medio obtenido para los modos de vibración de tensión de carbonilo registrados para complejos cuadrados de iridio(I), $IrCl(CO)_2(PMe_2Ar')$, y con la constante de acoplamiento escalar, $^1J_{PSe}$, obtenida para los correspondientes seleniuros de fosfina. Por otra parte, el estudio de las propiedades estéricas de los ligandos fosfina de terfenilo comprende la comparación del Ángulo Cónico de Tolman con medidas de Ángulo Sólido y de Volumen Ocupado. Posteriormente, se investiga el mecanismo de una reacción de activación C–H que tiene lugar en un complejo neutro de iridio(I) que contiene un ligando fosfina de terfenilo. La naturaleza hemilabil de estos ligandos es fundamental para estabilizar compuestos catiónicos e insaturados de iridio(I), para los que se describen procesos de reorganización de ligandos (CO y olefina).

ABBREVIATIONS

Me	methyl, -CH_3
Et	ethyl, -CH_2CH_3
^{i}Pr	*iso*-propyl, -$CH(CH_3)_2$
^{t}Bu	*tert*-butyl, CMe_3
Ph	phenyl, -C_6H_5
Ar	aryl
Ar’	terphenyl
Xyl	xylyl, 2,6-$Me_2C_6H_3$
Dipp	diisopropylphenyl, 2,6-$^{i}Pr_2C_6H_3$
BAr_F	$[\{3,5\text{-}(CF_3)_2\text{-}C_6H_3)_4\}B]^-$
COD	cyclooctadiene
COE	cyclooctene
THF	tetrahydrofuran, C_4H_8O
acac	acetylacetonate
L	2 electron donor ligand
C_5Me_5	pentamethyl cyclopentadienyl
NHC	N-Heterocyclic Carbene
CPK model	Corey Pauling and Koltun space filling model
κ	ligand hapticity
η	number of atoms of a ligand directly bound to a metal center
ν	infrared vibrational frequency (cm^{-1})
min	minutes
h	hours

equiv.	equivalents
Anal. Calc.	analysis calculated
Exp.	experimental
Kcal	kilocalorie
TEP	Tolman Electronic Parameter
TCA	Tolman Cone Angle
ECA	Equivalent Cone Angle
$\%V_{Bur}$	percentage of volume occupied in the first oxidation step
g	grams
mmol	millimol
mL	milliliter
Å	angstrom
º	degree
C	Celsius
K	Kelvin
ref.	reference
ORTEP	crystallographic representation (Oak Ridge Thermal Ellipsoid Program)
IR	infrared
k	rate constant
HAT	Hydrogen Atom Transfer
FLP	Frustrated Lewis Pair
TMOFLP	Transition Metal Only Frustrated Lewis Pair
OA	Oxidative Addition
RE	Reductive Elimination

σ-BM	σ-Bond Metathesis
MAσBM	Metal Assisted σ-Bond Metathesis
σ-CAM	σ-Complex Assisted Metathesis
OATS	Oxidatively Added Transition State
AMLA	Ambiphilic Metal Ligand Assistance
CMD	Concerted Metalation Deprotonation
bipy	2,2'-bipyridine
py	pyridine
NAD	Nicotinamide Adenine Dinucleotide
PCET	Proton Coupled Electron Transfer
DFT	Density Functional Theory
TS	Transition State
LMO	Localized Molecular Orbital
QTAIM	Quantum Theory of Atoms in Molecules
IRC	Intrinsic Reaction Coordinate
SMD	Solvation Model based on Density
SCF	Self-Consistent Field

NMR Abbreviations

NMR	Nuclear Magnetic Resonance
δ	chemical shift in ppm
ppm	parts per million
NOESY	Nuclear Overhauser Enhancement SpectroscopY
EXSY	EXchange SpectroscopY
COSY	^{1}H-^{1}H correlation spectroscopy
HSQC	^{1}H-^{13}C correlation spectroscopy (Heteronuclear Single Quantum Coherence)
HMBC	^{1}H-^{13}C correlation spectroscopy (Heteronuclear Multiple Bond Correlation)
s	singlet
d	doublet
t	triplet
sept	septet
m	multiplet
br.	broad
$^{n}J_{AB}$	coupling constant (Hz) between A and B nuclei separated by n bonds
Hz	hertz

Chapter I

C−H Activation at Unsaturated Ir(III) Complexes

I.1 INTRODUCTION

I.1.1 Transition Metal Mediated C−H Activation

Carbon−hydrogen bonds are present in the vast majority of organic molecules, yet most of them cannot be employed in fruitful reactions. The inertness of the usually non-polar bond and the difficulty of achieving selective transformations between the many, chemically similar C−H bonds present in organic molecules make their functionalization a challenging process.[1] Despite these obstacles, the importance of C−H activation cannot be overstated, for it represents a crucial tool for the chemical industry. While the use of hydrocarbons as fuels takes advantage of the energy content of their chemical bonds, it overlooks their potential as cheap feedstocks, because of the unavailability of efficient methods to turn them into synthetically valuable compounds.[2] This issue is best exemplified by the simplest of all hydrocarbons, methane, the main component of natural and shale gas and therefore a very abundant, extremely important feedstock.[3] The activation of one of its strong C−H bonds requires very high temperatures, and much research has been devoted to achieve its direct[4] and efficient conversion into valuable raw materials,[5] including higher hydrocarbons,[6] borylated products[7] and

---

[1] Bergman, R. G. *Nature* **2007**, *446*, 391.
[2] Labinger, J. A.; Bercaw, J. E. *Nature* **2002**, *417*, 507.
[3] Caballero, A.; Pérez, P. J. *Chem. Soc. Rev.*, **2013**,*42*, 8809.
[4] Methane is used in industry to produce CO and H_2, the so-called syngas.
[5] Gunsalus, N. J.; Koppaka, A.; Park, S. H.; Bischof, S. M.; Hashiguchi, B. G.; Periana, R. A. *Chem. Rev.* **2017**, *117*, 8521.
[6] a) Belgued, M., Pareja, P., Amariglio, A., Amariglio, H. *Nature* **1991**, *352*, 789; b) Guo, X.; Fang, G.; Li, G.; Ma, H.; Fan, H.; Yu, L.; Ma, C.; Wu, X.; Deng, D.; Wei, M.; Tan, D.; Si, R.; Zhang, S.; Li, J.; Sun, L.; Tang, Z.; Pan, X.; Bao, X. *Science* **2014**, *344*, 616; c) Morejudo, S. H.; Zanon, R.; Escolastico, S.; Yuste-Tirados, I.; Malerod-Fjeld, H.; Vestre, P. K.; Coors, W. G.; Martinez, A.; Norby, T.; Serra, J. M.; Kjølseth, C. *Science* **2016**, *353*, 563.

oxidated derivatives. Since the latter encompass carboxylic acids,[8] esters[9] and especially methanol,[10] such a process would revolutionize the chemical industry by providing at the same time a valuable feedstock and a liquid fuel (Figure 1).

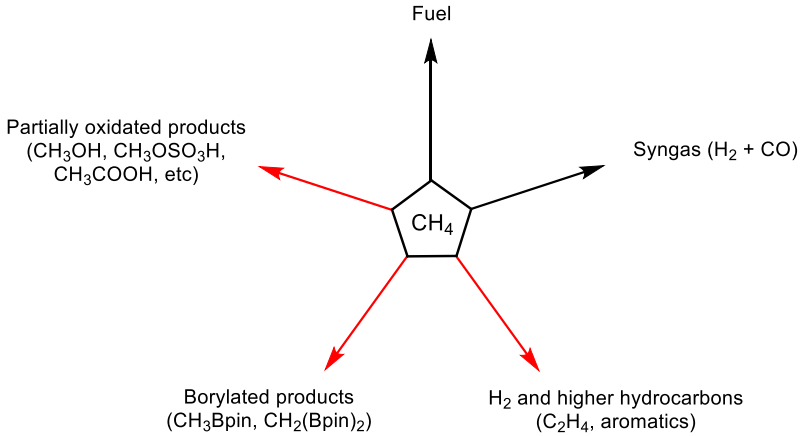

Figure 1. Current (black) and potentially feasible (red) industrial uses of methane.

---

[7] a) Cook, A. K.; Schimler, S. D.; Matzger, A. J.; Sanford, M. S. *Science* **2016**, *351*, 1421; b) Smith, K. T.; Berritt, S.; Gonzalez-Moreiras, M.; Ahn, S.; Smith, M. R.; Baik, M. H.; Mindiola, D. J. *Science* **2016**, *351*, 1424.

[8] a) Lin, M.; Sen, A. *Nature* **1994**, *368*, 613; b) Periana, R. A., Mironov, O., Taube, D., Bhalla, G., Jones, C. J. *Science* **2003**, *301*, 814; c) Cui, X.; Li, H.; Wang, Y.; Hu, Y.; Hua, L.; Li, H.; Han, X.; Liu, Q.; Yanf, F.; He, L.; Chen, X.; Li, Q.; Xiao, J.; Deng, D.; Bao, X. *Chem* **2018**, *4*, 1902.

[9] a) Periana, R. A.; Taube, D. J.; Gamble, S.; Taube, H.; Satoh, T.; Fujii, H. *Science* **1998**, *280*, 560; b) Caballero, A.; Despagnet-Ayoub, E.; Díaz-Requejo, M. M.; Díaz-Rodríguez, A.; Gonzalez-Nuñez, M. E.; Mello, R.; Muñoz, B. K.; Ojo, W.-S.; Asensio, G.; Etienne, M.; Perez, P. J. *Science* **2011**, *332*, 835.

[10] a) Periana, R. A.; Taube, D. J.; Evitt, E. R.; Löffler, D. G.; Wentrcek, P. R.; Voss, G.; Masuda, T. *Science* **1993**, *259*, 340; b) Hammond, C.; Forde, M. M.; Rahim, M. H. A.; Thetford, A.; He, Q.; Jenkins, R. L.; Dimitratos, N.; Lopez-Sanchez, J. A.; Dummer, N. F.; Murphy, D. M.; Carley, A. F.; Taylor, S. H.; Willock, D. J.; Stangland, E. E.; Kang, J.; Hagen, H.; Kiely, C. J.; Hutchings, G. J. *Angew. Chem., Int. Ed.* **2012**, *51*, 5129; c) Sushkevich, V.L., Palagin, D., Ranocchiari, M., van Bokhoven, J.A.; *Science* **2017**, *356*, 523 e) Agarwal, N.; Freakley, S. J.; McVicker, R. U.; Althahban, S. M.; Dimitratos, N.; He, Q.; Morgan, D. J.; Jenkins, R. L.; Willock, D. J.; Taylor, S. H.; Kiely, C. J.; Hutchings, G. J. *Science* **2017**, *358*, 223.

C−H bond activation is also invaluable in fine and pharmaceutical chemistry, for it allows single-step, late-stage carbon-carbon (C−C) and carbon-heteroatom (C−X) bond formation reactions, which are key for the synthesis of natural and biologically active products,[11] Scheme 1. Hydrogen isotope exchange constitutes another relevant application of C−H bond activation for the pharmaceutical industry, as the enhanced inertness of C−D (where D stands for deuterium) bonds towards metabolic oxidation provide longer-living drugs.[12] In the same line, the selective incorporation of tritium, the radioactive and heaviest isotope of hydrogen, is essential for drug discovery and in clinical studies.[13]

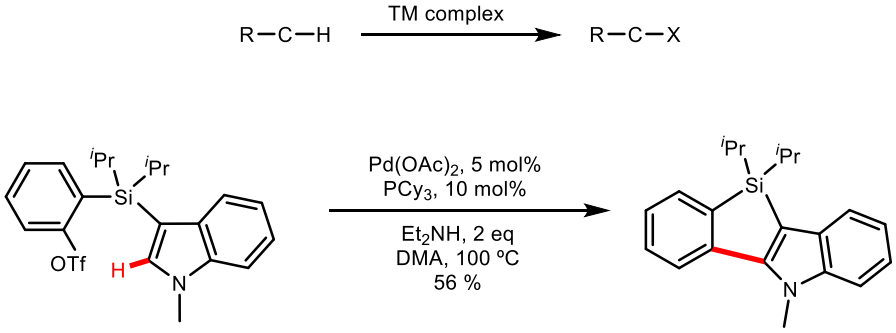

[11] a) Godula, K.; Sames, D. *Science* **2006**, *312*, 67; b) Rech, J. C.; Yato, M.; Duckett, D.; Ember, B.; LoGrasso, P. V.; Bergman, R. G.; Ellman, J. A. *J. Am. Chem. Soc.* **2007**, *129*, 490; c) Davies, H. M. L.; Manning, J. R. *Nature* **2008**, *451*, 417; d) McMurray, L.; O'Hara, F.; Gaunt, M. J. *Chem. Soc. Rev.* **2011**, *40*, 1885; e) Yamaguchi, J.; Yamaguchi, A. D.; Itami, K. *Angew. Chem. Int. Ed.* **2012**, *51*, 8960; f) Wencel-Delord, J.; Glorius, F. *Nat. Chem.* **2013**, *5*, 369; g) He, J.; Hamann, L. G. H.; Davies, H. M. L.; Beckwith, R. E. J. *Nat. Commun.* **2015**, *6*, 5943.

[12] a) Loh, Y. Y.; Nagao, K.; Hoover, A. J.; Hesk, D.; Rivera, N. R.; Colletti, S. L.; Davies, I. W.; MacMillan, D. W. C. *Science* **2017**, *358*, 1182; b) Atzrodt, J.; Derdau, V.; Kerr; W. J.; Reid, M. *Angew. Chem. Int. Ed.* **2018**, *57*, 3022.

[13] a) Elmore, C. S.; John, E. M. *Annu. Rep. Med. Chem.* Academic Press **2009**, 44, 515; b) Atzrodt, J.; Derdau, V.; Fey, T.; Zimmermann, J. *Angew. Chem. Int. Ed.* **2007**, *46*, 7744.

Scheme 1. General scheme (X = D, C, heteroatom) and a prototypical example of transition metal-mediated selective intramolecular functionalization of a C−H bond.[14]

The preeminence of transition metals in the field of catalytic C−H bond functionalization is well known, although many organocatalytic processes have been developed, including Frustrated Lewis Pairs and radical strategies.[15] As a paramount example, the activation of the C−H bond of benzene was reported in the seminal work of Dimroth,[16] in 1898, and Kharasch,[17] in 1931 (Scheme 2).

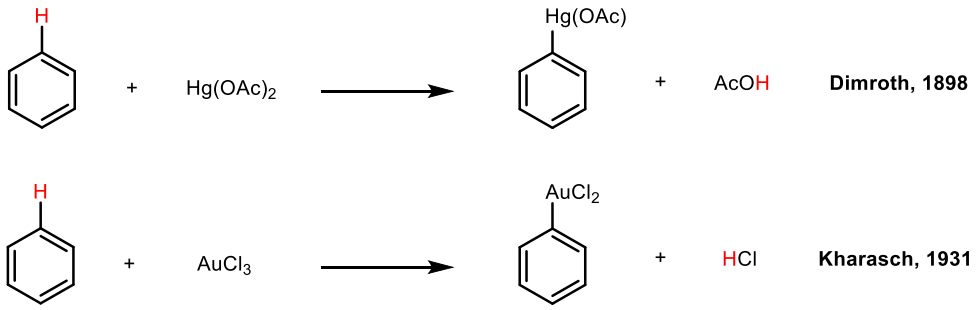

Scheme 2. First examples of the C−H activation of benzene.

In 1955, Murahashi[18] reported a cobalt-catalyzed C−H functionalization of an arene under harsh conditions. In the following years, Chatt[19] disclosed

[14] Shimizu, M., Mochida, K., Hiyama, T. *Angew. Chem. Int. Ed.* **2008**, *47*, 9760.
[15] a) Pan, S. C. *Beilstein J. Org. Chem.* **2012,** *8*, 1374; b) Légaré, M. A.; Courtemanche, M. A.; Rochette, E.; Fontaine, F. G. *Science* **2015**, *349*, 513 c) Qin, Y.; Zhu, L.; Luo, S. *Chem. Rev.* **2017**, *117*, 9433; d) Yi, H.; Zhang, G.; Wang, H.; Huang, Z.; Wang, J.; Singh, A. K.; Lei, A. *Chem. Rev.* **2017**, *117*, 9016.
[16] a) Dimroth, O. *Ber.* **1898**, *31*, 2154; b) Dimroth, O. *Chem. Ber.* **1902**, *35*, 2032.
[17] Kharasch, M.S.; Isbell, H.S. *J. Am. Chem. Soc.* **1931**, *53*, 3053.
[18] Murahashi, S. *J. Am. Chem. Soc.* **1955**, *77*, 6403.
[19] Chatt, J.; Watson, H. R. *J. Chem. Soc.*, **1962**, 2545.

the oxidative addition of naphthalene to a Ru(0) complex, whereas Shilov[20] made pioneer advances in the catalytic oxidation of alkanes to alcohols and alkyl halides, Scheme 3.

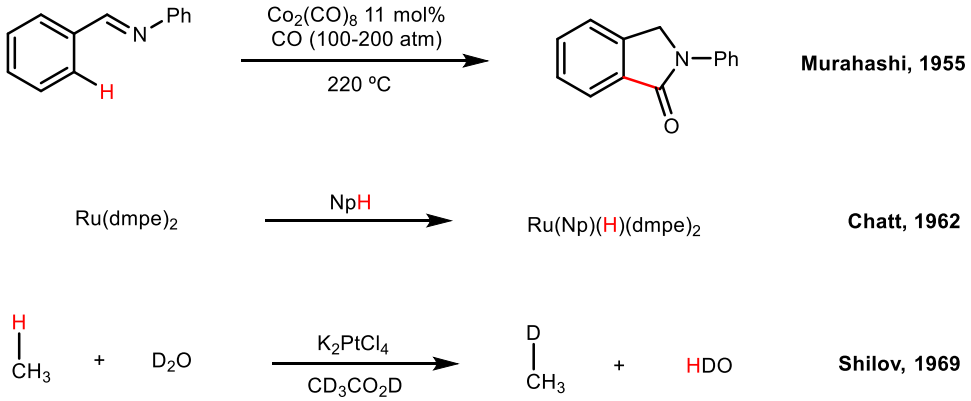

Scheme 3. Early examples of C−H bond activation and functionalization.

A wide variety of strategies for C−H activation and functionalization has emerged after those early examples described in Schemes 2 and 3. A common feature in active metal systems is the use of robust spectator ligands such as cyclopentadienyl, phosphine or pincer ligands of several types, among others. These ligands are known to provide kinetic stabilization to the metal center while being not reactive towards intramolecular C−H activation processes that would quench catalytic turnover.[21] Besides classic thermal activation, many examples of

[20] a) Gol'dshleger, N.F.; Tyabin, M.B.; Shilov, A.E.; Shteinman, A. A. *Zh. Fiz. Khim.* **1969**, *43*, 2174 b) Gol'dshleger, N. F.; Shteinman, A. A.; Shilov, A. E.; Eskova, V. V. *Zh. Fiz. Khim.* **1972**, *46*, 1353.

[21] a) van der Boom, M. E.; Milstein, D. *Chem. Rev.* **2003**, *103*, 1759; b) Clot, E.; Chen, J.; Lee; D.-H.; Sung, S. Y.; Appelhans, L. N.; Faller, J. W.; Crabtree, R. H.; Eisenstein, O. *J. Am. Chem. Soc.* **2004**, *126*, 8795; c) Crabtree, R. H. *J. Organomet. Chem.* **2005**, *690*, 5451.

photoinduced[22] (Scheme 4, a) and electrochemical[23] (Scheme 4, b) activation and functionalization of C−H bonds have been disclosed.

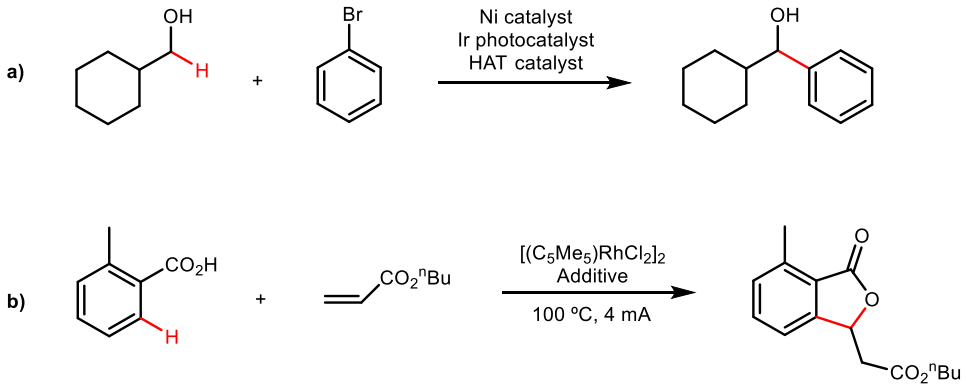

Scheme 4. a) Prototypical example of C−H functionalization employing photoredox catalysis (HAT stands for Hydrogen Atom Transfer). b) Prototypical example of a Rh-catalyzed C−H activation employing electricity as the oxidant.

As stated above, one of the challenges in the field of C−H functionalization is controlling the regioselectivity of the reaction, since there are usually many different C−H bonds of similar strength in any organic molecule. In this context, the use of permanent and transient directing groups within the

[22] a) Shaw, M. H.; Shurtleff, V. W.; Terrett, J. A.; Cuthbertson, J. D. MacMillan, D. W. C. *Science* **2016**, *352*, 1304; b), Perry, I. B.; Brewer, T. F.; Sarver, P. J.; Schultz, D. M.; DiRocco, D. A.; MacMillan, D. W. C. *Nature* **2018**, *560*, 70; c) Twilton, J.; Le, C.; Zhang, P.; Shaw, M. H.; Evans, R. W.; MacMillan, D. W. C. Nat. Rev. Chem. **2017**, *1*, 0052; d) Twilton, J.; Christensen, M.; DiRocco, D. A.; Ruck, R. T.; Davies, I. W.; MacMillan, D. W. C. *Angew. Chem. Int. Ed.* **2018**, *57*, 5369.

[23] a) Shrestha, A.; Lee, M.; Dunn, A. L.; Sanford, M. S. *Org. Lett.*, **2018**, *20*, 204; b) Sauermann, N.; Mei, R.; Ackermann, L. *Angew. Chem. Int. Ed.* **2018**, *57*, 5090; c) Qiu, Y.; Kong, W.-J.; Struwe, J.; Sauermann, N.; Rogge, T.; Scheremetjew, A.; Ackermann, L. *Angew. Chem. Int. Ed.* **2018**, *57*, 5828; d) Qiu, Y.; Stangier, M.; Meyer, T. H.; Oliveira, J. C. A.; Ackermann, L. *Angew. Chem. Int. Ed.* **2018**, *57*, 14179.

organic molecule to be functionalized,[24] and the exploitation of proton accepting coligands, specially carboxylates,[25] have shown great success (Scheme 5, a and b). The regioselective functionalization of C−H bonds in reactions involving radicals have also been explored with remarkable efficiency[26] (Scheme 5, c).

[24] a) Das, S.; Incarvito, C. D.; Crabtree, R. H.; Brudvig, G. W. *Science* **2006**, *312*, 1941; b) Lyons, T. W.; Sanford, M. S. *Chem. Rev.* **2010**, 110, 1147; c) Engle, K. M.; Mei, T.-S.; Wasa, M.; Yu, J.-Q. *Acc. Chem. Res.* **2012**, *45*, 788; d) Ros, A.; Fernandez, R.; Lassaletta, J. M. *Chem. Soc. Rev.* **2014**, *43*, 3229; e) Zhang, F.-L.; Hong, K.; Li, T.-J.; Park, H.; Yu, J.-Q. *Science* **2016**, *351*, 252; f) Topczewski, J. J.; Cabrera, P. J.; Saper, N. I.; Sanford, M. S. *Nature* **2016**, *531*, 220 g) Gandeepan, P.; Ackermann, L. *Chem* **2018**, *4*, 199.

[25] a) Tenn, W. J.; Young, K. J. H.; Bhalla, G.; Oxgaard, J.; Goddard, W. A.; Periana, R. A. *J. Am. Chem. Soc.* **2005**, *127*, 14172; b) Ess, D. H.; Gunnoe, T. B.; Cundari, T. R.; Goddard, W. A.; Periana, R. A. *Organometallics* **2010**, *29*, 6801; c) Ackermann, L. *Chem. Rev.* **2011**, *111*, 1315; d) Maleckis, A.; Kampf, J. W.; Sanford, M. S. *J. Am. Chem. Soc.* **2013**, *135*, 6618; e) Ackermann, L. *Acc. Chem. Res.* **2014**, *47*, 281; f) Davies, D. L.; Macgregor, S. A.; McMullin, C. L. *Chem. Rev.* **2017**, *117*, 8649.

[26] a) Boursalian, G. B.; Ham, W. S.; Mazzotti, A. R.; Ritter, T. *Nat. Chem.* **2016**, *8*, 810; b) Yi, H.; Zhang, G.; Wang, H.; Huang, Z.; Wang, J.; Singh, A. K.; Lei, A. *Chem. Rev.* **2017**, *117*, 9016; c) Serpier, F.; Pan, F.; Ham, W. S.; Jacq, J.; Genicot, C.; Ritter, T. *Angew. Chem. Int. Ed.* **2018**, *57*, 10697.

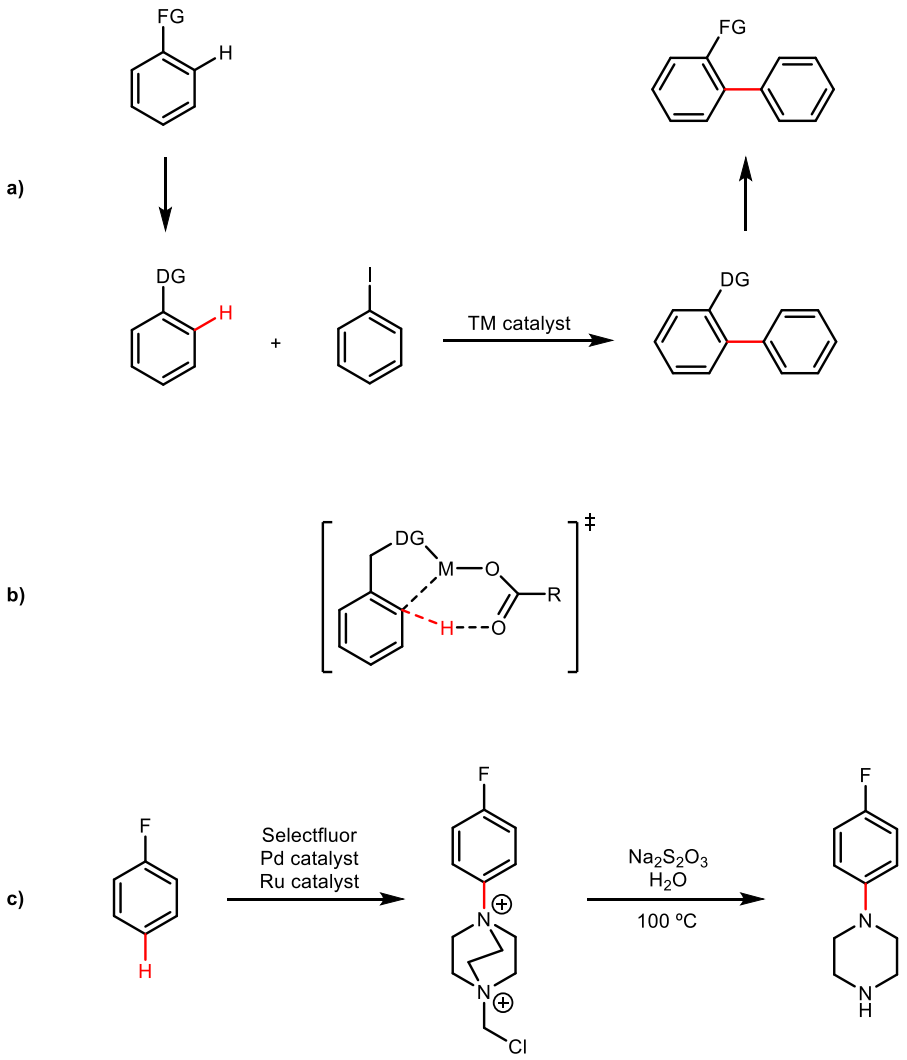

Scheme 5. a) Directing group (DG) strategy employed to achieve regioselectivity in C−H functionalization. b) Prototypical carboxylate assisted C−H activation. c) *para*-selective C−H functionalization enabled by radical substitution.

In the past years, much knowledge has been acquired regarding the mechanisms by which transition metal complexes can selectively cleave

C−H bonds.[27] Some of the disclosed paths such as the 1,2-addition and the metalloradical activation will not be discussed in this section. Instead, we will focus on the oxidative addition, σ-bond metathesis and electrophilic substitution mechanisms. Intermediate scenarios[28] between the oxidative addition-reductive elimination (OA-RE) mechanism that implicates an oxidated intermediate, and σ-bond metathesis (σ-BM) are depicted in Figure 2. They include metal assisted σ-bond metathesis (MAσBM), σ-complex assisted metathesis (σ-CAM, also known as oxidatively added transition state, OATS) and oxidative hydrogen migration (OHM).

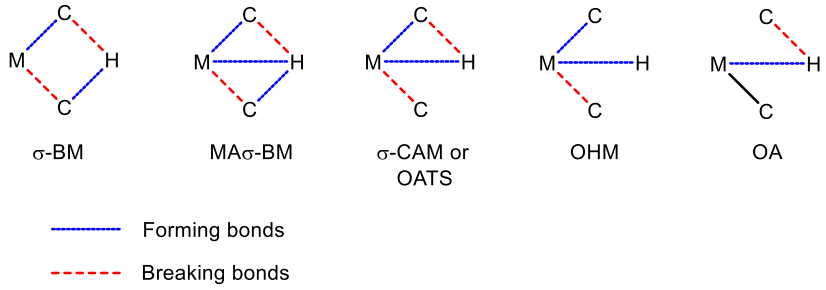

Figure 2. Transition state model connectivity for several C−H activation pathways.

Low valent, late transition metal complexes can perform C−H activation via mechanisms ranging from σ-bond metathesis to oxidative addition. The latter is also accessible for electron poor, late transition metal complexes in intermediate oxidation state, such as Ru, Pd and Pt (II), or Rh and Ir (III). However, the electrophilicity of these species usually promotes strong σ-donation from the C−H bond concomitant with weak π-back-donation, so that the enhanced acidity of the C−H bond in the intermediate agostic/sigma complex can be best exploited by base deprotonation

[27] Hartwig, J. F. *J. Am. Chem. Soc.* **2016**, *138*, 2.
[28] a) Roudesly, F.; Oble, J.; Poli, G. *J. Mol. Catal. A: Chem* **2017**, *426*, 275; b)Vastine, B. A.; Hall, M. B. *J. Am. Chem. Soc.* **2007**, *129*, 12068.

(Scheme 6). Decisive mechanistic advances have been made with the investigation of C−H bond activation at electrophilic (η^5-C_5Me_5)Ir(III) centers.[29]

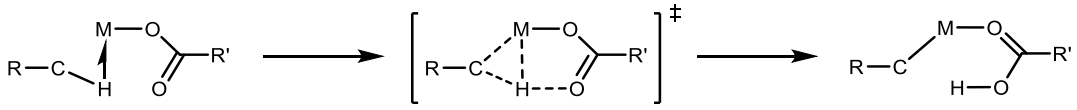

Scheme 6. Electrophilic C−H activation in an agostic or σ-complex.

On these grounds, it is clear that late transition metals present comparatively superior capacity towards C−H activation. Consequently, homogeneous C−H functionalization has been dominated by complexes of this kind. Particularly successful are those belonging to the second (Ru, Rh, Pd) and third (Ir, Pt) rows, although relevant advances have been recently achieved employing first row transition metal complexes, including Fe,[30] Co,[31] Ni[32] and Cu.[33]

[29] a) Klei, S. R.; Tilley, T. D.; Bergman, R. G. *J. Am. Chem. Soc.* **2000**, *122*, 1816; b) Balcells, D.; Clot, E.; Eisenstein, O.; *Chem. Rev.* **2010**, *110*, 749; c) Carlsen, R.; Wohlgemuth, N.; Carlson, L.; Ess, D. H. *J. Am. Chem. Soc.* **2018**, *140*, 11039.

[30] Shang, R.; Ilies, L.; Nakamura, E. *Chem. Rev.* **2017**, *117*, 9086.

[31] a) Moselage, M.; Li, J.; Ackermann, L. *ACS Catal.* **2016**, *6*, 498; b) Yoshino, T.; Matsunaga, S. *Adv. Organomet. Chem.* **2017**, *68*, 197.

[32] a) Zhou, W.; Zheng, S.; Schultz, J. W.; Rath, N. P.; Mirica, L. M. *J. Am. Chem. Soc.* **2016**, *138*, 5777; b) Chong, E.; Kampf, J. W.; Ariafard, A.; Canty, A. J.; Sanford, M. S. *J. Am. Chem. Soc.* **2017**, *139*, 6058.

[33] a) Gava, R.; Olmos, A.; Noverges, B.; Varea, T.; Álvarez, E.; Belderrain, T. R.; Caballero, A.; Asensio, G.; Pérez, P. J. *ACS Catal.* **2015**, *5*, 3726; b) Guo, X.-X.; Gu, D.-W.; Wu, Z.; Zhang, W. *Chem. Rev.* **2015**, *115*, 1622.

I.1.2 Iridium Complexes in C−H Activation

During the last 40 years, relevant breakthroughs were achieved in the C−H activation field by exploiting the reactivity of iridium complexes (Scheme 7). For instance, Crabtree[34] and Felkin[35] reported alkane dehydrogenation mediated by Ir complexes. This area of research was further developed by Goldman and Jensen with the use of pincer ligands,[36] and later extended thanks to the discovery of highly efficient alkane metathesis processes.[37]

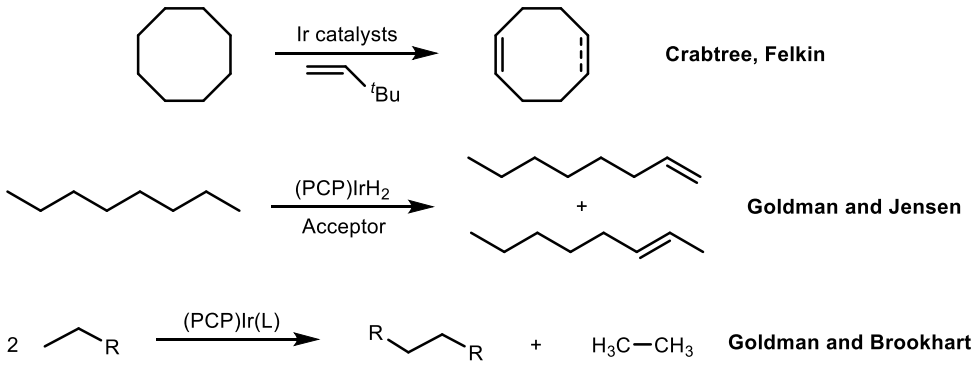

Scheme 7. Early reports on alkane dehydrogenation mediated by Ir complexes.

Inspired by the pioneering work of Green,[38] Bergman[39] and Graham[40] simultaneously reported in 1982 the oxidative addition of saturated hydrocarbons to photochemically generated iridium(I) cyclopentadienyl

[34] Crabtree, R. H., Mihelcic, J. M.; Quirk, J. M. *J. Am. Chem. Soc.* **1979**, *101*, 7738.
[35] Felkin, H.; Fillebeen-Khan, T.; Gault, Y.; Holmes-Smith, R.; Zakrzewski, J. *Tetrahedron Lett.* **1984**, *25*, 1279.
[36] Liu, F.; Pak, E. B.; Singh, B.; Jensen, C. M.; Goldman, A. S. *J. Am. Chem. Soc.* **1999**, *121*, 4086.
[37] Goldman, A. S.; Roy, A. H.; Huang, Z.; Ahuja, R.; Schinski, W.; Brookhart, M. *Science* **2006**, *312*, 257.
[38] Green, M. L. H.; Knowles, P. J. *J. Chem. Soc. D* **1970**, *0*, 1677.
[39] Janowicz, A.H.; Bergman, R. G. *J. Am. Chem. Soc.* **1982**, *104*, 352.
[40] Hoyano, J. K.; Graham, W.A.G. *J. Am. Chem. Soc.* **1982**, *104*, 3723.

complexes. In 1995, the group of Bergman reported a cationic [(η^5-C_5Me_5)Ir(III)] complex that permitted the facile activation of hydrocarbons, including methane[41] (Scheme 8).

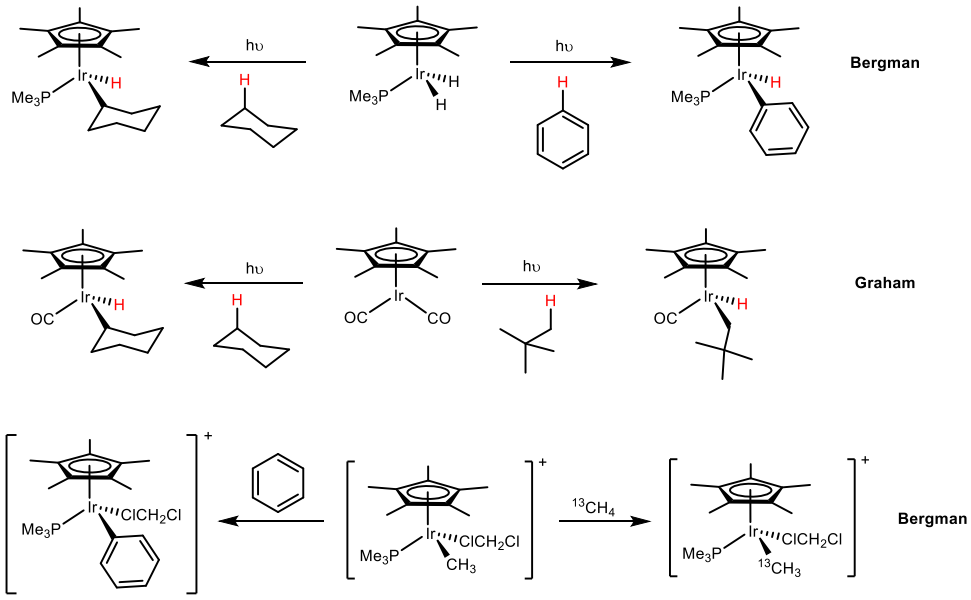

Scheme 8. Bergman and Graham advances in the C−H activation of hydrocarbons employing Ir(C_5Me_5) complexes.

A few years later, Iverson and Smith achieved the catalytic borylation of unactivated hydrocarbons employing neutral [(η^5-C_5Me_5)Ir(III)] complexes,[42] a topic further developed by Hartwig and Miyaura[43] (Scheme 9).

[41] Arndtsen, B. A.; Bergman, R. G. *Science* **1995**, *270*, 1970.
[42] Iverson, C. N.; Smith, M. R. *J. Am. Chem. Soc.* **1999**, *121*, 7696.
[43] Ishiyama, T.; Takagi, J.; Ishida, K.; Miyaura, N.; Anastasi, N. R.; Hartwig, J. F. *J. Am. Chem. Soc.* **2002**, *124*, 390.

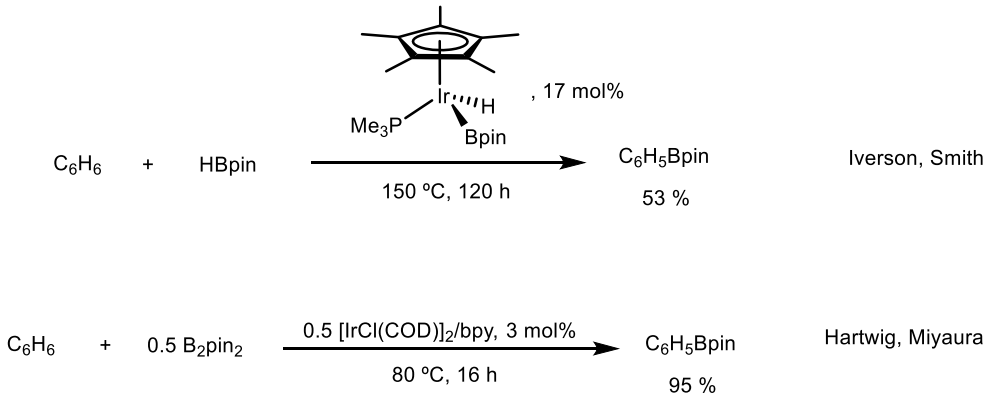

Scheme 9. Early advances in iridium mediated borylation of arenes.

More recently, Crabtree and coworkers employed the same type of cyclopentadienyl iridium complexes as catalysts for the C−H hydroxylation of alkanes with water[44] (Scheme 10).

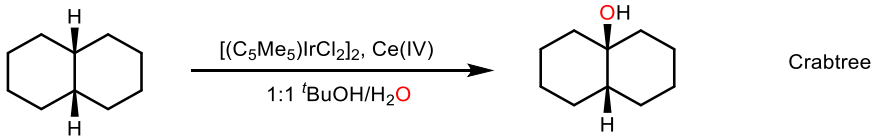

Scheme 9. Iridium(III)-catalyzed alkane hydroxylation.

Our research group has had a long-standing interest in the study of C−H bond activation reactions promoted by rhodium and, principally, iridium complexes stabilized by coordination to ancillary ligands of the types hydrotris(pyrazolyl)borate and cyclopentadienyl types.[45] Aside from

[44] a) Zhou, M.; Schley, N. D.; Crabtree, R. H. *J. Am. Chem. Soc.* **2010**, *132*, 12550; b) Zhou, M.; Balcells, D.; Parent, A. R.; Crabtree, R. H.; Eisenstein, O. *ACS Catal.* **2012**, *2*, 208.

[45] For early work from our group see for example: a) Pérez, P. J.; Poveda, M. L.; Carmona, E. *J. Chem. Soc., Chem. Commun.* **1992**, 8; b) Boutry, O.; Gutiérrez, E.; Monge, A.; Nicasio, M. C.; Pérez, P. J.; Carmona, E. *J. Am. Chem. Soc.* **1992**, *114*, 7288; c) Gutiérrez, E.; Monge, A.; Nicasio, M. C.; Poveda, M. L.; Carmona, E. *J. Am. Chem. Soc.* **1994**, *116*, 791; d) Alvarado, Y.; Boutry, O.; Gutiérrez, E.; Monge, A.; Nicasio, M. C.; Poveda, M. L.; Pérez, P. J.; Ruíz, C.;

activation of a single C−H bond, e.g. of C_6H_6, double C−H bond activation processes leading to heteroatom stabilized iridium carbenes were often encountered.[45h,i] Moreover, the migratory insertion chemistry of cationic iridium alkylidenes, i.e. $[Ir=C(H)R]^+$, was also investigated[45f,h] showing that such species can actively participate in C−C bond forming reactions. This possibility had been considered unlikely by the group of Bergman[46] but was subsequently reinforced by studies on cationic (η^5-C_5Me_5)Ir(III) complexes bound to the bis(xylyl) phosphine $PMe(Xyl)_2$ (Xyl = 2,6-$C_6H_3Me_2$) which is prone to cyclometallation[47] (Scheme 10).

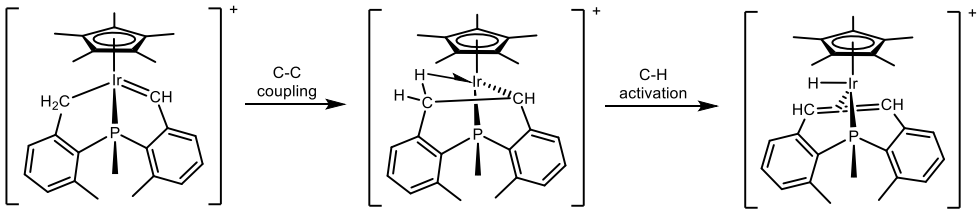

Scheme 10. C−H bond activation derived from an Ir(III) alkylidene.

Bianchini, C.; Carmona, E. *Chem. Eur. J.* **1997**, *3*, 860; e) Gutiérrez-Puebla, E.; Monge, A.; Nicasio, M. C.; Pérez, P. J.; Poveda, M. L.; Carmona, E. *Chem. Eur. J.* **1998**, *4*, 2225; f) Alías, F. M.; Poveda, M. L.; Sellin, M.; Carmona, E. *J. Am. Chem. Soc.* **1998**, *120*, 5816; g) Slugovc, C.; Padilla-Martínez, I.; Sirol, S.; Carmona, E. *Coord. Chem. Rev.* **2001**, *213*, 129; h) Carmona, E.; Paneque, M.; Poveda, M. L. *Dalton Trans.* **2003**, 4022; i) Conejero, S.; Paneque, M.; Poveda, M. L.; Santos, L. L.; Carmona, E. *Acc. Chem. Res.* **2010**, *43*, 572.

[46] Klei, S. R.; Golden, J. T.; Burger, P.; Bergman, R. G. *J. Mol. Catal. A Chem.* **2002**, *189*, 79.

[47] Campos, J.; López-Serrano, J.; Álvarez, E.; Carmona, E. *J. Am. Chem. Soc.* **2012**, *134*, 7165.

I.1.3 Non-Innocent Behavior of Phosphine and Cyclopentadienyl Ligands.

In the majority of the reactions promoted by transition metal complexes of both phosphine- and cyclopentadienyl-type ligands, including the aforementioned C−H activations, the ligands behave as spectators and provide thermal or kinetic stability, inhibiting decomposition or other side reactions. Indeed, the protective role they exert is one of the main reasons justifying the widespread utilizations of these ligands. Under certain conditions, however, these commonly used ligands can directly participate in the chemistry taking place at the metal complex. Gaining a deep knowledge of these unforeseen reactions is crucial, since they may strongly influence catalytic outcomes[48] or even lead to catalyst deactivation.[49] A typical example of non-innocent behavior is the facile cyclometalation that certain phosphines undergo upon coordination to late transition metals.[50] More recently, surprising examples describing the nickel- and palladium-

[48] a) Doyle, T. J.; Milner, P. J.; Kinzel, T.; Zhang, Y.; Takase, M. K.; Buchwald, S. L. *J. Am. Chem. Soc.* **2011**, *133*, 18106; b) Milner, P. J.; Maimone, T. J.; Su, M.; Chen, J.; Müller, P.; Buchwald, S. L. *J. Am. Chem. Soc.* **2012**, 134, 19922; c) Sather, A. C.; Lee, H. G.; De La Rosa, V. Y.; Yang, Y.; Müller, P.; Buchwald, S. L. *J. Am. Chem. Soc.* **2015**, *137*, 13433; d) Sather, A. C.; Buchwald, S. L. *Acc. Chem. Res.* **2016**, *49*, 2146.

[49] Crabtree, R. H. *Chem. Rev.* **2015**, *115*, 127.

[50] a) Zhang, S.; Chu, X.; Li, T.; Wang, Z.; Zhu, B. *ACS Omega* **2018**, *3*, 4522; b) Guenther, J.; Mallet-Ladeira, S.; Estevez, L.; Miqueu, K.; Amgoune, A.; Bourissou, D. *J. Am. Chem. Soc.* **2014**, *136*, 1778; c) Kiener, C. A.; Shu, C.; Incarvito, C.; Hartwig, J. F. *J. Am. Chem. Soc.* **2003**, *125*, 14272; d) Montag, M.; Leitus, G.; Shimon, L. J. W.; Ben-David, Y.; Milstein, D. *Chem. Eur. J.* **2007**, *13*, 9043; e) Millard, M. D.; Moore, C. E.; Rheingold, A. L.; Figueroa, J. S. *J. Am. Chem. Soc.* **2010**, *132*, 8921; f) Han, Y.-F.; Jin, G.-X. *Chem. Soc. Rev.* **2014**, *43*, 2799.

mediated dearomatization of dialkylbiaryl phosphines have been reported[48a,b;51] (Figure 3).

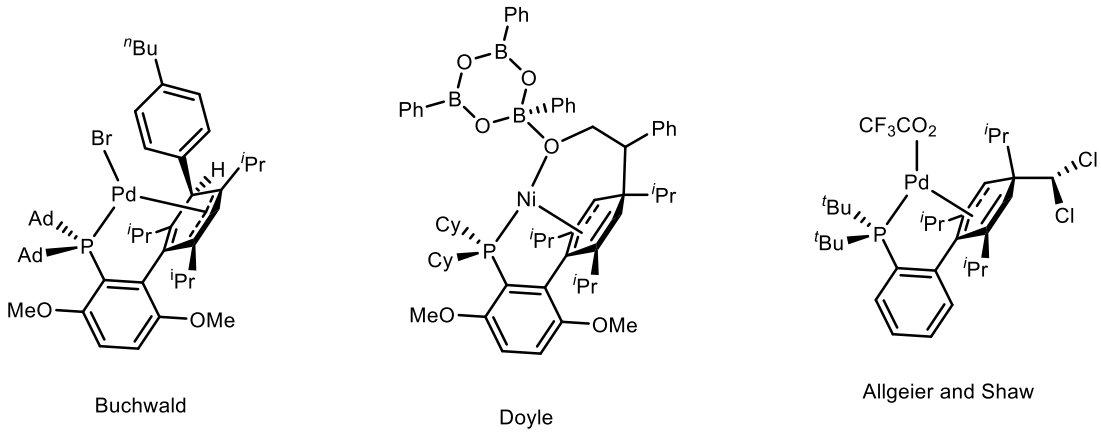

Figure 3. Dearomatized dialkylbiaryl phosphines.

For cyclopentadienyl ligands, in particular C_5Me_5, the activation of one of the methyl groups has been known for decades. This activation typically implies either deprotonation[52] or hydride abstraction.[53] Metal-to-ring hydride transfer[54] processes have also been documented for late transition

[51] a) Nielsen, D. K.; Doyle, A. G. *Angew. Chem. Int. Ed.* **2011**, *50*, 6056; b) Allgeier, A. M.; Shaw, B. J.; Hwang, T. L.; Milne, J. E.; Tedrow, J. S.; Wilde, C. N. *Organometallics* **2012**, *31*, 519.

[52] a) Glueck, D. S.; Bergman, R. G. *Organometallics* **1990**, *9*, 2862; b) Fan, L.; Wei, C.; Aigbirhio, F. I.; Turner, M. L.; Gusev, O. V.; Morozova, L. N.; Knowles, D. R. T.; Maitlis, P. M. *Organometallics* **1996**, *15*, 98; c) Rais, D.; Bergman, R. G. *Chem. - Eur. J.* **2004**, *10*, 3970; d) Caldwell, H.; Pregosin, P. S. *Organometallics* **2008**, *27*, 1591; e) Bernechea, M.; Berenguer, J. R.; Lalinde, E.; Torroba, J. *Organometallics* **2009**, *28*, 312; f) Thomas, H. P.; Marr, A. C.; Morgan, P. J.; Saunders, G. C. *Organometallics* **2018**, *37*, 1339.

[53] Meredith, J. M.; Goldberg, K. I.; Kaminsky, W.; Heinekey, D. M. *Organometallics* **2012**, *31*, 8459.

[54] a) Paneque, M.; Maitlis, P. M. *J. Chem. Soc., Chem. Commun.* **1989**, 105; b) Jones, W. D.; Kuykendall, V. L.; Selmeczy, A. D. *Organometallics* **1991**, *10*, 1577; c) Quintana, L. M. A.; Johnson, S. I.; Corona, S. L.; Villatoro, W.; Goddard, W. A.; Takase, M. K.; VanderVelde, D. G.; Winkler, J. R.; Gray, H. B.; Blakemore, J. D. *Proc. Natl. Acad. Sci. USA* **2016**, *113*, 6409; d) Pitman, C. L.;

metal complexes (Figure 4). Notably, there appears to be no report on the concerted activation of both a tertiary phosphine and a cyclopentadienyl ligand in a single system.

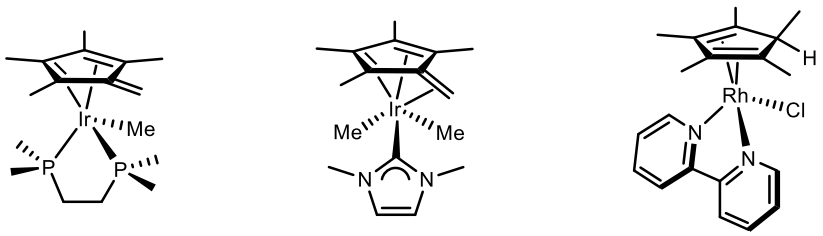

Bergman Heinekey Miller

Figure 4. Some examples of C_5Me_5 participation in the reactivity of late transition metal complexes.

Recently, Miller[54d] proposed that the cyclopentadienyl ligand in [(η^5-C_5Me_5)Rh(bipy)Cl] (bipy = 2,2'-bipyridine) could be responsible for catalytic hydride transfer to NAD^+ (NAD = Nicotinamide Adenine Dinucleotide; Figure 5), while Peters disclosed that protonated decamethylcobaltocenium, [(C_5Me_5)Co(η^4-C_5Me_5H)]$^+$, could act as a potent proton coupled electron transfer (PCET) reagent in the catalytic conversion of dinitrogen into ammonia.[55] These findings suggest that the non-innocent behaviour of the C_5Me_5 ligand could be extended from anecdotic stoichiometric reactions to the development of effective catalytic cycles.

Finster, O. N. L.; Miller, A. J. M. *Chem. Commun.* **2016**, *52*, 9105; e) Zamorano, A.; Rendón, N.; Valpuesta, J. E. V.; Álvarez, E.; Carmona, E. *Inorg. Chem.* **2015**, *54*, 6573.

[55] Chalkley, M.; Del Castillo, T. J.; Matson, B. D.; Roddy, J. P.; Peters, J. C. *ACS Cent. Sci*. **2017**, *3*, 217.

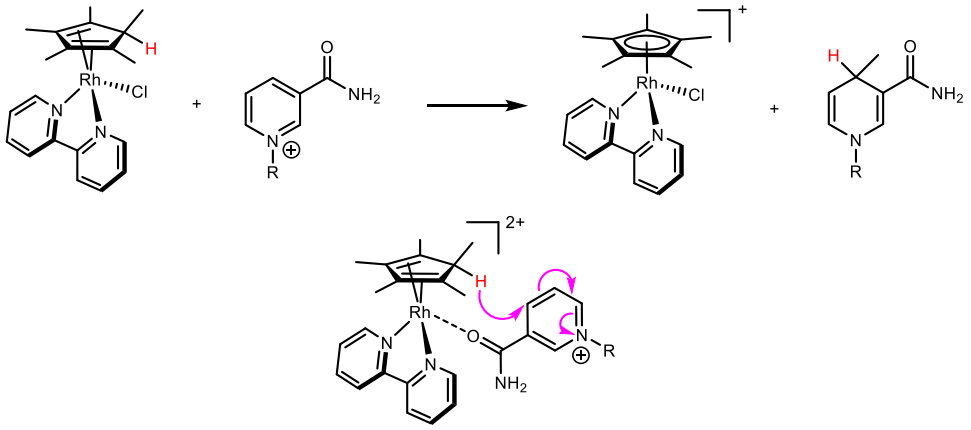

Figure 5. Reduction of NAD^+ (top) and proposed participation of the C_5Me_5H ligand in the hydride transfer (bottom).

The forthcoming *Results and Discussion* section of this Chapter revolves around C−H bond activation processes taking place at (η^5-C_5Me_5)Ir(III) complexes, for which a combined experimental and computational approach disclosed, for the first time, non-innocent behavior of both the cyclopentadienyl ligand and a coordinated terphenyl phosphine. The two molecular fragments which can reversibly form a C−C bond and even *mediate* a C−H activation step, both in solution and in the solid state.

I.2 RESULTS AND DISCUSSION

I.2.1 Synthesis of Cyclopentadienyl Terphenyl Phosphine Complexes

Cyclopentadienyls, C_5R_5, and tertiary phosphines, PR_3, are unquestionably two of the most important classes of ligands in organometallic chemistry and catalysis.[56] As stated in the Introduction, transition metal mediated C−H bond activation is a crucial transformation with great potential for the functionalization of hydrocarbons. In this field, fundamental mechanistic advances have been made with the study of C−H bond activation at electrophilic (η^5-C_5Me_5)Ir(III) centers.[29] In recent years, our group synthesized a family of rhodium and iridium complexes, for which the ambidentate character of a metalated aryl phosphine ligand (Figure 6) provided a rich chemistry, including catalytic applications in the isotopic labeling of hydrosilanes, as well as in the deutero- and tritio-silylation of ketones.[47,57] These findings prompted us to explore the reactivity of analogous complexes of dialkyl terphenyl phosphines in iridium chemistry. The term terphenyl stands for 2,6-diarylphenyl substituents. Evidently, these ligands present many similarities with Buchwald´s dialkylbiaryl phosphines,[58] which have shown outstanding properties in catalysis[59] (Figure 6).

---

[56] Crabtree, R. H. *J. Organomet. Chem.* **2005**, *690*, 5451.
[57] a) Campos, J.; Esqueda, A. C.; Carmona, E. *Chem. Eur. J.* **2010**, *16*, 419; b) Campos, J.; Esqueda, A. C.; López-Serrano, J.; Sánchez, L.; Cossío, F. F.; de Cózar, A.; Álvarez, E.; Maya, C.; Carmona, E. *J. Am. Chem. Soc.* **2010**, *132*, 16765; c) Rubio, M.; Campos, J.; Carmona, E. *Org. Lett.* **2011**, *13*, 5236; d) Campos, J.; Espada, M. F.; López-Serrano, J.; Carmona, E. *Inorg. Chem.* **2013**, *52*, 6694.
[58] Old, D. W.; Wolfe, J. P.; Buchwald, S. L. *J. Am. Chem. Soc.* **1998**, *120*, 9722.
[59] a) Martin, R.; Buchwald, S. L. *Acc. Chem. Res.* **2008**, *41*, 1461 b) Sather, A. C.; Buchwald, S. L. *Acc. Chem. Res.* **2016**, *49*, 2146.

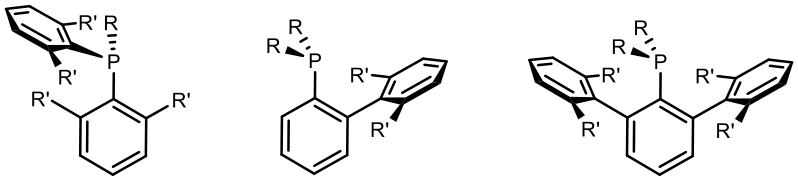

Figure 6. General structure of bis(aryl), Buchwald and terphenyl phosphines. R and R' stand for alkyl or H groups.

The terphenyl group, widely employed as a hydrocarbyl ligand by Power and coworkers, is a very reliable moiety for the stabilization of unsaturated reactive species. A paradigmatic example is the isolation of compound $Cr_2Ar^{Dipp}{}_2$, the first dimetallic complex with a quintuple M-M bond[60] (Figure 7). The stabilization of these and other low-coordinate compounds derives, in part, from the participation of dispersive interactions.[61]

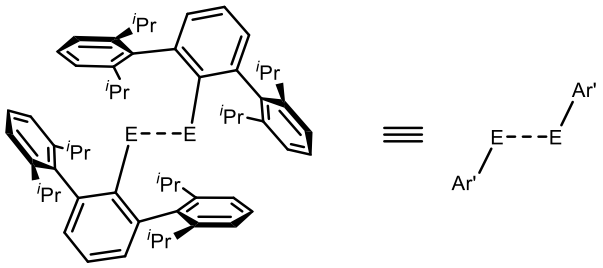

[60] Nguyen, T.; Sutton, A. D.; Brynda, M.; Fettinger, J. C.; Long, G. J.; Power, P. P. *Science* **2005**, *310*, 844.

[61] a) Ndambuki, S.; Ziegler, T. *Inorg. Chem.*, **2012**, *51*, 7794; b) Seidu, I.; Seth, M.; Ziegler, T. *Inorg. Chem.* **2013**, *52*, 8378; c) Lin, C.-Y.; Guo, J.-D.; Fettinger, J. C.; Nagase, S.; Grandjean, F.; Long, G.; Chilton, N. F.; Power, P. P. *Inorg. Chem.* **2013**, *52*, 13584; d) Rekken, B. D.; Brown, T. M.; Fettinger, J. C.; Lips, F.; Tuononen, H. M.; Herber, R. H.; Power, P. P. *J. Am. Chem. Soc.* **2013**, *135*, 10134; e) Wagner, C. L.; Tao, L.; Thompson, E. J.; Stich, T. A.; Guo, J.; Fettinger, J. C.; Berben, L. A.; Britt, R. D.; Nagase, S.; Power, P. P. *Angew. Chem. Int. Ed.* **2016**, *55*, 10444; f) Liptrot, D. J.; Power, P. P. *Nat. Rev. Chem.* **2017**, *1*, 4.

Figure 7. Main group and transition metal dimers stabilized by bulky terphenyl groups (E = Pb, formal bond order =1; E = Si, Ge, Sn, formal bond order = 3; E = Cr, formal bond order = 5; Ar' = terphenyl group).

The use of ligands that incorporate a terphenyl moiety has allowed the isolation of very reactive species, like terminal iron and cobalt carbynes stabilized by coordination to terphenyl isonitriles[62] or bimetallic terphenyl phosphine complexes of Au(I)[63] in which two $Au(PMe_2Ar')^+$ fragments are bridged by the simplest hydrocarbyl units, CH_3, $CH{=}CH_2$ and C≡CH (Figure 8). Terphenyl phosphine ligands were also instrumental in the development of the first Transition-Metal-Only Frustrated Lewis Pair.[64]

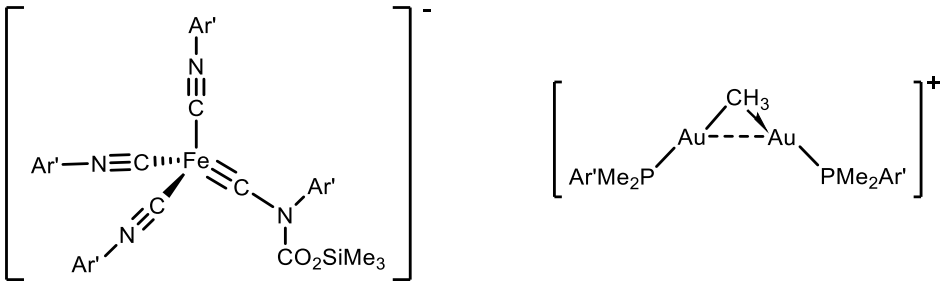

Figure 8. An anionic iron carbyne and a methyl-bridged digold complex, stabilized by ligands containing a terphenyl moiety (Ar').

This Chapter describes our results on the reactivity of Ir(III) complexes constructed around an η^5-C_5Me_5 ring and one of two selected terphenyl phosphines, namely $PMe_2Ar^{Xyl}{}_2$ and $PMe_2Ar^{Dipp}{}_2$ (Xyl = 2,6-$Me_2C_6H_3$, Dipp = 2,6-$^i Pr_2C_6H_3$), whose structures are depicted in Scheme 11. Using

[62] a) Mokhtarzadeh, C. C.; Moore, C. E.; Rheingold, A. L.; Figueroa, J. S. *Angew. Chem. Int. Ed.* **2017**, *56*, 10894; b) Mokhtarzadeh, C. C.; Moore, C. E.; Rheingold, A. L.; Figueroa, J. S. *J. Am. Chem. Soc.* **2018**, *140*, 8100.
[63] Espada, M. F.; Campos, J.; López-Serrano, J.; Poveda, M. L.; Carmona, E. *Angew. Chem. Int. Ed.* **2015**, *54*, 15379.
[64] Campos, J. *J. Am. Chem. Soc.* **2017**, *139*, 2944.

$[(\eta^5\text{-}C_5Me_5)IrCl_2]_2$ as a precursor, we found notable differences in reactivity for these two phosphines. Whereas the smaller, xylyl derived phosphine readily coordinated to the metal to yield the expected piano-stool, neutral complex **1(Xyl)**, the bulkier, diisopropylphenyl substituted ligand remained unreacted even after prolonged heating at 50 ºC (Scheme 11). As it will be discussed later in section **I.2.3**, the strong steric hindrance that needs be overcome to form **1(Dipp)** was found to be a relevant feature in reactions where chloride anions were displaced from the first coordination sphere of the metal.

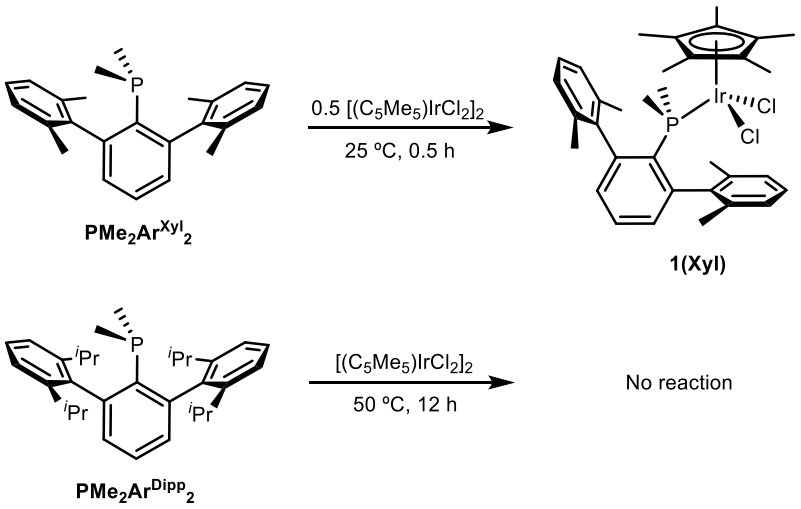

Scheme 11. Reactivity of dimethyl terphenyl phosphines towards $[(\eta^5\text{-}C_5Me_5)IrCl_2]_2$.

The phosphorus atom of complex **1(Xyl)** resonates as a sharp singlet at −29.9 ppm in the $^{31}P\{^1H\}$ spectrum, in accordance with the expected κ^1-P coordination.[65] In the ^1H NMR spectra, slow rotation around the P−*ipso*-C_6H_3 bond was responsible for two distinct sets of signals corresponding to the benzylic and *meta* protons of the flanking xylyl rings, which were

[65] Marin, M.; Moreno, J. J.; Navarro-Gilabert, C.; Álvarez, E.; Maya, C.; Peloso, R.; Nicasio, M. C.; Carmona, E. *Chem. Eur. J.* **2018**, *in press.*

found to be exchanging in the EXSY experiment. Chemical exchange cross peaks with minor amounts of free $PMe_2Ar^{Xyl}_2$ were also detected, proving that the Ir−P bond is labile in this species. The structure of complex **1(Xyl)** was confirmed by means of X-Ray crystallography (Figure 9). At variance with prior results from our group using related systems based on bis(aryl) phosphines[57a], **1(Xyl)** did not evolve to any cyclometalated structure even in the presence of organic bases.

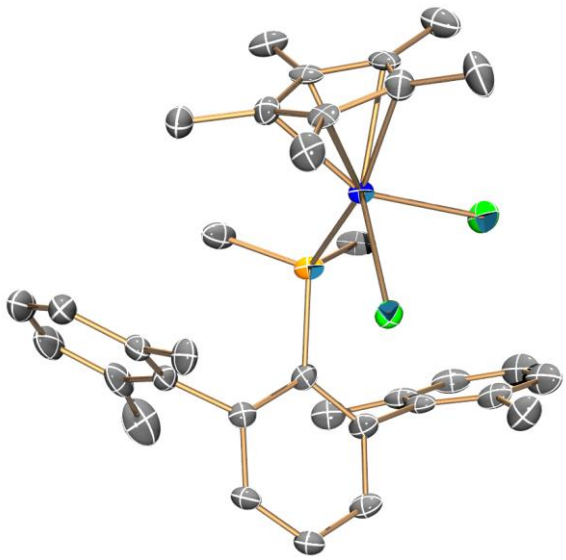

Figure 9. ORTEP diagram of complex **1(Xyl)**. Hydrogen atoms are excluded for clarity and thermal ellipsoids are set at 50 % probability.

As briefly noted, no reaction between $[(\eta^5\text{-}C_5Me_5)IrCl_2]_2$ and $PMe_2Ar^{Dipp}_2$ takes place at room temperature or at 50 ºC. Notwithstanding, upon addition of one equivalent of the sodium salt of the weakly coordinating BAr_F anion (BAr_F = $[\{3,5\text{-}(CF_3)_2\text{-}C_6H_3)_4\}B]^-$), to these unreacted solution mixtures a drastic color change, from orange to intense dark-brown, almost black, was observed. A marked high-frequency change of the phosphorus resonance in the $^{31}P\{^1H\}$ experiment relative to the free phosphine (from −41.3 to 6.6 ppm) and the appearance of a doublet at 1.22 ppm associated

with the 15 C_5Me_5 protons ($^4J_{HP}$ = 1.5 Hz) in the ^1H spectrum of the mixture, constituted unambiguous proof that coordination of the bulky phosphine had taken place to afford a new species, **2(Dipp)**$^+$ (Scheme 12). Complex **1(Xyl)** also reacted with $NaBAr_F$, yielding a similar, intense dark-red solution with analogous $^{31}P\{^1H\}$ and ^1H features, suggesting the formation of the related species **2(Xyl)**$^+$. The flanking aryl rings of the terphenyl phosphine ligand in type **2**$^+$ complexes appear equivalent in the ^1H and $^{13}C\{^1H\}$ NMR spectra, suggesting either fast exchange or a symmetrical disposition, both situations being incompatible with the existence of strong metal-arene interactions.

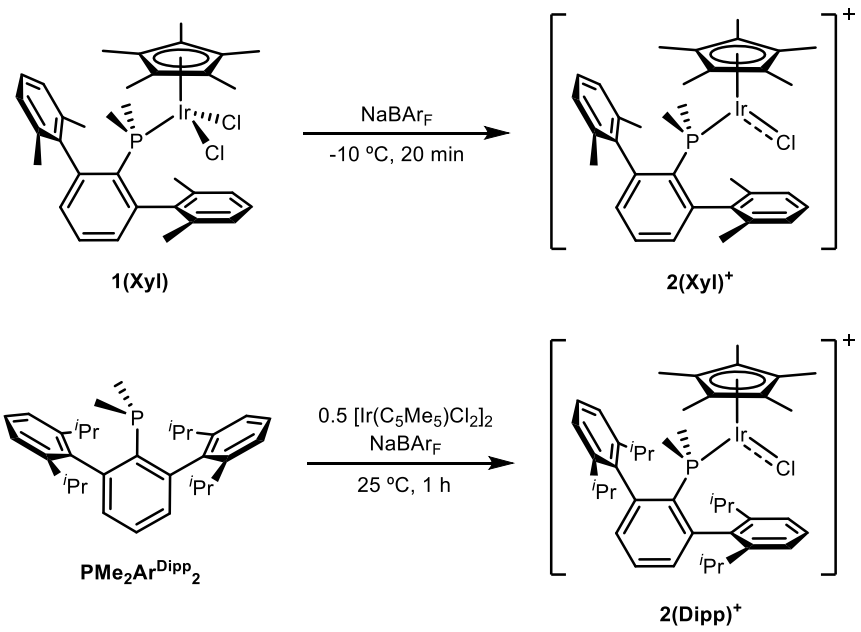

Scheme 12. Synthesis of type **2**$^+$ complexes.

Although for most biaryl and terphenyl phosphine complexes metal unsaturation is often compensated by means of so-called secondary π-arene

interactions,[59a,66] the intense dark coloration of these complexes and X-Ray crystallography studies of single crystals of the new compounds (Figure 10) disclosed the absence of significant arene-metal bonding. Contrarily, the closest Ir−C_{arene} distances found for **2(Xyl)**$^+$ were 3.918(3) (C_{ortho}) and 4.039(4) (C_{ipso}) Å, whereas for **2(Dipp)**$^+$ shorter values of 3.124(4) (C_{ortho}) and 3.160(4) (C_{ipso}) Å were registered. Along with the large metal-arene distances, the shortening of the Ir−Cl bond (Ir−Cl distances (Å): **1(Xyl)** = 2.401(1) and 2.391(1), **2(Xyl)**$^+$ = 2.278(1), **2(Dipp)**$^+$ = 2.347(1)) suggested that in the solid state the chloride ligand was acting as a π donor. Similar Ru−Cl shortening was reported in [(η^5-C_5Me_5)Ru(Cl)(P^iPr_3)].[67] Caulton and coworkers proposed also π-stabilization in (C_5Me_5)Ru(X)(PR_3) and related compounds.[68]

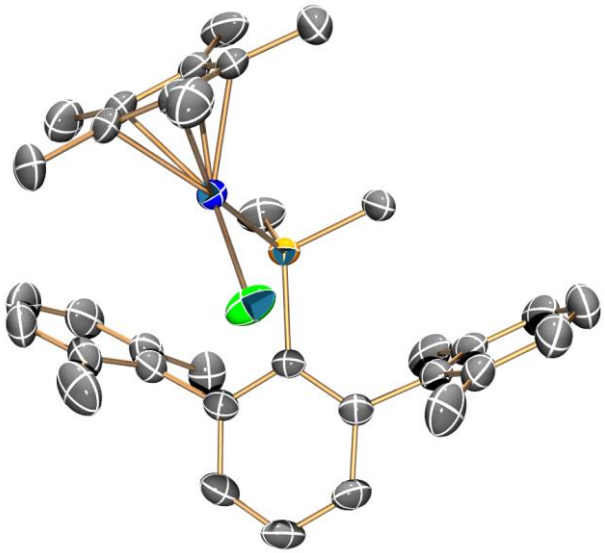

[66] Moreno, J. J.; Espada, M. F.; Krüger, E.; López-Serrano, J.; Campos, J.; Carmona, E. *Eur. J. Inorg. Chem.* **2018**, 2309.
[67] Campion, B. K.; Heyn, R. H.; Tilley, T. D. *J. Chem. Soc., Chem. Commun.* **1988**, 278.
[68] Johnson, T. J.; Folting, K.; Streib, W. E.; Martin, J. D.; Huffman, J. C.; Jackson, S. A.; Eisenstein, O.; Caulton, K. G. *Inorg. Chem.* **1995**, *34*, 488.

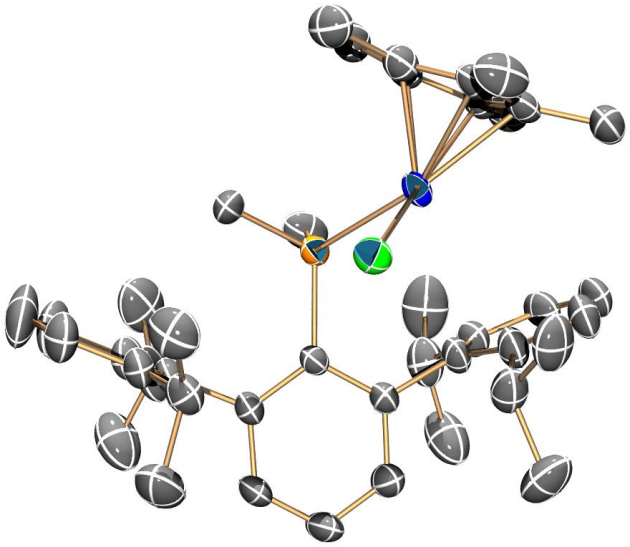

Figure 10. ORTEP diagrams of the cations of complex **2(Xyl)**$^{+}$ (top) and **2(Dipp)**$^{+}$ (bottom). Hydrogen atoms are excluded for clarity and thermal ellipsoids are set at 50 % probability.

Low-temperature ^{1}H NMR studies were carried out to ascertain the solution behavior of complex **2(Dipp)**$^{+}$, for which the above-mentioned metrical parameters (Ir−Cl and Ir−C_{arene} distances) suggested the possibility of detecting a metal-arene-bonded species that might be concealed by kinetic energy at room temperature. Upon lowering the temperature to −30 ºC, the slow exchange regime was attained for the rotation around the P−*ipso*-C_6H_3 bond ($\Delta G^{\ddagger}$ = 12.8 kcal·mol^{-1}, determined by means of line-shape analysis) splitting the signals corresponding to the ^{i}Pr methine protons and the aromatic *m*-Dipp protons in two sets. Further cooling to −80 ºC did not increase the complexity of the spectrum with additional signal splitting. The observed low-temperature pattern, similar to that of complex **1(Xyl)**, implied the existence of a pseudo symmetry plane containing the P, Ir and Cl atoms, which ruled out a permanent metal-arene interaction in this complex. Despite these findings, metal-

arene bonding was found to play a key role in the reactivity of the system, as disclosed in forthcoming sections.

Although the purported neutral complex **1(Dipp)** could not be accessed through the aforementioned route, a formally hexacoordinated complex was achieved by treating complex **2(Dipp)**$^+$ with CO (Scheme 13). This reaction was carried out both in solution and in the solid-state. In the latter case, dark crystals of **2(Dipp)**$^+$ immediately turned bright yellow upon exposure to CO. The corresponding solution $^{31}P\{^1H\}$ NMR spectrum of **2(Dipp)**$^+$ revealed a remarkable chemical shift change of nearly 40 ppm for the ^{31}P resonance upon CO addition (from 6.6 to −33.2 ppm). The new signal can be attributed to the formation of the CO adduct and is consistent with monodentate P-coordination of $PMe_2Ar^{Dipp}{}_2$.[65] The fluxional behavior of complex **2(Dipp)**$^+$**·CO** was noticed thanks to the presence of broad signals in the room temperature ^1H NMR spectrum. Upon cooling at −20 ºC, these signals sharpened, giving rise to four different signals corresponding to the inequivalent methine protons of the ^{i}Pr groups, in agreement with the lack of symmetry expected for this chiral molecule. Exchange peaks in the EXSY experiment suggested that the rotation around the P−*ipso*-C_6H_3 bond, responsible for the observed fluxionality, is not completely hindered at this temperature. In the $^{13}C\{^1H\}$ spectrum, a doublet was detected within the characteristic region for metal carbonyls, at 167.9 ppm, $^2J_{CP}$ = 19 Hz, which was unambiguously assigned to the incorporated CO ligand. A band at 2059 cm^{-1} in the IR spectrum (Nujol) of **[2(Dipp)·CO]BAr$_F$** can be assigned to the CO stretching frequency, further confirming the formation of the carbon monoxide adduct.

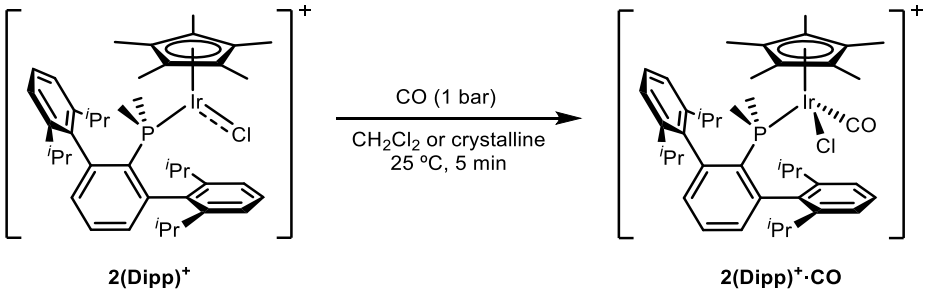

Scheme 13. Reactivity of **2(Dipp)**$^{+}$ towards CO.

I.2.2 Dicationic Complexes as Intermediates in C−H Activation

Dichloromethane solutions of complex **2(Xyl)**$^+$ underwent an unmistakable color change from red-black to yellow-red upon standing for *ca.* 4 hours at room temperature, a process that was found to be accelerated by the presence of water. Product crystallization from CH_2Cl_2/Et_2O solvent mixtures yielded a new iridium complex, **3(Xyl)**$^+$, along with $[(\eta^5\text{-}C_5Me_5)IrCl_2]_2$ and $[HPMe_2Ar^{Xyl}_2]BAr_F$ (Scheme 14). The latter two compounds were identified by comparison of their NMR spectra with those of authentic samples. In turn, **3(Xyl)**$^+$ was unequivocally characterized as a pseudoallylic species formed via remote ζ C−H activation of a benzylic C−H bond of one of the Xyl substituents. It thus appears that the HCl released in the formation of **3(Xyl)**$^+$ decomposed unreacted **2(Xyl)**$^+$ to yield the above-mentioned side products. Given that an increase in the steric requirements of coligands often results in enhanced kinetic stability that may hinder undesirable side reactions, it was not surprising to find that the otherwise structurally similar complex **2(Dipp)**$^+$ possessed much superior solution stability.

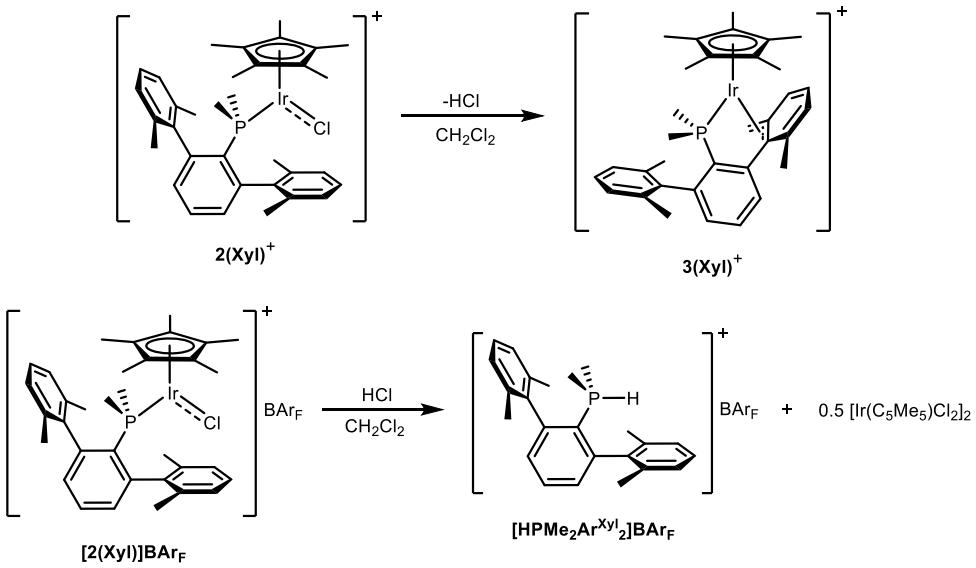

Scheme 14. Thermal evolution of **2(Xyl)**$^+$.

Bearing in mind the remarkable reactivity often exhibited by dicationic iridium complexes,[69] the reactions of complexes **2**$^+$ with a second equivalent of $NaBAr_F$ were carried out. Somewhat surprisingly, although the expected dicationic $[(\eta^5\text{-}C_5Me_5)Ir(PR_2Ar')]^{2+}$ species resulting from chloride abstraction could not be isolated, this procedure permitted the high yield syntheses of complexes **3(Xyl)**$^+$ and **3(Dipp)**$^+$. As shown in Scheme 15, the addition of $NaBAr_F$ to solutions containing the monocationic complex **2(Xyl)**$^+$ led rapidly to the pseudoallylic complex **3(Xyl)**$^+$. The latter complex results, as briefly cited, from remote electrophilic ζ C−H activation of a Xyl ring methyl group, presumably with elimination of HCl. In contrast, the analogous formation of **3(Dipp)**$^+$ from **2(Dipp)**$^+$ was very slow at room temperature and required heating at 40 ºC for several days for completion. It is reasonable to ascribe the

[69] Lehman, M. C.; Gary, J. B.; Boyle, P. D.; Sanford, M. S.; Ison, E. A. *ACS Catal*. **2013**, *3*, 2304.

sluggishness of the latter process to the absence of an effective Brönsted-Lowry base that could facilitate removal of the generated HCl. Consistent with this hypothesis, the deliberate addition of 1-2 equivalents of H_2O permitted the synthesis of complex **3(Dipp)**$^+$ under mild conditions (see Experimental Section). In like manner, the reaction of $PMe_2Ar^{Dipp}{}_2$ with $[(\eta^5\text{-}C_5Me_5)Ir(H_2O)_3](SO_4)$[70] proceeded rapidly to afford **3(Dipp)**$^+$.

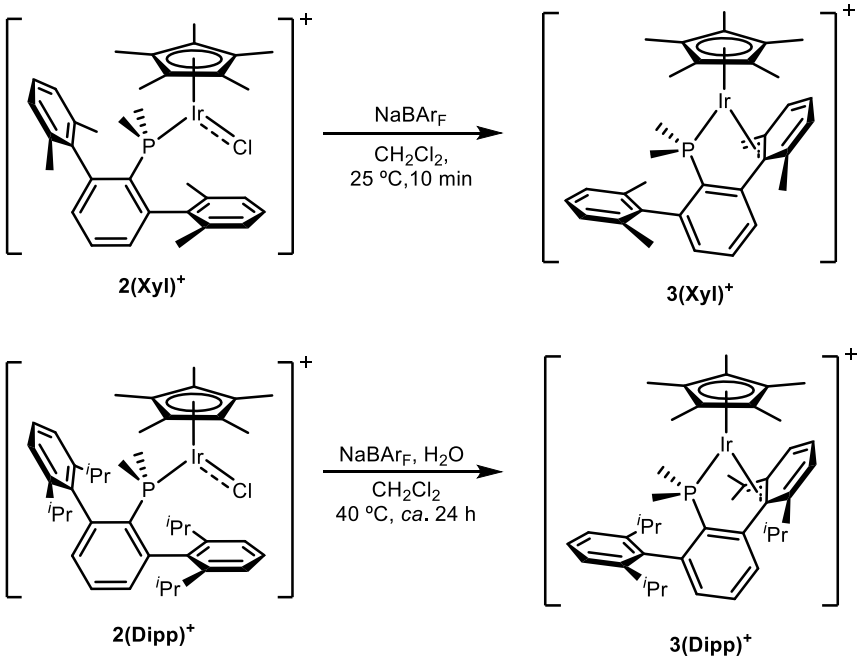

Scheme 15. Synthesis of type **3**$^+$ complexes starting from **2**$^+$ and $NaBAr_F$.

The BAr_F salts of the two pseudo-allyl complexes **3(Xyl)**$^+$ and **3(Dipp)**$^+$ were fully characterized by multinuclear NMR spectroscopy and X-Ray crystallography. The lack of symmetry exhibited by these complexes gave rise to complex NMR spectra. For **3(Xyl)**$^+$, distinct ^{1}H NMR resonances corresponding to the *syn* and *anti* pseudoallylic protons are seen as multiplets at 3.14 and 1.04 ppm, with $^2J_{HH}$ = 3.9 and $^3J_{HP}$ = 1 and 14 Hz,

[70] Ogo, S.; Makihara, N.; Watanabe, Y. *Organometallics* **1999**, *18*, 5470.

respectively. The corresponding carbon atom gives a $^{13}C\{^1H\}$ signal at 26.3 ppm ($^2J_{CP}$ = 4 Hz), whereas the C_{ortho} and C_{ipso} atoms involved in η^3-bonding can be found as doublets ($^2J_{CP}$ = 1 Hz) at 89.1 and 83.2 ppm, respectively. Whereas non-metalated xylyl rings exhibit $^3J_{HH}$ couplings of *ca*. 7.5 Hz, the partial loss of aromaticity of the metalated aryl ring of complex **3(Xyl)**$^+$ gives rise to $^3J_{HH}$ couplings above (8.6 Hz, *m*'-Xyl'−*p*-Xyl') and below average (6.5 Hz, *m*-Xyl'−*p*-Xyl'), Figure 11.[71] The NMR spectra of **3(Dipp)**$^+$ was found to be similar to those of **3(Xyl)**$^+$, except for the $^{13}C\{^1H\}$ resonance of the Ir*C*Me$_2$ carbon (44.1 ppm) and the proton resonances of the corresponding methyl groups (1.65 and 0.53 ppm in the ^1H NMR).

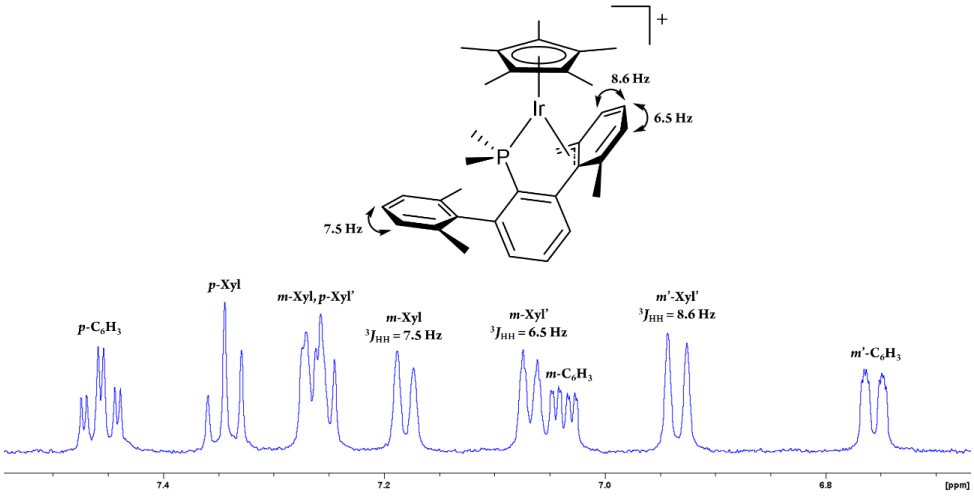

Figure 11. Aromatic region of the ^1H NMR spectrum of complex **3(Xyl)**$^+$.

Single-crystals of the two complexes **3**$^+$ were also investigated by X-ray crystallography (Figure 12), confirming that a flanking ring of the phosphine has undergone ζ C−H activation to give a pseudoallylic product.

[71] The apostrophe is used to differentiate the atom or ring that is closer to the metal center. Thus, Xyl' and Xyl designate coordinated and free xylyl rings, respectively. In turn, *m*'-Xyl' in **3(Xyl)**$^+$ refers to the *meta* position of the bound xylyl ring that is in closer proximity to the metal center.

For complex **3(Dipp)**$^+$, relevant metrical parameters are: Ir−CMe_2 = 2.224(3), Ir−C_{ortho} = 2.197(3) and Ir−C_{ipso} = 2.257(3) Å. Values of *ca*. 2.21 Å were found for the corresponding Ir−C distances in **3(Xyl)**$^+$.

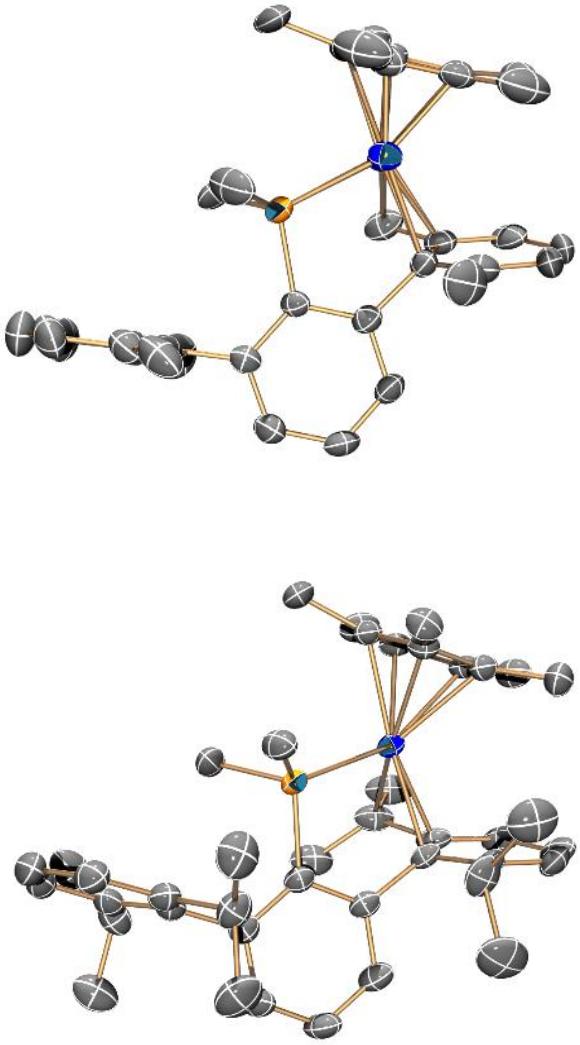

Figure 12. ORTEP diagrams of the cations of complexes **3(Xyl)**$^+$ (top) and **3(Dipp)**$^+$ (bottom). Hydrogen atoms are omitted for clarity and thermal ellipsoids are set at 50 % probability.

Pseudoallylic coordination of aryl phosphine ligands to group 9 transition metals (Rh and Ir) has frequently been encountered in our group. Thus, earlier work showed that $PMeXyl_2$ is prone to cyclometallation to yield five-membered metalacyclic structures upon reaction with Ir(III) and Rh(III) precursors in the presence of a base. For bis(aryl) phosphine ligands such as $PMeXyl_2$ ring strain and the partial loss of aromaticity associated to the pseudoallylic structure makes the κ^1-P,κ^3-C coordination very labile so that it can be easily displaced by weakly coordinating ligands, alike CH_3CN or THF. In the absence of additional ligands, these species could also access an almost isoenergetic κ^1-P,κ^1-C isomer. Therefore, generation of a vacant site and substrate coordination to the metal center, two fundamental features in transition metal-mediated homogeneous catalysis, were facile processes (Scheme 16).[47]

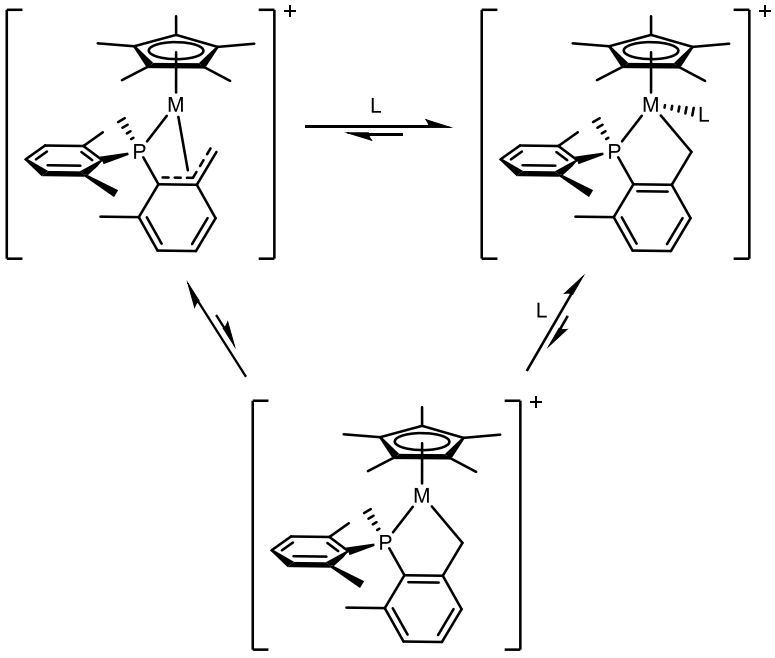

Scheme 16. Equilibria determined for metalated bis(aryl) phosphine ligand complexes (M = Rh, Ir; L = Lewis base, e.g. CH_3CN).

Despite the structural similarities of complexes **3**$^{+}$ with the aforementioned species, it is not surprising to find that their reactivity is more limited. Probably, the lack of ring strain in the longer-range metallacyclic structure could cause the pseudoallylic interaction to be less labile, to the point that it was not displaced by poor donor ligands, such as CH_3CN. In addition, no reactivity towards H_2 or D_2 was detected, which was observed, at variance with the signature reactivity of the bis(aryl) phosphine system. However, prolonged heating of **3(Xyl)**$^{+}$ under 1 bar of CO led to the carbonyl adduct, **3(Xyl)·CO**$^{+}$. This complex was be isolated and characterized as featuring κ^1-P,κ^1-C coordination of the terphenyl phosphine ligand (Scheme 17).

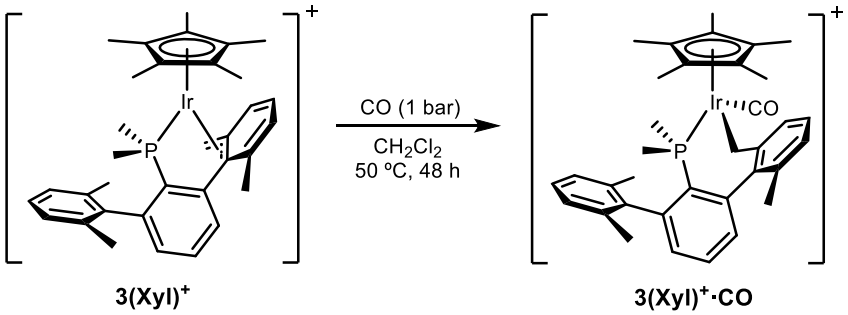

Scheme 17. Reactivity of **3(Xyl)**$^{+}$ towards CO.

Similarly to **2(Dipp)**$^{+}$, the $^{31}P\{^{1}H\}$ spectrum of **3(Xyl)·CO**$^{+}$ revealed a remarkable low-frequency shift relative to **3(Xyl)**$^{+}$ of nearly 60 ppm (from 13.6 to −46.3 ppm) in its $^{31}P\{^{1}H\}$ NMR resonance. The aromaticity of the coordinated xylyl ring was restored in **3(Xyl)·CO**$^{+}$, as unambiguously reflected in the ^{1}H NMR spectrum by the values of *ca*. 7.5 Hz found for all the aromatic $^{3}J_{HH}$ coupling constants. The methylene protons in **3(Xyl)·CO**$^{+}$ resonate as doublets of doublets (AMX spin system) at 2.87 and 2.56 ppm, in marked contrast with the corresponding chemical shifts found for **3(Xyl)**$^{+}$ (3.14 and 1.04 ppm). The $^{13}C\{^{1}H\}$ NMR spectrum provided further evidence for the proposed structural assignment of

3(Xyl)·CO^{+}, as the coordinated carbonyl group gives rise to a doublet ($^{2}J_{CP}$ = 13 Hz) registered at 167.3 ppm. The *ortho*' and *ipso* carbon atoms of the coordinated xylyl ring experience a significant high-frequency shift upon disengagement from the metal center, giving rise to a singlet and a doublet ($^{3}J_{CP}$ = 3 Hz) at 146.7 and 136.2 ppm, respectively (*cf.* the doublets ($^{2}J_{CP}$ = 1 Hz) at 89.1 and 83.2 ppm recorded for **3(Xyl)**$^{+}$). The methylenic carbon atom also presents a remarkable chemical shift variation, appearing as a doublet ($^{2}J_{CP}$ = 6 Hz) at 7.6 ppm ($\Delta\delta$ = −18.7 ppm relative to **3(Xyl)**$^{+}$). The wavenumber of the IR band associated with the CO stretching frequency, 2035 cm^{-1} (Nujol), represents a significant variation when compared to that found for **2(Dipp)**$^{+}$**·CO** (2059 cm^{-1}). Despite employing a different phosphine, it is safe to assume that the variation mainly arises from the stronger sigma donating character of the $ArCH_2$− moiety compared to the chloride ligand.[72]

[72] Thomson, J.; Baird, M. C. *Can. J. Chem.* **1973**, *51*, 1179.

I.2.2.1 Computational Studies on Electrophilic C−H Activation

The mechanism of the C−H bond activation to form complexes **3(Xyl)**$^+$ and **3(Dipp)**$^+$ was investigated by DFT methods.[73] The most accessible pathway involves initial Cl^- dissociation to afford an ion-pair comprising dicationic $[(\eta^5\text{-}C_5Me_5)Ir(PMe_2Ar')]^{2+}$, in which the phosphine is bound in a κ^1-P,κ^3-C_{arene} fashion (Figure 13) and Cl^-, which resides in the outer coordination sphere. For **2(Xyl)**$^+$, this process entails a barrier of 18.4 kcal/mol and gives a species 16.5 kcal/mol above **2(Xyl)**$^+$. A series of facile rearrangements of the dicationic complex yield an intermediate (+19.3 kcal/mol) featuring a ζ C−H agostic interaction. The acidity of the agostic proton in this dicationic species promotes its facile abstraction by the Cl^- ion via a transition state at +22.0 kcal/mol, this representing the overall barrier to the C−H activation process (Figure 14).

[73] Calculations were performed with the Gaussian 09 program employing the hybrid functional PBE0. Geometry optimizations were carried out without geometry constraints and included solvent (dichloromethane) and dispersion effects (Grimme´s D3 parameter set). 50%-corrected free energy variations (ΔG_{50}°) were employed to account for translational entropy overestimation.

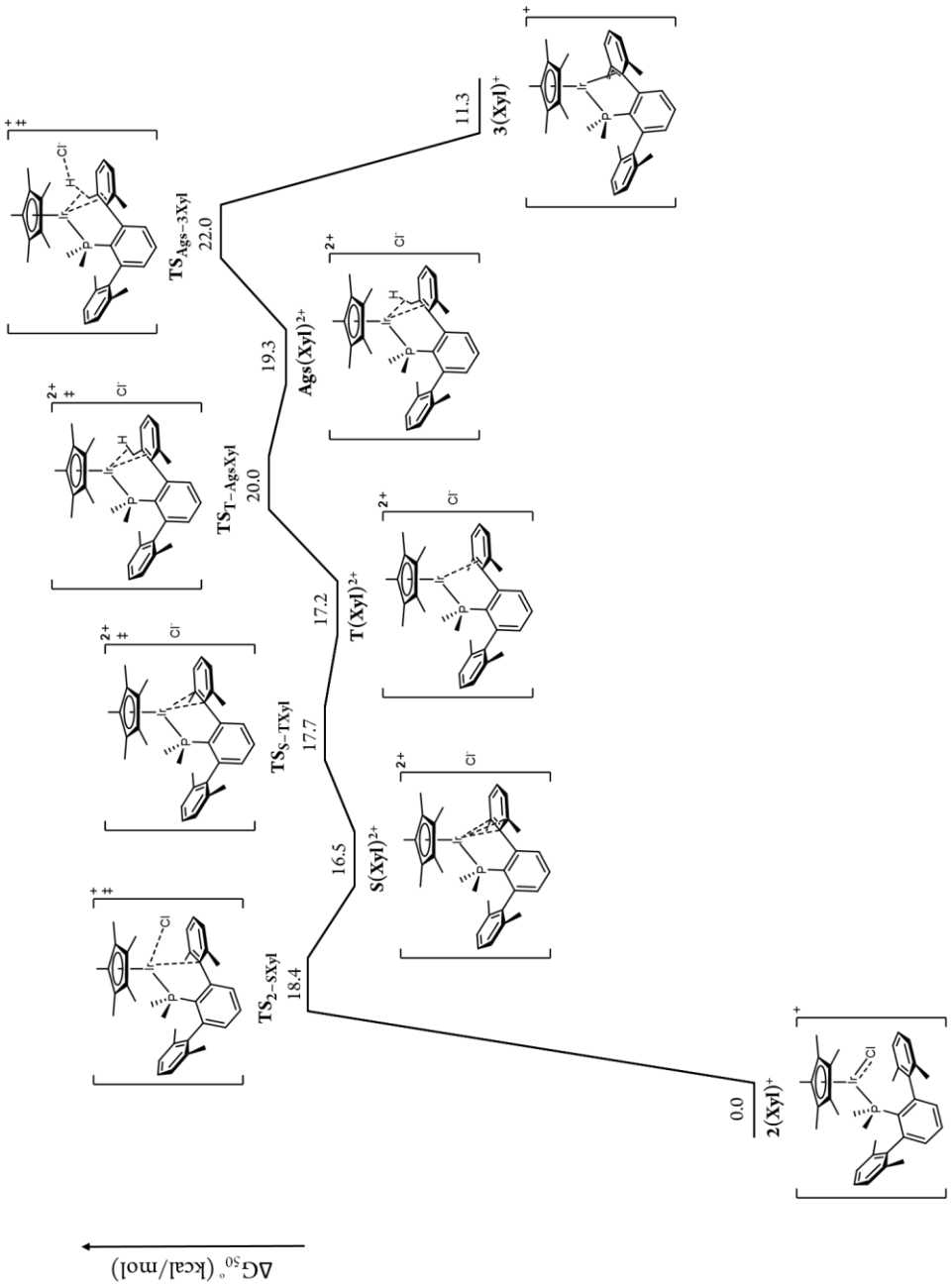

Figure 13. ΔG_{50}° profile for the conversion of **2(Xyl)**$^{+}$ into **3(Xyl)**$^{+}$ and HCl.

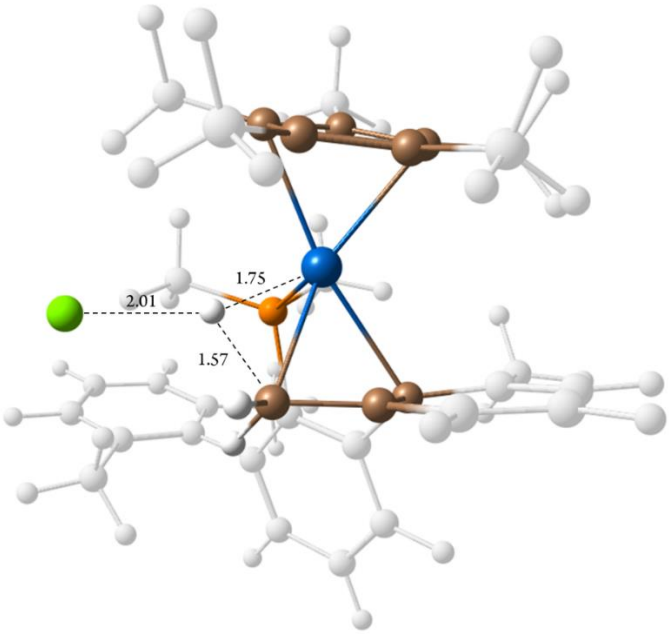

Figure 14. Molecular geometry of the transition state for the abstraction of the agostic proton by chloride (**TS$_{Ags–3Xyl}$**).

In contrast, the analogous chloride-mediated deprotonation in **2(Dipp)**$^+$ does not occur at the dicationic agostic complex, but requires an additional C−H oxidative cleavage step to form an Ir(V) hydride, which is then deprotonated by Cl^- (Figures 15-17). The overall barrier in this case is 24.7 kcal/mol, 2.7 kcal/mol higher than that in **2(Xyl)**$^+$ and so consistent with the observed enhanced solution stability of the former. The formation of [HPMe$_2$Ar$^{'}$]BAr$_F$ and [(η^5-C$_5$Me$_5$)IrCl$_2$]$_2$ from **2**$^+$ and HCl seems to be the driving force of the reaction in both systems. In the presence of NaBAr$_F$, the irreversible formation of NaCl is the driving force of the reaction. Chloride trapping by the sodium cation inhibits the formation of [(η^5-C$_5$Me$_5$)IrCl$_2$]$_2$, permitting the clean synthesis of type **3**$^+$ complexes along with [H(S)$_n$]BAr$_F$ (S = adventitious solvent molecules, i.e. H$_2$O). The latter was removed by washing with 1:1 mixtures of pentane and diethyl ether.

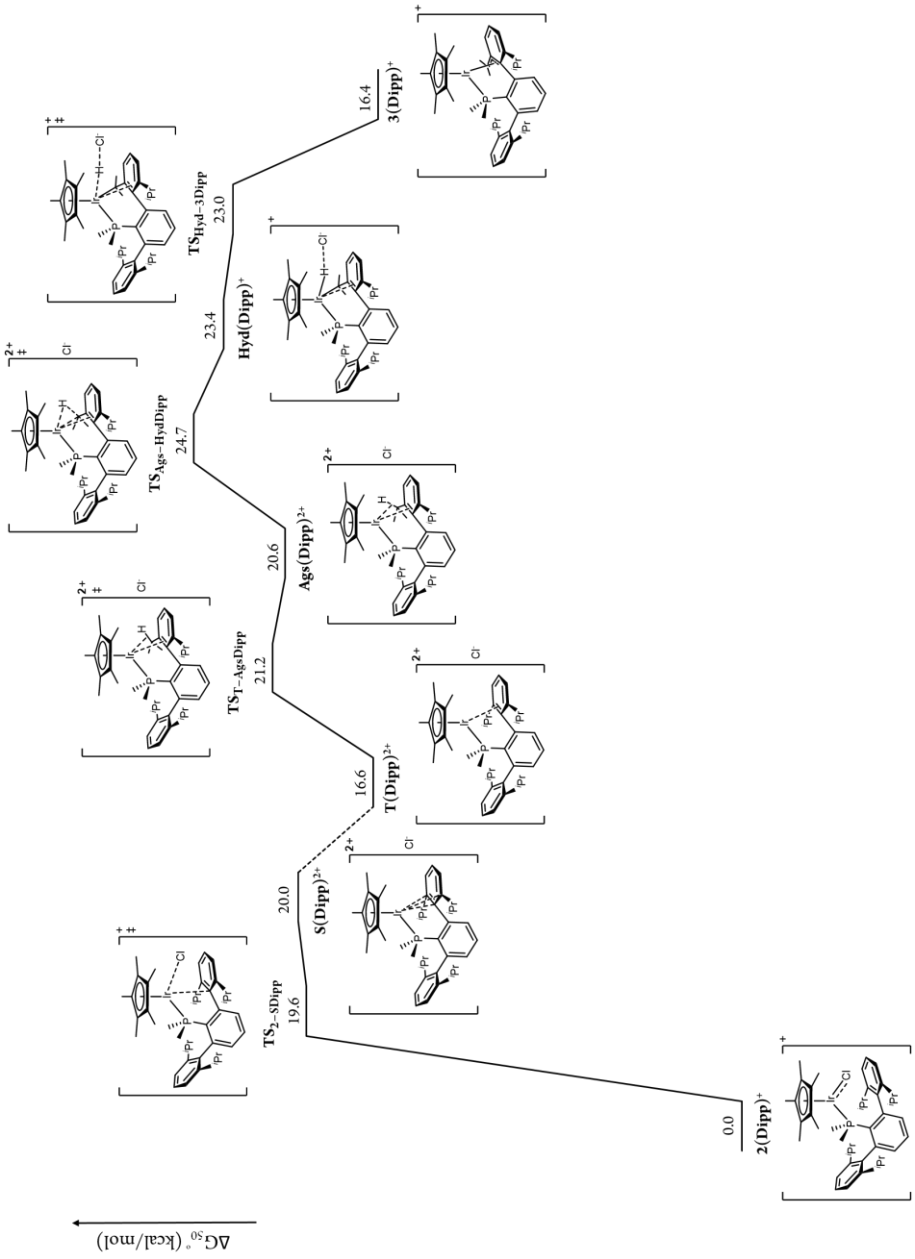

Figure 15. ΔG_{50}° profile for the conversion of **2(Dipp)**$^{+}$ into **3(Dipp)**$^{+}$ and HCl. A transition state connecting intermediates **S(Dipp)**$^{2+}$ and **T(Dipp)**$^{2+}$ could not be found.

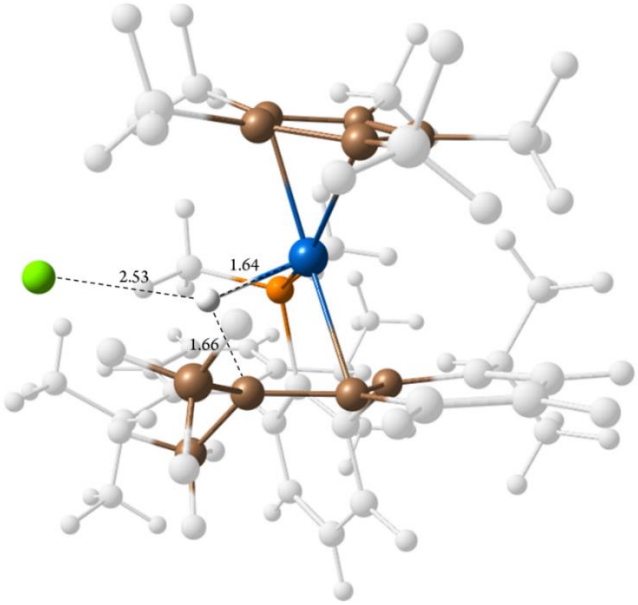

Figure 16. Molecular geometry of the transition state for the oxidative addition of the agostic proton to form an Ir(V) hydride (**TS$_{\mathbf{Ags-HydDipp}}$**).

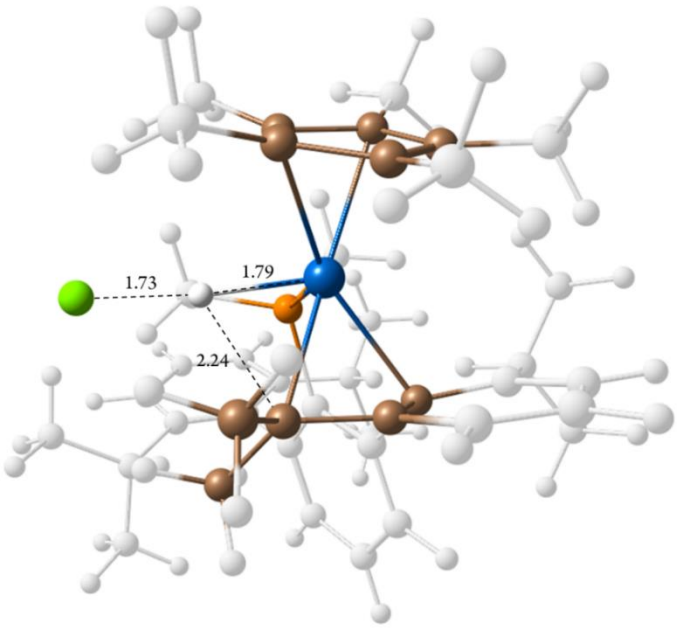

Figure 17. Molecular geometry of the transition state for the chloride deprotonation of the hydridic proton (**TS$_{\mathbf{Hyd-3Dipp}}$**).

I.2.2.2 Electrophilic C−H Activation: Alternative Pathways

The unsaturated character of complex **2(Xyl)**$^+$ prompted us to consider alternative reaction pathways, in which the C−H activation event could take place at the vacant coordination site, with no need of prior chloride dissociation. The operating mechanism in the related Bergman system is still a matter of debate nowadays. Thus, while early DFT (static) studies[74] favored stepwise oxidative addition-reductive elimination pathways, with the participation of Ir(V) intermediates, recent studies[29c] suggest that the Ir(V) stage may be bypassed in some cases.

In our case, it is remarkable that agostic complexes, which are frequently proposed as intermediates in these transformations, could not be located as minima for type **2**$^+$ complexes. Both concerted and stepwise pathways were taken into consideration in the DFT study of alternative C−H bond activation at **2(Xyl)**$^+$. The stepwise route, via the oxidative addition of the benzylic C−H bond, yields an Ir(V) hydride complex, **IrV(Xyl)**$^+$, (Figures 18 and 19), which in turn reductively eliminates HCl to generate **3(Xyl)**$^+$. However, an overall barrier of 35.0 kcal/mol, found for the reductive coupling step, makes this pathway highly unlikely.

[74] Niu, S.; Hall, M. B. *J. Am. Chem. Soc.* **1998**, *120*, 6169.

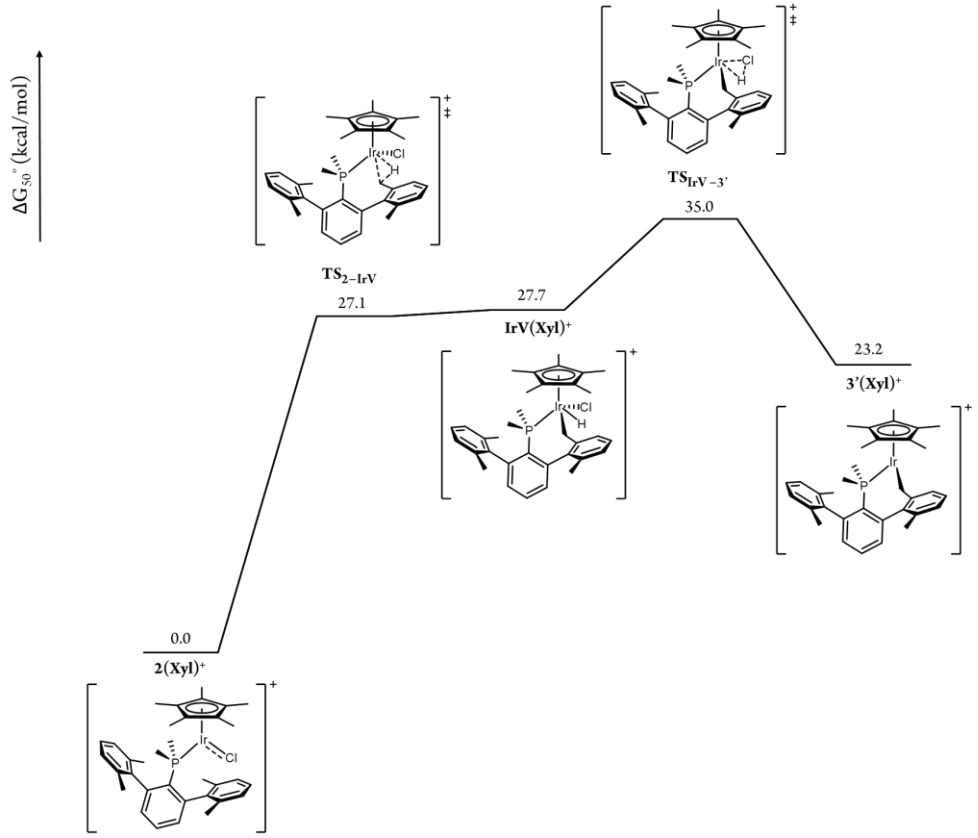

Figure 18. ΔG_{50}° profile for the conversion of **2(Xyl)**$^{+}$ into an Ir(V) hydride complex, followed by reductive elimination of HCl to yield **3'(Xyl)**$^{+}$, an η^{1}−allyl isomer of **3(Xyl)**$^{+}$.

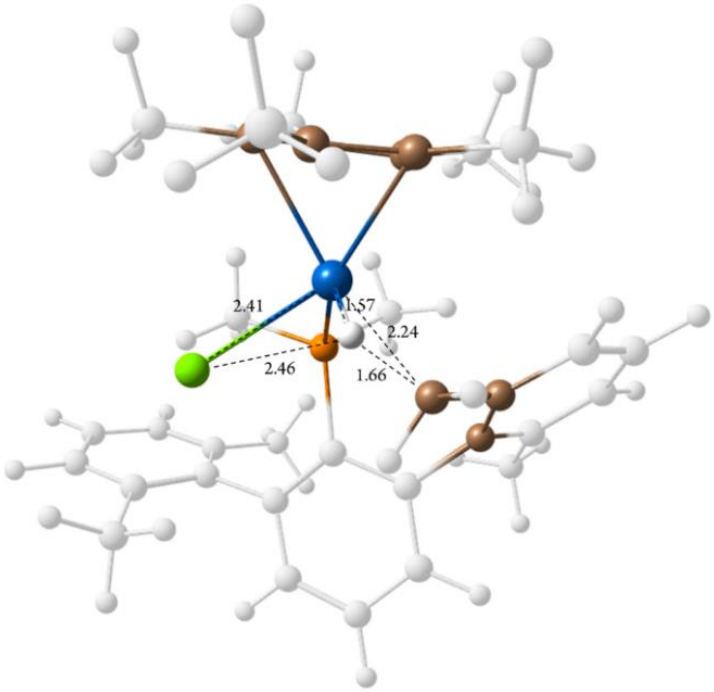

Figure 19. Molecular geometry of the transition state for the oxidative addition of the benzylic proton at **2(Xyl)**$^{+}$ (**TS**$_{2\text{–IrVXyl}}$).

A second alternative route that was also considered involves the concerted cleavage of a C−H bond promoted by a metal and an intramolecular base,[75] which in the case of complexes **2**$^{+}$ could be the chloride ligand. In this mechanism, known as *Ambiphilic Metal-Ligand Assistance* (AMLA),[76] there is a synergic role of the electron-deficient metal center and the proximate basic moiety in the activation of the C−H bond (Figure 20). Carboxylate ligands excel at this cooperative transformation and have been

[75] a) Lapointe, D.; Fagnou, K. *Chem. Lett.* **2010**, *39*, 1118; b) Davies, D. L.; Donald, S. M. A.; Macgregor, S. A. *J. Am. Chem. Soc.* **2005**, *127*, 13754; c) Davies, D. L.; Donald, S. M. A.; Al-Duaij, O.; Macgregor, S. A.; Pölleth, M. *J. Am. Chem. Soc.* **2006**, *128*, 4210.

[76] Boutadla, Y.; Davies, D. L.; Macgregor, S. A.; Poblador-Bahamonde, A. L. *Dalton Trans.* **2009**, 5820.

extensively used in C−H activation strategies,[77] as the change in the coordination mode to κ^1-O generates a vacant site adjacent to the base, which permits, upon formation of an agostic complex, to carry out the C−H activation through a six-membered transition state (AMLA-6).

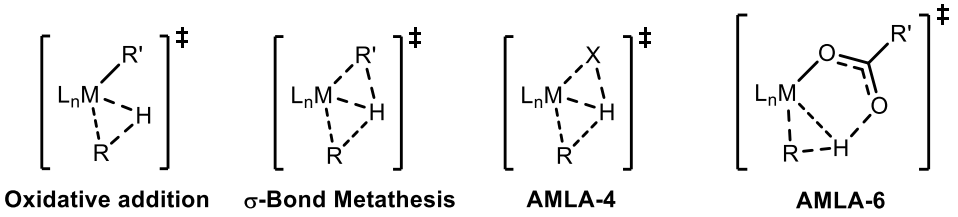

Figure 20. R−H bond activation mechanisms (R = H, hydrocarbyl, boryl; X = heteroatom with lone pairs).

AMLA-4 processes have also been defined and studied and we therefore evaluated if a concerted metalation deprotonation (CMD) event could take place at **2(Xyl)**$^+$. As previously mentioned, a monocationic agostic complex derived from **2(Xyl)**$^+$ could not be located as a minimum, making the search for the transition state associated to this process not trivial. First, we examined the relaxed potential energy scan for the elongation of the Ir−Cl bond and chose the geometry that presented an Ir−Cl bond distance of 3.01 Å, 0.58 Å shorter than that found for the transition state associated with Cl^- release. Then we carried out a second scan, shortening the distance between the Ir and the benzylic carbon atoms while keeping the Ir−Cl froze at 3.01 Å. This provided a reasonable starting geometry to launch a TS search, in which the Ir−Cl bond length was kept at 3.01 Å. Two imaginary frequencies, of −1051 and −53 cm^{-1}, were associated to the resulting geometry, the one with the greater absolute value corresponding to the sought transformation. Constraint-free TS search, starting from this

[77] Davies, D. L.; Macgregor, S. A.; McMullin, C. *Chem. Rev.* **2017**, *117*, 8649.

geometry, provided a true TS for the CMD process, which was found to be exceedingly high in energy, 35.1 kcal/mol above **2(Xyl)**$^+$ (Figures 21 and 22).

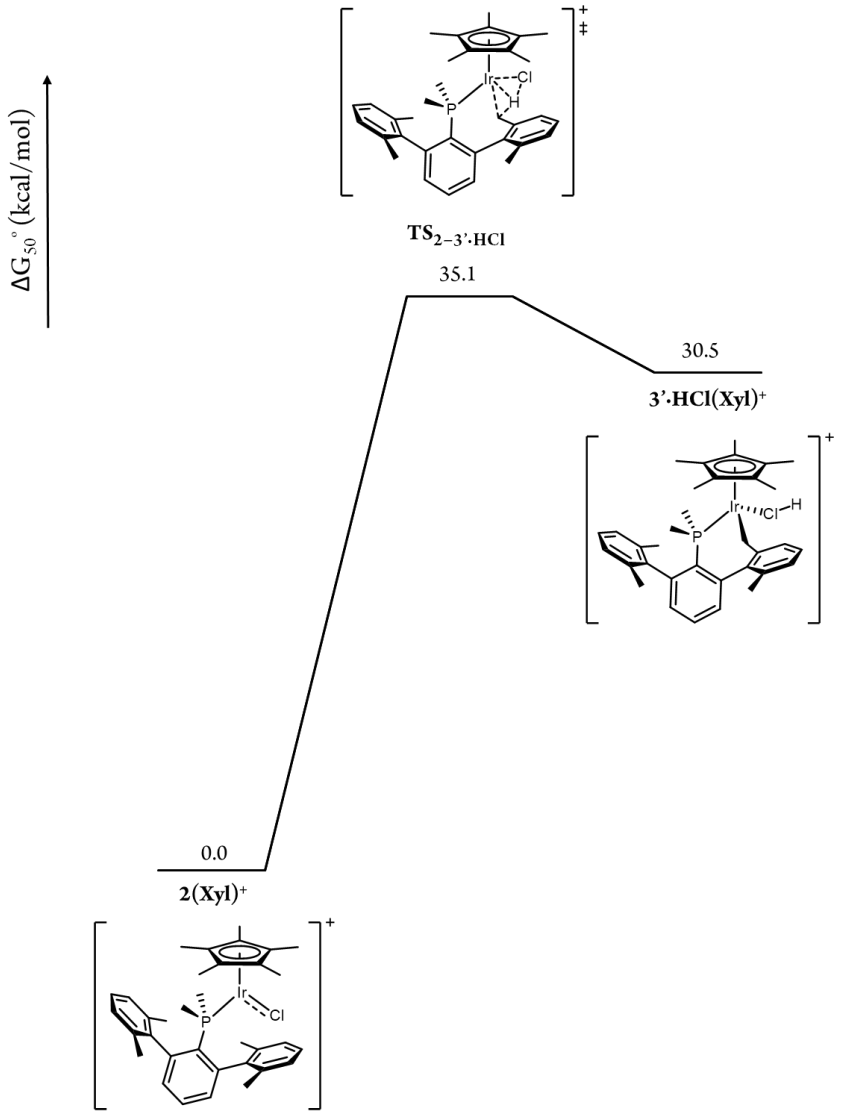

Figure 21. ΔG_{50}° profile for the concerted conversion of **2(Xyl)**$^+$ into **3'·HCl(Xyl)**$^+$.

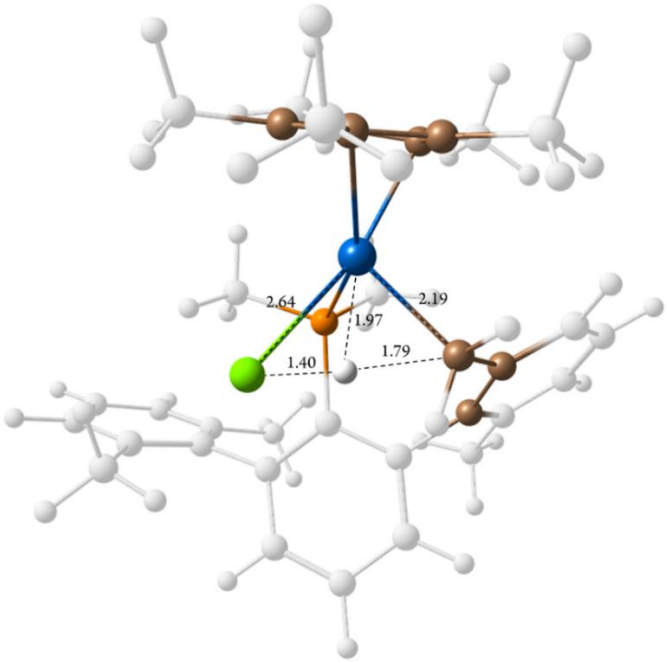

Figure 22. Molecular geometry of the AMLA-4/CMD transition state at **2(Xyl)**$^+$ (**TS 2−3'·HCl**$_{Xyl}$).

Yet a further alternative, a pericyclic-like mechanism for the conversion of **2(Xyl)**$^+$ into **3(Xyl)**$^+$ could be envisioned (Figure 23). Despite many attempts, transition states associated to this type of process could not be located; relaxed potential energy scans suggest that this pathway is not likely to be feasible, as the process entails a barrier of *ca*. 50 kcal/mol.

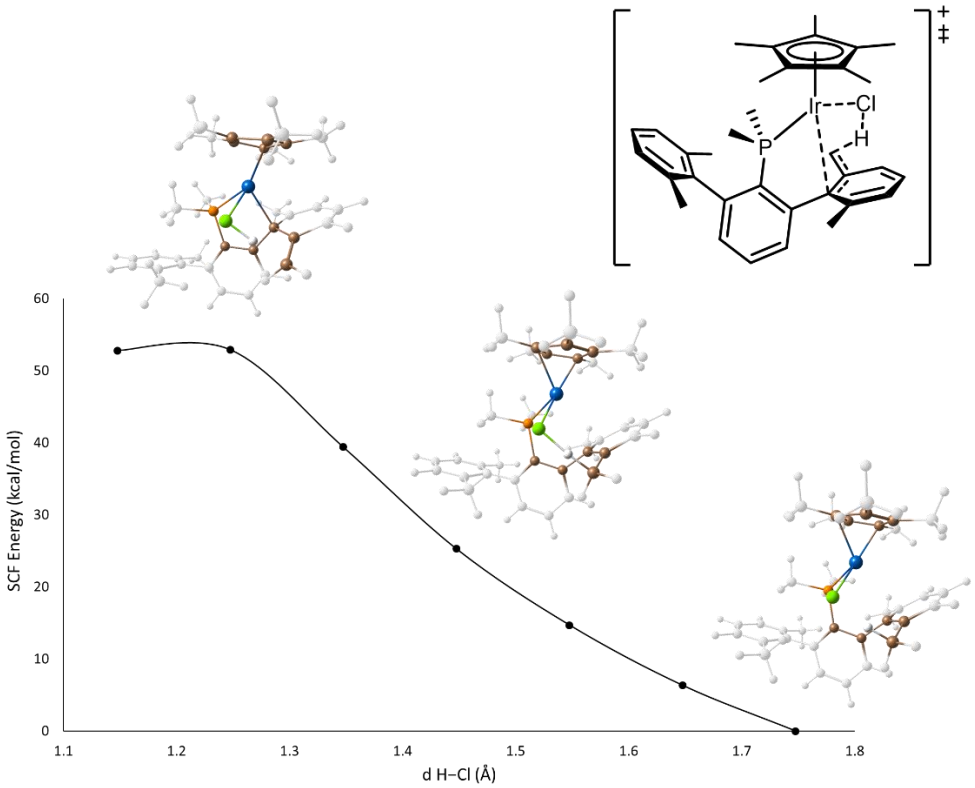

Figure 23. Hypothetical pericyclic-like TS for the conversion of **2(Xyl)**$^{+}$ into **3(Xyl)**$^{+}$ and relaxed energy scan of the H−Cl distance in complex **2(Xyl)**$^{+}$.

I.2.3 Base-Promoted, C_5Me_5-Mediated C−H and C−C Bond Formation

As the formation of cationic pseudoallyls, **3(PMe$_2$Ar')$^+$**, from the corresponding chlorides, **2(PMe$_2$Ar')$^+$**, implies electrophilic C−H activation and elimination of HCl, we considered it of interest to study the use of an external Brönsted base such as NEt_3 to facilitate HCl elimination. In stark contrast with the slow reaction of **2(Dipp)$^+$** with $NaBAr_F$, which could be qualitatively followed by the slow fading of the dark coloration, the addition of a slight excess of NEt_3 to solutions of **2(Dipp)$^+$** immediately turned the solution orange; **3(Dipp)$^+$** formed quantitatively as shown by ^{1}H NMR after stirring at room temperature for about 24 hours. Interestingly, examination of the reaction mixture by NMR revealed the formation of an intermediate, **4(Dipp)$^+$ (Scheme**, responsible for a $^{31}P\{^1H\}$ singlet resonance at −4.4 ppm, clearly distinguishable from those of **2(Dipp)$^+$** and **3(Dipp)$^+$** at 6.6 and 9.8 ppm, respectively. Optimization of the reaction temperature and time by NMR showed that intermediate **4(Dipp)$^+$** was formed as the only observable product when **2(Dipp)$^+$** and NEt_3 were allowed to react at −20 ºC for 2 hours.

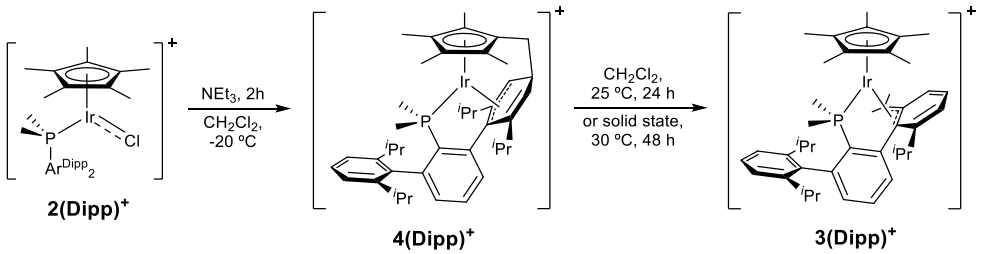

Scheme 18. NEt_3 assisted formation of complex **4(Dipp)$^+$** from **2(Dipp)$^+$**, and solution and solid-state isomerization of **4(Dipp)$^+$** to **3(Dipp)$^+$**.

Variable temperature multinuclear NMR and X-Ray studies provided unequivocal evidence of the remarkable chemical and structural changes

that occur *en route* to **3(Dipp)**$^+$. Although **3(Dipp)**$^+$ and **4(Dipp)**$^+$ are isomers, the latter exhibits very different atom connectivity, for it contains a 10-membered metallacyclic unit resulting from deprotonation of the C_5Me_5 ring,[52] followed by nucleophilic attack[52b,d] at the *para* carbon atom of the coordinated Dipp ring, which becomes dearomatized.[48,51] In solution, two degenerate pseudoallylic structures undergo fast exchange at room temperature, but reach the slow-exchange regime at −30 ºC (Scheme 19, Figure 24). Line shape analysis gave $\Delta G^{\ddagger}$ = 12.9 kcal/mol.

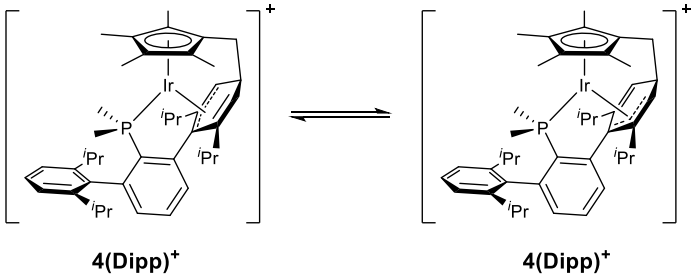

Scheme 19. Exchange of the allyl and alkene positions in **4(Dipp)**$^+$.

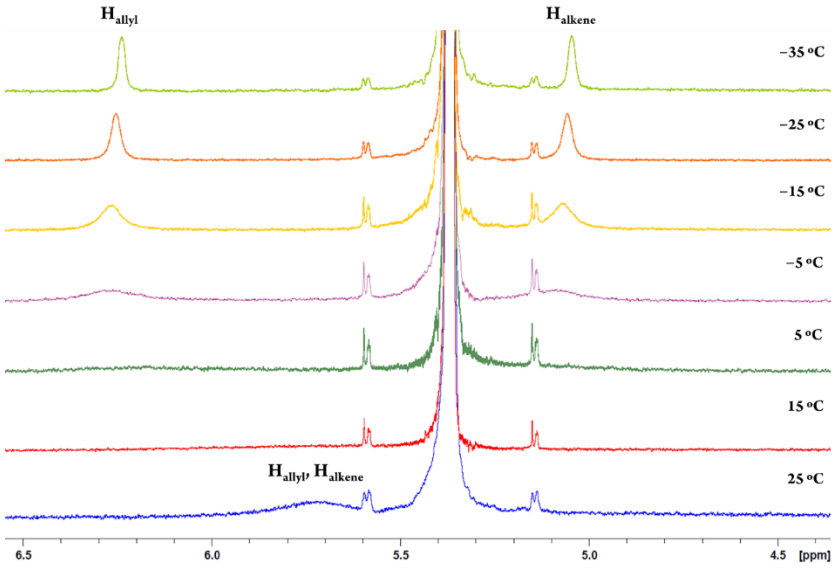

Figure 24. Solution dynamic behaviour of **4(Dipp)**$^+$ analyzed by variable temperature ^{1}H NMR.

Although initial NMR studies were carried out in CD_2Cl_2, the limited solubility of **4(Dipp)**$^+$ in this solvent at low temperature precluded full characterization. The complex displayed increased solubility in acetone-d^6, but it was countered by a worse dispersion pattern of the ^{1}H NMR resonances that impeded full assignment. These inconveniences were overcome employing THF-d_8 at −30 ºC.

The absence of a doublet attributable to the 15 H atoms of the C_5Me_5 ligand in the phosphine complex suggests that free rotation of the cyclopentadienyl terminus is hampered in **4(Dipp)**$^+$. At −30 ºC, singlets at 2.58, 2.03, 1.88 and 1.47 ppm are assigned to the $C_5\mathit{Me}_4$ protons whereas the diastereotopic $C_5Me_4C\mathit{H}_2$ protons resonate as doublets of doublets centered at 3.27 and 2.46 ppm, as a consequence of additional coupling to the adjacent $C\mathit{H}CH_2$ proton (former *p*-Dipp), which was detected at 3.56 ppm. The dearomatization of a flanking aryl ring of the phosphine ligand was also made evident by two exchanging broad singlets at 6.61 and 5.14 ppm, that corresponded to the allylic and alkene protons, respectively, and coalesced into a broad hump around 5.9 ppm at 25 ºC. Only 6 out of the 9 original aromatic protons remained in the corresponding region. Regarding the $^{13}C\{^1H\}$ spectrum, whereas the $C_5\mathit{Me}_4$ nuclei were found in the 8-12 ppm region, the $C_5Me_4\mathit{C}H_2$ atom resonated at 23.6 ppm. The signal corresponding to the $\mathit{C}HCH_2$ atom was detected at 63.1 ppm, whereas the allylic and alkenic $\mathit{C}H$ atoms were found at 86.3 and 116.6 ppm, respectively.

The X-ray structure shown in Figure 25 revealed that beyond the η^5 coordination of the $C_5Me_4C\mathit{H}_2$ moiety, the now activated phosphine ligand binds to iridium through the phosphorus atom (d(Ir−P) = 2.281(1) Å) and three adjacent carbon atoms of the dearomatized ring. The resulting

pseudoallylic structure is characterized by Ir−C bond distances of 2.166(4) (to C_{ipso}), 2.178(4) (C_{ortho}) and 2.255(5) Å (C_{meta}). The newly formed C−C bond has a length of 1.560(6) Å, while the dearomatization of the ring becomes also evident from the *ca*. 38º dihedral angle formed by the C_{meta}−C_{ortho}−C_{ipso} and C_{ortho}−C_{ipso}−C_{ortho} planes.

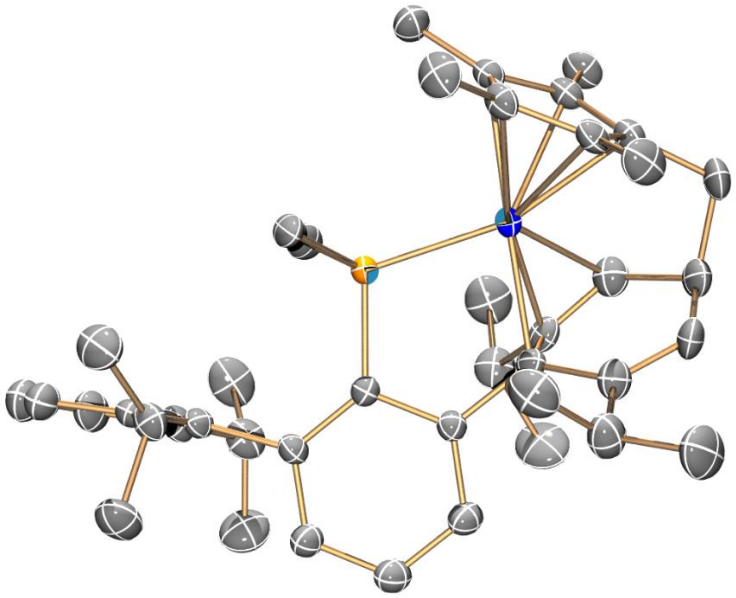

Figure 25. ORTEP diagram of the cation of complex **4(Dipp)**$^+$. Hydrogen atoms are excluded for clarity and thermal ellipsoids are set at 50 % probability.

The orange intermediate **4(Dipp)**$^+$ converted cleanly into the yellow pseudoallyl product **3(Dipp)**$^+$ after circa 24 hours of stirring at room temperature (Scheme 18). The isomerization required neither base (NEt_3) nor acid ($HNEt_3^+$) catalysis, since pure, isolated samples of **[4(Dipp)]BAr$_F$** transformed neatly in CH_2Cl_2 solutions into complex **3(Dipp)**$^+$. In addition, it was most notable to find that the **4(Dipp)**$^+$-to-**3(Dipp)**$^+$ isomerization, which implies C−C bond cleavage and C−H bond cleavage and formation, occurred also easily in the solid state after requiring 2 days at 30 ºC for

completion.[78] The isomerization in solution was monitored by $^{31}P\{^{1}H\}$ NMR spectroscopy at 25 ºC and showed a first order dependence on the concentration of **4(Dipp)**$^{+}$ (Figure 26), resulting in a first order rate, k = $3.1 \cdot 10^{-5}$, which corresponds to a half-life of *ca*. 6 h and $\Delta G^{\ddagger}_{298}$ of 23.6 kcal/mol. No observable intermediates were detected.

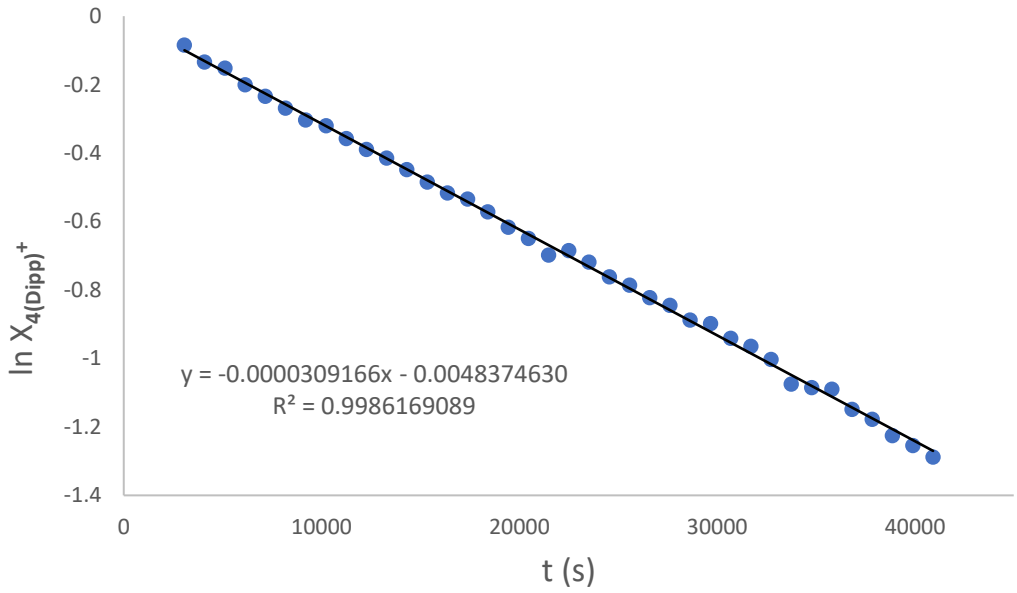

Figure 26. Plot of the natural logarithm of the molar fraction of **4(Dipp)**$^{+}$ against time.

[78] a) Pike, S. D.; Weller, A. S. *Phil. Trans. R. Soc. A* **2015**, *373*, 20140187; b) Pike, S. D.; Chadwick, F. M.; Rees, N. H.; Scott, M. P.; Weller, A. S.; Krämer, T.; Macgregor, S. A. *J. Am. Chem. Soc.* **2015**, *137*, 820; c) Pike, S. D.; Thompson, A. L.; Algarra, A. G.; Apperley, D. C.; Macgregor, S. A.; Weller, A. S. *Science* **2012**, *337*, 1648; d) Chaplin, A. B.; Green, J. C.; Weller, A. S. *J. Am. Chem. Soc.* **2011**, *133*, 13162; e) Huang, Z.; White, P. S.; Brookhart, M. *Nature* **2010**, *465*, 598; f) Bianchini, C.; Farnetti, E.; Graziani, M.; Kaspar, J.; Vizza, F. *J. Am. Chem. Soc.* **1993**, *115*, 1753.

I.2.3.1 Computational Investigation of the Rearrangement of 2(Dipp)$^+$ into 4(Dipp)$^+$ and 3(Dipp)$^+$.

The conversion of **2(Dipp)**$^+$ into **3(Dipp)**$^+$ through **4(Dipp)**$^+$ was also studied computationally. The following section contains our findings on these studies, whereas the corresponding reactivity of **2(Xyl)**$^+$ will be discussed in a separate section.

As represented in the simplified, free energy profile for the overall process depicted in Figure 27, the amine-mediated C_5Me_5 deprotonation of complex **2(Dipp)**$^+$ (17.4 kcal·mol^{-1}, **TS$_{2-A}$**) may lead to the formation of a neutral, Ir(I) fulvene complex (9.2 kcal·mol^{-1}, **A**). The generated triethylammonium cation provides further assistance in the chloride releasing step (20.2 kcal·mol^{-1}, **TS$_{A-B}$**) to yield complex **B** (1.0 kcal·mol^{-1}). **B** is a cationic fulvene complex for which metal unsaturation is compensated by means of a π-arene interaction with one of the flanking aryl rings of the phosphine, and presents an appropriate geometry to undergo C−C bond formation via **TS$_{B-4}$** at 17.7 kcal/mol. We propose that this ring dearomatization step proceeds with concomitant metal re-oxidation to give Ir(III) complex **4(Dipp)**$^+$ at −2.1 kcal/mol. Isomerization of **4(Dipp)**$^+$ to **3(Dipp)**$^+$ involves the reversible formation of Ir(I) complex **B** via **TS$_{B-4}$**. Then, attack of the fulvene moiety in **B** to the C−H of one *iso*-propyl group of the proximate aryl ring (19.4 kcal/mol, **TS$_{B-C}$**) re-oxidizes the metal center to Ir(III) and gives the η^1-allyl complex **C** at 7.6 kcal/mol. Isomerization to the corresponding η^3-allyl occurs via **TS$_{C-3}$** (18.9 kcal/mol) yielding **3(Dipp)**$^+$ at −11.5 kcal/mol.

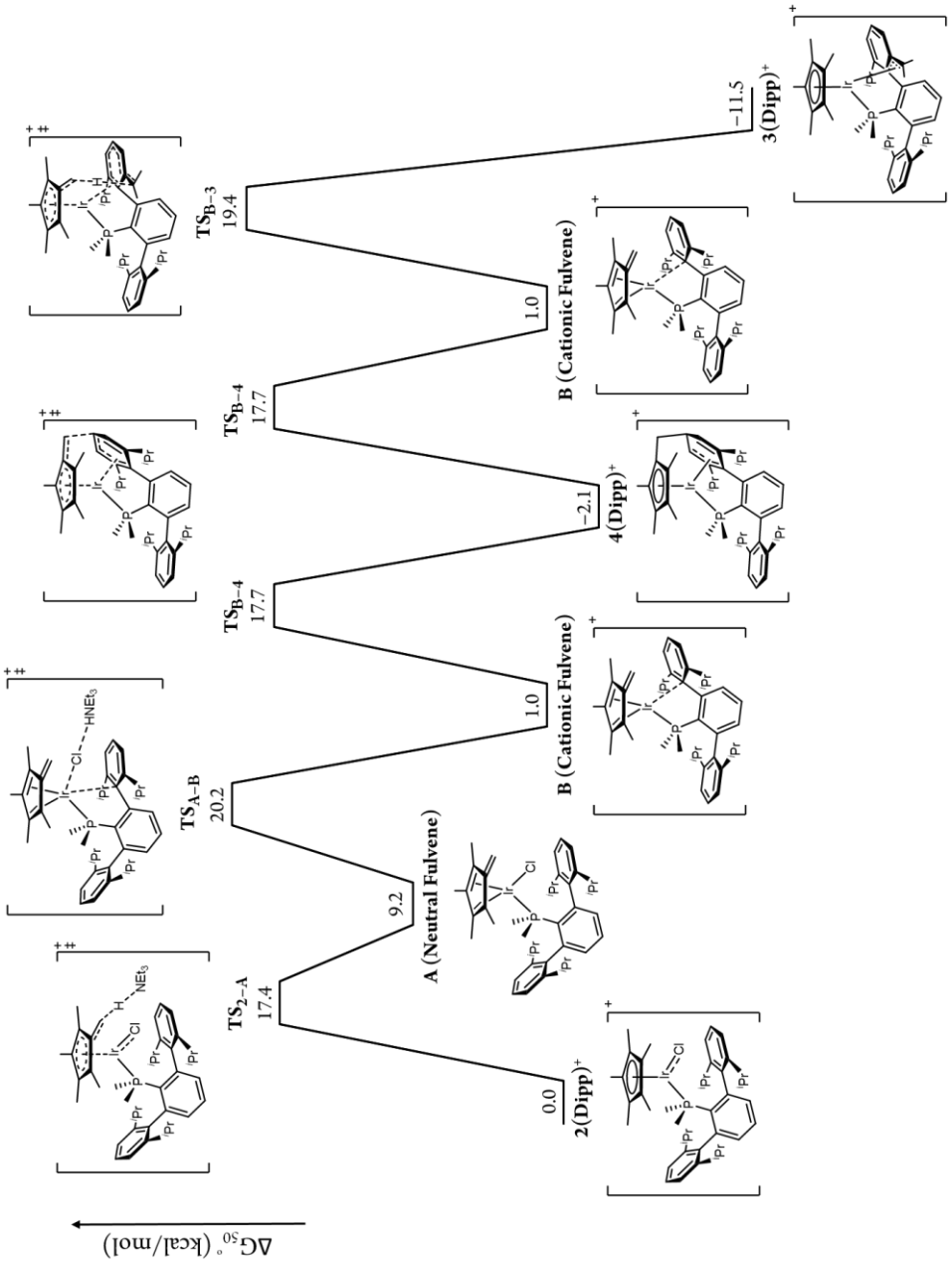

Figure 27. ΔG_{50}° profile for the conversion of **2(Dipp)**$^{+}$ into **3(Dipp)**$^{+}$ through **4(Dipp)**$^{+}$.

A step-by-step, detailed analysis is obliged to fully comprehend these complex, unusual transformations. As mentioned in the introduction, C_5Me_5 ring methyl activation implying either deprotonation[52] or hydride abstraction,[53] as well as metal-to-ring hydride transfer,[54] are well documented reactions. C_5Me_5 deprotonation is normally carried out using strong bases,[79] so that the acid-base reaction becomes the driving force compensating the loss of aromaticity of the cyclopentadienyl ring. However, functionalization of the C_5Me_5 ligand, including hydrogen isotope exchange as the simplest example, can be achieved under mild conditions.[52d,e] The relatively fast (2 h) reaction of **2(Dipp)**$^+$ at −20 ºC with NEt_3 suggest a certain degree of acidity of the ring methyl protons.[80] Although the cationic character of the complex is expected to increase the acidity of the aforementioned protons, the thermodynamic driving force for the deprotonation is, with no doubt, the formation of **4(Dipp)**$^+$ (Figure 28). Nevertheless, to some extent kinetic facilitation could be derived from the stability of the conjugated base of **2(Dipp)**$^+$, which is a 16-electron, square-planar Ir(I) fulvene complex (**A**). For endergonic reactions of this kind, it is reasonable to expect that enhanced stability of the product be accompanied by a certain kinetic facilitation (Figure 29).

[79] a) Miguel-Garcia, J. A.; Maitlis, P. M. *J. Chem. Soc., Chem. Commun.* **1990**, 1472; b) Gusev, O. V.; Rubezhov, A. Z.; Miguel-Garcia, J. A.; Maitlis, P. M. *Mendeleev Commun.* **1991**, *1*, 21.
[80] a) Kang, J. W.; Maitlis, P. M. *J. Organomet. Chem.*, **1971**, *30*, 127; b) Nutton, A.; Maitlis, P. M. *J. Chem. Soc., Dalton Trans.* **1981**, 2335.

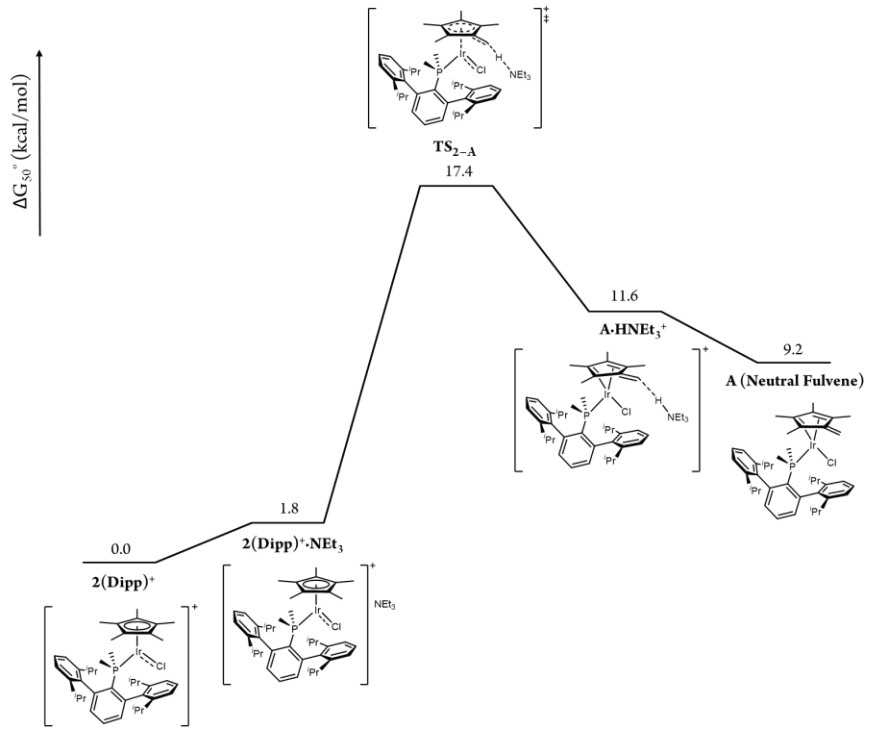

Figure 28. ΔG_{50}° profile for the deprotonation of **2(Dipp)**$^{+}$ to yield the neutral fulvene complex **A**.

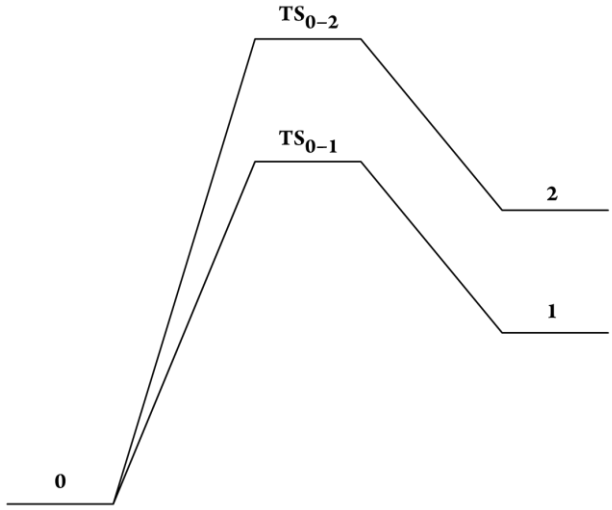

Figure 29. General profile for model endergonic reactions, for which transition states are energetically closer to products.

The geometry of **TS2–A** is depicted in Figure 30. Similar energies were obtained for upper-side amine attacks.

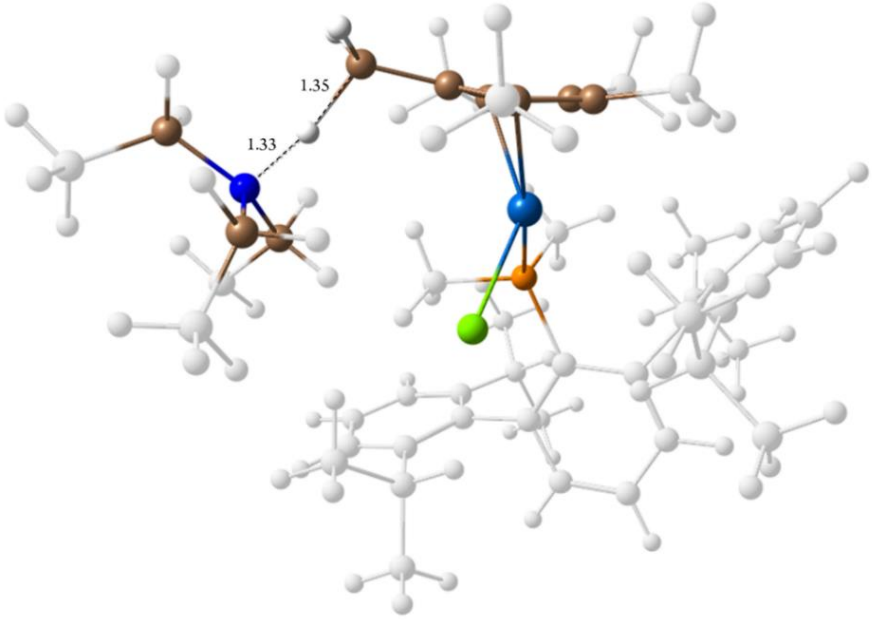

Figure 30. Molecular geometry of the transition state for the deprotonation of the C_5Me_5 (**TS2–A**).

I.2.3.2 Localized Molecular Orbital (LMO) Analysis.

Over the years, many approaches have been devised to serve as a bridge between chemical intuition and molecular wave functions. Among them, Population Analysis,[81] Molecular Orbital Analysis[82] and Bader´s theory of atoms in molecules[83] have become very popular and are widely used. Molecular Orbital Localization is another powerful tool to visualize, interpret and rationalize the results of electronic structure calculations that, despite dating back to the work of Boys in the sixties,[84] has been scarcely used by the organometallic community.[85] Molecular orbitals are spread over the molecule, making it difficult to extract valuable information upon visual inspection (Figure 31, left). Upon localization, molecular orbitals "reconcile" with the intuitive Valence Bond Theory, exposing valuable information regarding bonding, connectivity and oxidation states (Figure 31, center). Determining the mass center (centroid) of localized molecular orbitals (LMOs) further facilitates the interpretation of the electronic structure (Figure 31, right).

[81] a) Mulliken, R. S. *J. Chem. Phys.* **1955**, *23*, 1833; b) Mayer, I. *Chem. Phys. Lett.* **1983**, *97*, 270; c) Lowdin, P. O. *Phys. Rev.* **1955**, *97*, 1474.
[82] Reed, A. E.; Curtiss, L. A.; Weinhold, F. *Chem. Rev.* **1988**, *88*, 899.
[83] Bader, R. F. W. *Atoms in Molecules: A Quantum Theory*, Oxford University Press, Oxford, **1995**.
[84] a) Boys, S. F. *Rev. Mod. Phys.* **1960**, *32*, 296; b) Foster, J. M.; Boys, S. F. *Rev. Mod. Phys.* **1960**, *32*, 300.
[85] Vidossich, P.; Lledós, A. *Dalton Trans.* **2014**, *43*, 11145.

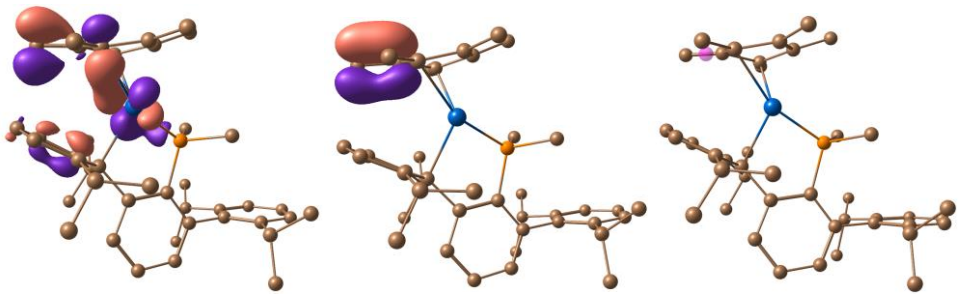

Figure 31. Left: molecular orbital delocalized over the fulvene moiety, the metal center and a Dipp ring. Center: Localized molecular orbital corresponding to the fulvene π-bond. Right: Mass center of the LMO belonging to the fulvene.

Following the evolution of relevant Valence Bond-like localized orbitals (or their centroids) along the Intrinsic Reaction Coordinate (IRC) from the transition states sheds light on the electronic rearrangements along the reaction pathway. Thus, if we are looking at occupied orbitals in a closed-shell system, the movement of the centroids resembles the motion of couples of electrons. This analysis allows a description of elemental steps of chemical reactions in terms of the arrow pushing or curved arrow formalism, first introduced by Robinson[86] and extensively used in organic chemistry ever since.

[86] Kermack, W. O.; Robinson, R. *J. Chem. Soc., Trans.* **1922**, *121*, 427.

I.2.3.3 C_5Me_5 Deprotonation

To gain deeper understanding of the complex base-promoted transformation of **2(Dipp)**$^+$ into **3(Dipp)**$^+$, we carried out localized molecular orbital studies along the IRCs of the processes that implied a change in the oxidation state of the metal center. Thus, as already mentioned, the attack of the lone-pair of the amine to the C_5Me_5 unit (**TS$_{2-A}$**) is accompanied by the formation of a π bond corresponding to the fulvene moiety (Figure 32) and it is concomitant with (formal) reduction to Ir(I).

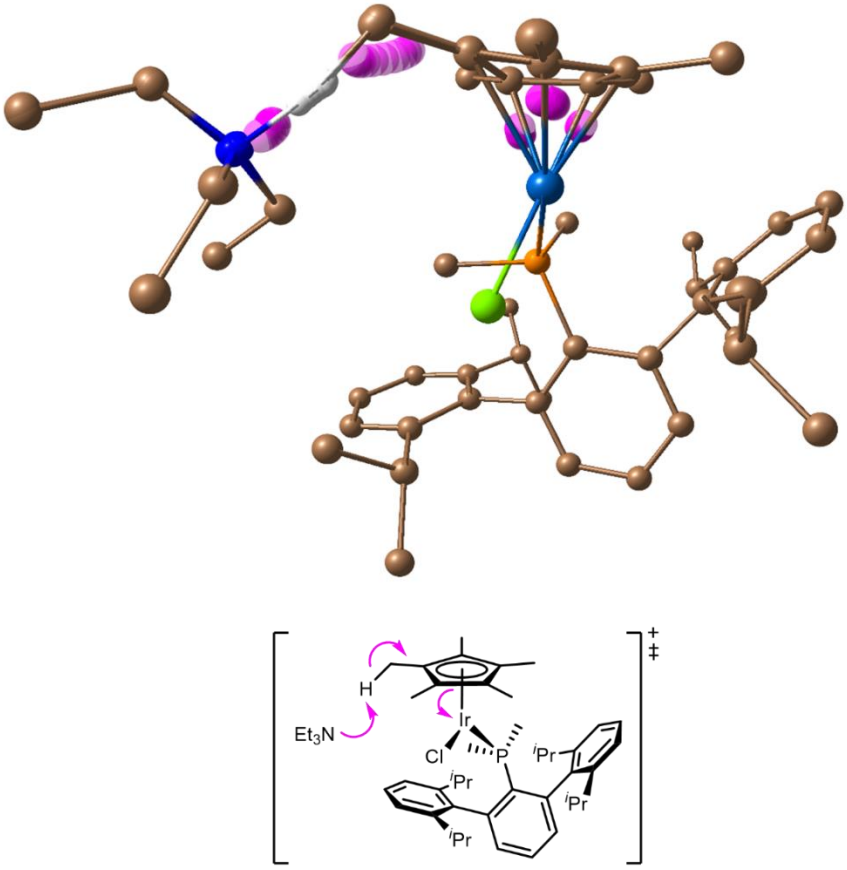

Figure 32. Localized molecular orbital study of the intrinsic reaction coordinate (IRC) of **TS$_{2-A}$**. Non-participating H atoms were omitted for

clarity. Curved arrows show the rearrangements of pair of electrons along the reaction pathway.

However, significant reduction to Ir(I) is not as apparent as in other examples discussed in following sections (*vide* Figures 39 and 45). This is based on the variation of the distances between the Ir atom and the centroids of the orbitals of the Ir-C_5Me_5 linkage along with C_5Me_5 deprotonation. The sinking of one of the centroids into the Ir atom, as the bonding orbital evolves into a metal-localized one, would be indicative of a 2-electron metal reduction. We hypothetically considered that the ionic interaction displayed in intermediate **A·HNEt$_3$** could favor a carbanionic, Ir(III) resonant form (Figure 33, right) tested this hypothesis by means of molecular orbital localization at intermediates **A·HNEt$_3$** and **A** (Figure 34). Although the sum of the three Ir-centroid distances was smaller for complex **A** in accordance with a greater Ir(I)-like character, the difference was too small (3.77 (**A**) vs 3.81 (**A·HNEt$_3$**), Å) to be visually telling, and possibly to be significant.

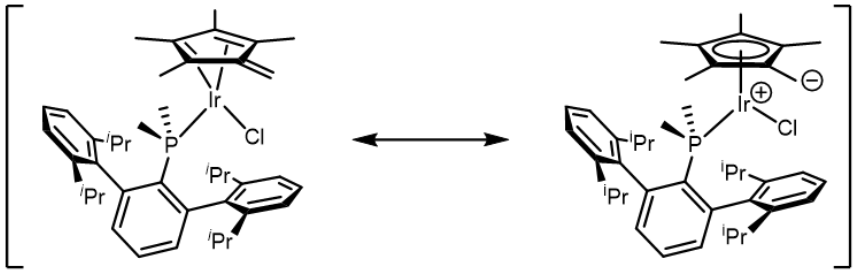

Figura 33. Ir(I) and Ir(III) resonant forms of the calculated intermediate **A**.

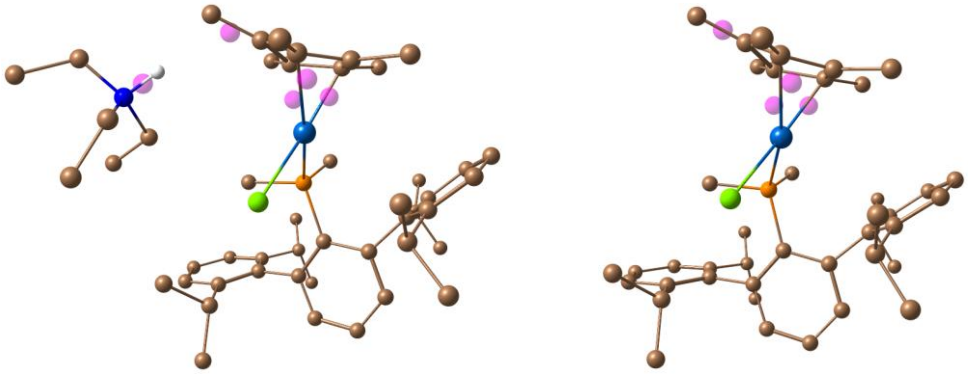

A·HNEt3 **A**

Figure 34. Centroids of relevant localized molecular orbitals for intermediates **A·HNEt$_3$** and **A**.

I.2.3.4 C–C Bond Formation

Calculations support that C_5Me_5 deprotonation, *en route* to complex **4(Dipp)**$^+$, takes place before chloride release (**TS2-SDipp** is higher in energy than **TS2–A**). The second stage of the proposed mechanism for the formation of **3(Dipp)**$^+$ *via* **4(Dipp)**$^+$ involves C−C bond formation between the *C*H_2 of the fulvene and the para carbon of a Dipp ring. This step may take place from neutral, **A**, or cationic, **B**, fulvenes, which can be connected by chloride elimination thanks to the assistance of the generated ammonium, $HNEt_3^+$. The vacant coordination site at the metal center is then filled by a π-arene interaction (see figure 35). Since comparable ΔG_{50} barriers have been found for the C−C bond formation reaction taking place at either intermediate **A** or **B** ($\Delta G_{50}^{\ddagger}$ = 20.2 kcal/mol for **A**, 20.4 kcal/mol for **B**, Figures 36 and 40), both pathways are discussed in forthcoming sections.

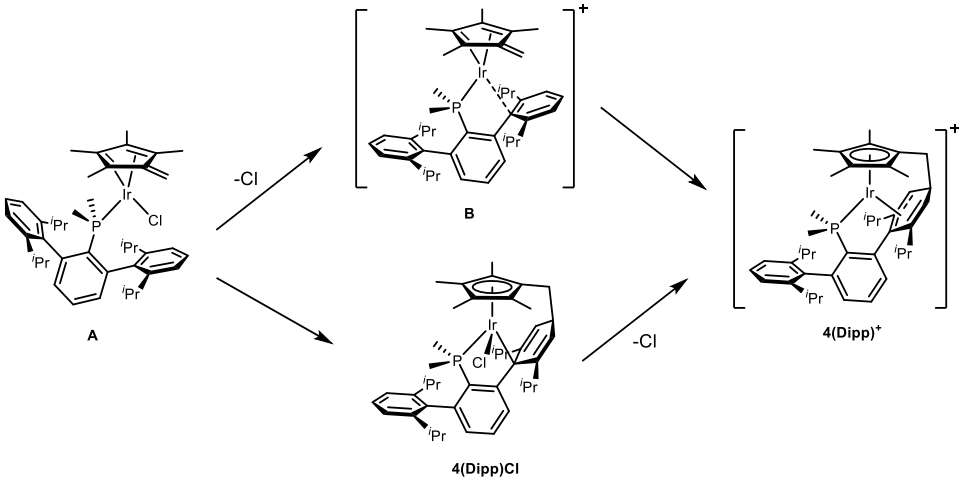

Figure 35. Possible C−C bond formation pathways from intermediate **A**: through the cationic fulvene **B** (top) or the neutral complex **4(Dipp)Cl** (bottom).

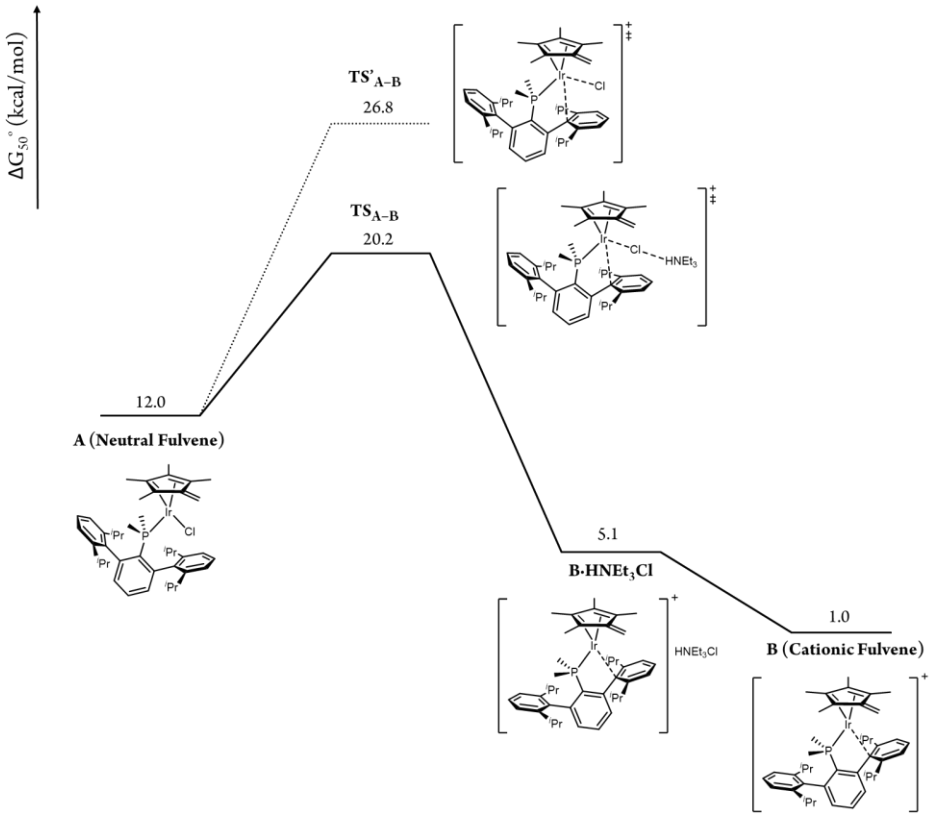

Figure 36. ΔG_{50}° profile for the chloride release at intermediate **A** to yield the cationic fulvene complex **B**. The relative energy of the transition state for unassisted chloride release is also shown.

I.2.3.5 C−C Bond Formation at the Cationic Fulvene Complex B

Conformational analysis revealed that the energy barrier associated with C−C bond formation at complex **B** is to some extent dependent on the orientation of the ^{i}Pr groups of the corresponding Dipp ring. A detailed energy profile including the conformational rearrangements taking place prior to the C−C coupling step is depicted in Figure 37.

$TS_{B\text{-}B'}$ (9.4 kcal/mol) gives **B'** at 2.8 kcal/mol after the rotation of one of the ^{i}Pr groups of **B**. As a transition state connecting intermediates **B'** and **B''** (10.1 kcal/mol) could not be found, the 10.5 kcal/mol barrier proposed for the rotation of the fulvene was estimated by means of relaxed energy scans. C−C bond formation (see Figure 38) takes place through **TS_{B-4}** (17.7 kcal/mol), yielding the formally 16-electron complex **4'** at 8.3 kcal/mol, for which its metalated cyclohexadiene unit displays a boat-like conformation. Isomerization to the 18e, η^3 pseudoallyl complex **4''** (9.3 kcal/mol) occurs via **$TS_{4'\text{-}4''}$** at 14.3 kcal/mol. Stepwise rotation of the allylic and alkenic *iso*-propyl groups give **4(Dipp)$^{+}$** through **$TS_{4''\text{-}4'''}$** and **$TS_{4'''\text{-}4}$** at 12.0 and 1.0 kcal/mol, respectively.

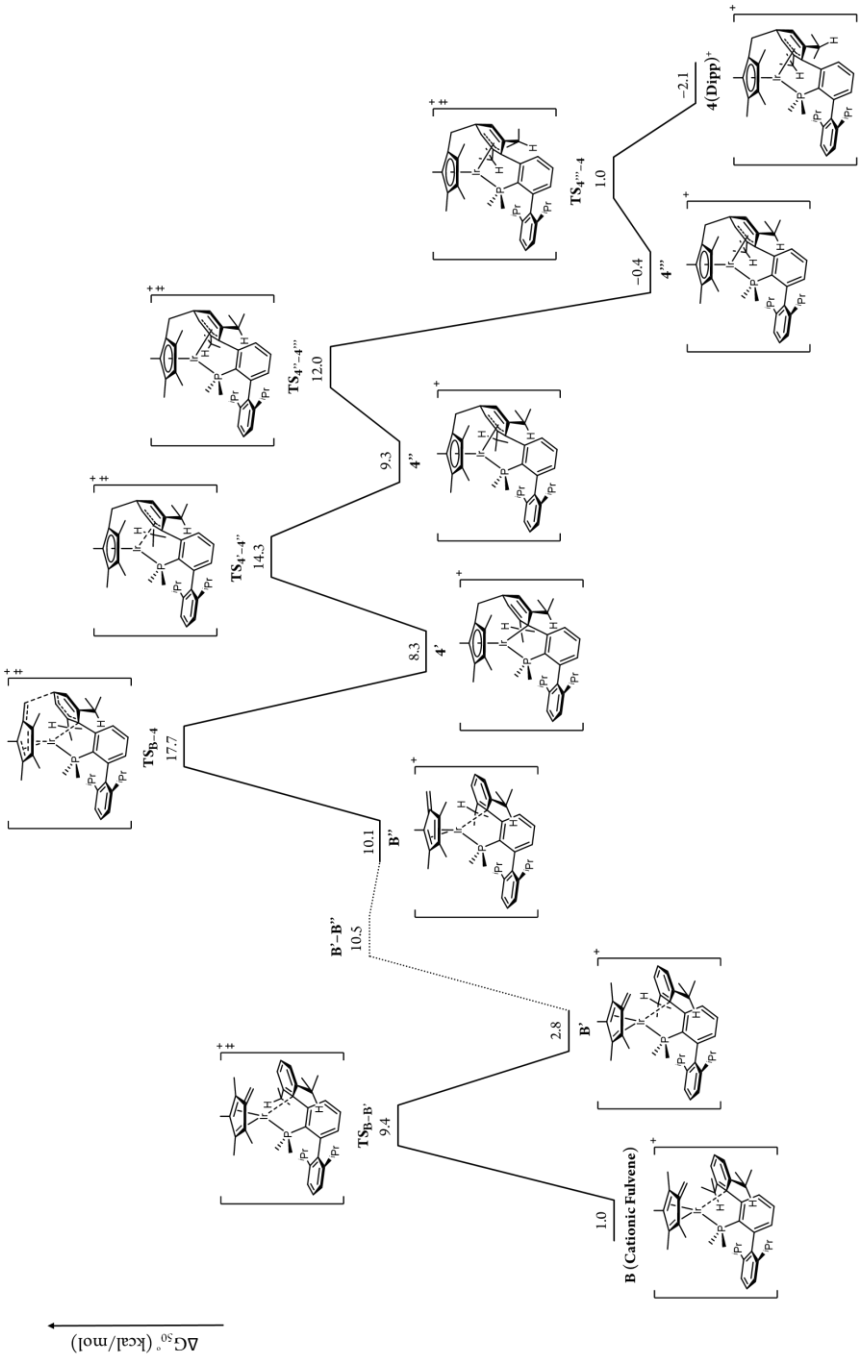

Figure 37. ΔG_{50}° profile for the lowest-energy pathway connecting complexes **B** and **4(Dipp)**$^+$.

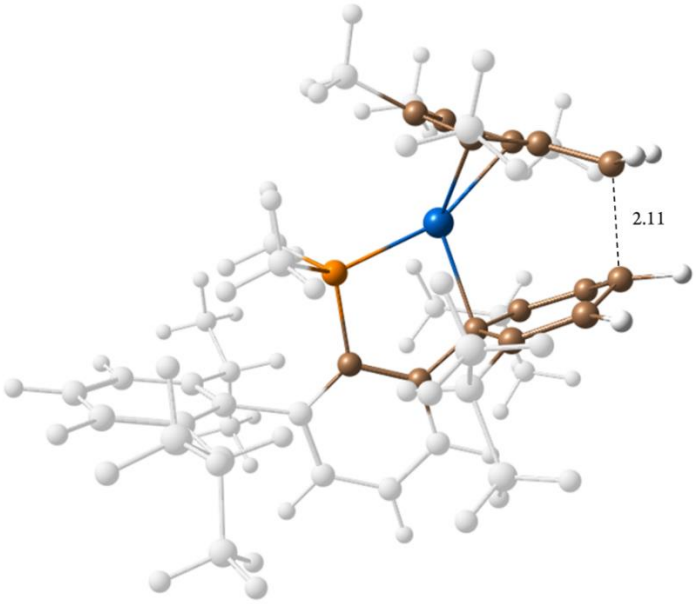

Figure 38. Molecular geometry of the transition state for the formation of the C−C bond at **B**, which is concomitant with ring dearomatization (**TS$_{B-4}$**).

The LMO study performed for the C−C coupling at complex **B** (Figure 39) permits an in-depth analysis of this elemental step. Nucleophilic attack of the fulvene moiety to the *para* carbon atom of the coordinated Dipp ring is concomitant with ring dearomatization and metal oxidation. Accordingly, the π LMO of the C=CH$_2$ unit of the fulvene evolves into a σ *C*H$_2$−*C*H bonding orbital implicating the Dipp ring *para* carbon atom, while a metal-centered LMO progresses to participate in the bonding with the cyclopentadienyl ligand. At the same time, one of the π LMOs of the Dipp ring transforms into a new covalent σ Ir-C bond. The remaining π electrons of the Dipp ring also rearrange as expected for the concomitant dearomatization.

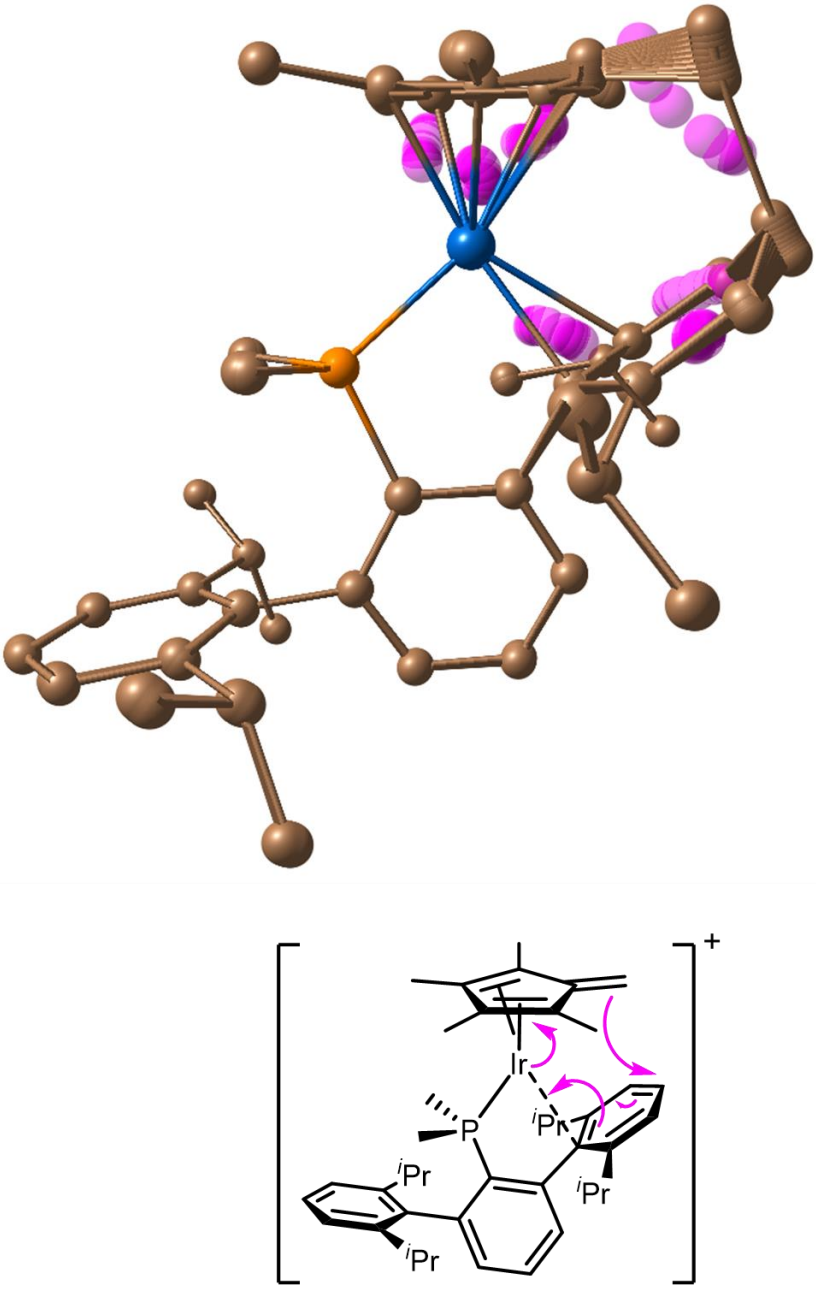

Figure 39. Localized molecular orbital study of the intrinsic reaction coordinate (IRC) of **TS$_{B-4}$**. H atoms were omitted for clarity.

I.2.3.6 C−C Bond Formation at the Neutral Fulvene Complex A

The C−C bond formation event could also occur at the neutral fulvene **A** (Figure 40). **$TS_{A-4DippCl}$** (20.4 kcal/mol, Figure 41), involves a similar electronic rearrangement to give the neutral Ir(III) complex **4DippCl** at 4.3 kcal/mol. Chloride release (**$TS_{4DippCl-4Dipp+}$**, 19.1 kcal/mol) gives a cationic η^1-allyl specie alike **4'** (Figure 37), which easily rearranges to the η^3-allyl, **4(Dipp)$^+$**.

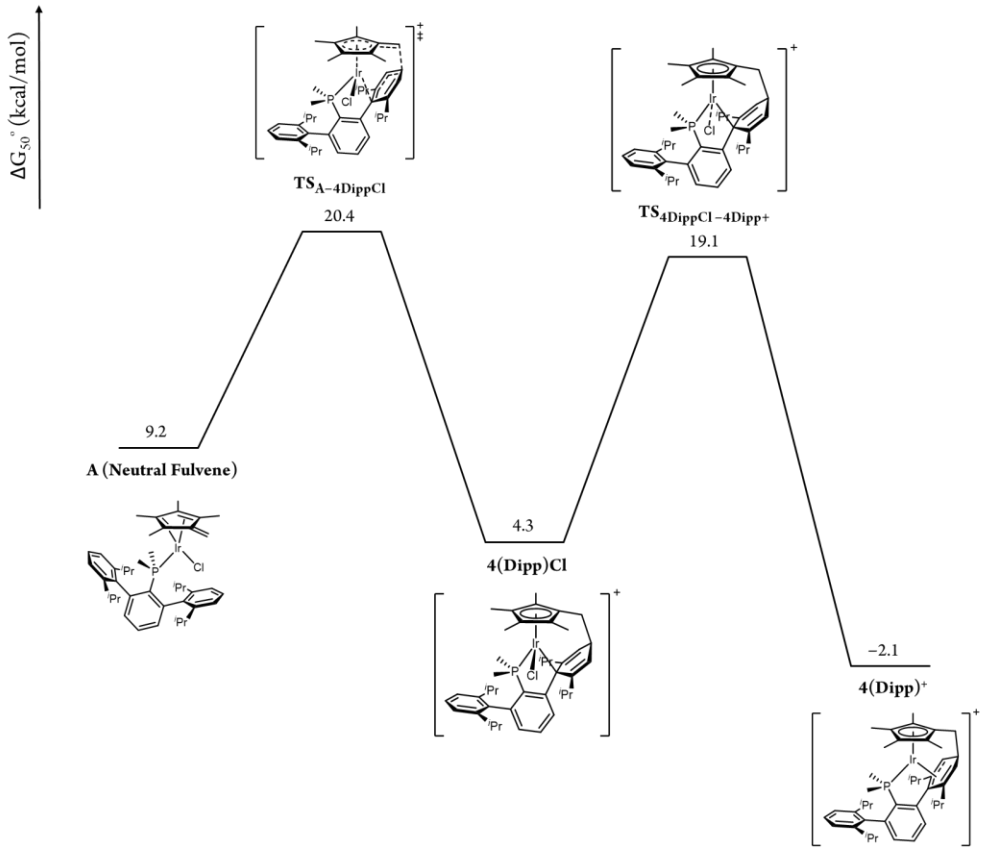

Figure 40. ΔG_{50}° profile for the C−C bond formation taking place at the neutral fulvene **A**.

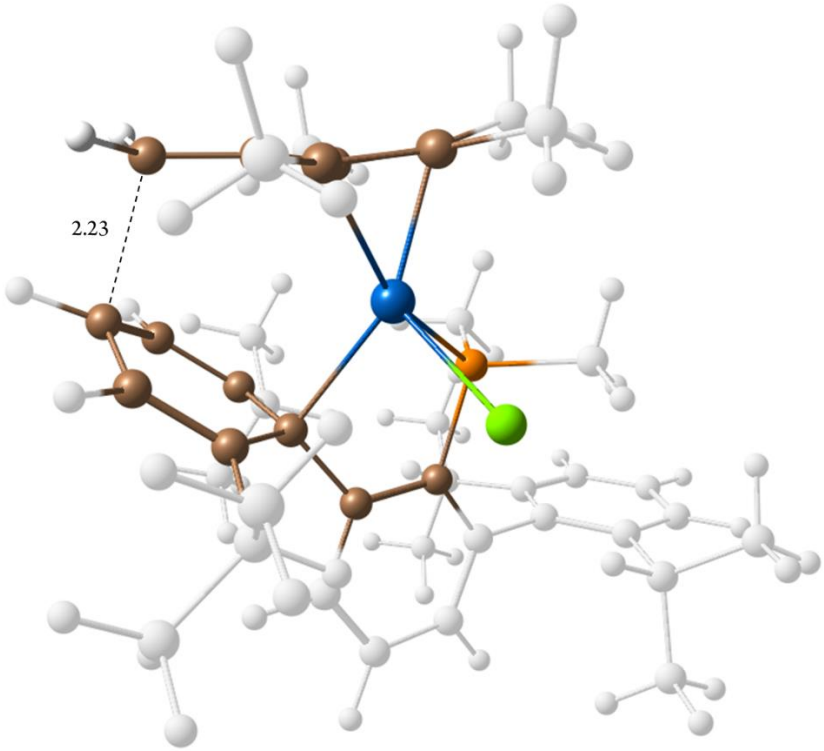

Figure 41. Molecular geometry of the transition state for the formation of the C−C bond at **A**.

I.2.3.7 C−C Bond Formation: Alternative Pathway

To complete this computational analysis, we considered the potential role of a tuck-in complex, since many examples of this kind of structure have been reported,[53] as a key intermediate in the C−C bond forming process. Although accessible in terms of energy ($\Delta G^{\ddagger}$ = 9 kcal/mol from **B,** Figure 42), relaxed energy scans reveal that the tuck-in complex is unlikely to take part in the formation of **4(Dipp)**$^{+}$; compromising the electron pair that forge the C−C bond in an interaction with the metal center does not facilitate the process.

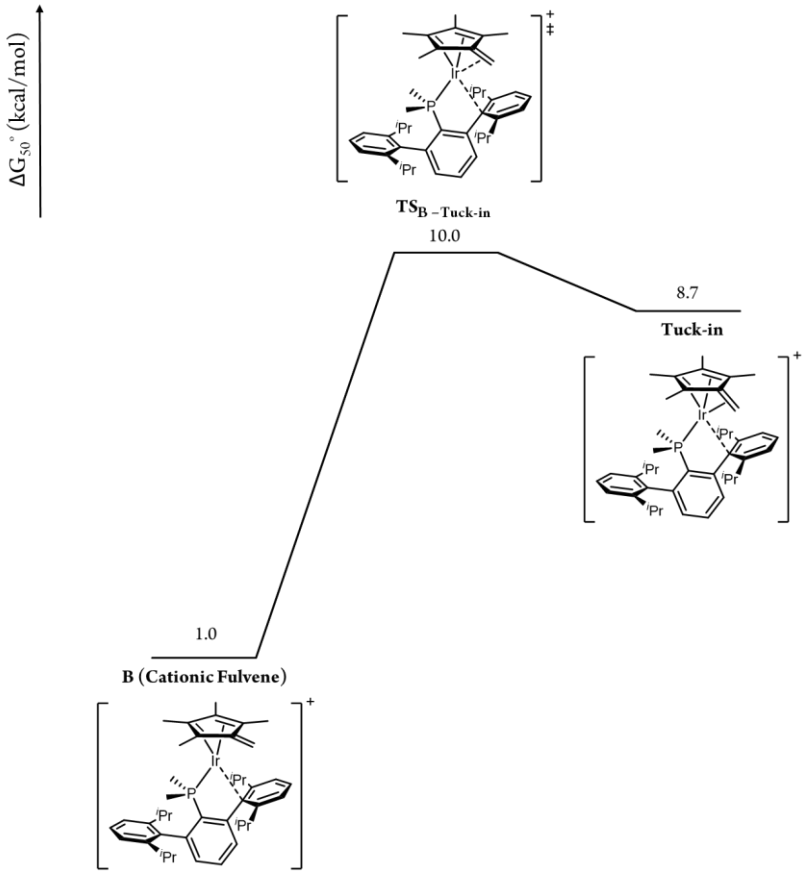

Figure 42. ΔG_{50}° profile for the conversion of the cationic fulvene complex **B** into a tuck-in complex.

I.2.3.8 Isomerization of 4(Dipp)$^+$

As already stated, the isomerization of **4(Dipp)**$^+$ into **3(Dipp)**$^+$ implies the cleavage of the newly formed C−C bond and the transfer of the methine H atom, C−*H* of an ^{i}Pr group, to restore the C_5Me_5 unit. The lowest-energy pathway for this transformation (Figure 43) comprises C–C bond cleavage (through $\mathbf{TS_{B\text{-}4}}$) to yield complex **B**, in which the direct attack of the fulvene moiety to a non-activated Me_2C−H bond ($\mathbf{TS_{B\text{-}C}}$, at 19.4 kcal/mol) triggers a complex electron rearrangement that gives complex **C**, an η^1 allyl, at 7.6 kcal/mol. Isomerization to the thermodynamic, observed product, **3(Dipp)**$^+$ (–11.5 kcal/mol) occurs via $\mathbf{TS_{C\text{-}3}}$ at 18.9 kcal/mol. Interestingly, the distance between Ir and the migrating H at $\mathbf{TS_{B\text{-}C}}$ is 3.21 Å, suggesting that there is no significant interaction between these atoms, nor even direct participation of the metal center in this step.

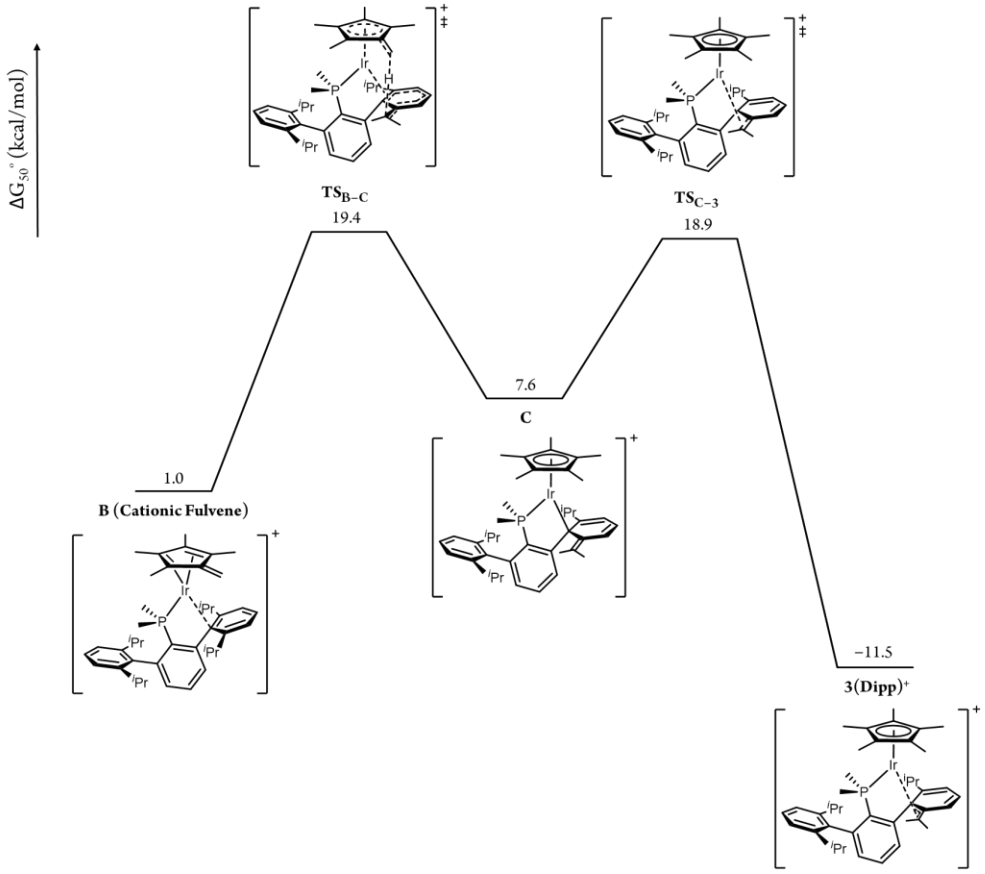

Figure 43. ΔG_{50}° profile for the isomerization of **B** to **3(Dipp)**$^{+}$.

Metrical parameters, particularly a long Ir−H bond distance (3.21 Å) found for **TS$_{B–C}$** (Figure 44) reveal that direct participation of the metal center in the hydrogen atom transfer step can be ignored.

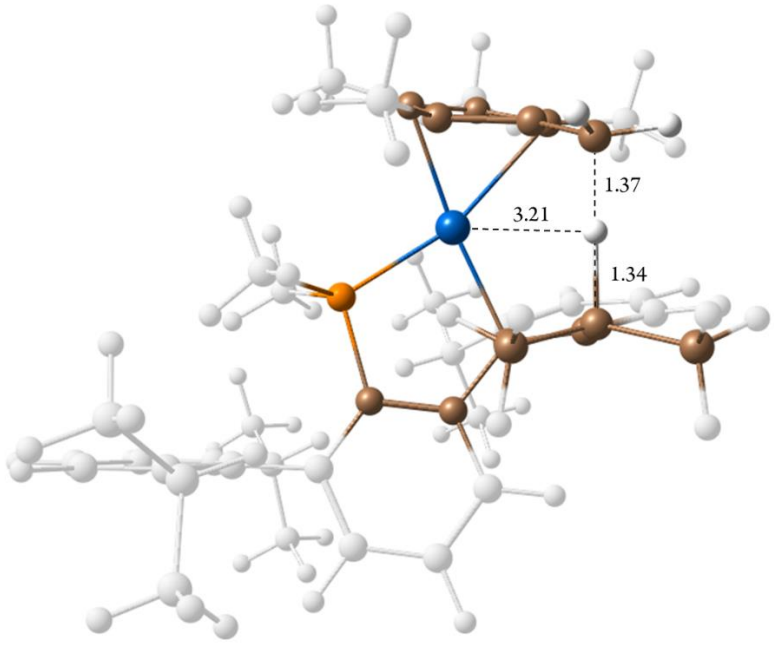

Figure 44. Molecular geometry of the transition state for the attack of the fulvene moiety of the C−H bond of one *iso*-propyl group (**TS$_{B-C}$**).

The LMOs study provided insight not only into the isomerization process but also on the complex electron rearrangement it involves (Figure 45). Attack of the fulvene moiety to the C−*H* atom is reflected by the evolution of the C=CH_2 π bond of the fulvene into a new σ C-H bond. Also, the Me_2C−H bond of the *iso*-propyl substituent converts into a new π C=CMe_2 LMO, whereas rearrangement of the π electrons of the corresponding aryl ring turns one π C=C LMO into a new σ Ir−C bond. Finally, one Ir-centered LMO evolves into a new bond with the C_5Me_5 ligand, consistent with reoxidation to Ir(III).

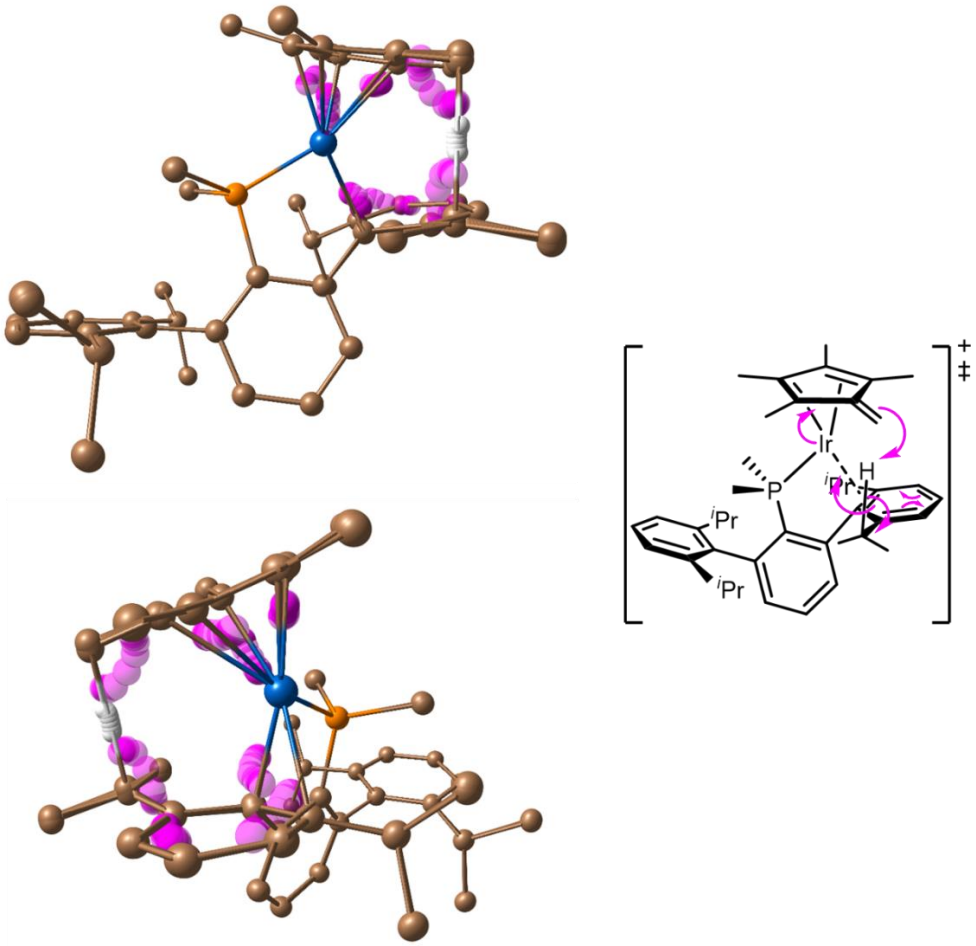

Figure 45. Two viewpoints of the LMO study of the IRC of **TS$_{B–C}$**. Non-participating H atoms were omitted for clarity.

I.2.3.9 Isomerization of 4(Dipp)$^+$: Alternative Pathways

Alternative mechanisms for this isomerization would proceed through oxidative cleavage of the C−H bond at accessible 16-electron complexes. In the case of Ir(I) complexes of type **B** and **Tuck-in**, this pathway would yield an Ir(III) hydride that could subsequently migrate to the $C_5Me_4CH_2$ unit. However, these pathways were found to be uncompetitive because of high kinetic barriers, as shown in Figures 46 and 47.

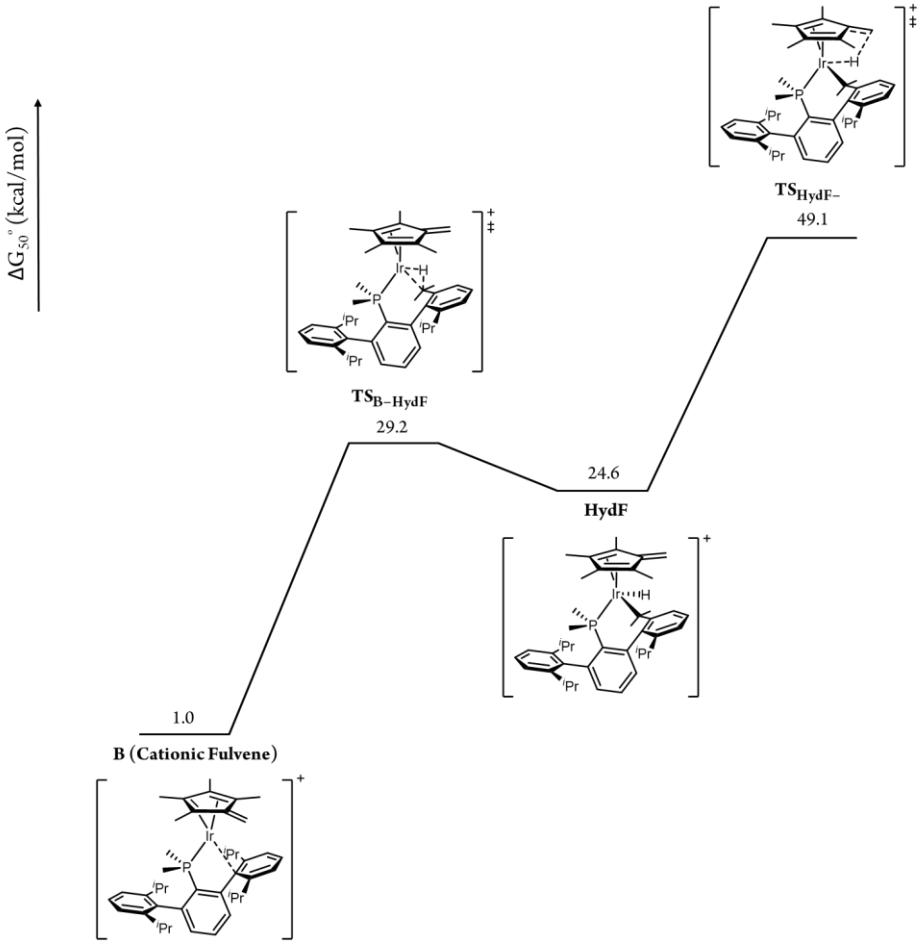

Figure 46. ΔG_{50}° profile for the oxidative addition of a C−H bond at the cationic fulvene complex **B** and further hydride migration to the fulvene moiety.

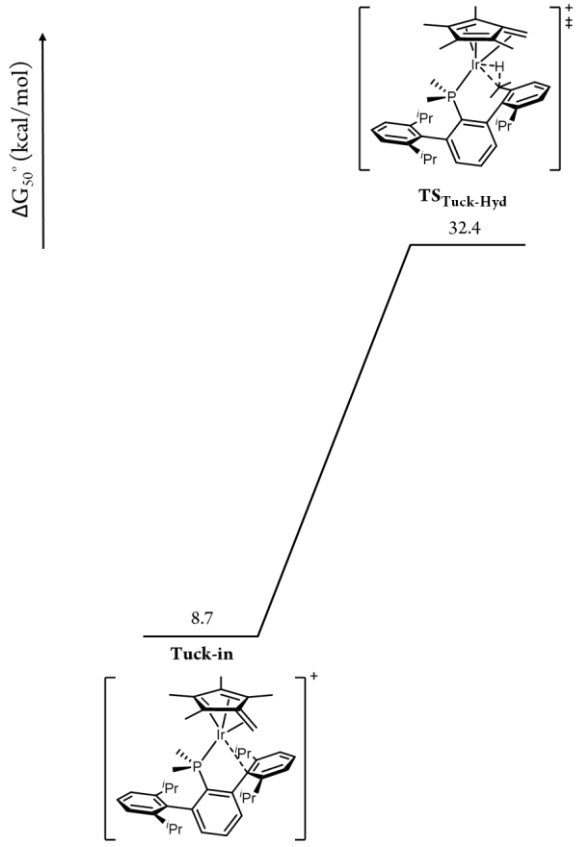

Figure 47. ΔG_{50}° profile for the oxidative addition of a C−H bond at the **Tuck-in** complex.

An important conclusion that may be derived from the above results is that ligands alike C_5Me_5 and PR_3, usually regarded as innocent can play a fundamental role in key transformations such as C−H activation and reversible C−C bond formation, whereas the contribution of the metal center that makes such reactivity feasible is its participation in a redox cycle such as the Ir(I)-Ir(III) discussed above. Such a behavior should be considered in the future to account for C−H activation mediated by transition metal complexes bearing C_5Me_5 ligands, especially in the presence of a Brönsted base.

I.2.4 Reactivity of 2(Xyl)$^+$ towards NEt$_3$

Despite the structural similarity between the two terphenyl phosphine ligands discussed within this Chapter, the outcome of the reaction of complex **2(Xyl)**$^+$ and NEt_3 was very different to that of **2(Dipp)**$^+$. At 25 ºC, the reaction yielded a complex mixture of products, and only traces of **3(Xyl)**$^+$ were detected by $^{31}P\{^1H\}$ NMR. Low temperature NMR monitoring revealed the immediate formation of **4(Xyl)**$^+$, which was characterized by a singlet at −2.5 ppm in the $^{31}P\{^1H\}$ NMR at −30 ºC (CD_2Cl_2). For comparison, **4(Dipp)**$^+$ resonates at −3.9 ppm under the same conditions. At −50 ºC, two clearly distinguishable exchanging ^1H NMR singlets were located at 6.09 and 4.85 ppm, once more reminiscent of the allylic and alkenic protons identified for **4(Dipp)**$^+$ (6.17 and 4.97 ppm in CD_2Cl_2, Figure 48). The exchange rate for the interconversion between the two equivalent pseudoallylic structures was faster for the xylyl system, with an associated barrier of $\Delta G^{\ddagger}$ = 10.7 kcal/mol, as calculated by line shape analysis (cf. the 12.9 kcal/mol found for **4(Dipp)**$^+$). Although compound **4(Xyl)**$^+$ could not be isolated and fully characterized, both its $^{31}P\{^1H\}$ and ^1H signature chemical resonances and its observed dynamic behavior in solution support an analogous formulation to that elucidated for **4(Dipp)**$^+$.

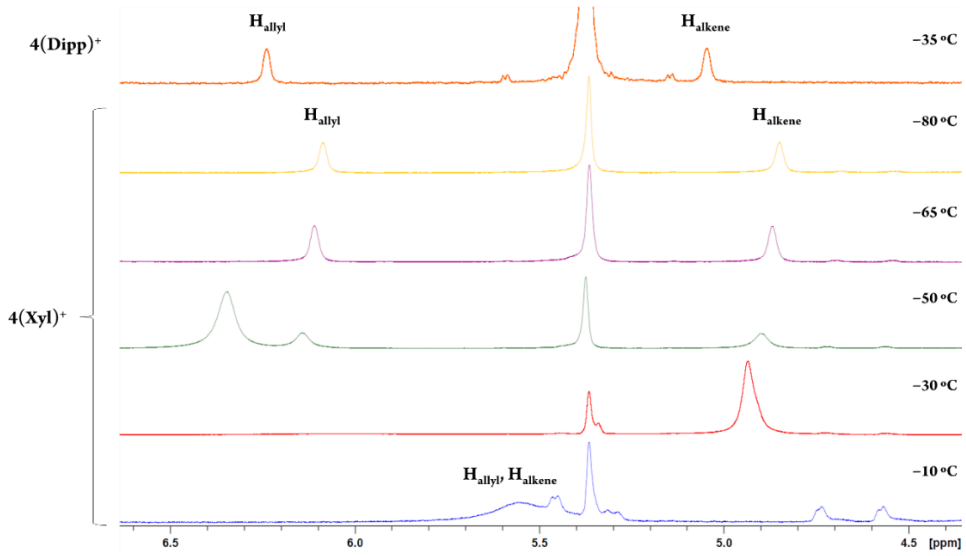

Figure 48. Solution dynamic behaviour of **4(Xyl)**$^+$ analyzed by variable temperature ^{1}H NMR, and comparison with **4(Dipp)**$^+$.

One of the reasons that precluded isolation of **4(Xyl)**$^+$ in pure form is the fact that its formation was accompanied by equimolar amounts of **1(Xyl)** and [HNEt$_3$]BAr$_F$ (Scheme 20), which presumably derive from unreacted starting material (**2(Xyl)**$^+$) and the in situ generated [HNEt$_3$]Cl. This behavior was not observed for the bulkier ligand PMe$_2$Ar$^{Dipp}_2$, where formation of **1(Dipp)** was never detected. **1(Xyl)** and [HNEt$_3$]BAr$_F$ are in equilibrium with [**2(Xyl)]BAr$_F$**] and [HNEt$_3$]Cl. In turn, complex **4(Xyl)**$^+$ was found to be reactive towards the latter leading to the new compound **5(Xyl)**$^+$, identified as the product resulting from the formal addition of HCl to **4(Xyl)**$^+$. Monitoring the reaction progress at low temperature (Figure 49) permitted the isolation of **5(Xyl)**$^+$, characterized by a ^{31}P NMR resonance at 9.7 ppm. In fact, this species was the only discernible organometallic product if sufficient time (12 h at −30 ºC) is allowed for the reaction. It is important to mention that compound **5(Xyl)**$^+$, isolated as a yellow

microcrystalline solid, remains stable at room temperature in solution only in the absence of NEt_3.

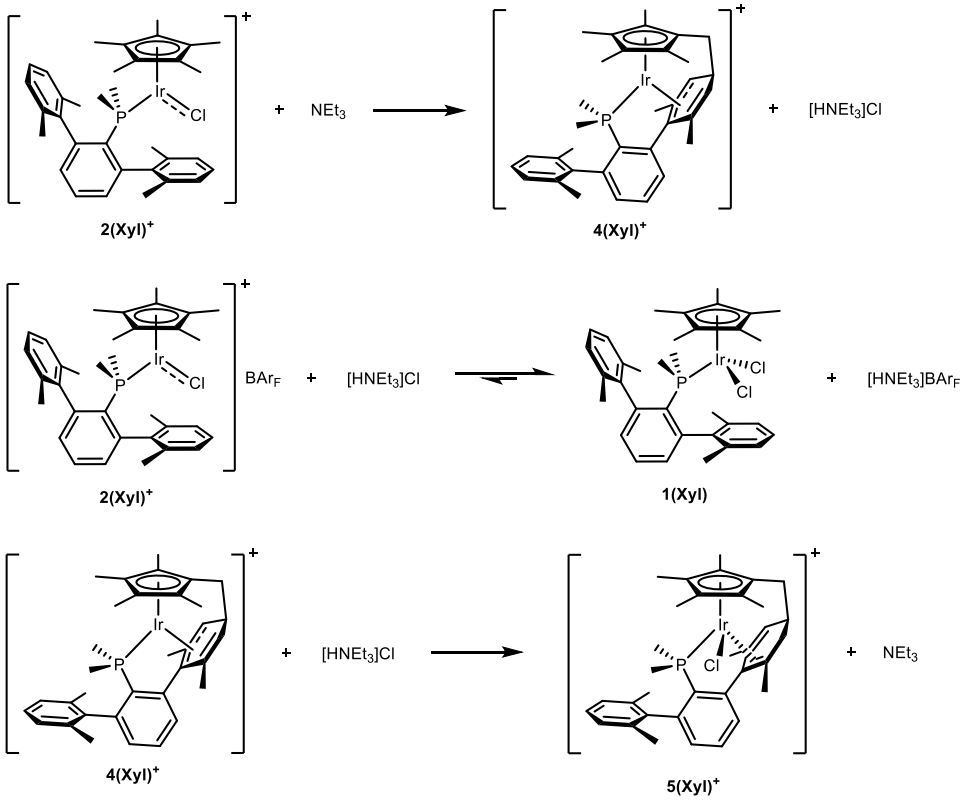

Scheme 20. NEt_3-catalyzed isomerization of **2(Xyl)**$^+$ into **5(Xyl)**$^+$ via **4(Xyl)**$^+$.

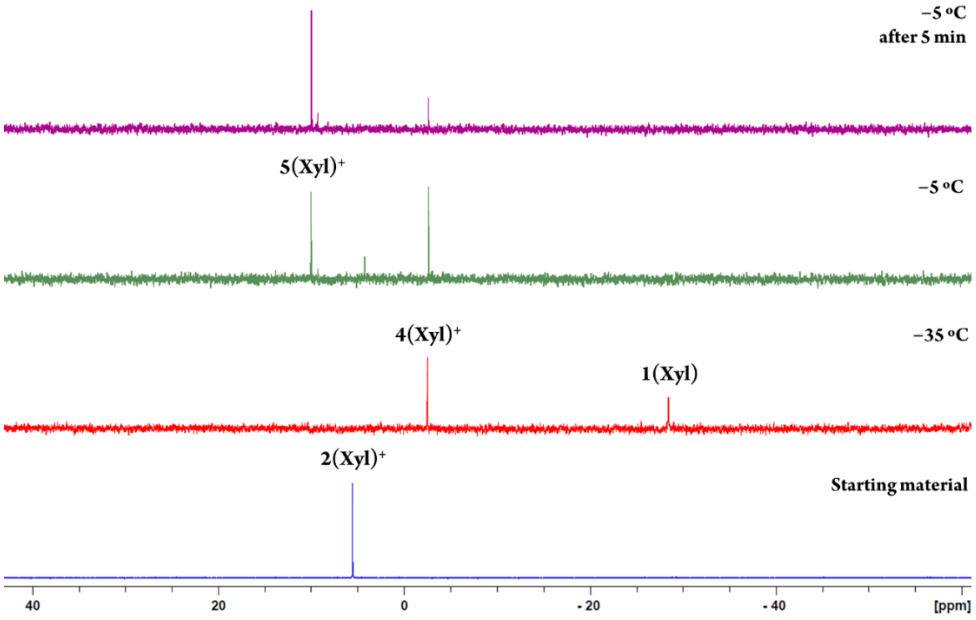

Figure 49. Low temperature $^{31}P\{^{1}H\}$ NMR monitoring of the reaction of equimolar quantities of **2(Xyl)**$^{+}$ (bottom) and NEt_3.

The molecular complexity of **5(Xyl)**$^{+}$ was originally inferred from multinuclear NMR spectroscopy and further confirmed by X-ray diffraction studies. Its ^{1}H NMR spectrum presents unequivocal evidence for the dearomatization of a xylyl ring due to the formation of a C−C bond with the cyclopentadienyl ligand. Nonetheless, at variance with compounds **4**$^{+}$ no fluxionality was detected by solution ^{1}H NMR. ^{1}H resonances for only six protons can be found in the aromatic region, whereas multiplets recorded upfield (5.44 and 3.01 ppm) can confidently be assigned to the alkenic *m*-CHXyl' and allylic *p*-Xyl' protons, respectively. A resonance at 2.06 ppm is attributed to a methylene group arising from protonation of one of the *meta* positions of the dearomatized xylyl ring. The methyl groups of the C_5Me_4 moiety give rise to four distinct ^{1}H signals (1.97, 1.83, 1.54 and 1.11 ppm), while the $C_5Me_4CH_2$ protons resonate at 2.00 ppm. Lastly, the methyl groups of the dearomatized xylyl ring lead to resonances

at 1.57 and 1.14 ppm, whereas corresponding signals for the non-coordinated ring appear at 2.07 and 1.89 ppm. The proposed η^2, alkene-type Xyl ring coordination is also supported by the ^{13}C chemical shifts of the dearomatized xylyl ring. The non-coordinated, originally *ortho* carbon resonates at 136.6 ppm in the $^{13}C\{^1H\}$ spectrum, *cf.* the bound *ipso* and *ortho* carbon atoms (84.0 and 82.8 ppm, respectively). The alkene meta carbon appears at 126.3 ppm, whereas the sp^3-hybridized methylene counterpart resonates at 38.5 ppm. Similarly, the also sp^3-hybridized carbon atom bonded to the $C_5Me_4CH_2$ moiety is responsible for the signal recorded at 31.9 ppm.

As stated above, the molecular structure of complex **5(Xyl)**$^+$ was authenticated by X-Ray crystallography (Figure 50), that further confirmed the formation of a C−C bond (1.551(9) Å) between a the $C_5Me_4CH_2$ moiety derived from the cyclopentadienyl ligand and the *para* carbon atom of one of the flanking xylyl rings. The η^2-coordination of the resulting cyclohexadiene unit is characterized by Ir-C bond distances of 2.273(6) and 2.257(5) Å for the *ortho* and *ipso* carbon atoms, respectively, whereas the non-coordinated *ortho* carbon was located far from the metal center at 3.151(6) Å. Despite the cationic character of complex **5(Xyl)**$^+$, the Ir−Cl bond distance (2.384(1) Å) is similar to that found for **1(Xyl)**, and both are significantly longer than those featured by complexes **2**$^+$ (**2(Xyl)**$^+$ = 2.278(1), **2(Dipp)**$^+$ = 2.347(1) Å), reinforcing the hypothesis that the chloride ligand may act as a σ and π donor in the latter unsaturated species.

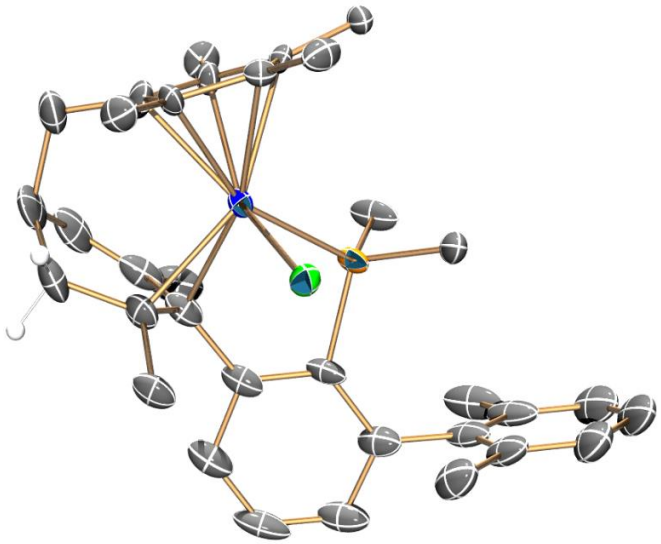

Figure 50. ORTEP diagram of the cation of complex **5(Xyl)**$^{+}$. Non-relevant hydrogen atoms are excluded for clarity and thermal ellipsoids are set at 50 % probability.

I.2.4.1 Computational Study of the Formation of 5(Xyl)$^+$

To unveil the reasons behind the sheer differences in the reactivity of complexes **2(Xyl)**$^+$ and **2(Dipp)**$^+$ against NEt_3, we conducted additional DFT calculations for the former system (Figure 51). The profile for the base-promoted formation of **3(Xyl)**$^+$ from **2(Xyl)**$^+$ is qualitatively similar to that disclosed previously for the Dipp system. Although for the xylyl complex the reaction is thermodynamically more favorable (−16.2 instead of −11.5 kcal/mol), a noticeable increase was found for the barrier associated to the fulvene attack to the benzylic C−H atom (26.8 kcal/mol relative to **4(Xyl)**$^+$, *cf*. the 21.5 kcal/mol found for the Dipp system, Figure 52) to yield **C Xyl**, that displays η^3-coordination of the allylic moiety (instead of the η^1 mode found for **C Dipp**). The higher barrier constitutes the rate limiting step for the xylyl system and seems to be responsible for the dissimilar reactivity exhibited by the two phosphines. Thus, the less accessible C−H deprotonation step permits other alternative pathways to compete and lead to a different reaction outcome, precluding the formation of **3(Xyl)**$^+$ in the presence of NEt_3.

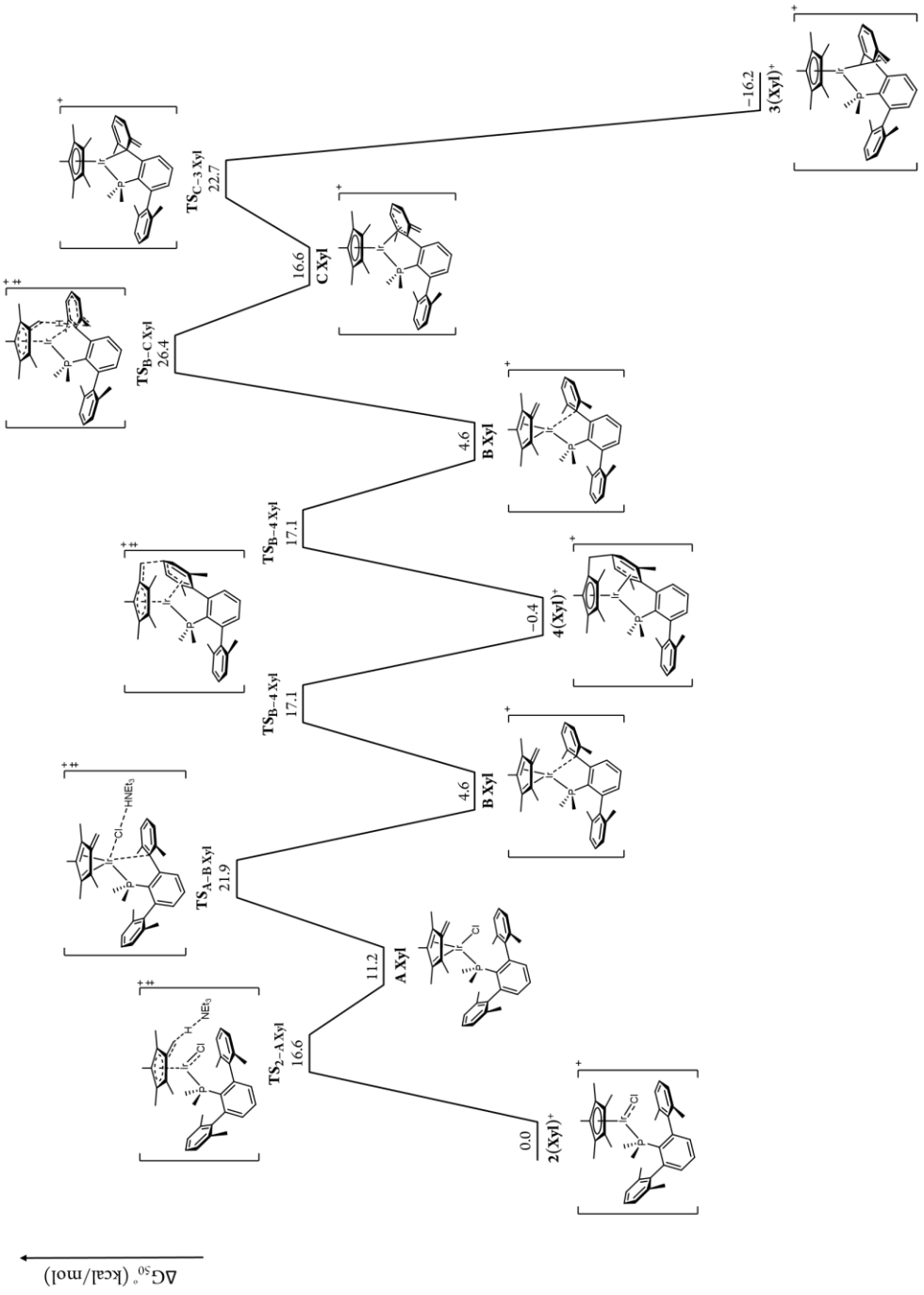

Figure 51. ΔG_{50}° profile for the conversion of **2(Xyl)**$^{+}$ into **4(Xyl)**$^{+}$ and **3(Xyl)**$^{+}$ promoted by NEt_3.

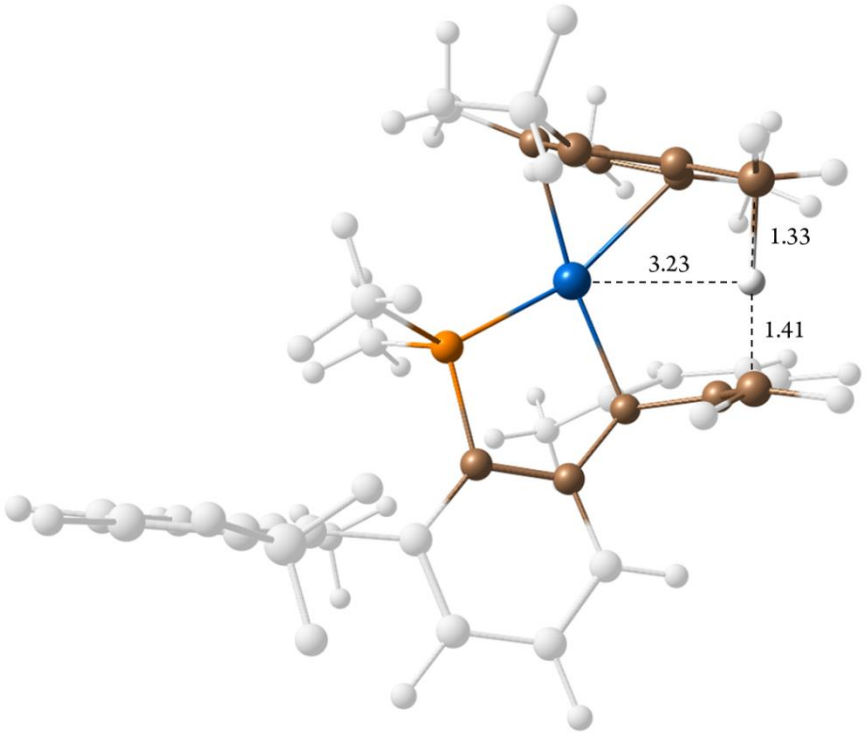

Figure 52. Molecular geometry of the transition state for the attack of the fulvene moiety at the benzylic C−H bond of the flanking xylyl ring (**$TS_{B–C\ Xyl}$**).

It is worth recalling that for the Dipp system the nature of the key species preceding the C−C bond formation event could not be defined unambiguously ($\Delta G_{50}^{\ddagger}$ = 20.2 kcal/mol for **A**, 20.4 kcal/mol for **B**; see Figures 36 and 40). In contrast, calculations based on the xylyl phosphine supports a carbon-carbon bond formation step through the neutral fulvene **A Xyl**, via **$TS_{AXyl–4XylCl}$** (17.5 kcal/mol, Figures 53 and 54). Thus, dissociation of the chloride ligand (8.3 kcal/mol, **$TS_{4XylCl–4Xyl+}$**) from **4(Xyl)Cl** (0.8 kcal/mol) followed by facile η^1-to-η^3 isomerization gives the observed intermediate, **4(Xyl)$^+$**, at −0.4 kcal/mol. In contrast, C−C bond formation from cationic fulvene **B Xyl** (Figure 51) requires surmounting a

barrier of 21.9 kcal/mol (**TS_{A-BXyl}**), that is, 4.4 kcal/mol higher than **$TS_{AXyl-4XylCl}$.**

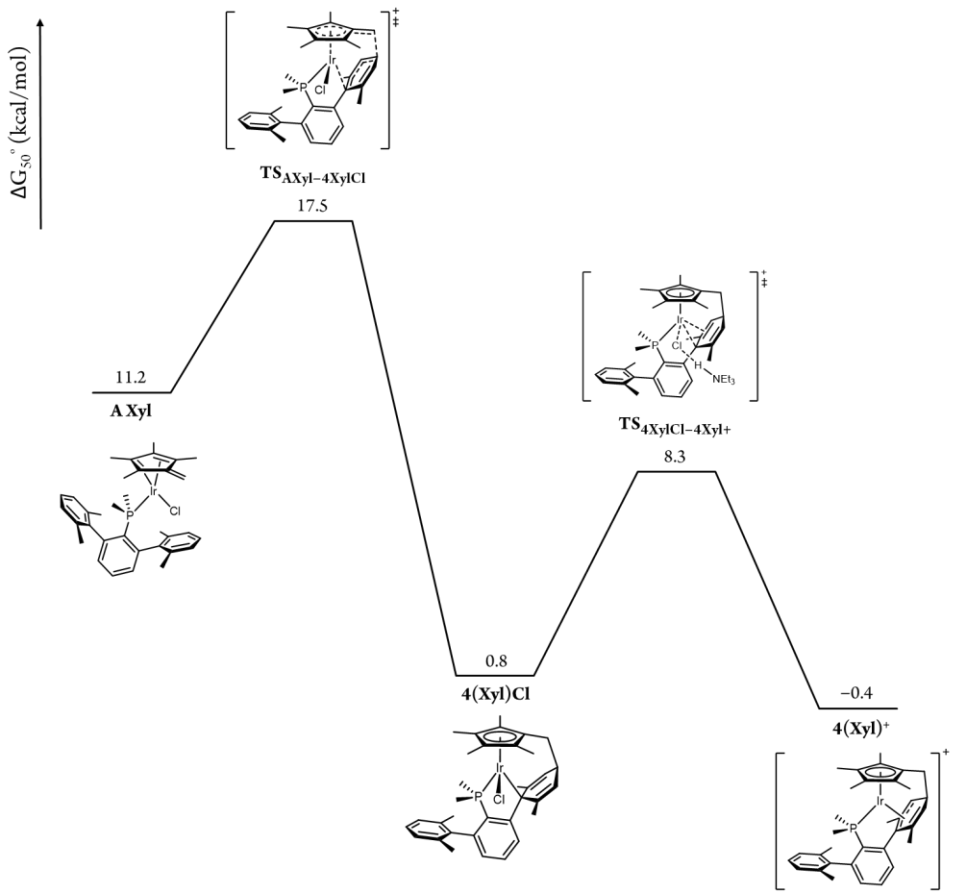

Figure 53. ΔG_{50}° profile for the C−C bond formation taking place at the neutral fulvene **A Xyl**.

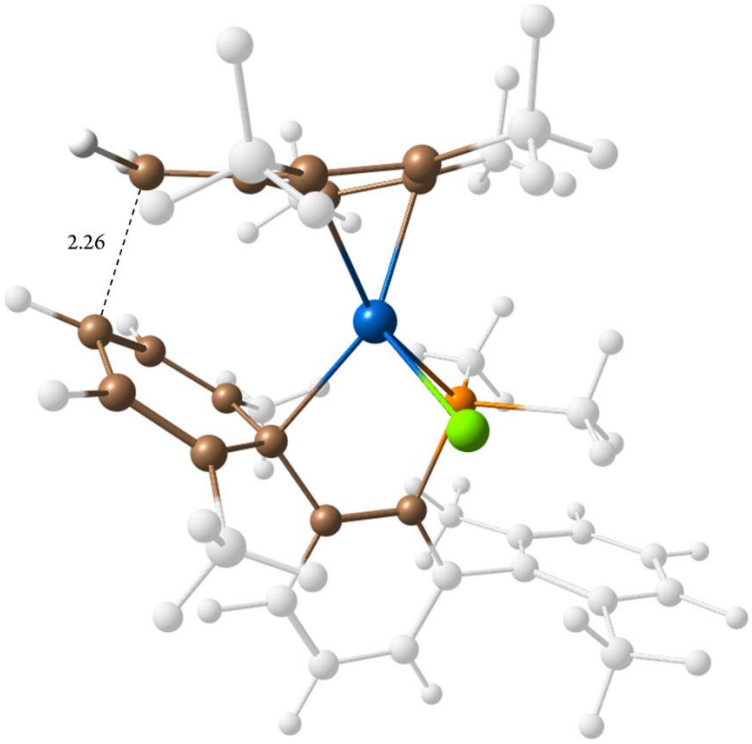

Figure 54. Molecular geometry of the transition state for the formation of the C−C bond at **A Xyl**.

I.2.4.2 Conversion of 4(Xyl)$^+$ to 5(Xyl)$^+$

The aforementioned findings prompted us to study the formal addition of HCl (from the [HNEt$_3$]Cl present in the reaction medium) to **4(Xyl)**$^+$. This species, with free energy −0.4 kcal/mol relative to **2(Xyl)**$^+$, readily incorporates a chloride anion via **TS$_{4Xyl+-4XylCl}$** (8.3 kcal/mol, Figure 55) to give the neutral complex **4(Xyl)Cl** at 0.8 kcal/mol. Protonation of the former *meta* carbon atom closer to the chloride ligand occurred through **TS$_{4XylCl-5Xyl+}$** at 11.3 kcal/mol (Figure 56), yielding complex **5(Xyl)**$^+$ at −4.0 kcal/mol (*cf*. **3(Xyl)**$^+$ at −16.2 kcal/mol). In agreement with our experimental findings, it may be concluded that **5(Xyl)**$^+$ is the kinetic product of a complex base-promoted isomerization of **2(Xyl)**$^+$, which indeed contrasts with the formation of **3(Xyl)**$^+$ in the absence of external base. It is therefore evident that the present work has disclosed an interesting case of a base-dependent competing isomerization path involving C−H bond activation along with C−C bond formation.

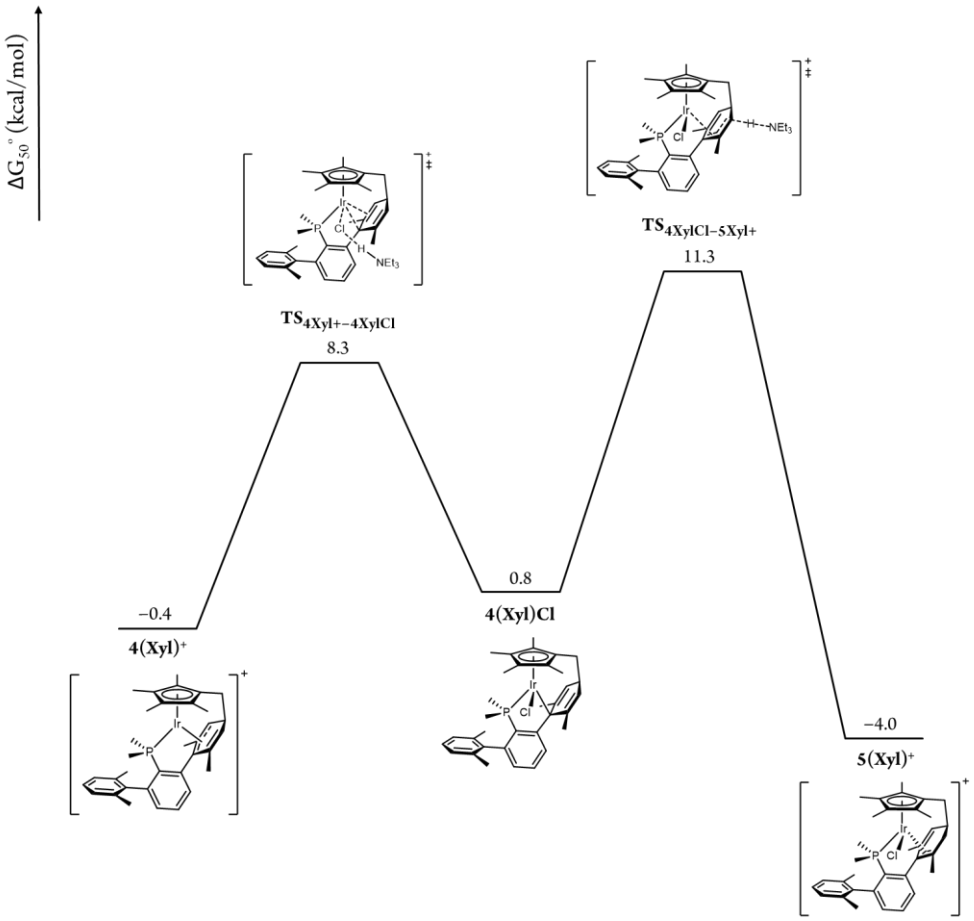

Figure 55. ΔG_{50}° profile for the formal incorporation of HCl to **4(Xyl)**$^{+}$ to yield complex **5(Xyl)**$^{+}$.

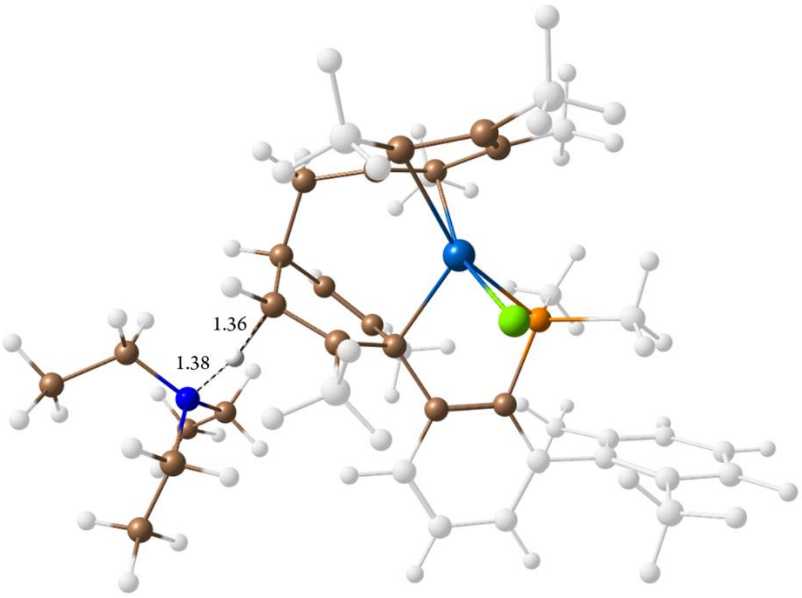

Figure 56. Molecular geometry of the transition state for the protonation of the allylic carbon (**TS$_{4XylCl-5Xyl+}$**).

An alternative mechanism for the formation of **5(Xyl)$^{+}$**, in which protonation of the *m*-allylic carbon is followed by chloride coordination to the thus formed dicationic complex, (**4(Xyl)H^{2+}**), was found to be considerably less favorable because of a significantly higher (26.0 kcal/mol) kinetic barrier leading to the formation of a dicationic intermediate, **4(Xyl)H^{2+}** (Figure 57).

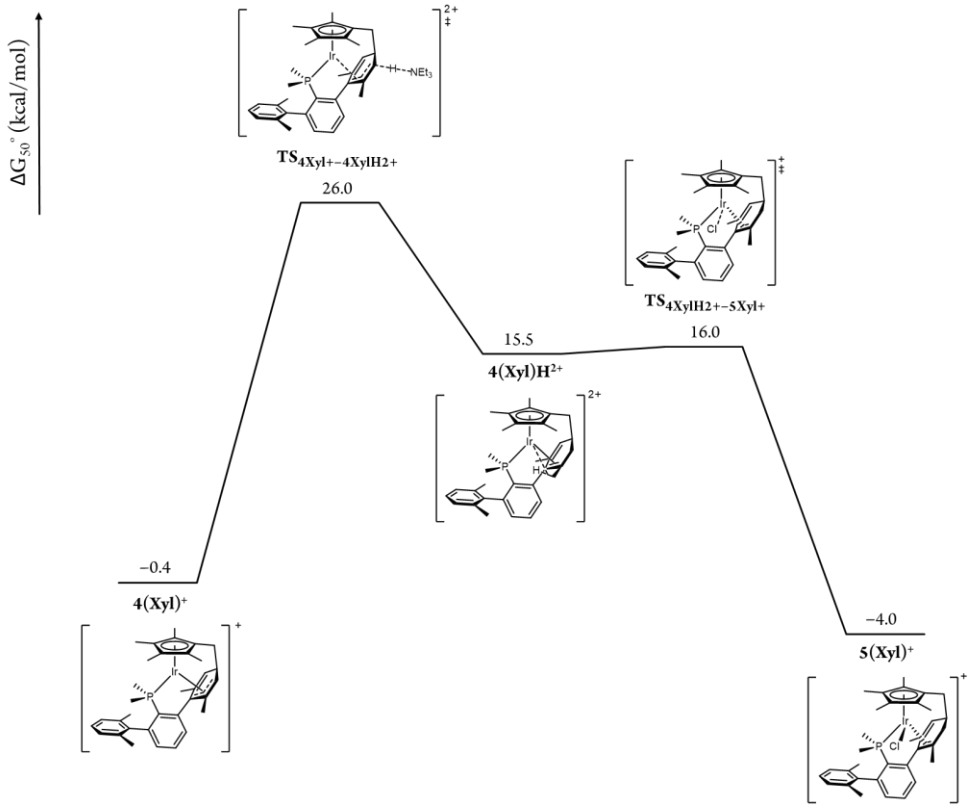

Figure 57. ΔG_{50}° profile for the transformation of **4(Xyl)**$^{+}$ into **5(Xyl)**$^{+}$ via a dicationic intermediate, **4(Xyl)H**$^{2+}$.

I.2.4.3 Computational Study of the Potential Formation of 5(Dipp)$^+$

For the sake of comparison, we decided to computationally explore the potential formation of **5(Dipp)$^+$**, derived from the bulkier $PMe_2Ar^{Dipp}{}_2$ phosphine (Figure 58). Energy barriers were, however, higher than for the Xyl system as a consequence of the steric hindrance exerted by the *iso*-propyl groups around the coordination environment of the metal center. Considering that these barriers are comparable to those found for the formation of **3(Dipp)$^+$**, we postulate that the selectivity towards the latter is due to thermodynamic reasons, that is, formation of **5(Dipp)$^+$** from **4(Dipp)$^+$** and $[HNEt_3]Cl$ is not exergonic.

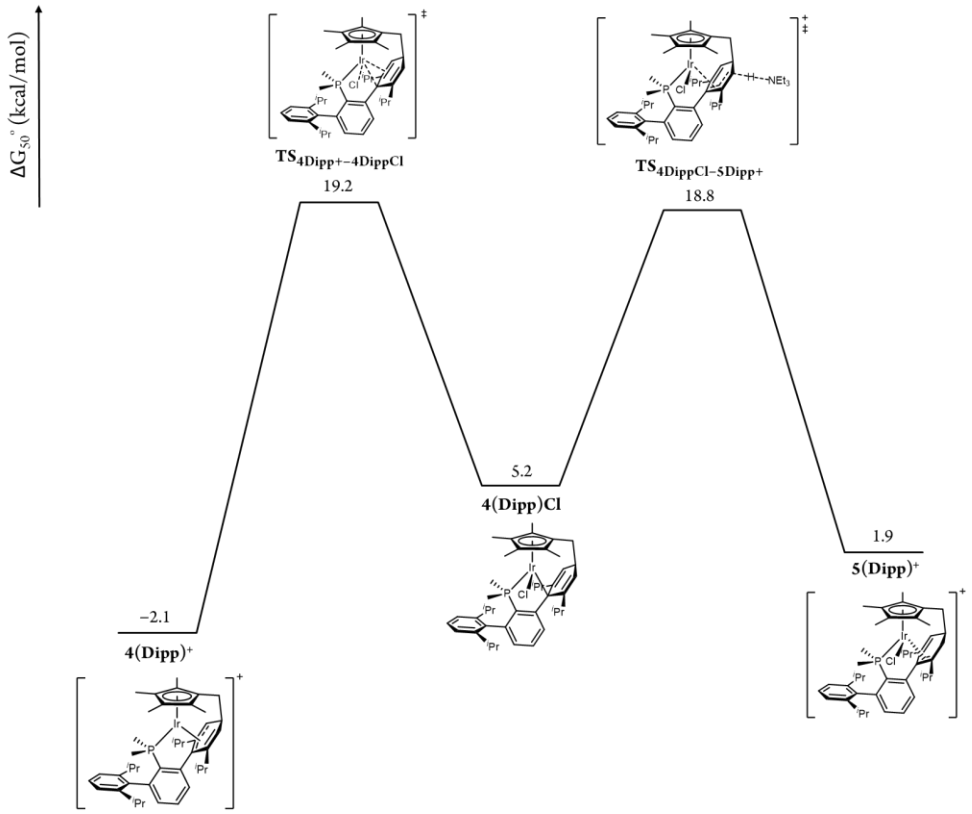

Figure 58. ΔG_{50}° profile for the formal incorporation of HCl to **4(Dipp)$^+$** to yield complex **5(Dipp)$^+$**.

I.2.5 Reactivity of the Cationic Chloride Complex [(η^5-C_5Me_5)Ir(Cl)($PMe_2Ar^{Dipp}_2$)]$^+$, 2(Dipp)$^+$, Towards LiMe, H_2 and $PhSiH_3$

I.2.5.1 Reactivity of 2(Dipp)$^+$ Towards LiMe

Numerous fundamental breakthroughs in organometallic chemistry have been achieved over the years exploiting the unique reactivity and structural diversity of transition-metal methyl complexes.[87] For instance, the distinctive reactivity of the σ-M−C bond, along with the small size of the methyl group and the impossibility to undergo β-H elimination were key features for the isolation of the first methylidene complex ($M=CH_2$)[88] (Figure 59), for the low temperature characterization of a σ-CH_4 complex[89] and not least for the mild C−H activation of alkanes and arenes,[41] to cite a few paradigmatic examples.

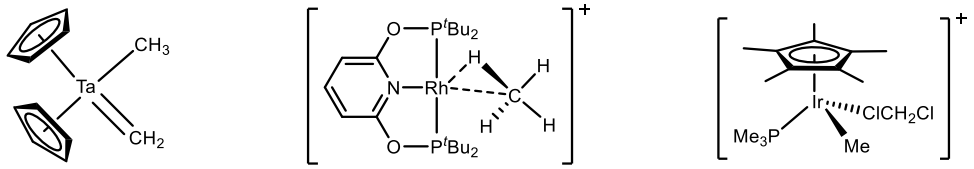

Figure 59. First methylidene (left) and σ−CH_4 (center) complexes, and Bergman´s C−H activation system (right).

As a natural extension of the results described in previous sections of this Thesis, we investigated the possibility of accessing the analogue of Bergman´s complex, [(η^5-C_5Me_5)Ir(Me)(PMe_3)($ClCH_2Cl$)]$^+$, containing the bulky $PMe_2Ar^{Dipp}_2$ in place of PMe_3. Our choice of the cited terphenyl phosphine was reinforced by the enhanced stability towards

[87] Campos, J.; López-Serrano, J.; Peloso, R.; Carmona, E. *Chem. Eur. J.* **2016**, *22*, 6432.
[88] Schrock, R. R. *J. Am. Chem. Soc.* **1975**, *97*, 6577.
[89] Bernskoetter, W. H.; Schauer, C. K.; Goldberg, K. I.; Brookhart, M. *Science* **2009**, *326*, 553.

cyclometallation exhibited by complex **[2(Dipp)]BAr$_F$** (see Sections I.2.1 and I.2.2). To this aim the reaction of the latter complex with LiMe was performed as represented in Scheme 21.

Addition of equimolar amounts of LiMe to diethyl ether solutions of the cationic chloride complex **[2(Dipp)]BAr$_F$** resulted in an instantaneous color change from dark to bright red due to the formation of a new species, the also cationic complex **6(Dipp)$^+$** (Scheme 21). The new complex features a $^{31}P\{^1H\}$ NMR resonance at 5.1 ppm, therefore similar to that of **2(Dipp)$^+$** (6.6 ppm). The large $\Delta\delta$ shift relative to free $PMe_2Ar^{Dipp}_2$ (−41.3 ppm) of about 46 ppm may be indicative of the existence of weak Ir−C_{arene} interactions involving one of the phosphine lateral Dipp units.[65] The room temperature ^1H NMR spectrum features broad resonances, suggestive of solution dynamic processes. Although lowering the temperature to −20 ºC slowed down the exchange and provided sharp, well-resolved resonances, the highly characteristic ^1H NMR signal associated with the η^5-C_5Me_5 protons (e.g. for **2(Dipp)$^+$** 1.22 ppm, d, $^4J_{HP}$ = 1.5 Hz, 15H) could not be found, clearly evincing that the desired complex, [(η^5-C_5Me_5)Ir(Me)($PMe_2Ar^{Dipp}_2$)]$^+$, was not an observable reaction product. As discussed next, 1D and 2D NMR experiments were instead in agreement with methylation of the C_5Me_5 ring and formation of an hexamethylcyclopentadiene ligand, η^4-C_5Me_6 (Scheme 21).

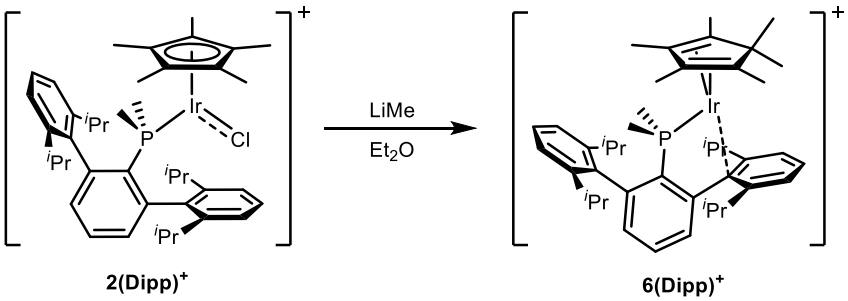

Scheme 21. Synthesis of **6(Dipp)**$^+$ from **2(Dipp)**$^+$ and LiMe.

As briefly mentioned, at −20 ºC complex **6(Dipp)**$^+$ exhibits a rigid solution structure. The complexity of the ^{1}H NMR spectrum is consistent with the absence of symmetry in the molecules of **6(Dipp)**$^+$, such that six ^{1}H resonances, each with relative intensity corresponding to 3H, are recorded in the 1.84-0.32 ppm range for the Me groups of the newly formed C_5Me_6 ligand. Likewise, the four Dipp *iso*-propyl substituents are inequivalent and originate corresponding multiplets centered at 2.64, 2.32, 2.15 and 2.00 ppm (see Experimental Section) for the methine C*H*Me$_2$ protons. In the ^{13}C{^{1}H} NMR spectrum, the low-frequency shift of one of the *ipso* carbon atoms of the flanking aryl rings (120.4 ppm, *cf*. the 135.7 ppm value for the corresponding carbon of the non-coordinated Dipp ring) suggests the existence of a weak π-arene interaction with the iridium center. One of the *ortho* carbon atoms of this ring could also participate in the bonding, resulting in η^2-coordination of the arene, as its chemical shift (132.5 ppm) is significantly shifted to lower frequencies compared to its counterparts (141.5 ppm for the other *ortho* carbon within the same ring, and 146.5 and 146.9 ppm for the ones belonging to the free Dipp). The fluxional behavior of **6(Dipp)**$^+$ could arise from the exchange of the coordinated and free Dipp rings. This rearrangement could occur through formally 14-electron species[65,66] or via the rotation of the C_5Me_6 fragment,

presumably through a tetrahedral coordination environment[90] (Figure 60). Since no exchange peaks can be recorded in a 2D EXSY experiment for the clearly distinguishable *m*-C_6H_3 protons of the central aryl ring, the former process can be ruled out.

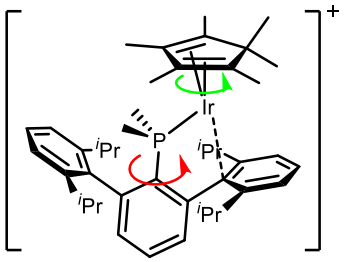

Figure 60. Possible rotational modes to account for the dynamic solution behaviour of **6(Dipp)**$^+$.

The molecular structure of complex **6(Dipp)**$^+$ was unequivocally determined by single-crystal X-Ray crystallography (Figure 61). In agreement with the above NMR observations, an η^1-arene coordination was preferred in the solid state. The Ir−C_{arene} bonding is characterized by an Ir−C_{ipso} bond distance of 2.249(4) Å, and by significantly longer, and therefore weaker, Ir−C_{ortho} interactions of length 2.544(5) and 2.686(4) Å. Despite this weakness, η^2-coordination is also a reasonable proposal.

[90] a) Marinelli, G.; Rachidi, I. E.-I.; Streib, W. E.; Eisenstein, O.; Caulton, K. G. *J. Am. Chem. Soc.* **1989**, *111*, 2346; b) Geer, A. M.; Julián, A.; López, J. A.; Ciriano, M. A.; Tejel, C. *Chem. Eur. J.* **2018**, *24*, 1.

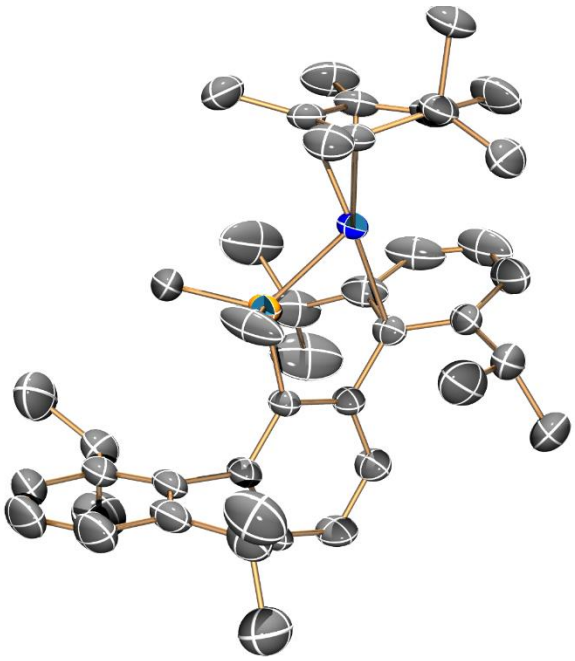

Figure 61. ORTEP diagram of the cation of complex **6(Dipp)**$^{+}$. Hydrogen atoms are excluded for clarity and thermal ellipsoids are set at 50 % probability.

I.2.5.2 Computational Studies of the Reactivity of 2(Dipp)$^+$ Towards LiMe

We considered of interest to examine the mechanism for the formation of complex **6(Dipp)**$^+$ by DFT calculations. As starting point, a reductive coupling between the methyl and C_5Me_5 ligands of the Ir(III) complex $[(\eta^5\text{-}C_5Me_5)Ir(Me)(PMe_2Ar^{Dipp}{}_2)]^+$, which could be favored by steric congestion around the metal center, was envisioned. The above complex could result from chloride-by-methyl metathesis in **2(Dipp)**$^+$, facilitated by precipitation of LiCl. Nevertheless, computational work revealed the non-feasibility of this reductive step, for it entailed a barrier of 35.6 kcal/mol (ΔG_{50}) relative to $[(\eta^5\text{-}C_5Me_5)Ir(Me)(PMe_2Ar^{Dipp}{}_2)]^+$ (Figure 62).

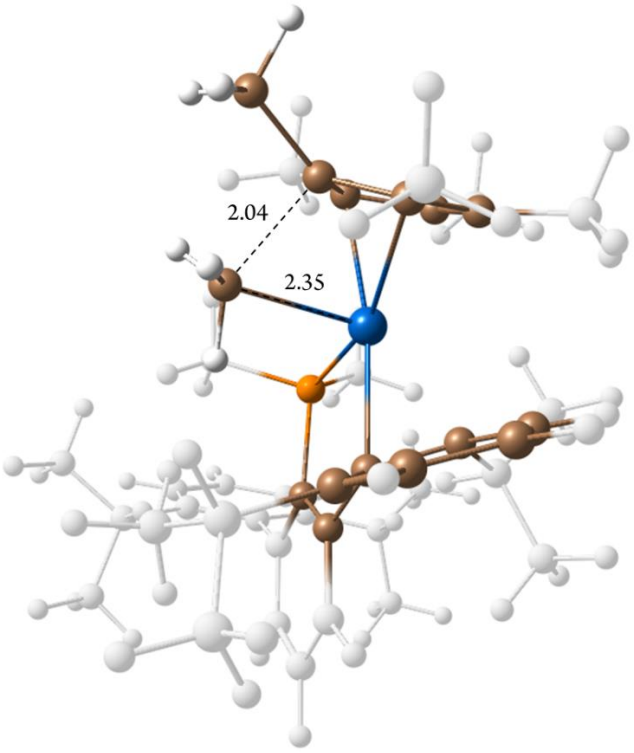

Figure 62. Molecular geometry of the transition state for reductive coupling at $[(\eta^5\text{-}C_5Me_5)Ir(Me)(PMe_2Ar^{Dipp}{}_2)]^+$.

As a reasonable alternative, we analyzed the possibility of the reductive coupling event taking place at the neutral, 18-electron (η^5-C_5Me_5)Ir(Me)(Cl)($PMe_2Ar^{Dipp}_2$) species. This complex could stem from direct attack of a molecule of LiMe to the electrophilic cationic Ir(III) center, concomitant with the formation of $LiBAr_F$. The two conformers represented in Figure 63 were evaluated, but both yielded exceedingly high energy barriers for the reductive coupling (38.8 and 41.2 kcal/mol relative to the corresponding minimum), inconsistent with the experimental observations.

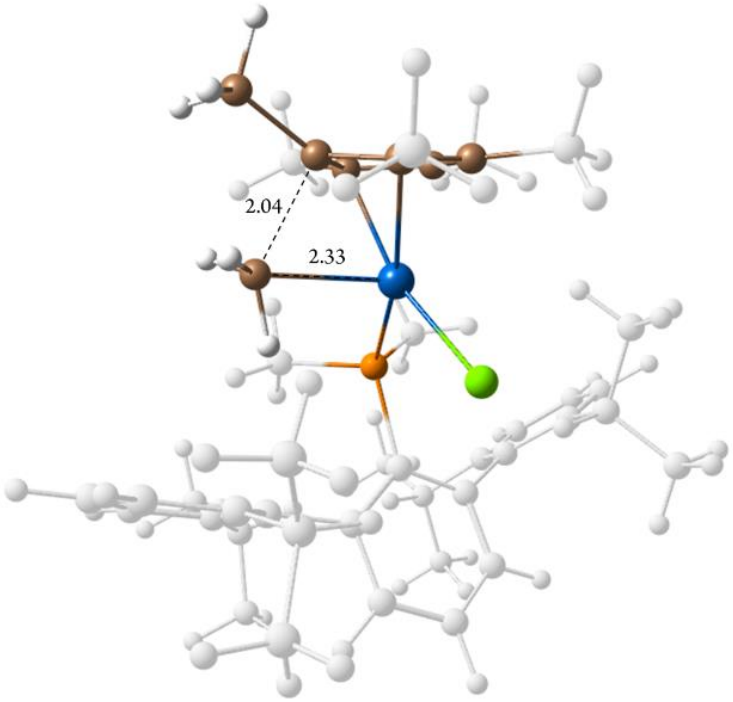

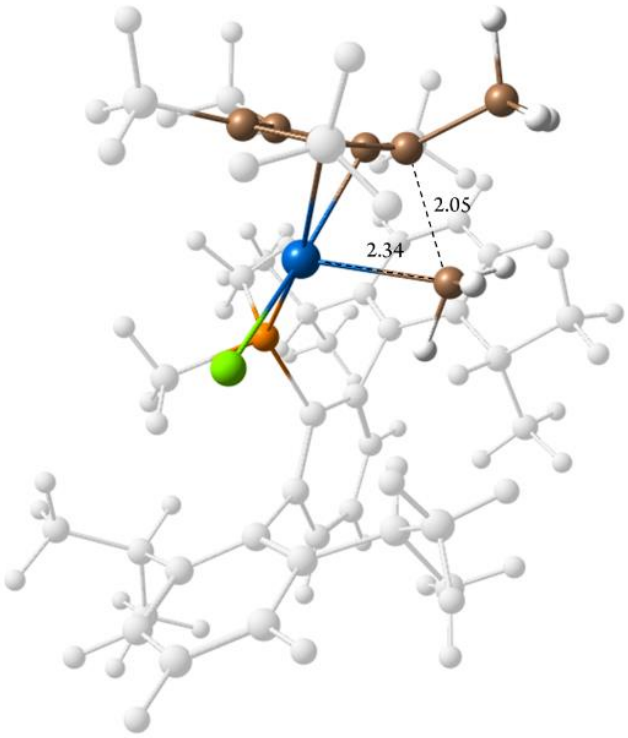

Figure 63. Molecular geometries of the transition states of the reductive coupling, found at 38.8 (left) and 41.2 kcal/mol (ΔG_{50}) (right) relative to the corresponding (η^5-C_5Me_5)Ir(Me)(Cl)($PMe_2Ar^{Dipp}_2$) isomer.

Our failure to explain the formation of complex **6(Dipp)**$^+$ through the rather classical foregoing routes, both implying the participation of an Ir−Me functionality, led us to explore a more unconventional reaction path that does not require direct participation of the Ir(III) center. To this aim, we explored the feasibility of a direct attack of the molecule of LiMe to the *exo* face of the η^5-C_5Me_5 ligand. The transition state for this reaction is shown in Figure 64 and the C−C bond formation step that yielded a neutral Ir(I) complex at −25.6 kcal/mol relative to reactants required surmounting a barrier of only 10.6 kcal/mol. Subsequent chloride release gave complex **6(Dipp)**$^+$ through an accessible barrier ($\Delta G_{50}^{\ddagger}$ = 18.6 kcal/mol).

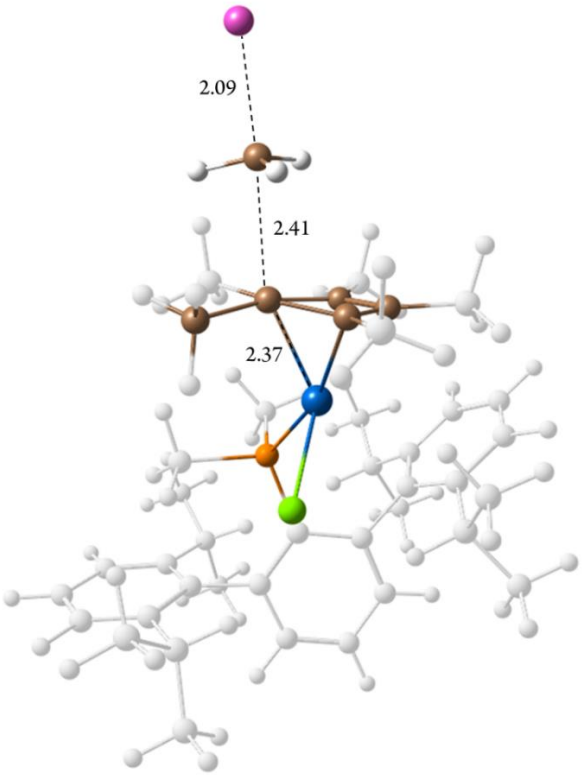

Figure 64. Molecular geometry of the transition state for the direct attack of LiMe to the C_5Me_5 in **2(Dipp)**$^+$.

Though geometry optimizations included solvent effects (diethyl ether) with the SMD continuum model, a monomeric, unsolvated LiMe molecule could display exacerbated reactivity. Incorporation of one, two or three explicit solvent molecules (Me_2O) resulted in increasingly reduced ΔG_{50} barriers of 8.6, 6.4 and 4.5 kcal/mol, respectively, giving the corresponding products at −29.6, −37.6 and −46.8 kcal/mol, respectively, relative to the reactants. Therefore, incorporation of explicit solvent molecules stabilizes, as expected, the transition state and the products due to the higher unsaturated character of the Li cation in these stages compared to the reactants. The molecular geometry of the transition state stabilized by three explicit ether molecules is depicted in Figure 65.

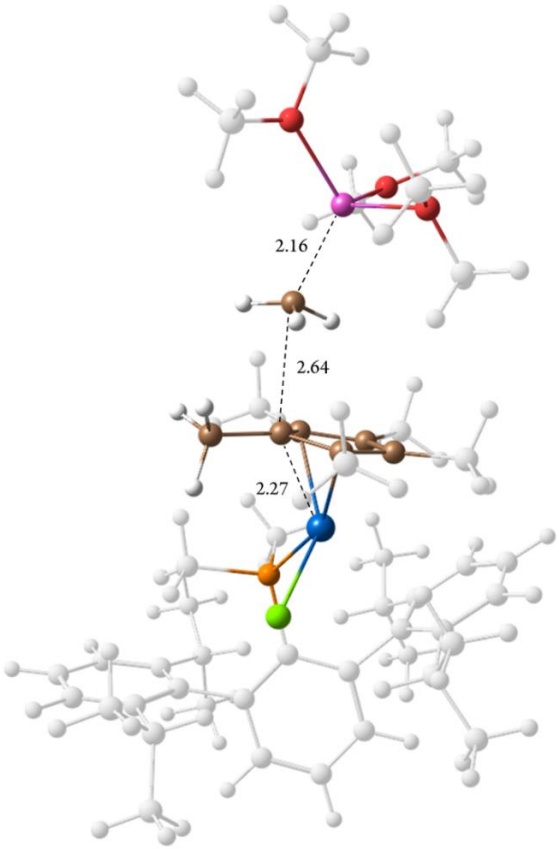

Figure 65. Molecular geometry of the transition state for the attack of $(Me_2O)_3LiMe$ to **2(Dipp)**$^+$.

At this stage, it is worth recalling that the already presented results concerning the reactivity of complexes **2**$^+$ towards NEt_3 (see Sections I.2.3 and I.2.4) clearly demonstrated that the Brönsted-Lowry acidity of the methyl groups of the C_5Me_5 ligand can be exploited to highlight the non-innocent behavior of the pentamethyl cyclopentadienyl ligand. Now, the experimental and computational studies on the reactivity of **2(Dipp)**$^+$ towards LiMe reveal that these species also display remarkable electrophilicity of the internal carbon atoms of the C_5Me_5 ring. In the two cases, readily accessible square-planar Ir(I) complexes appear to be key intermediates.

I.2.5.3 Reactivity of 2(Dipp)$^+$ towards H_2 and $PhSiH_3$

The pioneering work of Crabtree and coworkers[91] paved the way for the development of olefin hydrogenation catalysis employing iridium complexes.[92] Along these years, many fundamental advances have also been achieved by exploiting the unique reactivity of the simplest molecule, dihydrogen, in organometallic iridium chemistry,[93] including naturally the development of σ-H_2 complexes.[94]

We were interested in disclosing the reactivity towards H_2 of some of the cationic Ir(III)-PMe_2Ar' complexes described earlier, complementing in this manner anterior investigations on analogous Rh and Ir complexes stabilized by coordination to $PMeXyl_2$ and related bis(aryl)phosphine ligands.[57b] Compared to these species, complexes of type **3**$^+$, which as discussed in section **I.2.2** of this Thesis are cationic [(η^5-C_5Me_5)Ir(PMe_2Ar')]$^+$ complexes where the terphenyl phosphine ligand, $PMe_2Ar^{Xyl}_2$ or $PMe_2Ar^{Dipp}_2$, has undergone remote ζ C−H activation, and is therefore bonded to iridium in a κ^1-P, η^3-pseudoallylic fashion, were found to display considerably reduced reactivity. This relative inertness is probably due to the difficulty of accessing low-energy intermediates with a vacant coordination site. In contrast, the parent complexes **2(Xyl)**$^+$ and **2(Dipp)**$^+$ feature formally five-coordinate structures. Given that **2(Xyl)**$^+$ is

[91] Crabtree, R. H.; Morris, G. E. *J. Organomet. Chem*. **1977**, *135*, 395.
[92] Kolychev, E. L.; Kronig, S.; Brandhorst, K.; Freytag, M.; Jones, P. G.; Tamm, M. *J. Am. Chem. Soc.* **2013**, *135*, 12448 and references therein.
[93] a) Pons, V.; Heinekey, D. M. *J. Am. Chem. Soc.* **2003**, *125*, 8428; b) Göttker-Schnetmann, I.; Heinekey, D. M.; Brookhart, M. *J. Am. Chem. Soc.* **2006**, *128*, 17114; c) Goldberg, J. M.; Goldberg, K. I.; Heinekey, D. M.; Burgess, S. A.; Lao, D. B.; Linehan, J. C. *J. Am. Chem. Soc.* **2017**, *139*, 12638.
[94] a) Crabtree, R. H. *Acc. Chem. Res.* **1990**, *23*, 95; b) Kubas, G. J. Metal Dihydrogen and Sigma-Bond Complexes. Structure, Theory and Reactivity. Kluwer Academic: New York, **2001**; c) Kubas, G. J. *J. Organomet. Chem.* **2014**, *751*, 33.

characterized by rather limited solution stability, its $PMe_2Ar^{Dipp}{}_2$ counterpart, **2(Dipp)$^+$**, was chosen for this study.

At room-temperature, exposure of a CD_2Cl_2 solution of complex **2(Dipp)$^+$** to 1 bar of H_2 did not result in an observable color change. Similarly, no variations relative to free **2(Dipp)$^+$** were detected in the ^1H and $^{31}P\{^1H\}$ NMR spectra, as can be seen in Figure 66 (**B** and **A**, respectively). Upon cooling at −30 ºC, a temperature-dependent equilibrium was, however, stablished. Thus, a new $^{31}P\{^1H\}$ resonance appeared at −27.4 ppm whereas in the ^1H NMR spectrum a doublet was recorded with δ −11.7 and $^2J_{HP}$ = 9 Hz. The Δδ value of *ca*. 14 ppm observed for the 31P resonance of the new complex relative to the free phosphine is consistent with κ^1-P coordination. In turn, the low-frequency 1H NMR signal at −11.7 ppm suggests incorporation of a molecule of H_2, forming either an Ir-(σ-H_2) complex or a bis(hydride), $Ir(H)_2$, isomeric structure. To distinguish between these possibilities, additional NMR studies, as well as DFT calculations, were performed.

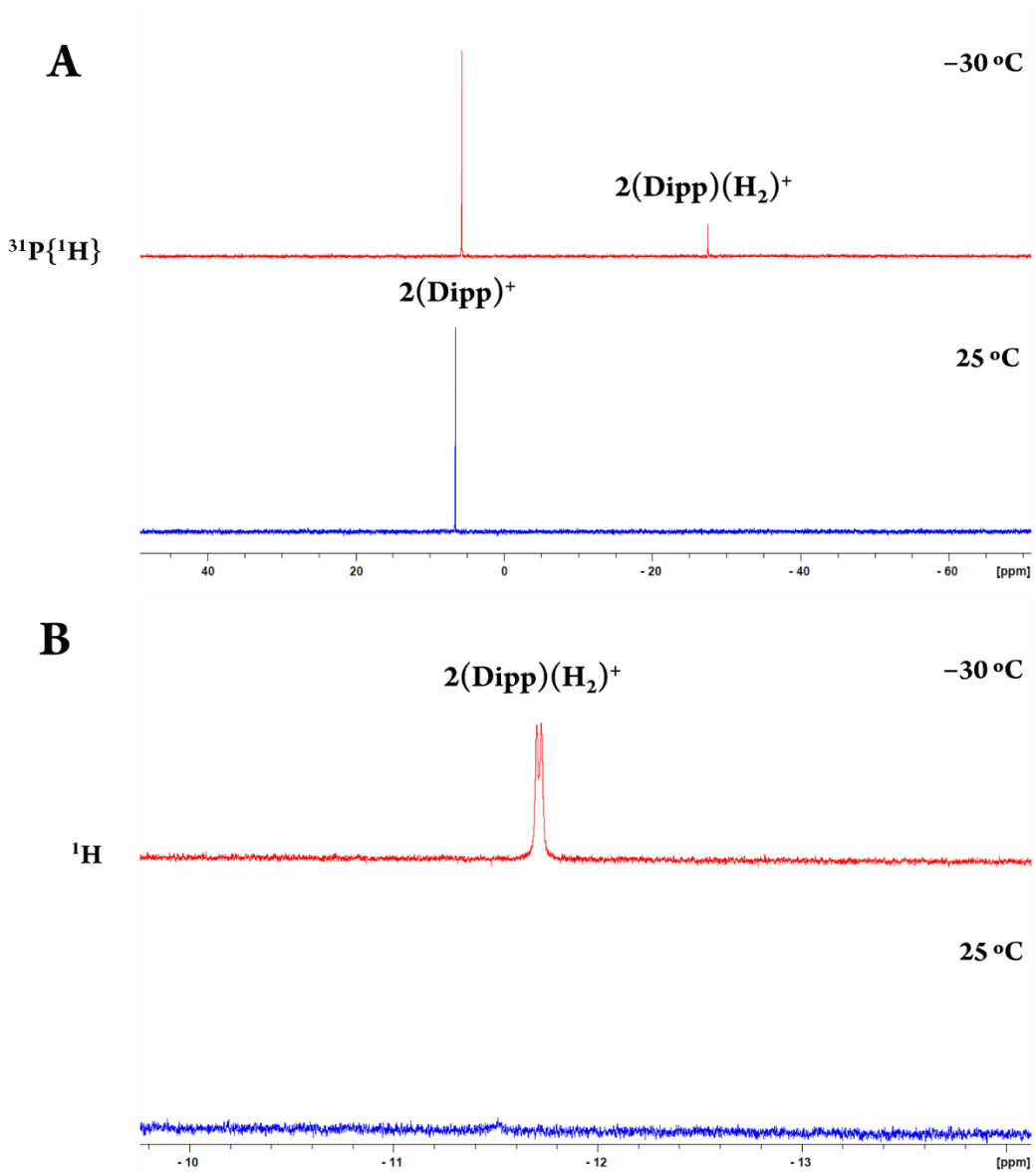

Figure 66. Selected regions of the $^{31}P\{^{1}H\}$ (**A**, top) and ^{1}H (**B**, bottom) NMR spectra of **2(Dipp)**$^{+}$ under H_2 atmosphere (1 bar) at –30 ºC and at room temperature.

Spin-lattice relaxation time, T_1, measurements were accomplished in the temperature interval from −80 to 25 ºC. A minimum T_1 value was registered at −40 ºC. Its magnitude of 180 ms clearly indicates a

bis(hydride) formulation for the newly generated complex.[95] The two isomeric structures, namely **2(Dipp)(σ-H$_2$)$^+$** and **2(Dipp)(H)$_2^+$**, were studied computationally by DFT methods. Figure 67 shows the calculated geometries for the two molecules. Although they were found to have relatively close energies (ΔG_{50}), in agreement with the NMR observations **2(Dipp)(H)$_2^+$** was computed to be 2.3 kcal/mol more stable than the σ-H$_2$ complex **2(Dipp)(σ-H$_2$)$^+$**. The Ir(V) dihydride is characterized by computed Ir−H distances of 1.56 and 1.57 Å, and by a long H−H separation of 1.68 Å. In contrast, for **2(Dipp)(σ-H$_2$)$^+$** the calculated distance between hydrogen atoms of 1.03 Å is in accord with a slightly stretched σ complex[96] while the associated Ir−H distances of 1.62 and 1.64 Å are longer than corresponding separations in the bis(hydride) isomer.

[95] Hamilton, D. G.; Crabtree, R. H. *J. Am. Chem. Soc.* **1988**, *110*, 4126.
[96] a) Klooster, W. T.; Koetzle, T. F.; Jia, G.; Fong, T. P.; Morris, R. H.; Albinati, A. *J. Am. Chem. Soc.* **1994**, *116*, 7677; b) Barea, G.; Esteruelas, M. A.; Lledós, A.; López, A. M.; Tolosa, J. I. *Inorg. Chem.* **1998**, *37*, 5033; c) Crabtree, R. H. *Chem. Rev.* **2016**, *116*, 8750.

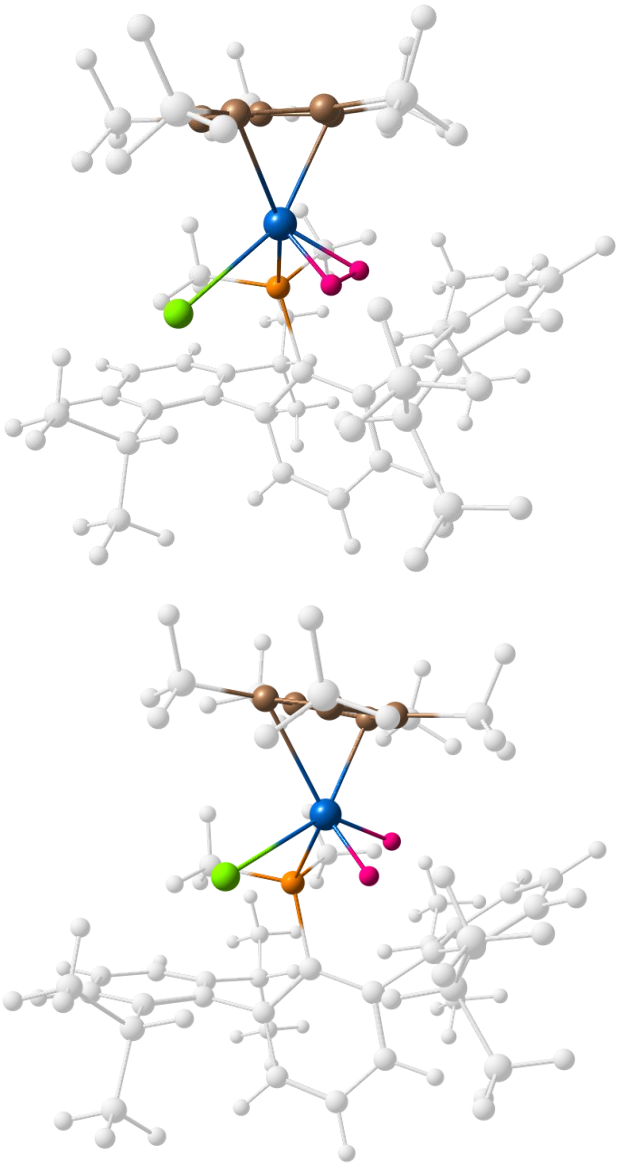

Figure 67. Calculated molecular geometries of **2(Dipp)(H$_2$)$^+$** and **2(Dipp)(H)$_2^+$**.

When solutions of complex **2(Dipp)$^+$** were allowed to react with 1 bar of H_2 at room temperature overnight, irreversible changes were clearly noticed. Thus, the color of the solution varied from the initial dark brown

to yellow-red. Besides, the ^{1}H NMR spectrum revealed the formation of a new hydride complex, **7(Dipp)$^{+}$**, responsible for the appearance of a doublet resonance at −18.3 ppm ($^{2}J_{HP}$ = 39 Hz). Once more, the ^{31}P{^{1}H} NMR spectrum of the new complex is simple, as it contains a singlet at −3.3 ppm. Note, however, that at variance with **2(Dipp)(H)$_2$$^{+}$**, the Δδ value is now of about 38 ppm, suggesting the P-coordination to iridium is complemented by Ir−C_{arene} binding to one of the side Dipp rings.[65] In agreement with this assumption, the four ^{i}Pr substituents of the Dipp rings are non-equivalent, as evidenced, for instance, by the observation of four multiplets at 2.42, 2.31, 2.19 and 1.21 ppm, the latter overlapping partially with one of the eight methyl doublets arising from the *iso*-propyl terphenyl substituents. The existence of an (η^5-C_5Me_5)Ir moiety in complex **7(Dipp)$^{+}$** can be inferred beyond any doubt from the observation of a doublet resonance centered at 1.45 ppm, with relative intensity corresponding to 15H and $^{4}J_{HP}$ = 1 Hz. Since a close analysis of the reaction mixture demonstrated the presence of by-products [(η^5-C_5Me_5)$IrCl_2$]$_2$ and [$HPMe_2Ar^{Dipp}_2$]BAr_F, it can be proposed that provided that a sufficient reaction time is given to **2(Dipp)$^{+}$**-plus-H_2 mixtures, elimination of HCl occurs, yielding the above side products along with the mono-hydride [(η^5-C_5Me_5)Ir(H)($PMe_2Ar^{Dipp}_2$)]$^{+}$, **7(Dipp)$^{+}$**. Scheme 22 summarizes the chemical evolution of CH_2Cl_2 solutions of **2(Dipp)$^{+}$** in the presence of H_2.

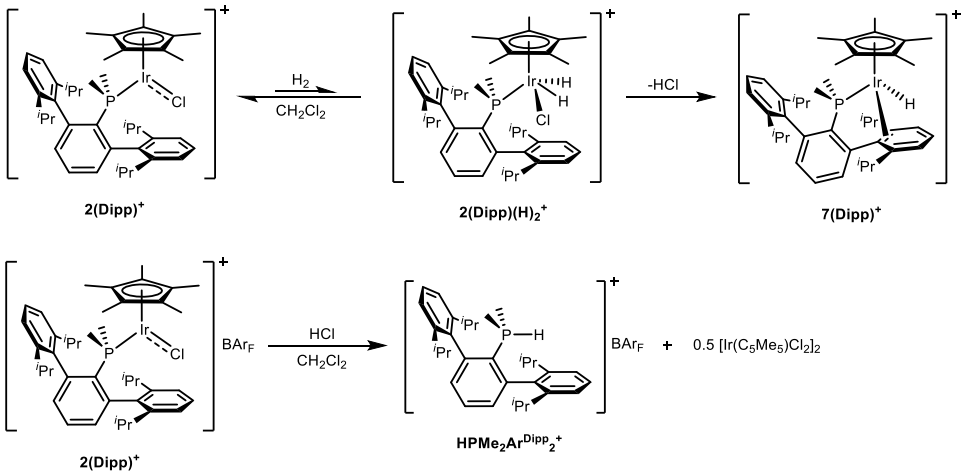

Scheme 22. Evolution of **2(Dipp)**$^+$ under a H_2 atmosphere.

The intrinsic complexity of the reaction just discussed justifies generation of complex **7(Dipp)**$^+$ in very low yields, making difficult its isolation from crude reaction mixtures. Accordingly, an alternative, direct route to **7(Dipp)**$^+$ was sought. Given that in a formal sense generation of **7(Dipp)**$^+$ from **2(Dipp)**$^+$ involves simply converting the Ir−Cl bond of the latter into the Ir−H bond of the former, the reaction of **[2(Dipp)]BAr$_F$** with $PhSiH_3$ was performed, allowing isolation of **[7(Dipp)]BAr$_F$** in very high yields (90 %) as a yellow solid. Crystals of this compound suitable for X-Ray studies were isolated by slow evaporation of a saturated dichloromethane-hexane solvent mixture.

Before describing the solid-state structure of the molecules of **7(Dipp)**$^+$ some additional comments on the spectroscopic properties seem appropriate. Apart from the already cited ^{1}H NMR resonance at −18.3 ppm, the Ir−H unit gives rise to a medium-intensity IR absorption at 2306 cm^{-1}. The also mentioned inequivalence of the phosphine Dipp rings imposed by the existence of Ir−C_{arene} interactions involving one of these substituents, can also be deduced from the scalar coupling values found for

the *meta* protons of the coordinated aryl substituent with the corresponding *para* hydrogen atom. Thus, the fixed configuration of double and single C−C bonds within this ring leads to values of 6.4 (*m*) and 8.7 (*m*') Hz, instead of the typical 7.6 Hz coupling constant. In addition, the $^{13}C\{^{1}H\}$ resonance of the coordinated *ipso* carbon appears at 96.3 ppm, i.e. 39.7 ppm shifted to lower frequencies compared to its non-coordinated counterpart. Moreover, the also coordinated *ortho* carbon resonates at 101.4 ppm, whereas δ values for *o*-Dipp' and *o*-Dipp carbon atoms are 152.3, 147.6 and 146.9 ppm. All these data strongly support η^2-coordination of a side Dipp ring.

X-Ray crystallography (Figure 68) provided definitive confirmation of the proposed structural assignment. **7(Dipp)**$^+$ features an Ir−H bond distance of 1.48(4) Å, whereas the bound Ir−C_{ipso} and Ir−C_{ortho} bonds have lengths of 2.342(4) and 2.361(4) Å, respectively. These bond distances, along with the lack of exchange observed by NMR and the significant quaternarization observed for the bound *ipso* and *ortho* carbon atoms suggest a strong interaction of the arene with the metal center. The localization of the electron density of the π-bond in the arene-metal bond could also be reflected in the remarkable upfield shift of the proximal C*H*Me_2 (1.21 ppm, *cf*. the 2.3 ppm average value for the other C*H*Me_2 protons).

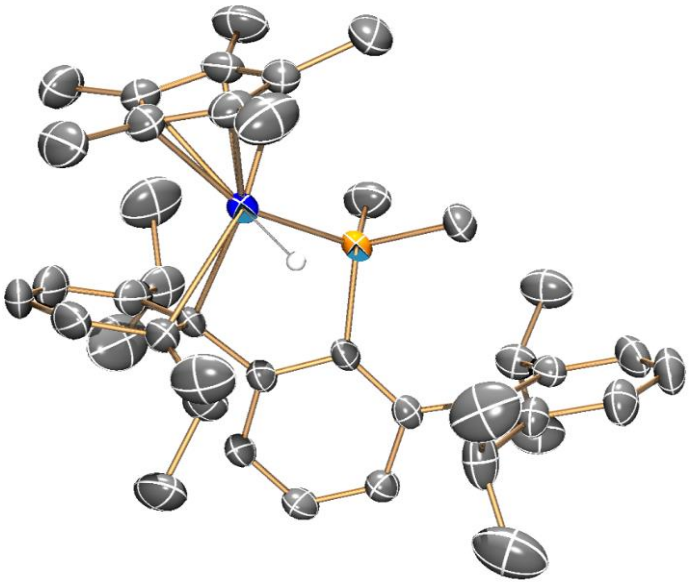

Figure 68. ORTEP diagram of the cation of complex **7(Dipp)**$^{+}$. Non-relevant hydrogen atoms are excluded for clarity and thermal ellipsoids are set at 50 % probability.

I.2.6 Transition Metal Only Frustrated Lewis Pair Reactivity

The past decade witnessed the emergence of Frustrated Lewis Pair (FLP) chemistry, which enabled main-group compounds to activate small molecules through reactivity patterns once believed to be exclusive of transition metals.[97]. Notwithstanding these remarkable advances, the reluctance of main group elements to partake in fundamental organometallic reactions such as oxidative addition or reductive elimination, has prevented a wider use of FLPs in catalysis. Accordingly, integrating Lewis basic and Lewis acidic transition metal complexes as FLP components seems to be a promising approach to increase their catalytic potential. Fundamental breakthroughs achieved by the groups of Wass,[98] Erker,[99] and Bourissou,[100] among others, paved the way for the recent development of a FLP solely constructed around transition metal complexes[64] (Figure 69). The latter, comprising as constituents Au(I) and Pt(0) neutral phosphine complexes, displayed typical FLP behavior towards acetylene, yielding vinylene and acetylide complexes, and against

[97] Stephan, D. W. *Acc. Chem. Res.*, **2015**, *48*, 306.
[98] a) Forrest, S. J. K.; Clifton, J.; Fey, N.; Pringle, P. G.; Sparkes, H. A.; Wass, D. F. *Angew. Chem. Int. Ed.* **2015**, *54*, 2223; b) Metters, O. J.; Forrest, S. J. K.; Sparkes, H. A.; Manners, I.; Wass, D. F. *J. Am. Chem. Soc.* **2016**, *138*, 1994; c) Metters, O. J.; Flynn, S. R.; Dowds, C. K.; Manners, I. Wass, D. F. *ACS Catal.* **2016**, *6*, 6601.
[99] a) Xu, X.; Kehr, G.; Daniliuc, C. G.; Erker, G. *J. Am. Chem. Soc.* **2014**, *136*, 12431; b) Xu, X.; Kehr, G.; Daniliuc, C. G.; Erker, G. *Organometallics* **2015**, *34*, 2655; c) Xu, X.; Kehr, G.; Daniliuc, C. G.; Erker, G. *J. Am. Chem. Soc.* **2015**, *137*, 4550; d) Normand, A. T.; Richard, P.; Balan, C.; Daniliuc, C. G.; Kehr, G.; Erker, G.; Le Gendre, P. *Organometallics* **2015**, *34*, 2000; e) Normand, A. T.; Daniliuc, C. G.; Wibbeling, B.; Kehr, G.; Le Gendre, P.; Erker, G. *J. Am. Chem. Soc.* **2015**, *137*, 10796.
[100] a) Devillard, M.; Bouhadir, G.; Bourissou, D. *Angew. Chem. Int. Ed.* **2015**, *54*, 730; b) Devillard, M.; Declercq, R.; Nicolas, E.; Ehlers, A. W.; Backs, J.; Saffon-Merceron, N.; Bouhadir, G.; Slootweg, J. C.; Uhl, W.; Bourissou, D. *J. Am. Chem. Soc.* **2016**, *138*, 4917.

dihydrogen, achieving in this case the heterolytic cleavage of this simple molecule.

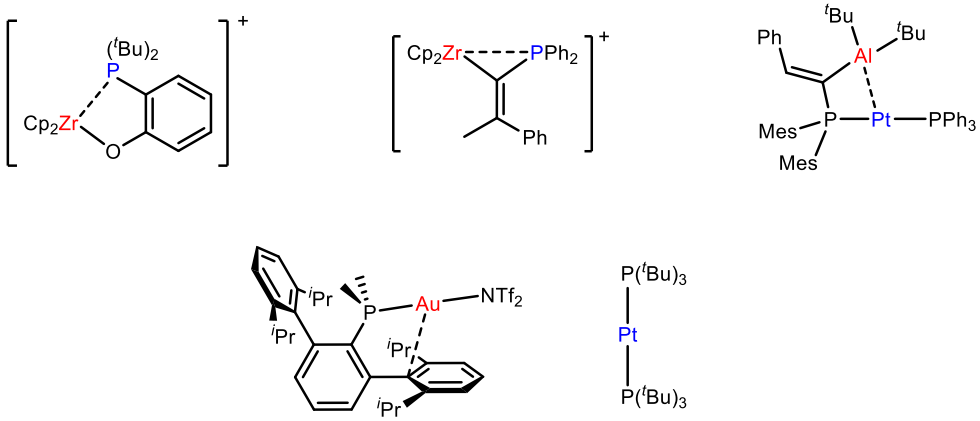

Figure 69. Frustrated Lewis Pairs including transition metal centers reported by the groups of Wass(left), Erker (center), Bourissou (right) and our group (bottom).

To contribute to this emerging field, we selected **2(Dipp)**$^+$ as a bulky Lewis acid fragment, given not only the characteristic chemistry disclosed in previous sections, but also the known electrophilic character of cationic Ir(III) complexes, particularly in low-coordination environments.[101] We decided to combine this compound with Pt(P^tBu_3)$_2$, whose basic behavior has already been exploited by our group,[64] with the aim of constructing a Transition Metal Only Frustrated Lewis Pair (TMOFLP). Although metal-metal bonded heterobimetallic species can display cooperative activation of small molecules[102] and even catalyze relevant processes,[103] enhanced reactivity is expected for non-bonded systems.[104]

[101] Cleary, B. P.; Eisenberg, R. *Inorganica Chim. Acta* **1995**, *240*, 135.
[102] a) Jayarathne, U.; Parmelee, S. R.; Mankad, N. P. *Inorg. Chem.* **2014**, *53*, 7730; b) Zhang, H.; Wu, B.; Marquard, S. L.; Litle, E. D.; Dickie, D. A.;

In our case, the bulkiness of the phosphine ligands that stabilize both the iridium and platinum fragments prevented the formation of a metal-only Lewis adduct, as no broadening nor chemical shift changes were apparent in the NMR spectra upon mixing **2(Dipp)**$^+$ and Pt(P^tBu_3)$_2$. Nevertheless, in the presence of **2(Dipp)**$^+$ Pt(P^tBu_3)$_2$ displayed Brönsted basicity so that **4(Dipp)**$^+$ was formed along with PtHCl(P^tBu_3)$_2$. After a sufficiently long reaction time, the former evolved further to **3(Dipp)**$^+$ (Scheme 23). The acid-base reaction was however slow at room temperature ($t_{1/2}$ ≈ 2 h, 25 ºC, Figure 70), particularly when compared to the use of Et_3N as the base ($t_{1/2}$ ≈ 0.5 h, −20 ºC) permitting the study of the FLP behaviour of the system.

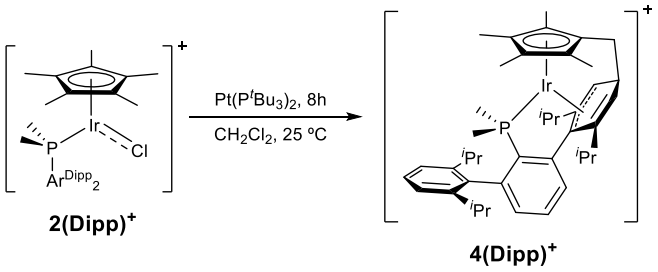

Scheme 23. Brönsted acid-base reactivity of **2(Dipp)**$^+$ and Pt(P^tBu_3)$_2$.

Bezpalko, M. W.; Foxman, B. M.; Thomas, C. M. *Organometallics*, **2017**, *36*, 3498; c) Poitras, A. M.; Knight, S. E.; Bezpalko, M. W.; Foxman, B. M.; Thomas, C. M. *Angew. Chem. Int. Ed.* **2018**, *57*, 1497.

[103] a) Mazzacano, T. J.; Mankad, N. P. *J. Am. Chem. Soc.* **2013**, *135*, 17258; b) Wu, B.; Gramigna, K. M.; Bezpalko, M. W.; Foxman, B. M.; Thomas, C. M. *Inorg. Chem.* **2015**, *54*, 10909; c) Karunananda, M. K.; Mankad, N. P. *J. Am. Chem. Soc.* **2015**, *137*, 14598; d) Pye, D. R.; Cheng, L.-J.; Mankad, N. P. *Chem. Sci.* **2017**, *8*, 4750; e) Coombs, J.; Perry, D.; Kwon, D.-H.; Thomas, C. M.; Ess, D. H. *Organometallics*, **2018**, *37*, 4195.

[104] Johnstone, T. C.; Wee, G. N. J. H.; Stephan, D. W. *Angew. Chem. Int. Ed.* **2018**, *57*, 5881.

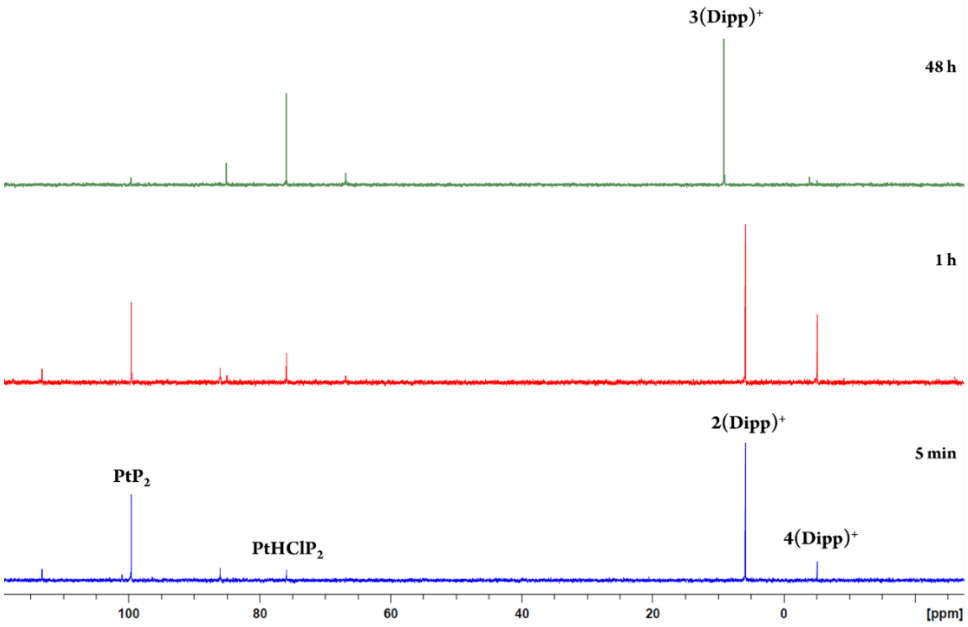

Figure 70. Room temperature evolution of **2(Dipp)**$^+$ and Pt(P^tBu_3)$_2$.

DFT calculations confirmed that the Pt-mediated deprotonation of the C_5Me_5 of **2(Dipp)**$^+$ was indeed feasible, displaying a barrier of 20.8 kcal/mol (ΔG_{50}) relative to the separated fragments (Figure 71). This study also supports the fact that the reaction with the platinum proceeds at a slower rate, since the barrier for the deprotonation by NEt_3 is noticeable smaller (17.4 kcal/mol).

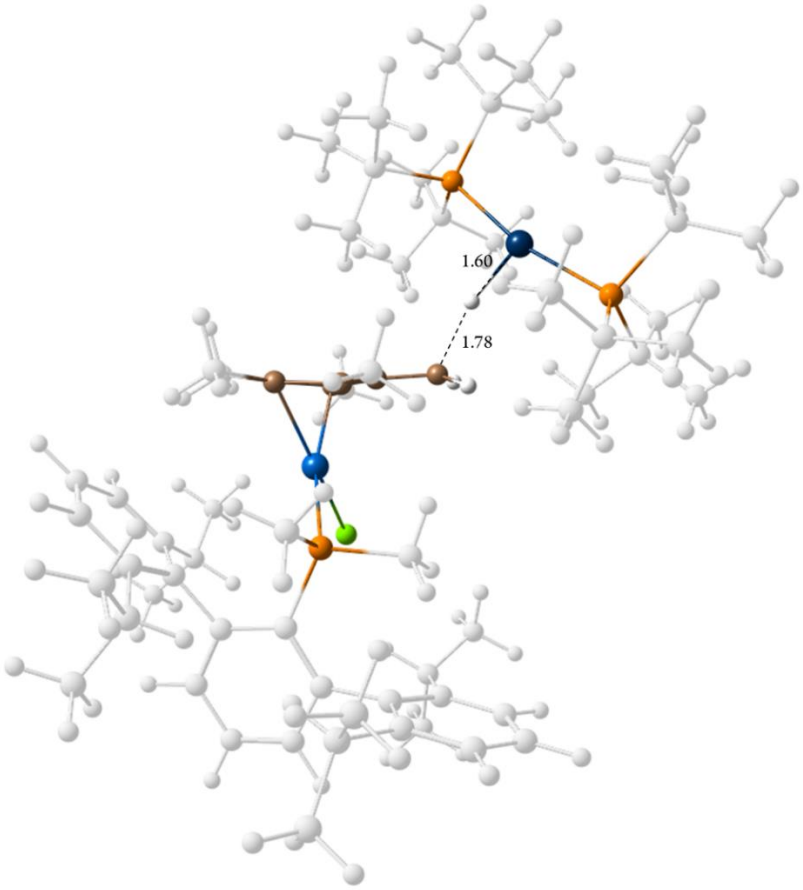

Figure 71. Molecular geometry of the transition state for the Pt-mediated C_5Me_5 deprotonation.

In contrast with the aforementioned Au(I)−Pt(0) system,[64] no cooperative activation of acetylene was registered with this Ir(III)−Pt(0) FLP and polyacetylene was the only reaction product. A different behavior was observed for H_2. Charging a CD_2Cl_2 solution of the FLP with H_2 promoted evident chemical changes, as evinced by a fast color change from dark brown to yellow. $^{31}P\{^1H\}$ and ^1H NMR analysis of the reaction mixture permitted the identification of **7(Dipp)**$^+$ and $PtHCl(P^tBu_3)_2$ as the final products of the reaction. $[PtH(P^tBu_3)_2]^+$ and a hydride-containing iridium

complex were spotted as intermediates, the latter being tentatively assigned as the neutral complex (η^5-C_5Me_5)Ir(Cl)(H)($PMe_2Ar^{Dipp}{}_2$), **2(Dipp)H** (Scheme 24 and Figure 72).

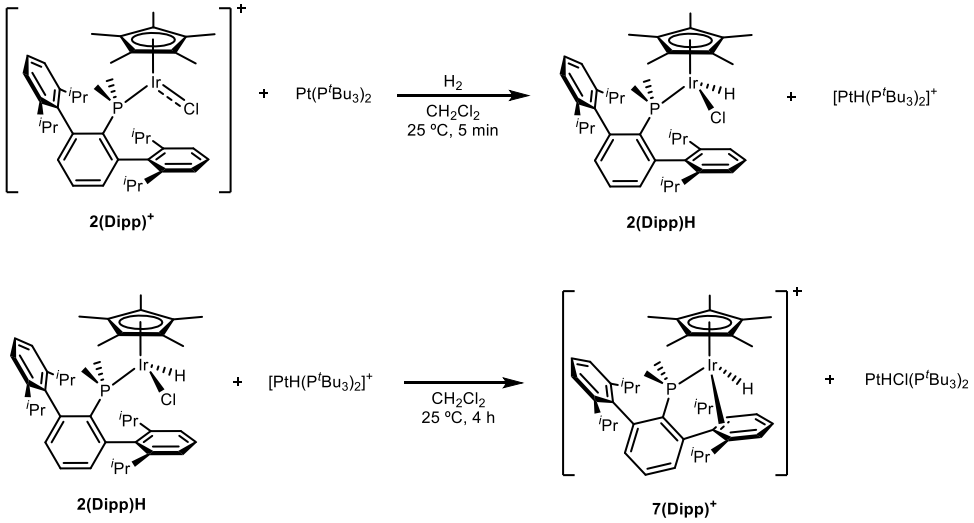

Scheme 24. Cooperative activation of H_2 by **2(Dipp)**$^+$ and Pt(P^tBu_3)$_2$.

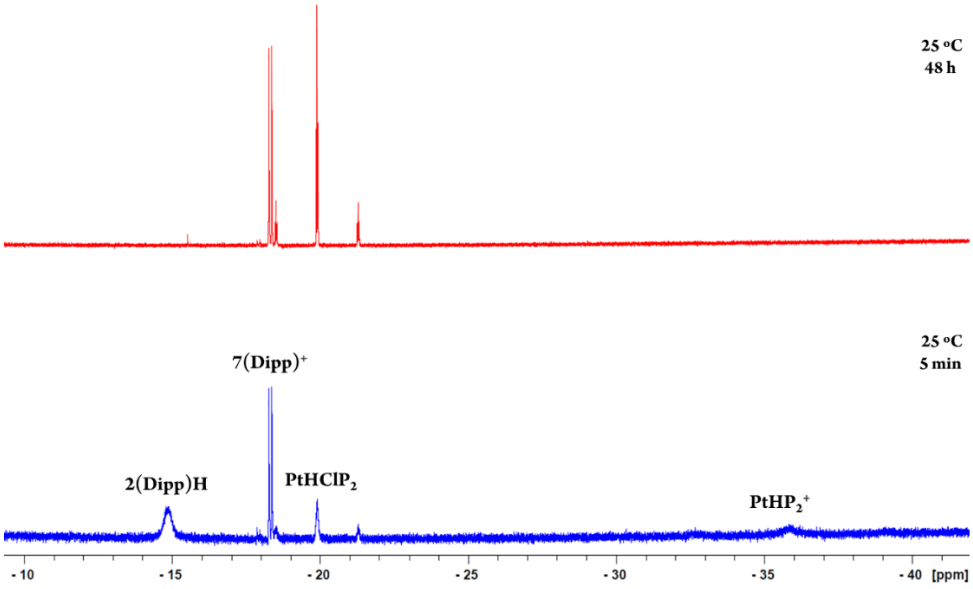

Figure 72. Hydridic region of the ^{1}H NMR spectrum corresponding to the room temperature heterolytic H_2 splitting by the Ir(III)-Pt(0) TMOFLP.

The cooperative activation of H_2 by the bimetallic pair becomes evident on the basis of the following facts. First, $Pt(P^tBu_3)_2$ does not react with H_2 in benzene, whereas in dichloromethane it reacts very slowly to form $PtHCl(P^tBu_3)_2$ and *trans*-$PtH_2(P^tBu_3)_2$. Furthermore, the rate of the reaction of **2(Dipp)**$^+$ with dihydrogen to yield **7(Dipp)**$^+$ and HCl was much slower than the one observed for the heterolytic splitting of H_2 at the Ir(III)−Pt(0) FLP. On these grounds, we decided to compute several alternative and cooperative mechanistic pathways to account for this reactivity. Among the potential mechanisms that will be discussed herein we were able to locate transition states for an FLP-like activation of H_2 (Figure 73, up) and for the Pt-mediated deprotonation of **2(Dipp)(H)$_2$**$^+$ (Figure 73, bottom).

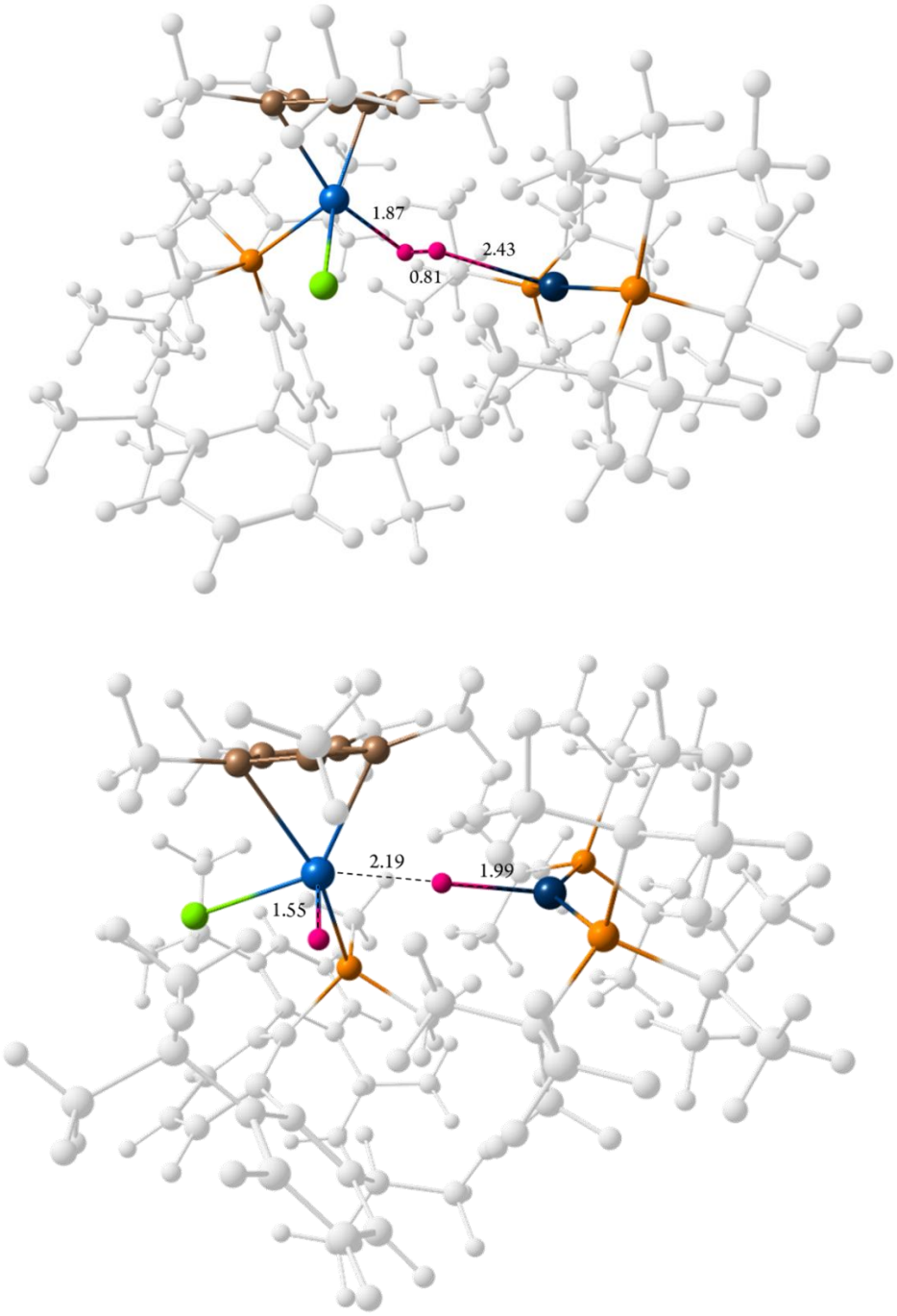

Figure 73. Molecular geometries of the transition states for the FLP H_2 splitting (up) and the Pt-mediated deprotonation of **2(Dipp)(H)**$_2^+$ (bottom).

The barrier associated to the Pt-mediated deprotonation of the Ir(V) dihydride is 37.5 kcal/mol (ΔG_{50}, relative to the isolated fragments) and therefore this pathway can be disregarded. The TS for an FLP-like cooperative activation was located at 23.2 kcal/mol, but the remarkable difference (38.6 kcal/mol) found between SCF and Gibbs free energies casts doubt on the accuracy of this result, which is heavily reliant on the G_{50} approximation.[105] With the aim of getting kinetic data relative to the H_2 splitting, the reaction was monitored by means of low temperature $^{31}P\{^1H\}$ and ^1H NMR (Figure 74). This study revealed that, at −30 ºC, **2(Dipp)**$^+$ catalyzes the hydrogenation of $Pt(P^tBu_3)_2$ to yield *trans*-$PtH_2(P^tBu_3)_2$. The latter further reacts with **2(Dipp)**$^+$, transferring a hydride to give $[PtH(P^tBu_3)_2]^+$ and **2(Dipp)H**, a neutral hydride, as the only detectable products at −15 ºC. Anion exchange to generate $PtHCl(P^tBu_3)_2$ and **7(Dipp)**$^+$ required approximately 5 hours at room temperature to reach completion.

[105] a) Kua, J.; Krizner, H. E.; De Haan, D. O. *J. Phys. Chem. A* **2011**, *115*, 1667; b) Han, L.-L.; Li, S.-J.; Fang, D.-C. *Phys. Chem. Chem. Phys.* **2016**, *18*, 6182.

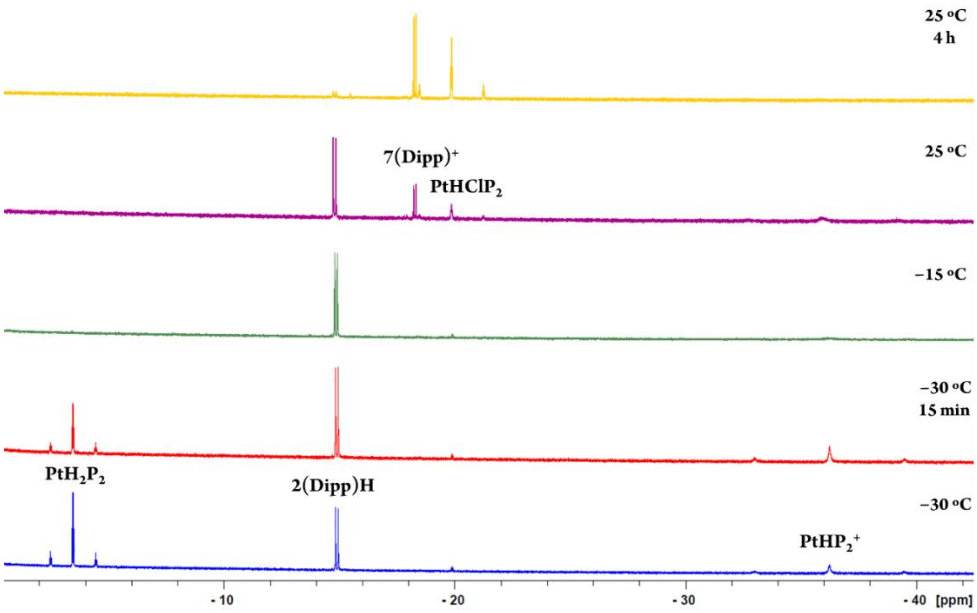

Figure 74. Hydride region (*ca*. 0 to −40 ppm) of the ^{1}H NMR spectrum corresponding to the low-temperature NMR monitoring of the reaction between the Ir(III)-Pt(0) TMOFLP and H_2.

To gain a better understanding of the system, the hydrogenation of $Pt(P^tBu_3)_2$ was studied computationally[106] (Figure 75). Oxidative addition of dihydrogen (13.9 kcal/mol) gives *cis*-$PtH_2(P^tBu_3)_2$ at 7.8 kcal/mol, whereas its conversion to the *trans* isomer requires surmounting a barrier of 36.7 kcal/mol. Therefore, this reaction cannot be observed at room temperature.

[106] Calculations were performed with the Gaussian 09 program employing the long-range-corrected hybrid functional ωB97XD. Geometry optimizations were carried out without geometry constraints and included solvent (benzene). 50%-corrected free energy variations (ΔG_{50}°) were employed to account for translational entropy overestimation.

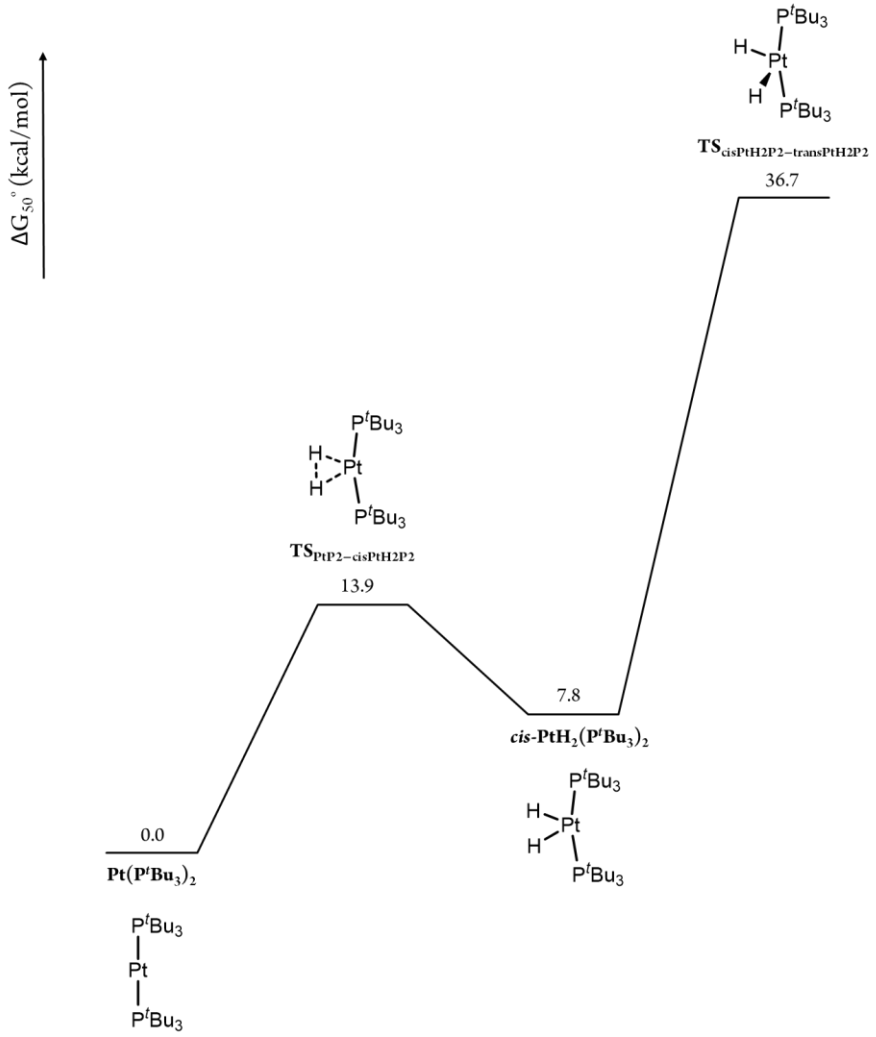

Figure 75. ΔG_{50}° profile for the formation and isomerization of *cis*-$PtH_2(P^tBu_3)_2$.

On these grounds, it seems reasonable to propose that **2(Dipp)**$^+$ might be lowering the barrier for the *cis-trans* isomerization of the accessible *cis*-$PtH_2(P^tBu_3)_2$. Although a transition state for this process could not be located with **2(Dipp)**$^+$, however, DFT calculations performed for a related terphenyl phosphine gold system revealed that the isomerization barrier

could be significantly lowered to 23.7 kcal/mol (ΔG_{50}), relative to the experimentally detected Au-Pt Lewis adduct and H_2 (Figure 76).

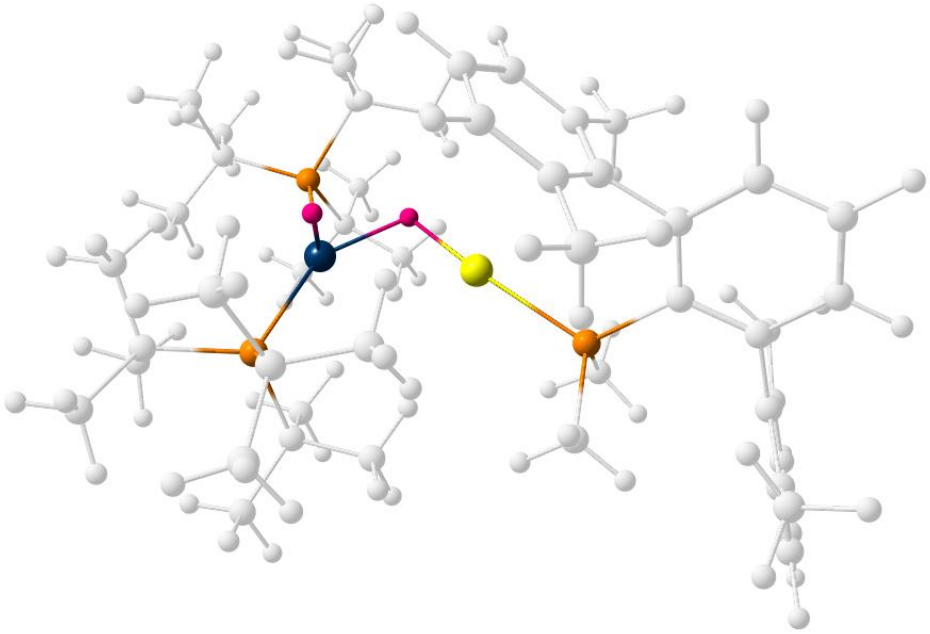

Figure 76. Molecular geometry of the TS associated with transition-metal Lewis-acid ($AuPMe_2Ar^{Xyl}{}_2^+$) facilitated isomerization of *cis*-$PtH_2(P^tBu_3)_2$.

Brönsted-acid mediation can also be envisioned, for under the reaction conditions, formation of **2(Dipp)(H)$_2^+$** could result in the generation of catalytic amounts of HCl. Under an atmosphere of H_2 the latter might facilitate formation of $[PtH_3(P^tBu_3)_2^+]Cl$ (Scheme 25).[107] Then, chloride-mediated deprotonation of the σ-H_2 moiety would give the thermodynamic *trans* isomer of $PtH_2(P^tBu_3)_2$, thus regenerating HCl.

[107] Gusev, D. G.; Notheis, J. U.; Rambo, J. R.; Hauger, B. E.; Eisenstein, O.; Caulton, K. G. *J. Am. Chem. Soc.* **1994**, *116*, 7409.

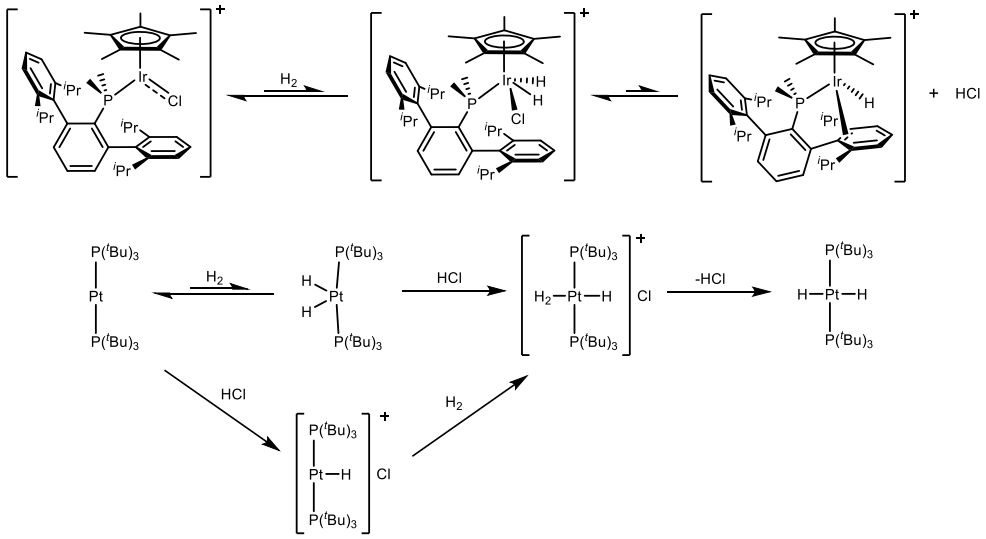

Scheme 25. Proposed mechanism for the formation of *trans*-$PtH_2(P^tBu_3)_2$.

I.2.7 Summary and Conclusions

El uso de fosfinas voluminosas de terfenilo ha permitido el aislamiento de complejos catiónicos e insaturados de Ir(III), que participan en activación C−H remota por medio de intermedios dicatiónicos. En presencia de una base de Brönsted, el carácter no inocente del ligando C_5Me_5 se ha puesto de manifiesto, ya que su fácil desprotonación promueve su participación en varios procesos, incluyendo reacciones de formación reversible de enlace C−C y activación C−H. Los cálculos DFT revelan que el centro metálico participa de manera indirecta por medio de ciclos redox Ir(I)−Ir(III). El ligando C_5Me_5 también muestra una notable electrofilia en la reacción del complejo de cloruro con LiMe. La reactividad de este complejo insaturado de Ir frente a H_2 también se exploró, incluyendo su potencial carácter como ácido de Lewis en Pares de Lewis Frustrados compuestos Solo por Metales de Transición.

The use of bulky terphenyl phosphine ligands has permitted the isolation of cationic, unsaturated chloride complexes of Ir(III), which participate in remote C−H activation reactions through dicationic intermediates. In the presence of a Brönsted base, a non-innocent behavior of the C_5Me_5 ligand has been disclosed, as its facile deprotonation promotes its involvement in several processes, including reversible C−C bond formation and C−H activation reactions. DFT calculations reveal that the metal center participates in an indirect fashion by means of Ir(I)−Ir(III) redox cycles. The C_5Me_5 ligand also displays remarkable electrophilicity in the reaction of the chloride complex with LiMe. The reactivity of this unsaturated Ir complex towards H_2 was also explored, including its potential Lewis acid behavior in a Transition Metal Only Frustrated Lewis Pair.

I.3 EXPERIMENTAL SECTION

I.3.1 General Considerations

All manipulations were carried out using standard Schlenk techniques, under high purity nitrogen. All solvents were dried and distilled under nitrogen prior to use. *n*-Pentane (C_5H_{12}) and *n*-hexane (C_6H_{14}) were distilled over sodium. Diethyl ether was distilled over sodium/benzophenone. CH_2Cl_2 and CD_2Cl_2 were dried over CaH_2. THF-d_8 was dried over 4 Å molecular sieves. $[Ir(C_5Me_5)Cl_2]_2$,[108] $NaBAr_F$,[109] $PtP(^tBu_3)_2$[110] and PMe_2Ar'[111] were prepared according to literature methods. All cationic complexes were isolated as salts of the BAr_F anion. NEt_3 was commercially available and used as received. Solution NMR spectra were recorded on Bruker AMX-300, DRX-400 and DRX-500 spectrometers. Spectra were referenced to external $SiMe_4$ (δ: 0 ppm) using the residual proton solvent peaks as internal standards (^{1}H NMR experiments), or the characteristic resonances of the solvent nuclei (^{13}C NMR experiments), while ^{31}P was referenced to H_3PO_4. Spectra recorded in the 300 MHz present an artifact at −23.9 ppm. Spectral assignments were made by routine one- and two-dimensional NMR experiments (^{1}H, ^{1}H{^{31}P}, ^{13}C{^{1}H}, ^{31}P{^{1}H}, COSY, NOESY, HSQC and HMBC) where appropriate. For elemental analyses a LECO TruSpec CHN elementary analyzer was utilized.

---

[108] White, C.; Yates, A.; Maitlis, P. M.; Heinekey, D. M. *Inorg. Synth.* **1992**, *29*, 228.
[109] Yakelis, N. A.; Bergman, R. G. *Organometallics* **2005**, *24*, 3579.
[110] Goel, R. G.; Ogini, W. O.; Srivastava, R. C. *J. Organomet. Chem.* **1981**, *214*, 405.
[111] a) Campos, J.; Ortega-Moreno, L.; Conejero, S.; Peloso, R.; López-Serrano, J.; Maya, C.; Carmona, E. *Chem. Eur. J.* **2015**, *21*, 8883; b) Ortega-Moreno, L.; Peloso, R.; Maya, C.; Suárez, A.; Carmona, E. *Chem. Commun.* **2015**, *51*, 17008.

Calculations were performed at the DFT level with the Gaussian 09 (Revision D.01) program.[112] The hybrid functionals PBE0[113] and ωB97XD[114] were used throughout the computational study. Dispersion effects were accounted for by using Grimme's D3 parameter set with Becke−Johnson (BJ) damping.[115] Geometry optimizations were carried out without geometry constraints, using the 6-31G(d,p)[116] basis set to represent the C, H, P, Cl and N atoms and the Stuttgart/Dresden Effective Core Potential and its associated basis set (SDD)[117] to describe the Ir, Pt and Au atoms. Bulk solvent effects (dichloromethane, diethylether, benzene) were included at the optimization stage with the SMD continuum model.[118] The stationary points and their nature as minima or saddle points (TS) were characterized by vibrational analysis, which also produced

[112] Frisch, M. J.; Trucks, G. W.; Schlegel, H. B.; Scuseria, G. E.; Robb, M. A.; Cheeseman, J. R.; Scalmani, G.; Barone, V.; Mennucci, B; Petersson, G. A.; Nakatsuji, H.; Caricato, M.; Li, X.; Hratchian, H. P.; Izmaylov, A. F.; Bloino, J.; Zheng, G.; Sonnenberg, J. L.; Hada, M.; Ehara, M.; Toyota, K.; Fukuda, R.; Hasegawa, J.; Ishida, M.; Nakajima, T.; Honda, Y.; Kitao, O.; Nakai, H.; Vreven, T.; Montgomery, J. A. J.; Peralta, J. E.; Ogliaro, F.; Bearpark, M.; Heyd, J. J.; Brothers, E.; Kudin, K. N.; Staroverov, V. N.; Kobayashi, R.; Normand, J.; Raghavachari, K.; Rendell, A.; Burant, J. C.; Iyengar, S. S.; Tomasi, J.; Cossi, M.; Rega, N.; Millam, J. M.; Klene, M.; Knox, J. E.; Cross, J. B.; Bakken, V.; Adamo, C.; Jaramillo, J.; Gomperts, R.; Stratmann, R. E.; Yazyev, O.; Austin, A. J.; Cammi, R.; Pomelli, C.; Ochterski, J. W.; Martin, R. L.; Morokuma, K.; Zakrzewski, V. G.; Voth, G. A.; Salvador, P.; Dannenberg, J. J.; Dapprich, S.; Daniels, A. D.; Farkas, O.; Foresman, J. B.; Ortiz, J. V.; Cioslowski, J.; Fox, D. J.; Gaussian 09, Revision D.01, Gaussian, Inc.: Wallingford CT, **2013**.

[113] Perdew, J. P.; Burke, K.; Ernzerhof, M. *Phys. Rev. Lett.* **1996**, *77*, 3865.

[114] Chai, J.-D.; Head-Gordon, M. *Phys. Chem. Chem. Phys.* **2008**, *10*, 6615.

[115] Grimme, S.; Antony, J.; Ehrlich, S.; Krieg, H. *J. Chem. Phys.* **2010**, *132*, 154104.

[116] a) Hehre, W. J.; Ditchfield, R.; Pople, J. A. *J. Phys. Chem.* **1972**, *56*, 2257; b) Hariharan, P. C.; Pople, J. A. *Theor. Chim. Acta.* **1973**, *28*, 213; c) Francl, M. M.; Pietro, W. J.; Hehre, W. J.; Binkley, J. S.; Gordon, M. S.; Defrees, D. J.; Pople, J. A. *J. Chem. Phys.* **1982**, *77*, 3654.

[117] Andrae, D.; Haeussermann, U.; Dolg, M.; Stoll, H.; Preuss, H. *Theor. Chim. Acta* **1990**, *77*, 123.

[118] Marenich, A. V.; Cramer, C. J.; Truhlar, D. G. *J. Phys. Chem. B* **2009**, *113*, 6378.

enthalpy (H), entropy (S) and Gibbs energy (G) data at 298.15 K. The minima connected by a given transition state were determined by Intrinsic Reaction Coordinate (IRC) calculations or by perturbing the transition states along the TS coordinate and optimizing to the nearest minimum. 50%-corrected free energy variations ($\Delta G50^{o}$), employed to account for translational entropy overestimation,[105,119] were found to be in best agreement with experimental findings. Localized molecular orbital studies were carried out following the Pipek-Mezey criterion[120] and the procedure described by Vidossich and Lledós.

[119] a) Ríos, P.; Rodríguez, A.; López-Serrano, J. *ACS Catal.* **2016**, *6*, 5715; b) Deubel, D. V. *J. Am. Chem. Soc.* **2008**, *130*, 665.
[120] Pipek, J.; Mezey, P.G. *J. Chem. Phys*. **1989**, *90*, 4916.

I.3.2 Synthesis and Characterization of New Complexes

Complex 1(Xyl)

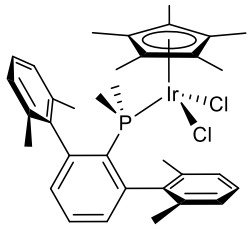

A solid mixture of $[IrCp^*Cl_2]_2$ (79.7 mg, 0.100 mmol) and $PMe_2Ar^{Xyl}{}_2$ (70.0 mg, 0.202 mmol) was dissolved in dry CH_2Cl_2 (10 mL) in a Schlenk flask provided with a stir bar. The reaction mixture was stirred for 30 min, yielding an orange solution. The solvent was then removed in vacuo and the product washed 3 times with 5 mL of pentane, to yield compound **1(Xyl)** as an analytically pure, air-stable orange solid (136.6 mg, 92%).

Anal. Calcd. for $C_{34}H_{42}Cl_2IrP$: C, 54.83; H, 5.68. **Found**: C, 54.74; H, 5.63.

^{1}H NMR (300 MHz, CD_2Cl_2, 25 ºC) δ: 7.43 (td, $^3J_{HH}$ = 7.6 Hz, $^5J_{HP}$ = 2.2 Hz, 1H, *p*-C_6H_3), 7.14 (t, $^3J_{HH}$ = 7.3 Hz, 2H, *p*-Xyl), 7.09 (br d, $^3J_{HH}$ = 6.6 Hz, 2H, *m*-Xyl), 6.96 (dd, $^3J_{HH}$ = 7.5 Hz, $^4J_{HP}$ = 2.7 Hz, 2H, *m*-C_6H_3), 6.94 (overlapped br d, $^3J_{HH} \approx 7$ Hz, 2H, *m*-Xyl), 2.48 (s, 6H, Me_{Xyl}), 1.89 (s, 6H, Me_{Xyl}), 1.39 (d, $^4J_{HP}$ = 2.0 Hz, 15H, C_5Me_5), 1.29 (d, $^2J_{HP}$ = 9.9 Hz, 6H, PMe_2).

^{13}C{^{1}H} NMR (100 MHz, CD_2Cl_2, 25 ºC) δ: 146.5 (d, $^2J_{CP}$ = 8 Hz, *o*-C_6H_3), 143.2 (*ipso*-Xyl), 138.6 (br, *o*-Xyl), 137.8 (*o*-Xyl), 131.3 (d, $^3J_{CP}$ = 9 Hz, *m*-C_6H_3), 130.2 (d, $^4J_{CP}$ = 2 Hz, *p*-C_6H_3), 129.5 (d, $^1J_{CP}$ = 38 Hz, *ipso*-C_6H_3), 128.6 (*m*-Xyl), 127.6 (*p*-Xyl), 126.6 (*m*-Xyl), 92.0 (d, $^2J_{CP}$ = 3

Hz, C_5Me_5), 24.4 (br, Me_{Xyl}), 22.1 (Me_{Xyl}), 19.0 (d, $^1J_{CP}$ = 36 Hz, PMe_2), 9.3 (C_5Me_5).

$^{31}P\{^1H\}$ NMR (120 MHz, CD_2Cl_2, 25 ºC) δ: −29.9.

Complex 2(Xyl)$^+$

To a CH_2Cl_2 solution (5 mL) of complex **1(Xyl)** (74.5 mg, 0.100 mmol) cooled to −20 ºC was added a $NaBAr_F$ dispersion in CH_2Cl_2 (88.6 mg, 0.100 mmol, 10 mL). The mixture was stirred at this temperature until a dark coloration fully developed (*ca.* 20 min). The solution was then filtered and the solvent evaporated under reduced pressure at −20 ºC The residue was washed with pentane (5 mL) to obtain the desired complex as a dark reddish solid (135.4 mg, 86%) Single crystals were grown from a saturated hexane-dichloromethane solution at −32 ºC.

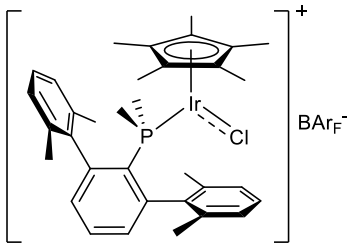

Anal. Calcd. for $C_{66}H_{54}BF_{24}ClIrP$: C, 50.41; H, 3.46. **Found**: C, 50.18; H, 3.32.

^{1}H NMR (400 MHz, CD_2Cl_2, 25 ºC) δ: 7.72 (s, 8H, *o*-Ar), 7.56 (s, 4H, *p*-Ar), 7.54 (td, $^3J_{HH}$ = 7.6 Hz, $^5J_{HP}$ = 2.1 Hz, 1H, *p*-C_6H_3), 7.38 (t, $^3J_{HH}$ = 7.6 Hz, 2H, *p*-Xyl), 7.12 (d, $^3J_{HH}$ = 7.6 Hz, 4H, *m*-Xyl), 6.93 (dd, $^3J_{HH}$ = 7.6 Hz, $^4J_{HP}$ = 3.4 Hz, 2H, *m*-C_6H_3), 2.00 (s, 12H, Me_{Xyl}), 1.58 (d, $^2J_{HP}$ = 10.4 Hz, 6H, PMe_2), 1.19 (d, $^4J_{HP}$ = 1.6 Hz, 15H, C_5Me_5).

^{13}C{^{1}H} NMR (100 MHz, CD_2Cl_2, −25 ºC) δ: 161.7 (q, $^1J_{CB}$ = 50 Hz, *ipso*-Ar), 146.1 (d, $^2J_{CP}$ = 11 Hz, *o*-Xyl), 138.8 (*o*-Xyl), 134.9 (d, $^3J_{CP}$ = 4 Hz, *ipso*-Xyl), 134.7 (*o*-Ar), 132.8 (*p*-C_6H_3), 132.5 (d, $^1J_{CP}$ ≈ 54 Hz, *ipso*-C_6H_3), 131.0 (d, $^3J_{CP}$ = 9 Hz, *m*-C_6H_3), 129.6 (*p*-Xyl), 128.7 (q, $^2J_{CF}$ = 31 Hz, *m*-Ar), 128.1 (*m*-Xyl), 124.5 (q, $^1J_{CF}$ = 272 Hz, CF_3), 117.5 (m, *p*-Ar),

95.1 (d, $^{2}J_{CP}$ = 2 Hz, C_5Me_5), 22.5 (Me_{Xyl}), 16.0 (d, $^{1}J_{CP}$ = 40 Hz, PMe_2), 9.0 (C_5Me_5).

$^{31}P\{^{1}H\}$ NMR (160 MHz, CD_2Cl_2, 25 ºC) δ: 5.5.

Complex 2(Dipp)$^+$

CH_2Cl_2 (10 mL) was added to a solid mixture of $[IrCp^*Cl_2]_2$ (119.5 mg, 0.150 mmol), $PMe_2Ar^{Dipp}_2$ (139.0 mg, 0.303 mmol) and $NaBAr_F$ (265.9 mg, 0.300 mmol). The resulting suspension was stirred until the dark coloration remained unchanged (1 h to ensure full conversion) and filtered. The solvent was evaporated under reduced pressure and the residue washed with pentane (10 mL) to obtain complex [**2(Dipp)]BAr$_F$** as a dark, brownish solid (441.4 mg, 87%).

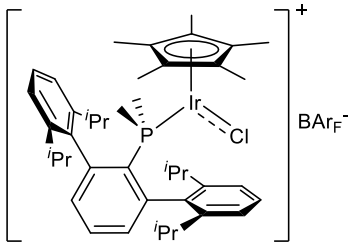

Anal. Calcd. for $C_{74}H_{70}BF_{24}ClIrP$: C, 52.75; H, 4.19. **Found**: C, 52.40; H, 4.31.

^{1}H NMR (500 MHz, CD_2Cl_2, 25 ºC) δ: 7.71 (s, 8H, *o*-Ar), 7.56 (s, 4H, *p*-Ar), 7.53 (t, $^3J_{HH}$ = 7.8 Hz, 2H, *p*-Dipp), 7.49 (td, $^3J_{HH}$ = 7.6 Hz, $^5J_{HP}$ = 1.8 Hz, 1H, *p*-C_6H_3), 7.30 (d, $^3J_{HH}$ = 7.8 Hz, 4H, *m*-Dipp), 7.19 (dd, $^3J_{HH}$ = 7.7 Hz, $^4J_{HP}$ = 3.5 Hz, 2H, *m*-C_6H_3), 2.52 (m, 4H, (C*H*Me_2)$_{Dipp}$), 1.55 (d, $^2J_{HP}$ = 10.5 Hz, 6H, PMe_2), 1.31 (d, $^3J_{HH}$ = 6.7 Hz, 12H, Me_{Dipp}), 1.22 (d, $^4J_{HP}$ = 1.5 Hz, 15H, C_5Me_5), 0.98 (d, $^3J_{HH}$ = 6.6 Hz, 12H, Me_{Dipp}).

^{13}C{^{1}H} NMR (100 MHz, CD_2Cl_2, 25 ºC) δ: 162.1 (q, $^1J_{CB}$ = 49 Hz, *ipso*-Ar), 147.5 (very broad, *o*-Dipp), 144.7 (d, $^2J_{CP}$ = 10 Hz, *o*-C_6H_3), 137.1 (d, $^3J_{CP}$ = 5 Hz, *ipso*-Dipp), 135.2 (*o*-Ar), 133.2 (d, $^3J_{CP}$ = 9 Hz, *m*-C_6H_3), 132.7 (d, $^1J_{CP}$ = 57 Hz, *ipso*-C_6H_3), 130.6 (*p*-Dipp), 129.9 (d, $^4J_{CP}$ = 3 Hz, *p*-C_6H_3), 129.3 (q, $^2J_{CF}$ = 31 Hz, *m*-Ar), 125.0 (q, $^1J_{CF}$ = 272 Hz, CF_3),

124.8 (very broad, *m*-Dipp), 117.9 (m, *p*-Ar), 95.7 (d, $^{2}J_{CP}$ = 3 Hz, C_5Me_5), 31.7 ($(CHMe_2)_{Dipp}$), 26.2 (Me_{Dipp}), 23.1 (br, Me_{Dipp}), 17.7 (d, $^{1}J_{CP}$ = 39 Hz, PMe_2), 9.9 (C_5Me_5).

$^{31}P\{^{1}H\}$ NMR (160 MHz, CD_2Cl_2, 25 ºC) δ: 6.6.

Complex 2(Dipp)$^{+}$·CO

A CH_2Cl_2 solution (5 mL) of complex [**2(Dipp)]BAr$_F$** (40.0 mg, 0.024 mmol) was charged with CO (1 bar). The solution was stirred for 5 min and the solvent was removed under reduced pressure, quantitatively affording the BAr_F salt of complex **2(Dipp)$^{+}$·CO** as a yellow solid. Crystalline starting material permitted to carry out the reaction in the solid-gas interphase. Crystals suitable for X-Ray diffraction were grown by slow evaporation of a saturated Et_2O solution. The NMR characterization was carried out in acetone-d_6 due to the limited solubility of this complex in CD_2Cl_2 at −20 ºC.

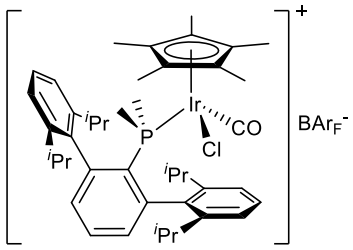

Anal. Calcd. for $C_{75}H_{70}BClF_{24}IrOP$: C, 52.59; H, 4.12. **Found**: C, 52.25; H, 4.50.

^{1}H NMR (400 MHz, $(CD_3)_2CO$, −20 ºC) δ: 7.81 (m, 8H, *o*-Ar), 7.72 (s, 4H, *p*-Ar), 7.68 (td, $^3J_{HH}$ = 7.6 Hz, $^5J_{HP}$ = 2.5 Hz, 1H, *p*-C_6H_3), 7.47 (t, $^3J_{HH}$ ≈ 7.6 Hz, 2H, *p*-Dipp), 7.45 (m, 1H, *m*-Dipp), 7.39 (dd, $^3J_{HH}$ = 7.8 Hz, $^4J_{HH}$ = 0.9 Hz, 1H, *m*-Dipp), 7.33 (ddd, $^3J_{HH}$ = 7.6 Hz, $^4J_{HP}$ = 3.9 Hz, $^4J_{HH}$ = 1.4 Hz, 1H, *m*-C_6H_3), 7.26 (m, 3H, *m*-Dipp), 7.23 (m, 1H, *m*-C_6H_3), 3.30 (sept, $^3J_{HH}$ = 6.7 Hz, 1H, (C*H*Me$_2$)$_{Dipp}$), 3.19 (sept, $^3J_{HH}$ = 6.7 Hz, 1H, (C*H*Me$_2$)$_{Dipp}$), 2.65 (sept, $^3J_{HH}$ = 6.7 Hz, 1H, (C*H*Me$_2$)$_{Dipp}$), 2.52 (sept, $^3J_{HH}$ = 6.8 Hz, 1H, (C*H*Me$_2$)$_{Dipp}$), 2.12 (d, $^2J_{HP}$ = 10.8 Hz, 3H, P*Me*Me), 1.91 (d, $^4J_{HP}$ = 2.2 Hz, 15H, C_5Me_5), 1.57 (d, $^2J_{HP}$ = 11.3 Hz, 3H, P*Me*Me), 1.35 (d, $^3J_{HH}$ ≈ 6.7 Hz, 3H, Me$_{Dipp}$), 1.33 (d, $^3J_{HH}$ ≈ 6.7 Hz, 3H, Me$_{Dipp}$), 1.31 (d,

$^{3}J_{HH}$ = 6.6 Hz, 3H, Me_{Dipp}), 1.27 (d, $^{3}J_{HH}$ = 6.7 Hz, 3H, Me_{Dipp}), 1.18 (d, $^{3}J_{HH}$ = 6.7 Hz, 3H, Me_{Dipp}), 1.15 (d, $^{3}J_{HH}$ = 6.7 Hz, 3H, Me_{Dipp}), 0.83 (d, $^{3}J_{HH}$ = 6.7 Hz, 3H, Me_{Dipp}), 0.69 (d, $^{3}J_{HH}$ = 6.6 Hz, 3H, Me_{Dipp}).

$^{13}C\{^{1}H\}$ NMR (100 MHz, $(CD_3)_2CO$, −20 ºC) δ: 167.9 (d, $^{2}J_{CP}$ = 19 Hz, CO), 162.3 (q, $^{1}J_{CB}$ = 50 Hz, *ipso*-Ar), 149.3 (*o*-Dipp), 148.0 (*o*-Dipp), 147.2 (*o*-Dipp), 146.6 (*o*-Dipp), 146.2 (d, $^{2}J_{CP}$ = 6 Hz, *o*-C_6H_3), 145.4 (d, $^{2}J_{CP}$ = 11 Hz, *o*-C_6H_3), 140.8 (*ipso*-Dipp), 139.7 (*ipso*-Dipp), 136.2 (d, $^{3}J_{CP}$ = 10 Hz, *m*-C_6H_3), 135.2 (*o*-Ar), 134.8 (d, $^{3}J_{CP}$ = 9 Hz, *m*-C_6H_3), 130.7 (*p*-Dipp), 130.5 (*p*-C_6H_3), 130.1 (*p*-Dipp), 129.7 (q, $^{2}J_{CF}$ = 32 Hz, *m*-Ar), 126.8 (*m*-Dipp), 125.4 (d, $^{1}J_{CP}$ = 54 Hz, *ipso*-C_6H_3), 125.0 (q, $^{1}J_{CF}$ = 272 Hz, CF_3), 124.7 (*m*-Dipp), 123.1 (*m*-Dipp), 122.9 (*m*-Dipp), 118.4 (m, *p*-Ar), 107.1 (C_5Me_5), 32.4 ($(CHMe_2)_{Dipp}$), 31.6 ($(CHMe_2)_{Dipp}$), 31.2 ($(CHMe_2)_{Dipp}$), 30.8 ($(CHMe_2)_{Dipp}$), 27.5 (Me_{Dipp}), 25.9 (Me_{Dipp}), 25.0 (Me_{Dipp}), 24.9 (Me_{Dipp}), 24.8 (Me_{Dipp}), 23.7 (Me_{Dipp}), 23.5 (d, $^{1}J_{CP} \approx 39$ Hz, P*Me*Me), 22.0 (Me_{Dipp}), 21.0 (Me_{Dipp}), 20.9 (d, $^{1}J_{CP}$ = 35 Hz, PMe*Me*), 9.4 (C_5Me_5).

$^{31}P\{^{1}H\}$ NMR (160 MHz, $(CD_3)_2CO$, 25 ºC) δ: −33.2.

IR (Nujol): ν(IrCO) 2059 cm^{-1}.

Complex 3(Xyl)$^+$

CH_2Cl_2 (5 mL) was added to an equimolar (0.020 mmol) mixture of complex [**2(Xyl)]BAr$_F$** (31.5 mg) and $NaBAr_F$ (17.7 mg). A brownish solution formed and was stirred until the resulting yellow coloration remained unchanged (*ca*. 10 min). The solution was filtered and the solvent removed under reduced pressure. The residue was washed with a 1:1 mixture of Et_2O and pentane (6 mL), yielding the BAr_F salt of complex **3(Xyl)$^+$** as a yellow solid (24.9 mg, 81%).

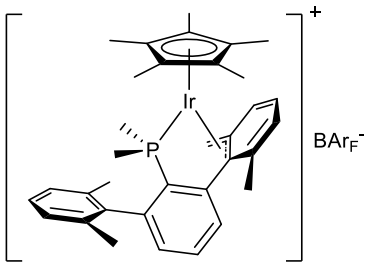

Anal. Calcd. for $C_{66}H_{53}BF_{24}IrP$: C, 51.61; H, 3.48. **Found**: C, 51.65; H, 3.22.

^{1}H NMR (400 MHz, CD_2Cl_2, 25 ºC) δ: 7.73 (s, 8H, *o*-Ar), 7.56 (s, 4H, *p*-Ar), 7.41 (td, $^3J_{HH}$ = 7.6 Hz, $^5J_{HP}$ = 2.5 Hz, 1H, *p*-C_6H_3), 7.30 (t, $^3J_{HH}$ = 7.6 Hz, 1H, *p*-Xyl), 7.21 (m, 2H, *p*-Xyl', *m*-Xyl), 7.13 (d, $^3J_{HH}$ = 7.5 Hz, 1H, *m*-Xyl), 7.02 (dt, $^3J_{HH}$ = 6.5 Hz, $^4J_{HH}$ = 1.0 Hz, 1H, *m*-Xyl'), 6.99 (qd, $^3J_{HH}$ = 7.4 Hz, $^4J_{HP}$ = 3.4 Hz, $^4J_{HH}$ = 1.1 Hz, 1H, *m*-C_6H_3), 6.89 (d, $^3J_{HH}$ = 8.6 Hz, 1H, *m*'-Xyl'), 6.72 (dq, $^3J_{HH}$ = 7.9 Hz, $^4J_{HP}$ = $^4J_{HH}$ = 1.1 Hz, 1H, *m*'-C_6H_3), 3.14 (dd, $^2J_{HH}$ = 3.9 Hz, $^3J_{HP}$ = 0.9 Hz, 1H, IrC*H*H), 2.03 (s, 3H, $Me_{Xyl'}$), 2.01 (s, 3H, Me_{Xyl}), 1.85 (s, 3H, Me_{Xyl}), 1.81 (d, $^2J_{HP}$ = 10.8 Hz, 3H, P*Me*Me), 1.53 (d, $^4J_{HP}$ = 1.9 Hz, 15H, C_5Me_5), 1.48 (d, $^2J_{HP}$ = 10.9 Hz, 3H, PMe*Me*), 1.04 (dd, $^3J_{HP}$ = 16.4 Hz, $^2J_{HH}$ = 3.9 Hz, 1H, IrCH*H*).

$^{13}C\{^{1}H\}$ NMR (100 MHz, CD_2Cl_2, 25 ºC) δ: 162.2 (q, $^{1}J_{CB}$ = 50 Hz, *ipso*-Ar), 145.8 (d, $^{2}J_{CP}$ = 31 Hz, *o*-C_6H_3), 145.5 (d, $^{2}J_{CP}$ = 3 Hz, *o*-C_6H_3), 143.9 (*o*-Xyl'), 138.2 (d, $^{3}J_{CP}$ = 2 Hz, *ipso*-Xyl), 137.2 (*o*-Xyl), 136.2 (*o*-Xyl), 135.2 (*o*-Ar), 133.5 (d, $^{4}J_{CP}$ = 3 Hz, *p*-C_6H_3), 132.1 (d, $^{3}J_{CP}$ = 6 Hz, *m*-C_6H_3), 131.6 (d, $^{3}J_{CP}$ = 15 Hz, *m*'-C_6H_3), 131.5 (*p*-Xyl'), 130.8 (d, $^{1}J_{CP}$ = 60 Hz, *ipso*-C_6H_3), 129.3 (q, $^{2}J_{CF}$ = 32 Hz, *m*-Ar), 129.2 (*p*-Xyl), 128.5 (*m*-Xyl), 128.0 (*m*-Xyl), 125.0 (q, $^{1}J_{CF}$ = 272 Hz, CF_3), 121.9 (*m*'-Xyl'), 121.1 (*m*-Xyl'), 117.9 (m, *p*-Ar), 96.3 (d, $^{2}J_{CP}$ = 2 Hz, C_5Me_5), 89.1 (d, $^{2}J_{CP}$ = 1 Hz, *o*'-Xyl'), 83.2 (d, $^{2}J_{CP}$ = 1 Hz, *ipso*-Xyl'), 26.3 (d, $^{2}J_{CP}$ = 4 Hz, $IrCH_2$), 21.6 ($Me_{Xyl'}$), 21.33 (Me_{Xyl}), 21.28 (Me_{Xyl}), 17.3 (d, $^{1}J_{CP}$ = 38 Hz, P*Me*Me), 13.6 (d, $^{1}J_{CP}$ = 40 Hz, PMe*Me*), 8.2 (C_5Me_5).

$^{31}P\{^{1}H\}$ NMR (120 MHz, CD_2Cl_2, 25 ºC) δ: 13.6.

Complex 3(Dipp)$^+$

CH_2Cl_2 (5 mL) was added to an equimolar (0.020 mmol) mixture of complex [**2(Dipp)]BAr$_F$** (33.7 mg) and $NaBAr_F$ (17.7 mg). 1-2 equivalents of H_2O were added to the initial brownish solution, which was stirred until the yellow coloration remained unchanged (*ca*. 24 h). The solution was filtered and the solvent removed under reduced pressure. The residue was washed with a 1:1 mixture of Et_2O and pentane (6 mL), yielding complex [**3(Dipp)]BAr$_F$** as a yellow solid (26.3 mg, 80%). Complex **[3(Dipp)]BAr$_F$** was cleanly and quantitatively obtained by allowing a CH_2Cl_2 solution of complex **[4(Dipp)]BAr$_F$** to stand at room temperature for *ca*. 24 hours. This transformation can also occur in the solid state in a similar reaction time. Single crystals were grown from a saturated hexane-dichloromethane solution at −32 ºC.

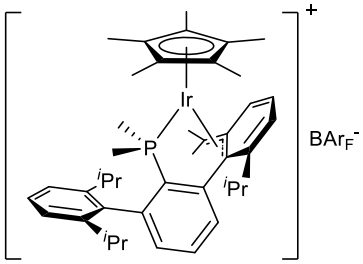

Anal. Calcd. for $C_{74}H_{69}BF_{24}IrP$: C, 53.92; H, 4.22. **Found**: C, 53.60; H, 4.21.

^{1}H NMR (500 MHz, CD_2Cl_2, 25 ºC) δ: 7.72 (s, 8H, *o*-Ar), 7.56 (s, 4H, *p*-Ar), 7.48 (t, $^3J_{HH}$ = 7.7 Hz, 1H, *p*-Dipp), 7.42 (dd, $^3J_{HH}$ = 8.7 Hz, $^3J_{HH}$ = 6.8 Hz, 1H, *p*-Dipp'), 7.34 (td, $^3J_{HH}$ = 7.6 Hz, $^5J_{HP}$ = 2.5 Hz, 1H, *p*-C_6H_3), 7.30 (m, 2H, *m*-Dipp), 7.26 (d, $^3J_{HH}$ = 6.8 Hz, 1H, *m*-Dipp'), 7.13 (d, $^3J_{HH}$ = 8.7 Hz, 1H, *m*'-Dipp'), 7.12 (qd, $^3J_{HH}$ = 7.5 Hz, $^4J_{HP}$ = 3.5 Hz, $^4J_{HH}$ = 1.0 Hz, 1H, *m*-C_6H_3), 6.60 (dq, $^3J_{HH}$ = 7.8 Hz, $^4J_{HP}$ = $^4J_{HH}$ = 1.0 Hz, 1H, *m*'-C_6H_3),

2.31 (sept, $^{3}J_{HH}$ = 6.7 Hz, 1H, ((C*H*Me$_2$)$_{Dipp}$), 2.26 (sept, $^{3}J_{HH}$ = 6.8 Hz, 1H, ((C*H*Me$_2$)$_{Dipp'}$), 2.19 (sept, $^{3}J_{HH}$ = 6.7 Hz, 1H, ((C*H*Me$_2$)$_{Dipp}$), 1.86 (d, $^{2}J_{HP}$ = 10.7 Hz, 3H, P*Me*Me), 1.65 (s, 3H, Me'$_{Dipp'}$), 1.57 (d, $^{2}J_{HP}$ = 10.9 Hz, 3H, PMe*Me*), 1.46 (d, $^{4}J_{HP}$ = 1.9 Hz, 15H, C$_5$Me$_5$), 1.29 (d, $^{3}J_{HH}$ = 6.8 Hz, 3H, Me$_{Dipp}$), 1.21 (d, $^{3}J_{HH}$ = 6.8 Hz, 3H, Me$_{Dipp}$), 1.19 (d, $^{3}J_{HH}$ = 6.8 Hz, 3H, Me$_{Dipp'}$), 1.00 (d, $^{3}J_{HH}$ = 6.6 Hz, 3H, Me$_{Dipp}$), 0.96 (d, $^{3}J_{HH}$ = 7.1 Hz, 3H, Me$_{Dipp'}$), 0.90 (d, $^{3}J_{HH}$ = 6.7 Hz, 3H, Me$_{Dipp}$), 0.53 (d, $^{4}J_{HP}$ = 1.5 Hz, 3H, Me'$_{Dipp'}$).

^{13}C{^{1}H} NMR (100 MHz, CD_2Cl_2, 25 ºC) δ: 162.2 (q, $^{1}J_{CB}$ = 50 Hz, *ipso*-Ar), 154.3 (*o*-Dipp'), 150.1 (d, $^{2}J_{CP}$ = 30 Hz, *o*-C$_6$H$_3$), 147.44 (*o*-Dipp), 147.40 (*o*-Dipp), 144.3 (d, $^{2}J_{CP}$ = 2 Hz, *o*-C$_6$H$_3$), 135.6 (d, $^{3}J_{CP}$ = 2 Hz, *ipso*-Dipp), 135.2 (d, $^{1}J_{CP}$ = 58 Hz, *ipso*-C$_6$H$_3$), 135.2 (*o*-Ar), 133.9 (d, $^{3}J_{CP}$ = 6 Hz, *m*-C$_6$H$_3$), 131.6 (d, $^{3}J_{CP}$ = 15 Hz, *m*'-C$_6$H$_3$), 131.5 (d, $^{4}J_{CP}$ = 3 Hz, *p*-C$_6$H$_3$), 130.3 (*p*-Xyl), 130.1 (*p*-Xyl'), 129.3 (q, $^{2}J_{CF}$ = 31 Hz, *m*-Ar), 125.0 (q, $^{1}J_{CF}$ = 272 Hz, CF$_3$), 123.7 (*m*-Dipp), 123.34 (d, $^{3}J_{CP}$ = 1 Hz, *m*'-Dipp), 123.30 (*m*-Dipp), 118.5 (*m*-Dipp'), 117.9 (m, *p*-Ar), 98.4 (d, $^{2}J_{CP}$ = 2 Hz, *C*$_5$Me$_5$), 86.9 (*o*'-Dipp'), 86.5 (d, $^{2}J_{CP}$ = 2 Hz, *ipso*-Dipp'), 44.1 (d, $^{2}J_{CP}$ = 5 Hz, Ir*C*Me$_2$), 34.0 (Me'$_{Dipp'}$), 31.9 ((*C*HMe$_2$)$_{Dipp'}$), 31.7 ((*C*HMe$_2$)$_{Dipp}$), 31.5 ((*C*HMe$_2$)$_{Dipp}$), 26.4 (Me$_{Dipp}$), 26.1 (Me$_{Dipp}$), 24.4 (Me$_{Dipp'}$), 24.3 (Me$_{Dipp'}$), 23.9 (d, $^{3}J_{CP}$ = 8 Hz, Me'$_{Dipp'}$), 21.7 (Me$_{Dipp}$), 21.2 (Me$_{Dipp}$), 18.9 (d, $^{1}J_{CP}$ = 40 Hz, P*Me*Me), 13.9 (d, $^{1}J_{CP}$ = 38 Hz, PMe*Me*), 8.3 (C$_5$*Me*$_5$).

^{31}P{^{1}H} NMR (160 MHz, CD_2Cl_2, 25 ºC) δ: 9.8.

Complex 3(Xyl)$^{+}$·CO

A CH_2Cl_2 solution (5 mL) of compound **[3(Xyl)]BAr$_F$** (30 mg, 0.020 mmol) was charged with CO (1 bar) and stirred for 48 h at 50 ºC. The solvent was evaporated under reduced pressure, quantitatively yielding the BAr_F derivative of complex **3(Xyl)$^{+}$·CO** as a yellow solid.

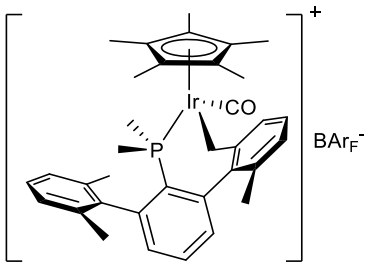

Anal. Calcd. for $C_{67}H_{53}BF_{24}IrOP$: C, 51.45; H, 3.42. **Found**: C, 51.38; H, 3.52.

^{1}H NMR (500 MHz, CD_2Cl_2, 25 ºC) δ: 7.72 (s, 8H, *o*-Ar), 7.66 (td, $^{3}J_{HH}$ = 7.6 Hz, $^{5}J_{HP}$ = 1.9 Hz, 1H, *p*-C_6H_3), 7.56 (s, 4H, *p*-Ar), 7.28 (t, $^{3}J_{HH}$ = 7.6 Hz, 1H, *p*-Xyl), 7.24 (t, $^{3}J_{HH}$ = 7.6 Hz, 1H, *p*-Xyl'), 7.17 to 7.10 (m, 4H, *m*-C_6H_3, *m*'-C_6H_3, *m*-Xyl), 7.05 (d, $^{3}J_{HH}$ = 7.6 Hz, 1H, *m*-Xyl'), 6.91 (d, $^{3}J_{HH}$ = 7.6 Hz, 1H, *m*'-Xyl'), 2.87 (dd, $^{2}J_{HH}$ = 7.8 Hz, $^{3}J_{HP}$ = 5.0 Hz, 1H, IrC*H*H), 2.56 (dd, $^{3}J_{HP}$ = 11.5 Hz, $^{2}J_{HH}$ = 7.8 Hz, 1H, IrCH*H*), 2.07 (s, 3H, Me_{Xyl}), 2.06 (s, 3H, Me_{Xyl}), 2.00 (s, 3H, $Me_{Xyl'}$), 1.88 (d, $^{4}J_{HP}$ = 1.9 Hz, 15H, C_5Me_5), 1.55 (d, $^{2}J_{HP}$ = 9.8 Hz, 3H, P*Me*Me), 1.25 (d, $^{2}J_{HP}$ = 11.2 Hz, 3H, PMe*Me*).

^{13}C{^{1}H} NMR (100 MHz, CD_2Cl_2, 25 ºC) δ: 167.3 (d, $^{2}J_{CP}$ = 13 Hz, CO), 162.2 (q, $^{1}J_{CB}$ = 50 Hz, *ipso*-Ar), 146.7 (*o*'-Xyl'), 146.1 (d, $^{2}J_{CP}$ = 11 Hz, *o*-C_6H_3), 142.2 (d, $^{2}J_{CP}$ = 6 Hz, *o*-C_6H_3), 140.8 (d, $^{3}J_{CP}$ = 2 Hz, *ipso*-Xyl), 137.2 (*o*-Xyl'), 137.1 (*o*-Xyl), 136.2 (d, $^{3}J_{CP}$ = 3 Hz, *ipso*-Xyl'), 135.6 (*o*-Xyl), 135.2 (*o*-Ar), 133.8 (d, $^{3}J_{CP}$ = 9 Hz, *m*'-C_6H_3), 132.3 (d, $^{4}J_{CP}$ = 3 Hz,

p-C_6H_3), 132.2 (d, $^3J_{CP}$ = 8 Hz, *m*-C_6H_3), 129.7 (*m*-Xyl'), 129.3 (*p*-Xyl), 129.3 (q, $^2J_{CF}$ = 31 Hz, *m*-Ar), 129.1 (*p*-Xyl'), 128.4 (*m*-Xyl), 128.1 (*m*-Xyl), 125.0 (q, $^1J_{CF}$ = 272 Hz, CF_3), 124.5 (*m*'-Xyl'), 119.6 (d, $^1J_{CP}$ = 52 Hz, *ipso*-C_6H_3), 117.9 (m, *p*-Ar), 102.7 (d, $^2J_{CP}$ = 2 Hz, C_5Me_5), 23.3 (Me_{Xyl}), 21.6 ($Me_{Xyl'}$), 21.4 (Me_{Xyl}), 20.3 (d, $^1J_{CP}$ = 46 Hz, P*Me*Me), 17.8 (d, $^1J_{CP}$ = 38 Hz, PMe*Me*), 9.5 (C_5Me_5), 7.6 (d, $^2J_{CP}$ = 6 Hz, $IrCH_2$).

$^{31}P\{^1H\}$ NMR (160 MHz, CD_2Cl_2, 25 ºC) δ: −46.3.

IR (Nujol): υ(IrCO) 2035 cm^{-1}.

Complex 4(Dipp)$^+$

To a CH_2Cl_2 solution of complex **[2(Dipp)]BAr$_F$** (120.0 mg, 0.071 mmol) at −20 ºC was added NEt_3 (20.0 µL, 0.142 mmol). The solution was stirred at this temperature until the orange coloration remained unchanged (*ca*. 2 h). The solvent was removed under reduced pressure and the residue was extracted with Et_2O at −30 ºC. The solvent was evaporated and the residue washed with pentane. Crystallization from CH_2Cl_2 at −32 ºC afforded the BAr_F salt of complex **4(Dipp)$^+$** as an orange, crystalline solid (72.9 mg, 62%).

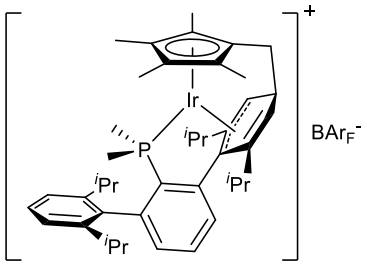

Anal. Calcd. for: $C_{74}H_{69}BF_{24}IrP$: C, 53.92; H, 4.22. **Found**: C, 53.78, H, 4.40.

^{1}H NMR (400 MHz, THF-d_8, −30 ºC) δ: 7.94 (dd, $^3J_{HH}$ = 7.7 Hz, $^4J_{HP}$ = 1.8 Hz, 1H, *m*'-C_6H_3), 7.85 (s, 8H, *o*-Ar), 7.66 (s, 4H, *p*-Ar), 7.59 (td, $^3J_{HH}$ = 7.6 Hz, $^5J_{HP}$ = 1.8 Hz, 1H, *p*-C_6H_3), 7.45 (t, $^3J_{HH}$ = 7.7 Hz, 1H, *p*-Dipp), 7.34 (d, $^3J_{HH}$ = 7.7 Hz, 1H, *m*-Dipp), 7.29 (m, 2H, *m*-Dipp, *m*-C_6H_3), 6.61 (br, 1H, H_{allyl}), 5.14 (br, 1H, H_{alkene}), 3.56 (br, overlapped, 1H, C*H*CH_2), 3.33 (br m, 1H, (C*H*Me_2)$_{alkene}$), 3.27 (dd, $^2J_{HH}$ ≈ 14 Hz, $^3J_{HH}$ ≈ 6 Hz, 1H, CHC*H*H), 2.58 (s, 3H, C_5Me_4), 2.46 (m, 2H, CHCH*H*, (C*H*Me_2)$_{Dipp}$), 2.10 (m, 1H, C*H*Me_2)$_{Dipp}$), 2.03 (s, 3H, C_5Me_4), 1.88 (s, 3H, C_5Me_4), 1.58 (d, $^2J_{HP}$ = 10.5 Hz, 3H, P*Me*Me), 1.47 (s, 3H, C_5Me_4), 1.36 (m, 1H,

C*H*Me$_2$)$_{allyl}$), 1.27 (d, $^3J_{HH}$ = 6.3 Hz, 3H, Me$_{Dipp}$), 1.19 (m, 9H, PMe*Me*, Me$_{Dipp}$, Me$_{alkene}$), 0.99 (m, 6H, Me$_{Dipp}$), 0.89 (m, 9H, Me$_{allyl,}$ Me$_{alkene}$).

^{13}C{^{1}H} NMR (100 MHz, THF-d$_8$, −30 ºC) δ: 162.7 (q, $^1J_{CB}$ = 50 Hz, *ipso*-Ar), 151.5 (d, $^2J_{CP}$ = 26 Hz, *o*-C$_6$H$_3$), 148.4 (*o*-alkene), 147.7 (*o*-Dipp), 147.4 (*o*-Dipp), 144.5 (*o*-C$_6$H$_3$), 136.9 (*ipso*-Dipp), 135.3 (*o*-Ar), 134.2 (d, $^1J_{CP}$ = 57 Hz, *ipso*-C$_6$H$_3$), 133.2 (d, $^3J_{CP}$ = 6 Hz, *m*-C$_6$H$_3$), 130.8 (*p*-C$_6$H$_3$), 130.3 (*p*-Dipp), 129.8 (q, $^2J_{CF}$ = 32 Hz, *m*-Ar), 129.6 (overlapped, *m*'-C$_6$H$_3$), 125.2 (q, $^1J_{CF}$ = 272 Hz, CF$_3$), 123.4 (*m*-Dipp), 122.2 (*C*$_5$Me$_4$), 118.1 (m, *p*-Ar), 116.6 (*m*-alkene), 113.7 (d, $^2J_{CP}$ = 8 Hz, *C*$_5$Me$_4$), 105.4 (*o*-allyl), 95.2 (*C*$_5$Me$_4$), 93.5 (*C*$_5$Me$_4$), 92.3 (*C*$_5$Me$_4$), 86.3 (*m*-allyl), 63.1 (*C*HCH$_2$), 61.0 (*ipso*-allyl), 32.0 ((*C*HMe$_2$)$_{Dipp}$), 31.9 (*C*HMe$_2$)$_{Dipp}$), 30.3 (*C*HMe$_2$)$_{alkene}$), 29.5 (d, $^3J_{CP}$ = 4 Hz, (*C*HMe$_2$)$_{allyl}$), 26.3 (Me$_{Dipp}$), 26.2 (Me$_{Dipp}$), 24.8 (Me$_{allyl}$), 23.6 (CH*C*H$_2$), 21.3 (Me$_{Dipp}$), 21.2 (Me$_{Dipp}$), 19.4 (Me$_{alkene}$), 19.3 (Me$_{alkene}$), 18.6 (Me$_{allyl}$), 16.5 (d, $^1J_{CP}$ = 39 Hz, P*Me*Me), 14.3 (d, $^1J_{CP}$ = 35 Hz, PMe*Me*), 11.3 (C$_5$*Me*$_4$), 11.9 (C$_5$*Me*$_4$), 8.8 (C$_5$*Me*$_4$), 8.2 (C$_5$*Me*$_4$).

^{31}P{^{1}H} NMR (160 MHz, THF-d$_8$, −30 ºC) δ: −3.5.

Complex 5(Xyl)$^+$

To a −35 ºC CH_2Cl_2 solution of complex [**2(Xyl)]BAr$_F$** (40.0 mg, 0.025 mmol) was added NEt_3 (3.7 µL, 0.050 mmol). The solution was kept at −32 ºC for 12 hours. The solvent was removed under reduced pressure and the yellow residue washed with pentane (10 mL) and extracted with Et_2O at −30 ºC (15 mL). The solvent was concentrated to approximately half the original volume and the same amount of hexane was carefully added to form a bilayer. Crystallization at −32 ºC afforded compound **[5(Xyl)]BAr$_F$** as a yellow, crystalline solid with *ca*. 70 % yield.

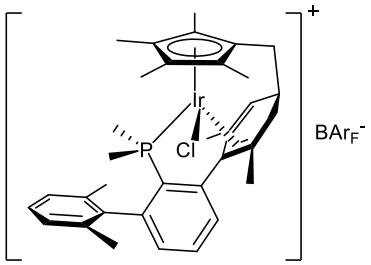

Anal. Calcd. for $C_{66}H_{54}BClF_{24}IrP$: C, 50.41, H, 3.46. **Found**: C, 50.34; H, 3.54.

^{1}H NMR (500 MHz, CD_2Cl_2, 25 ºC) δ: 7.72 (s, 8H, *o*-Ar), 7.61 (td, $^3J_{HH}$ = 7.6 Hz, $^5J_{HP}$ = 2.7 Hz, 1H, *p*-C_6H_3), 7.56 (s, 4H, *p*-Ar), 7.27 (t, $^3J_{HH}$ = 7.6 Hz, 1H, *p*-Xyl), 7.21 (m, 2H, *m*'-C_6H_3, *m*-Xyl), 7.12 (ddd, $^3J_{HH}$ = 7.4 Hz, $^4J_{HP}$ = 3.9 Hz, $^4J_{HH}$ = 1.0 Hz, 1H, *m*-C_6H_3), 7.10 (d, $^3J_{HH}$ = 7.6 Hz, 1H, *m*-Xyl), 5.44 (m, 1H, *m*-$CH_{Xyl'}$), 3.01 (m, 1H, *p*-Xyl'), 2.08 to 2.05 (m, 2H, *m*-CH_2), 2.07 (s, 3H, Me_{Xyl}), 2.03 to 1.97 (m, 2H, $C_5Me_4CH_2$), 1.97 (d, $^4J_{HP}$ = 4.3 Hz, 3H, C_5Me_4), 1.89 (s, 3H, Me_{Xyl}), 1.83 (d, $^4J_{HP}$ = 4.5 Hz, 3H, C_5Me_4), 1.81 (d, $^2J_{HP}$ = 10.6 Hz, 3H, P*Me*Me), 1.57 (m, 3H, $Me_{Xyl'}$), 1.54 (s, 3H, C_5Me_4), 1.14 (d, $^2J_{HP}$ = 12.0 Hz, 3H, PMe*Me*), 1.14 (s, 3H, $Me'_{Xyl'}$), 1.11 (s, 3H, C_5Me_4).

$^{13}C\{^1H\}$ NMR (100 MHz, CD_2Cl_2, −25 ºC) δ: 161.7 (q, $^1J_{CB}$ = 50 Hz, *ipso*-Ar), 147.2 (d, $^2J_{CP}$ = 28 Hz, *o*-C_6H_3), 144.8 (*o*-C_6H_3), 137.4 (m, *o*-Xyl, *ipso*-Xyl), 136.6 (*o*-Xyl'), 136.0 (d, $^1J_{CP}$ = 60 Hz, *ipso*-C_6H_3), 134.8 (*o*-Xyl), 134.7 (*o*-Ar), 133.9 (*p*-C_6H_3), 130.9 (d, $^3J_{CP}$ = 7 Hz, *m*-C_6H_3), 128.8 (overlapped, *p*-Xyl), 128.6 (q, $^2J_{CF}$ = 31 Hz, *m*-Ar), 127.9 (*m*-Xyl), 127.6 (d, $^NJ_{CP}$ ≈ 14 Hz, *m*'-C_6H_3), 127.5 (*m*-Xyl), 126.3 (*m*-$CH_{Xyl'}$), 124.5 (q, $^1J_{CF}$ = 272 Hz, CF_3), 117.5 (m, *p*-Ar), 114.3 (C_5Me_4), 107.7 (C_5Me_4), 102.5 (C_5Me_4), 97.1 (d, $^2J_{CP}$ = 10 Hz, C_5Me_4), 88.1 (C_5Me_4), 84.0 (*ipso*-Xyl'), 82.8 (*o*'-Xyl'), 38.5 (*m*-CH_2), 31.9 (*p*-Xyl'), 27.8 ($Me'_{Xyl'}$), 23.2 ($Me_{Xyl'}$), 21.2 (Me_{Xyl}), 20.8 (Me_{Xyl}), 17.5 (d, $^1J_{CP}$ = 37 Hz, P*Me*Me), 14.9 ($C_5Me_4CH_2$), 10.2 (d, $^1J_{CP}$ ≈ 45 Hz, PMe*Me*), 10.0 (C_5Me_4), 9.8 (C_5Me_4), 7.4 (C_5Me_4), 4.9 (C_5Me_4).

$^{31}P\{^1H\}$ NMR (200 MHz, CD_2Cl_2, 25 ºC) δ: 9.7.

Complex 6(Dipp)$^+$

To a Et_2O solution (10 mL) of complex **[2(Dipp)]BAr$_F$** (100.0 mg, 0.060 mmol) was added LiMe (0.04 mL, 1.6 M in Et_2O, 0.060 mmol). The bright red solution was filtered and the solvent evaporated under reduced pressure. The residue was washed with pentane (6 mL), yielding complex **[6(Dipp)]BAr$_F$** as an orange, microcrystalline solid in *ca*. 70% yield. Single crystals were grown from a saturated CH_2Cl_2-hexane solution at −32 ºC.

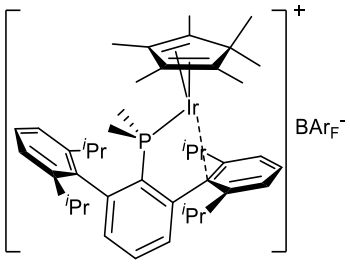

^{1}H NMR (400 MHz, CD_2Cl_2, −20 ºC) δ: 7.71 (m, 8H, *o*-Ar), 7.55 (s, 4H, *p*-Ar), 7.50 (td, $^3J_{HH}$ = 7.6 Hz, $^5J_{HP}$ = 2.1 Hz, 1H, *p*-C_6H_3), 7.43 (m, 2H, *p*-Dipp, *m*-Dipp'), 7.36 (d, $^3J_{HH}$ = 7.3 Hz, 1H, *m*-Dipp'), 7.30 (t, $^3J_{HH}$ = 7.6 Hz, 1H, *p*-Dipp'), 7.28 (d, $^3J_{HH}$ = 7.7 Hz, 1H, *m*-Dipp), 7.23 (d, $^3J_{HH}$ = 7.8 Hz, 1H, *m*-Dipp), 7.20 (ddd, $^3J_{HH}$ = 7.5 Hz, $^4J_{HP}$ = 2.8 Hz, $^4J_{HH}$ = 0.9 Hz, 1H, *m*-C_6H_3), 6.99 (ddd, $^3J_{HH}$ = 7.7 Hz, $^4J_{HP}$ = 2.0 Hz, $^4J_{HH}$ = 0.9 Hz, 1H, *m*'-C_6H_3), 2.64 (sept, $^3J_{HH}$ = 6.8 Hz, 1H, (C*H*Me$_2$)$_{Dipp'}$), 2.32 (sept, $^3J_{HH}$ = 6.7 Hz, 1H, (C*H*Me$_2$)$_{Dipp}$), 2.15 (sept, $^3J_{HH}$ = 6.7 Hz, 1H, (C*H*Me$_2$)$_{Dipp}$), 2.00 (sept, $^3J_{HH}$ = 6.8 Hz, 1H, (C*H*Me$_2$)$_{Dipp'}$), 1.86 (d, $^4J_{HP}$ = 1.1 Hz, 3H, C_5Me_6), 1.54 (s, 3H, C_5Me_6), 1.48 (d, $^2J_{HP}$ = 10.1 Hz, 3H, P*Me*Me), 1.35 (d, $^3J_{HH}$ = 7.0 Hz, 3H, Me$_{Dipp'}$), 1.30 (d, $^3J_{HH}$ = 7.1 Hz, 3H, Me$_{Dipp'}$), 1.24 (d, $^2J_{HP}$ = 10.3 Hz, 3H, PMe*Me*), 1.23 (d, $^3J_{HH}$ = 6.7 Hz, 3H, Me$_{Dipp}$), 1.19 (d, $^3J_{HH}$ = 6.7 Hz, 3H, Me$_{Dipp}$), 1.13 (s, 3H, C_5Me_6), 1.00 (d, $^3J_{HH}$ = 6.6 Hz, 3H, Me$_{Dipp}$), 0.90 (m, 6H, Me$_{Dipp}$, Me$_{Dipp'}$), 0.77 (s, 3H, C_5Me_6), 0.73 (s,

3H, C_5Me_6), 0.70 (d, $^3J_{HH}$ = 6.8 Hz, 3H, $Me_{Dipp'}$), 0.32 (d, $^4J_{HP}$ = 3.4 Hz, 3H, C_5Me_6).

$^{13}C\{^1H\}$ NMR (100 MHz, CD_2Cl_2, −20 ºC) δ: 161.7 (q, $^1J_{CB}$ = 50 Hz, *ipso*-Ar), 146.9 (*o*-Dipp), 146.5 (*o*-Dipp), 146.2 (d, $^2J_{CP}$ = 27 Hz, *o*-C_6H_3), 144.2 (*o*-C_6H_3), 141.5 (*o*-Dipp'), 137.6 (d, $^1J_{CP}$ = 53 Hz, *ipso*-C_6H_3), 135.7 (*ipso*-Dipp), 134.7 (*o*-Ar), 133.8 (d, $^3J_{CP}$ = 5 Hz, *m*-C_6H_3), 133.6 (*m*-Dipp'), 132.5 (m, *m*-Dipp', *o*-Dipp'), 131.7 (d, $^3J_{CP}$ = 13 Hz, *m*-C_6H_3), 131.1 (*p*-C_6H_3), 129.7 (*p*-Dipp), 128.7 (q, $^2J_{CF}$ = 32 Hz, *m*-Ar), 127.8 (*p*-Dipp'), 124.4 (q, $^1J_{CF}$ = 272 Hz, CF_3), 123.2 (overlapped, *m*-Dipp), 122.9 (*m*-Dipp), 122.5 (d, $^2J_{CP}$ = 15 Hz, C_5Me_6), 120.4 (overlapped, *ipso*-Dipp'), 117.5 (m, *p*-Ar), 114.6 (C_5Me_6), 78.3 (C_5Me_6), 61.9 (C_5Me_6), 56.7 (C_5Me_6), 34.2 ((CHMe$_2$)$_{Dipp'}$, (CHMe$_2$)$_{Dipp'}$), 31.4 ((CHMe$_2$)$_{Dipp}$), 31.2 ((CHMe$_2$)$_{Dipp}$), 29.7 (C_5Me_6), 26.1 (Me_{Dipp}), 25.7 (Me_{Dipp}), 24.7 ($Me_{Dipp'}$), 24.4 ($Me_{Dipp'}$), 24.2 ($Me_{Dipp'}$), 24.1 ($Me_{Dipp'}$), 21.4 (C_5Me_6), 21.2 (Me_{Dipp}), 21.1 (Me_{Dipp}), 15.7 (d, $^1J_{CP}$ = 39 Hz, PMe*Me*), 15.1 (d, $^1J_{CP}$ ≈ 39 Hz, P*Me*Me), 13.4 (C_5Me_6), 12.3 (C_5Me_6), 11.8 (C_5Me_6), 8.3 (C_5Me_6).

$^{31}P\{^1H\}$ NMR (120 MHz, CD_2Cl_2, 25 ºC) δ: 5.1.

Complex 7(Dipp)$^+$

To a Et_2O solution (5 mL) of complex **[2(Dipp)]BAr$_F$** (50 mg, 0.030 mmol) was added $PhSiH_3$ (7.3 µL, 0.060 mmol). The solution was stirred for 5 min and the solvent was removed under reduced pressure. The residue was dissolved in Et_2O (4 mL) and precipitated with pentane (16 mL), affording compound **[7(Dipp)]BAr$_F$** as a yellow solid in ca 90% yield. Crystals suitable for X-Ray diffraction were grown by slow evaporation of a saturated hexane-dichloromethane solution.

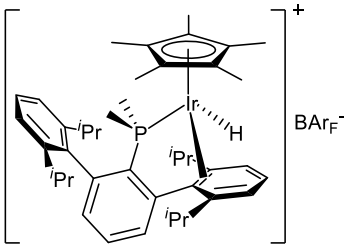

Anal. Calcd. for $C_{74}H_{71}BF_{24}IrP$: C, 53.86; H, 4.34. **Found**: C, 53.69; H, 4.61.

^{1}H NMR (400 MHz, CD_2Cl_2, 25 ºC) δ:7.72 (s, 8H, *o*-Ar), 7.56 (s, 4H, *p*-Ar), 7.47 (t, $^3J_{HH}$ = 7.8 Hz, 1H, *p*-Dipp), 7.45 (m, 1H, *p*-C_6H_3), 7.32 (dd, $^3J_{HH}$ = 7.8 Hz, $^4J_{HH}$ = 1.0 Hz, 1H, *m*-Dipp), 7.27 (dd, $^3J_{HH}$ = 7.8 Hz, $^4J_{HH}$ = 1.0 Hz, 1H, *m*-Dipp), 7.20 (ddd, $^3J_{HH}$ = 7.4 Hz, $^4J_{HP}$ = 3.6 Hz, $^4J_{HH}$ = 1.1 Hz, 1H, *m*-C_6H_3), 7.05 (m, 1H, *p*-Dipp'), 7.01 (dd, $^3J_{HH}$ = 8.7 Hz, $^4J_{HH}$ = 1.2 Hz, 1H, *m*'-Dipp'), 6.89 (ddd, $^3J_{HH}$ = 7.8 Hz, $^4J_{HP}$ = 2.3 Hz, $^4J_{HH}$ = 1.1 Hz, 1H, *m*'-C_6H_3), 6.86 (dd, $^3J_{HH}$ = 6.4 Hz, $^4J_{HH}$ = 1.2 Hz, 1H, *m*-Dipp'), 2.42 (sept, $^3J_{HH}$ = 6.8 Hz, 1H, ((C*H*Me$_2$)$_{Dipp}$), 2.31 (sept, $^3J_{HH}$ = 6.9 Hz, 1H, ((C*H*Me$_2$)$_{Dipp'}$), 2.19 (sept, $^3J_{HH}$ = 6.8 Hz, 1H, ((C*H*Me$_2$)$_{Dipp}$), 1.77 (d, $^2J_{HP}$ = 10.9 Hz, 3H, P*Me*Me), 1.48 (d, $^3J_{HH} \approx$ 6.8 Hz, 3H, Me'$_{Dipp'}$), 1.47 (d, $^2J_{HP} \approx$ 11.4 Hz, 3H, PMe*Me*), 1.45 (d, $^4J_{HP}$ = 1.1 Hz, 15H, C_5Me_5), 1.32 (d, $^3J_{HH}$ = 6.8 Hz, 3H, Me$_{Dipp}$), 1.21 (m, 4H, Me$_{Dipp}$, ((C*H*Me$_2$)'$_{Dipp'}$), 1.11 (d,

$^{3}J_{HH}$ = 6.7 Hz, 3H, $Me_{Dipp'}$), 1.03 (d, $^{3}J_{HH}$ = 6.6 Hz, 3H, Me_{Dipp}), 1.02 (d, $^{3}J_{HH}$ = 7.0 Hz, 3H, $Me_{Dipp'}$), 0.94 (d, $^{3}J_{HH}$ = 6.7 Hz, 3H, Me_{Dipp}), 0.68 (d, $^{3}J_{HH}$ = 6.6 Hz, 3H, $Me'_{Dipp'}$), −18.3 (d, $^{2}J_{HP}$ = 38.8 Hz, 1H, IrH).

$^{13}C\{^{1}H\}$ NMR (100 MHz, CD_2Cl_2, 25 ºC) δ: 162.2 (q, $^{1}J_{CB}$ = 50 Hz, *ipso*-Ar), 152.3 (*o*-Dipp'), 147.6 (*o*-Dipp), 147.1 (d, $^{2}J_{CP}$ = 26 Hz, *o*-C_6H_3), 146.9 (*o*-Dipp), 143.6 (d, $^{2}J_{CP}$ = 2 Hz, *o*-C_6H_3), 136.9 (d, $^{1}J_{CP}$ = 61 Hz, *ipso*-C_6H_3), 136.0 (*ipso*-Dipp), 135.2 (*o*-Ar), 133.7 (d, $^{3}J_{CP}$ = 7 Hz, *m*-C_6H_3), 131.3 (*p*-C_6H_3), 131.2 (d, $^{3}J_{CP} \approx$ 13 Hz, *m*'-C_6H_3), 130.3 (*p*-Dipp), 129.3 (q, $^{2}J_{CF}$ = 31 Hz, *m*-Ar), 129.2 (*m*'-Dipp'), 125.4 (*p*-Dipp'), 125.0 (q, $^{1}J_{CF}$ = 272 Hz, CF_3), 123.62 (*m*-Dipp), 123.59 (*m*-Dipp), 117.9 (m, *p*-Ar), 117.6 (*m*-Dipp'), 101.4 (*o*'-Dipp'), 99.3 (C_5Me_5), 96.3 (d, $^{2}J_{CP}$ = 2 Hz, *ipso*-Dipp'), 39.6 ((CHMe$_2$)'$_{Dipp'}$), 32.7 ((CHMe$_2$)$_{Dipp'}$), 31.7 ((CHMe$_2$)$_{Dipp}$), 31.5 ((CHMe$_2$)$_{Dipp}$), 26.5 (Me_{Dipp}), 26.0 (Me_{Dipp}), 25.6 ($Me'_{Dipp'}$), 24.8 ($Me_{Dipp'}$), 24.6 ($Me_{Dipp'}$, $Me'_{Dipp'}$), 21.8 (Me_{Dipp}, Me_{Dipp}), 20.7 (d, $^{1}J_{CP}$ = 49 Hz, PMe*Me*), 16.5 (d, $^{1}J_{CP}$ = 33 Hz, P*Me*Me), 9.0 (C_5Me_5).

$^{31}P\{^{1}H\}$ NMR (160 MHz, CD_2Cl_2, 25 ºC) δ: −3.3.

IR (CH_2Cl_2): υ(IrH) 2306 cm^{-1}.

REFERENCES

[1] Bergman, R. G. *Nature* **2007**, *446*, 391.

[2] Labinger, J. A.; Bercaw, J. E. *Nature* **2002**, *417*, 507.

[3] Caballero, A.; Pérez, P. J. *Chem. Soc. Rev.*, **2013**,*42*, 8809.

[5] Gunsalus, N. J.; Koppaka, A.; Park, S. H.; Bischof, S. M.; Hashiguchi, B. G.; Periana, R. A. *Chem. Rev.* **2017**, *117*, 8521.

[6] a) Belgued, M., Pareja, P., Amariglio, A., Amariglio, H. *Nature* **1991**, *352*, 789; b) Guo, X.; Fang, G.; Li, G.; Ma, H.; Fan, H.; Yu, L.; Ma, C.; Wu, X.; Deng, D.; Wei, M.; Tan, D.; Si, R.; Zhang, S.; Li, J.; Sun, L.; Tang, Z.; Pan, X.; Bao, X. *Science* **2014**, *344*, 616; c) Morejudo, S. H.; Zanon, R.; Escolastico, S.; Yuste-Tirados, I.; Malerod-Fjeld, H.; Vestre, P. K.; Coors, W. G.; Martinez, A.; Norby, T.; Serra, J. M.; Kjølseth, C. *Science* **2016**, *353*, 563.

[7] a) Cook, A. K.; Schimler, S. D.; Matzger, A. J.; Sanford, M. S. *Science* **2016**, *351*, 1421; b) Smith, K. T.; Berritt, S.; Gonzalez-Moreiras, M.; Ahn, S.; Smith, M. R.; Baik, M. H.; Mindiola, D. J. *Science* **2016**, *351*, 1424.

[8] a) Lin, M.; Sen, A. *Nature* **1994**, *368*, 613; b) Periana, R. A., Mironov, O., Taube, D., Bhalla, G., Jones, C. J. *Science* **2003**, *301*, 814; c) Cui, X.; Li, H.; Wang, Y.; Hu, Y.; Hua, L.; Li, H.; Han, X.; Liu, Q.; Yanf, F.; He, L.; Chen, X.; Li, Q.; Xiao, J.; Deng, D.; Bao, X. *Chem* **2018**, *4*, 1902.

[9] a) Periana, R. A.; Taube, D. J.; Gamble, S.; Taube, H.; Satoh, T.; Fujii, H. *Science* **1998**, *280*, 560; b) Caballero, A.; Despagnet-Ayoub, E.; Díaz-Requejo, M. M.; Díaz-Rodríguez, A.; Gonzalez-Nuñez, M. E.; Mello, R.; Muñoz, B. K.; Ojo, W.-S.; Asensio, G.; Etienne, M.; Perez, P. J. *Science* **2011**, *332*, 835.

[10] a) Periana, R. A.; Taube, D. J.; Evitt, E. R.; Löffler, D. G.; Wentrcek, P. R.; Voss, G.; Masuda, T. *Science* **1993**, *259*, 340; b) Hammond, C.; Forde, M. M.; Rahim, M. H. A.; Thetford, A.; He, Q.; Jenkins, R. L.; Dimitratos, N.; Lopez-Sanchez, J. A.; Dummer, N. F.; Murphy, D. M.; Carley, A. F.; Taylor, S. H.; Willock, D. J.; Stangland, E. E.; Kang, J.; Hagen, H.; Kiely, C. J.; Hutchings, G. J. *Angew. Chem., Int. Ed.* **2012**, *51*, 5129; c) Sushkevich, V.L., Palagin, D., Ranocchiari, M., van Bokhoven, J.A.; *Science* **2017**, *356*, 523 e) Agarwal, N.; Freakley, S. J.; McVicker, R. U.; Althahban, S. M.; Dimitratos, N.; He, Q.; Morgan, D. J.; Jenkins, R. L.; Willock, D. J.; Taylor, S. H.; Kiely, C. J.; Hutchings, G. J. *Science* **2017**, *358*, 223.

[11] a) Godula, K.; Sames, D. *Science* **2006**, *312*, 67; b) Rech, J. C.; Yato, M.; Duckett, D.; Ember, B.; LoGrasso, P. V.; Bergman, R. G.; Ellman, J. A. *J. Am. Chem. Soc.* **2007**, *129*, 490; c) Davies, H. M. L.; Manning, J. R. *Nature* **2008**, *451*, 417; d) McMurray, L.; O'Hara, F.; Gaunt, M. J. *Chem. Soc. Rev.* **2011**, *40*, 1885; e) Yamaguchi, J.; Yamaguchi, A. D.; Itami, K. *Angew. Chem. Int. Ed.* **2012**, *51*, 8960; f) Wencel-Delord, J.; Glorius, F. *Nat. Chem.* **2013**, *5*, 369; g) He, J.; Hamann, L. G. H.; Davies, H. M. L.; Beckwith, R. E. J. *Nat. Commun.* **2015**, *6*, 5943.

[12] a) Loh, Y. Y.; Nagao, K.; Hoover, A. J.; Hesk, D.; Rivera, N. R.; Colletti, S. L.; Davies, I. W.; MacMillan, D. W. C. *Science* **2017**, *358*, 1182; b) Atzrodt, J.; Derdau, V.; Kerr; W. J.; Reid, M. *Angew. Chem. Int. Ed.* **2018**, *57*, 3022.

[13] a) Elmore, C. S.; John, E. M. *Annu. Rep. Med. Chem.* Academic Press **2009**, 44, 515; b) Atzrodt, J.; Derdau, V.; Fey, T.; Zimmermann, J. *Angew. Chem. Int. Ed.* **2007**, *46*, 7744.

[14] Shimizu, M., Mochida, K., Hiyama, T. *Angew. Chem. Int. Ed.* **2008**, *47*, 9760.

[15] a) Pan, S. C. *Beilstein J. Org. Chem.* **2012,** *8*, 1374; b) Légaré, M. A.; Courtemanche, M. A.; Rochette, E.; Fontaine, F. G. *Science* **2015**, *349*, 513 c) Qin, Y.; Zhu, L.; Luo, S. *Chem. Rev.* **2017**, *117*, 9433; d) Yi, H.; Zhang, G.; Wang, H.; Huang, Z.; Wang, J.; Singh, A. K.; Lei, A. *Chem. Rev.* **2017**, *117*, 9016.

[16] a) Dimroth, O. *Ber.* **1898**, *31*, 2154; b) Dimroth, O. *Chem. Ber*. **1902**, *35*, 2032.

[17] Kharasch, M.S.; Isbell, H.S. *J. Am. Chem. Soc.* **1931**, *53*, 3053.

[18] Murahashi, S. *J. Am. Chem. Soc.* **1955**, *77*, 6403.

[19] Chatt, J.; Watson, H. R. *J. Chem. Soc.*, **1962**, 2545.

[20] a) Gol'dshleger, N.F.; Tyabin, M.B.; Shilov, A.E.; Shteinman, A. A. *Zh. Fiz. Khim.* **1969**, *43*, 2174 b) Gol'dshleger, N. F.; Shteinman, A. A.; Shilov, A. E.; Eskova, V. V. *Zh. Fiz. Khim.* **1972**, *46*, 1353.

[21] a) van der Boom, M. E.; Milstein, D. *Chem. Rev.* **2003**, *103*, 1759; b) Clot, E.; Chen, J.; Lee; D.-H.; Sung, S. Y.; Appelhans, L. N.; Faller, J. W.; Crabtree, R. H.; Eisenstein, O. *J. Am. Chem. Soc.* **2004**, *126*, 8795; c) Crabtree, R. H. *J. Organomet. Chem.* **2005**, *690*, 5451.

[22] a) Shaw, M. H.; Shurtleff, V. W.; Terrett, J. A.; Cuthbertson, J. D. MacMillan, D. W. C. *Science* **2016**, *352*, 1304; b), Perry, I. B.; Brewer, T. F.; Sarver, P. J.; Schultz, D. M.; DiRocco, D. A.; MacMillan, D. W. C. *Nature* **2018**, *560*, 70; c) Twilton, J.; Le, C.; Zhang, P.; Shaw, M. H.; Evans, R. W.; MacMillan, D. W. C.

Nat. Rev. Chem. **2017**, *1*, 0052; d) Twilton, J.; Christensen, M.; DiRocco, D. A.; Ruck, R. T.; Davies, I. W.; MacMillan, D. W. C. *Angew. Chem. Int. Ed.* **2018**, *57*, 5369.

[23] a) Shrestha, A.; Lee, M.; Dunn, A. L.; Sanford, M. S. *Org. Lett.*, **2018**, *20*, 204; b) Sauermann, N.; Mei, R.; Ackermann, L. *Angew. Chem. Int. Ed.* **2018**, *57*, 5090; c) Qiu, Y.; Kong, W.-J.; Struwe, J.; Sauermann, N.; Rogge, T.; Scheremetjew, A.; Ackermann, L. *Angew. Chem. Int. Ed.* **2018**, *57*, 5828; d) Qiu, Y.; Stangier, M.; Meyer, T. H.; Oliveira, J. C. A.; Ackermann, L. *Angew. Chem. Int. Ed.* **2018**, *57*, 14179.

[24] a) Das, S.; Incarvito, C. D.; Crabtree, R. H.; Brudvig, G. W. *Science* **2006**, *312*, 1941; b) Lyons, T. W.; Sanford, M. S. *Chem. Rev.* **2010**, 110, 1147; c) Engle, K. M.; Mei, T.-S.; Wasa, M.; Yu, J.-Q. *Acc. Chem. Res.* **2012**, *45*, 788; d) Ros, A.; Fernandez, R.; Lassaletta, J. M. *Chem. Soc. Rev.* **2014**, *43*, 3229; e) Zhang, F.-L.; Hong, K.; Li, T.-J.; Park, H.; Yu, J.-Q. *Science* **2016**, *351*, 252; f) Topczewski, J. J.; Cabrera, P. J.; Saper, N. I.; Sanford, M. S. *Nature* **2016**, *531*, 220 g) Gandeepan, P.; Ackermann, L. *Chem* **2018**, *4*, 199.

[25] a) Tenn, W. J.; Young, K. J. H.; Bhalla, G.; Oxgaard, J.; Goddard, W. A.; Periana, R. A. *J. Am. Chem. Soc.* **2005**, *127*, 14172; b) Ess, D. H.; Gunnoe, T. B.; Cundari, T. R.; Goddard, W. A.; Periana, R. A. *Organometallics* **2010**, *29*, 6801; c) Ackermann, L. *Chem. Rev.* **2011**, *111*, 1315; d) Maleckis, A.; Kampf, J. W.; Sanford, M. S. *J. Am. Chem. Soc.* **2013**, *135*, 6618; e) Ackermann, L. *Acc. Chem. Res.* **2014**, *47*, 281; f) Davies, D. L.; Macgregor, S. A.; McMullin, C. L. *Chem. Rev.* **2017**, *117*, 8649.

[26] a) Boursalian, G. B.; Ham, W. S.; Mazzotti, A. R.; Ritter, T. *Nat. Chem.* **2016**, *8*, 810; b) Yi, H.; Zhang, G.; Wang, H.; Huang, Z.; Wang, J.; Singh, A. K.; Lei, A. *Chem. Rev.* **2017**, *117*, 9016; c) Serpier, F.; Pan, F.; Ham, W. S.; Jacq, J.; Genicot, C.; Ritter, T. *Angew. Chem. Int. Ed.* **2018**, *57*, 10697.

[27] Hartwig, J. F. *J. Am. Chem. Soc*. **2016**, *138*, 2.

[28] a) Roudesly, F.; Oble, J.; Poli, G. *J. Mol. Catal. A: Chem* **2017**, *426*, 275; b)Vastine, B. A.; Hall, M. B. *J. Am. Chem. Soc.* **2007**, *129*, 12068.

[29] a) Klei, S. R.; Tilley, T. D.; Bergman, R. G. *J. Am. Chem. Soc.* **2000**, *122*, 1816; b) Balcells, D.; Clot, E.; Eisenstein, O.; *Chem. Rev.* **2010**, *110*, 749; c) Carlsen, R.; Wohlgemuth, N.; Carlson, L.; Ess, D. H. *J. Am. Chem. Soc.* **2018**, *140*, 11039.

[30] Shang, R.; Ilies, L.; Nakamura, E. *Chem. Rev.* **2017**, *117*, 9086.

[31] a) Moselage, M.; Li, J.; Ackermann, L. *ACS Catal.* **2016**, *6*, 498; b) Yoshino, T.; Matsunaga, S. *Adv. Organomet. Chem.* **2017**, *68*, 197.

[32] a) Zhou, W.; Zheng, S.; Schultz, J. W.; Rath, N. P.; Mirica, L. M. *J. Am. Chem. Soc.* **2016**, *138*, 5777; b) Chong, E.; Kampf, J. W.; Ariafard, A.; Canty, A. J.; Sanford, M. S. *J. Am. Chem. Soc.* **2017**, *139*, 6058.

[33] a) Gava, R.; Olmos, A.; Noverges, B.; Varea, T.; Álvarez, E.; Belderrain, T. R.; Caballero, A.; Asensio, G.; Pérez, P. J. *ACS Catal.* **2015**, *5*, 3726; b) Guo, X.-X.; Gu, D.-W.; Wu, Z.; Zhang, W. *Chem. Rev.* **2015**, *115*, 1622.

[34] Crabtree, R. H., Mihelcic, J. M.; Quirk, J. M. *J. Am. Chem. Soc.* **1979**, *101*, 7738.

[35] Felkin, H.; Fillebeen-Khan, T.; Gault, Y.; Holmes-Smith, R.; Zakrzewski, J. *Tetrahedron Lett.* **1984**, *25*, 1279.

[36] Liu, F.; Pak, E. B.; Singh, B.; Jensen, C. M.; Goldman, A. S. *J. Am. Chem. Soc.* **1999**, *121*, 4086.

[37] Goldman, A. S.; Roy, A. H.; Huang, Z.; Ahuja, R.; Schinski, W.; Brookhart, M. *Science* **2006**, *312*, 257.

[38] Green, M. L. H.; Knowles, P. J. *J. Chem. Soc. D* **1970**, *0*, 1677.

[39] Janowicz, A.H.; Bergman, R. G. *J. Am. Chem. Soc.* **1982**, *104*, 352.

[40] Hoyano, J. K.; Graham, W.A.G. *J. Am. Chem. Soc.* **1982**, *104*, 3723.

[41] Arndtsen, B. A.; Bergman, R. G. *Science* **1995**, *270*, 1970.

[42] Iverson, C. N.; Smith, M. R. *J. Am. Chem. Soc.* **1999**, *121*, 7696.

[43] Ishiyama, T.; Takagi, J.; Ishida, K.; Miyaura, N.; Anastasi, N. R.; Hartwig, J. F. *J. Am. Chem. Soc.* **2002**, *124*, 390.

[44] a) Zhou, M.; Schley, N. D.; Crabtree, R. H. *J. Am. Chem. Soc.* **2010**, *132*, 12550; b) Zhou, M.; Balcells, D.; Parent, A. R.; Crabtree, R. H.; Eisenstein, O. *ACS Catal.* **2012**, *2*, 208.

[45] a) Pérez, P. J.; Poveda, M. L.; Carmona, E. *J. Chem. Soc., Chem. Commun.* **1992**, 8; b) Boutry, O.; Gutiérrez, E.; Monge, A.; Nicasio, M. C.; Pérez, P. J.; Carmona, E. *J. Am. Chem. Soc.* **1992**, *114*, 7288; c) Gutiérrez, E.; Monge, A.; Nicasio, M. C.; Poveda, M. L.; Carmona, E. *J. Am. Chem. Soc.* **1994**, *116*, 791; d) Alvarado, Y.; Boutry, O.; Gutiérrez, E.; Monge, A.; Nicasio, M. C.; Poveda, M. L.; Pérez, P. J.; Ruíz, C.; Bianchini, C.; Carmona, E. *Chem. Eur. J.* **1997**, *3*, 860; e) Gutiérrez-Puebla, E.; Monge, A.; Nicasio, M. C.; Pérez, P. J.; Poveda, M. L.; Carmona, E. *Chem. Eur. J.* **1998**, *4*, 2225; f) Alías, F. M.; Poveda, M. L.; Sellin, M.; Carmona, E. *J. Am. Chem. Soc.* **1998**, *120*, 5816; g) Slugovc, C.; Padilla-

Martínez, I.; Sirol, S.; Carmona, E. *Coord. Chem. Rev.* **2001**, *213*, 129; h) Carmona, E.; Paneque, M.; Poveda, M. L. *Dalton Trans.* **2003**, 4022; i) Conejero, S.; Paneque, M.; Poveda, M. L.; Santos, L. L.; Carmona, E. *Acc. Chem. Res.* **2010**, *43*, 572.

[46] Klei, S. R.; Golden, J. T.; Burger, P.; Bergman, R. G. *J. Mol. Catal. A Chem.* **2002**, *189*, 79.

[47] Campos, J.; López-Serrano, J.; Álvarez, E.; Carmona, E. *J. Am. Chem. Soc.* **2012**, *134*, 7165.

[48] a) doyle, T. J.; Milner, P. J.; Kinzel, T.; Zhang, Y.; Takase, M. K.; Buchwald, S. L. *J. Am. Chem. Soc.* **2011**, *133*, 18106; b) Milner, P. J.; Maimone, T. J.; Su, M.; Chen, J.; Müller, P.; Buchwald, S. L. *J. Am. Chem. Soc.* **2012**, 134, 19922; c) Sather, A. C.; Lee, H. G.; De La Rosa, V. Y.; Yang, Y.; Müller, P.; Buchwald, S. L. *J. Am. Chem. Soc.* **2015**, *137*, 13433; d) Sather, A. C.; Buchwald, S. L. *Acc. Chem. Res.* **2016**, *49*, 2146.

[49] Crabtree, R. H. *Chem. Rev.* **2015**, *115*, 127.

[50] a) Zhang, S.; Chu, X.; Li, T.; Wang, Z.; Zhu, B. *ACS Omega* **2018**, *3*, 4522; b) Guenther, J.; Mallet-Ladeira, S.; Estevez, L.; Miqueu, K.; Amgoune, A.; Bourissou, D. *J. Am. Chem. Soc.* **2014**, *136*, 1778; c) Kiener, C. A.; Shu, C.; Incarvito, C.; Hartwig, J. F. *J. Am. Chem. Soc.* **2003**, *125*, 14272; d) Montag, M.; Leitus, G.; Shimon, L. J. W.; Ben-David, Y.; Milstein, D. *Chem. Eur. J.* **2007**, *13*, 9043; e) Millard, M. D.; Moore, C. E.; Rheingold, A. L.; Figueroa, J. S. *J. Am. Chem. Soc.* **2010**, *132*, 8921; f) Han, Y.-F.; Jin, G.-X. *Chem. Soc. Rev.* **2014**, *43*, 2799.

[51] a) Nielsen, D. K.; Doyle, A. G. *Angew. Chem. Int. Ed.* **2011**, *50*, 6056; b) Allgeier, A. M.; Shaw, B. J.; Hwang, T. L.; Milne, J. E.; Tedrow, J. S.; Wilde, C. N. *Organometallics* **2012**, *31*, 519.

[52] a) Glueck, D. S.; Bergman, R. G. *Organometallics* **1990**, *9*, 2862; b) Fan, L.; Wei, C.; Aigbirhio, F. I.; Turner, M. L.; Gusev, O. V.; Morozova, L. N.; Knowles, D. R. T.; Maitlis, P. M. *Organometallics* **1996**, *15*, 98; c) Rais, D.; Bergman, R. G. *Chem. - Eur. J.* **2004**, *10*, 3970; d) Caldwell, H.; Pregosin, P. S. *Organometallics* **2008**, *27*, 1591; e) Bernechea, M.; Berenguer, J. R.; Lalinde, E.; Torroba, J. *Organometallics* **2009**, *28*, 312; f) Thomas, H. P.; Marr, A. C.; Morgan, P. J.; Saunders, G. C. *Organometallics* **2018**, *37*, 1339.

[53] Meredith, J. M.; Goldberg, K. I.; Kaminsky, W.; Heinekey, D. M. *Organometallics* **2012**, *31*, 8459.

[54] a) Paneque, M.; Maitlis, P. M. *J. Chem. Soc., Chem. Commun.* **1989**, 105; b) Jones, W. D.; Kuykendall, V. L.; Selmeczy, A. D. *Organometallics* **1991**, *10*,

1577; c) Quintana, L. M. A.; Johnson, S. I.; Corona, S. L.; Villatoro, W.; Goddard, W. A.; Takase, M. K.; VanderVelde, D. G.; Winkler, J. R.; Gray, H. B.; Blakemore, J. D. *Proc. Natl. Acad. Sci. USA* **2016**, *113*, 6409; d) Pitman, C. L.; Finster, O. N. L.; Miller, A. J. M. *Chem. Commun.* **2016**, *52*, 9105; e) Zamorano, A.; Rendón, N.; Valpuesta, J. E. V.; Álvarez, E.; Carmona, E. *Inorg. Chem.* **2015**, *54*, 6573.

[55] Chalkley, M.; Del Castillo, T. J.; Matson, B. D.; Roddy, J. P.; Peters, J. C. *ACS Cent. Sci*. **2017**, *3*, 217.

[56] Crabtree, R. H. *J. Organomet. Chem.* **2005**, *690*, 5451.

[57] a) Campos, J.; Esqueda, A. C.; Carmona, E. *Chem. Eur. J.* **2010**, *16*, 419; b) Campos, J.; Esqueda, A. C.; López-Serrano, J.; Sánchez, L.; Cossío, F. F.; de Cózar, A.; Álvarez, E.; Maya, C.; Carmona, E. *J. Am. Chem. Soc.* **2010**, *132*, 16765; c) Rubio, M.; Campos, J.; Carmona, E. *Org. Lett.* **2011**, *13*, 5236; d) Campos, J.; Espada, M. F.; López-Serrano, J.; Carmona, E. *Inorg. Chem.* **2013**, *52*, 6694.

[58] Old, D. W.; Wolfe, J. P.; Buchwald, S. L. *J. Am. Chem. Soc.* **1998**, *120*, 9722.

[59] a) Martin, R.; Buchwald, S. L. *Acc. Chem. Res.* **2008**, *41*, 1461 b) Sather, A. C.; Buchwald, S. L. *Acc. Chem. Res.* **2016**, *49*, 2146.

[60] Nguyen, T.; Sutton, A. D.; Brynda, M.; Fettinger, J. C.; Long, G. J.; Power, P. P. *Science* **2005**, *310*, 844.

[61] a) Ndambuki, S.; Ziegler, T. *Inorg. Chem.*, **2012**, *51*, 7794; b) Seidu, I.; Seth, M.; Ziegler, T. *Inorg. Chem.* **2013**, *52*, 8378; c) Lin, C.-Y.; Guo, J.-D.; Fettinger, J. C.; Nagase, S.; Grandjean, F.; Long, G.; Chilton, N. F.; Power, P. P. *Inorg. Chem.* **2013**, *52*, 13584; d) Rekken, B. D.; Brown, T. M.; Fettinger, J. C.; Lips, F.; Tuononen, H. M.; Herber, R. H.; Power, P. P. *J. Am. Chem. Soc.* **2013**, *135*, 10134; e) Wagner, C. L.; Tao, L.; Thompson, E. J.; Stich, T. A.; Guo, J.; Fettinger, J. C.; Berben, L. A.; Britt, R. D.; Nagase, S.; Power, P. P. *Angew. Chem. Int. Ed.* **2016**, *55*, 10444; f) Liptrot, D. J.; Power, P. P. *Nat. Rev. Chem.* **2017**, *1*, 4.

[62] a) Mokhtarzadeh, C. C.; Moore, C. E.; Rheingold, A. L.; Figueroa, J. S. *Angew. Chem. Int. Ed.* **2017**, *56*, 10894; b) Mokhtarzadeh, C. C.; Moore, C. E.; Rheingold, A. L.; Figueroa, J. S. *J. Am. Chem. Soc.* **2018**, *140*, 8100.

[63] Espada, M. F.; Campos, J.; López-Serrano, J.; Poveda, M. L.; Carmona, E. *Angew. Chem. Int. Ed.* **2015**, *54*, 15379.

[64] Campos, J. *J. Am. Chem. Soc.* **2017**, *139*, 2944.

[65] Marin, M.; Moreno, J. J.; Navarro-Gilabert, C.; Álvarez, E.; Maya, C.; Peloso, R.; Nicasio, M. C.; Carmona, E. *Chem. Eur. J.* **2018**, *in press.*

[66] Moreno, J. J.; Espada, M. F.; Krüger, E.; López-Serrano, J.; Campos, J.; Carmona, E. *Eur. J. Inorg. Chem.* **2018**, 2309.

[67] Campion, B. K.; Heyn, R. H.; Tilley, T. D. *J. Chem. Soc., Chem. Commun.* **1988**, 278.

[68] Johnson, T. J.; Folting, K.; Streib, W. E.; Martin, J. D.; Huffman, J. C.; Jackson, S. A.; Eisenstein, O.; Caulton, K. G. *Inorg. Chem.* **1995**, *34*, 488.

[69] Lehman, M. C.; Gary, J. B.; Boyle, P. D.; Sanford, M. S.; Ison, E. A. *ACS Catal.* **2013**, *3*, 2304.

[70] Ogo, S.; Makihara, N.; Watanabe, Y. *Organometallics* **1999**, *18*, 5470.

[72] Thomson, J.; Baird, M. C. *Can. J. Chem.* **1973**, *51*, 1179.

[74] Niu, S.; Hall, M. B. *J. Am. Chem. Soc.* **1998**, *120*, 6169.

[75] a) Lapointe, D.; Fagnou, K. *Chem. Lett.* **2010**, *39*, 1118; b) Davies, D. L.; Donald, S. M. A.; Macgregor, S. A. *J. Am. Chem. Soc.* **2005**, *127*, 13754; c) Davies, D. L.; Donald, S. M. A.; Al-Duaij, O.; Macgregor, S. A.; Pölleth, M. *J. Am. Chem. Soc.* **2006**, *128*, 4210.

[76] Boutadla, Y.; Davies, D. L.; Macgregor, S. A.; Poblador-Bahamonde, A. L. *Dalton Trans.* **2009**, 5820.

[77] Davies, D. L.; Macgregor, S. A.; McMullin, C. *Chem. Rev.* **2017**, *117*, 8649.

[78] a) Pike, S. D.; Weller, A. S. *Phil. Trans. R. Soc. A* **2015**, *373*, 20140187; b) Pike, S. D.; Chadwick, F. M.; Rees, N. H.; Scott, M. P.; Weller, A. S.; Krämer, T.; Macgregor, S. A. *J. Am. Chem. Soc.* **2015**, *137*, 820; c) Pike, S. D.; Thompson, A. L.; Algarra, A. G.; Apperley, D. C.; Macgregor, S. A.; Weller, A. S. *Science* **2012**, *337*, 1648; d) Chaplin, A. B.; Green, J. C.; Weller, A. S. *J. Am. Chem. Soc.* **2011**, *133*, 13162; e) Huang, Z.; White, P. S.; Brookhart, M. *Nature* **2010**, *465*, 598; f) Bianchini, C.; Farnetti, E.; Graziani, M.; Kaspar, J.; Vizza, F. *J. Am. Chem. Soc.* **1993**, *115*, 1753.

[79] a) Miguel-Garcia, J. A.; Maitlis, P. M. *J. Chem. Soc., Chem. Commun.* **1990**, 1472; b) Gusev, O. V.; Rubezhov, A. Z.; Miguel-Garcia, J. A.; Maitlis, P. M. *Mendeleev Commun.* **1991**, *1*, 21.

[80] a) Kang, J. W.; Maitlis, P. M. *J. Organomet. Chem.*, **1971**, *30*, 127; b) Nutton, A.; Maitlis, P. M. *J. Chem. Soc., Dalton Trans.* **1981**, 2335.

[81] a) Mulliken, R. S. *J. Chem. Phys.* **1955**, *23*, 1833; b) Mayer, I. *Chem. Phys. Lett.* **1983**, *97*, 270; c) Lowdin, P. O. *Phys. Rev.* **1955**, *97*, 1474.

[82] Reed, A. E.; Curtiss, L. A.; Weinhold, F. *Chem. Rev.* **1988**, *88*, 899.

[83] Bader, R. F. W. *Atoms in Molecules: A Quantum Theory*, Oxford University Press, Oxford, **1995**.

[84] a) Boys, S. F. *Rev. Mod. Phys.* **1960**, *32*, 296; b) Foster, J. M.; Boys, S. F. *Rev. Mod. Phys.* **1960**, *32*, 300.

[85] Vidossich, P.; Lledós, A. *Dalton Trans.* **2014**, *43*, 11145.

[86] Kermack, W. O.; Robinson, R. *J. Chem. Soc., Trans.* **1922**, *121*, 427.

[87] Campos, J.; López-Serrano, J.; Peloso, R.; Carmona, E. *Chem. Eur. J.* **2016**, *22*, 6432.

[88] Schrock, R. R. *J. Am. Chem. Soc.* **1975**, *97*, 6577.

[89] Bernskoetter, W. H.; Schauer, C. K.; Goldberg, K. I.; Brookhart, M. *Science* **2009**, *326*, 553.

[90] a) Marinelli, G.; Rachidi, I. E.-I.; Streib, W. E.; Eisenstein, O.; Caulton, K. G. *J. Am. Chem. Soc.* **1989**, *111*, 2346; b) Geer, A. M.; Julián, A.; López, J. A.; Ciriano, M. A.; Tejel, C. *Chem. Eur. J.* **2018**, *24*, 1.

[91] Crabtree, R. H.; Morris, G. E. *J. Organomet. Chem*. **1977**, *135*, 395.

[92] Kolychev, E. L.; Kronig, S.; Brandhorst, K.; Freytag, M.; Jones, P. G.; Tamm, M. *J. Am. Chem. Soc.* **2013**, *135*, 12448 and references therein.

[93] a) Pons, V.; Heinekey, D. M. *J. Am. Chem. Soc.* **2003**, *125*, 8428; b) Göttker-Schnetmann, I.; Heinekey, D. M.; Brookhart, M. *J. Am. Chem. Soc.* **2006**, *128*, 17114; c) Goldberg, J. M.; Goldberg, K. I.; Heinekey, D. M.; Burgess, S. A.; Lao, D. B.; Linehan, J. C. *J. Am. Chem. Soc.* **2017**, *139*, 12638.

[94] a) Crabtree, R. H. *Acc. Chem. Res.* **1990**, *23*, 95; b) Kubas, G. J. Metal Dihydrogen and Sigma-Bond Complexes. Structure, Theory and Reactivity. Kluwer Academic: New York, **2001**; c) Kubas, G. J. *J. Organomet. Chem.* **2014**, *751*, 33.

[95] Hamilton, D. G.; Crabtree, R. H. *J. Am. Chem. Soc.* **1988**, *110*, 4126.

[96] a) Klooster, W. T.; Koetzle, T. F.; Jia, G.; Fong, T. P.; Morris, R. H.; Albinati, A. *J. Am. Chem. Soc.* **1994**, *116*, 7677; b) Barea, G.; Esteruelas, M. A.; Lledós,

A.; López, A. M.; Tolosa, J. I. *Inorg. Chem.* **1998**, *37*, 5033; c) Crabtree, R. H. *Chem. Rev.* **2016**, *116*, 8750.

[97] Stephan, D. W. *Acc. Chem. Res.*, **2015**, *48*, 306.

[98] a) Forrest, S. J. K.; Clifton, J.; Fey, N.; Pringle, P. G.; Sparkes, H. A.; Wass, D. F. *Angew. Chem. Int. Ed.* **2015**, *54*, 2223; b) Metters, O. J.; Forrest, S. J. K.; Sparkes, H. A.; Manners, I.; Wass, D. F. *J. Am. Chem. Soc.* **2016**, *138*, 1994; c) Metters, O. J.; Flynn, S. R.; Dowds, C. K.; Manners, I. Wass, D. F. *ACS Catal.* **2016**, *6*, 6601.

[99] a) Xu, X.; Kehr, G.; Daniliuc, C. G.; Erker, G. *J. Am. Chem. Soc.* **2014**, *136*, 12431; b) Xu, X.; Kehr, G.; Daniliuc, C. G.; Erker, G. *Organometallics* **2015**, *34*, 2655; c) Xu, X.; Kehr, G.; Daniliuc, C. G.; Erker, G. *J. Am. Chem. Soc.* **2015**, *137*, 4550; d) Normand, A. T.; Richard, P.; Balan, C.; Daniliuc, C. G.; Kehr, G.; Erker, G.; Le Gendre, P. *Organometallics* **2015**, *34*, 2000; e) Normand, A. T.; Daniliuc, C. G.; Wibbeling, B.; Kehr, G.; Le Gendre, P.; Erker, G. *J. Am. Chem. Soc.* **2015**, *137*, 10796.

[100] a) Devillard, M.; Bouhadir, G.; Bourissou, D. *Angew. Chem. Int. Ed.* **2015**, *54*, 730; b) Devillard, M.; Declercq, R.; Nicolas, E.; Ehlers, A. W.; Backs, J.; Saffon-Merceron, N.; Bouhadir, G.; Slootweg, J. C.; Uhl, W.; Bourissou, D. *J. Am. Chem. Soc.* **2016**, *138*, 4917.

[101] Cleary, B. P.; Eisenberg, R. *Inorganica Chim. Acta* **1995**, *240*, 135.

[102] a) Jayarathne, U.; Parmelee, S. R.; Mankad, N. P. *Inorg. Chem.* **2014**, *53*, 7730; b) Zhang, H.; Wu, B.; Marquard, S. L.; Litle, E. D.; Dickie, D. A.; Bezpalko, M. W.; Foxman, B. M.; Thomas, C. M. *Organometallics*, **2017**, *36*, 3498; c) Poitras, A. M.; Knight, S. E.; Bezpalko, M. W.; Foxman, B. M.; Thomas, C. M. *Angew. Chem. Int. Ed.* **2018**, *57*, 1497.

[103] a) Mazzacano, T. J.; Mankad, N. P. *J. Am. Chem. Soc.* **2013**, *135*, 17258; b) Wu, B.; Gramigna, K. M.; Bezpalko, M. W.; Foxman, B. M.; Thomas, C. M. *Inorg. Chem.* **2015**, *54*, 10909; c) Karunananda, M. K.; Mankad, N. P. *J. Am. Chem. Soc.* **2015**, *137*, 14598; d) Pye, D. R.; Cheng, L.-J.; Mankad, N. P. *Chem. Sci.* **2017**, *8*, 4750; e) Coombs, J.; Perry, D.; Kwon, D.-H.; Thomas, C. M.; Ess, D. H. *Organometallics*, **2018**, *37*, 4195.

[104] Johnstone, T. C.; Wee, G. N. J. H.; Stephan, D. W. *Angew. Chem. Int. Ed.* **2018**, *57*, 5881.

[105] a) Kua, J.; Krizner, H. E.; De Haan, D. O. *J. Phys. Chem. A* **2011**, *115*, 1667; b) Han, L.-L.; Li, S.-J.; Fang, D.-C. *Phys. Chem. Chem. Phys.* **2016**, *18*, 6182.

[107] Gusev, D. G.; Notheis, J. U.; Rambo, J. R.; Hauger, B. E.; Eisenstein, O.; Caulton, K. G. *J. Am. Chem. Soc.* **1994**, *116*, 7409.

[108] White, C.; Yates, A.; Maitlis, P. M.; Heinekey, D. M. *Inorg. Synth.* **1992**, *29*, 228.

[109] Yakelis, N. A.; Bergman, R. G. *Organometallics* **2005**, *24*, 3579.

[110] Goel, R. G.; Ogini, W. O.; Srivastava, R. C. *J. Organomet. Chem.* **1981**, *214*, 405.

[111] a) Campos, J.; Ortega-Moreno, L.; Conejero, S.; Peloso, R.; López-Serrano, J.; Maya, C.; Carmona, E. *Chem. Eur. J.* **2015**, *21*, 8883; b) Ortega-Moreno, L.; Peloso, R.; Maya, C.; Suárez, A.; Carmona, E. *Chem. Commun.* **2015**, *51*, 17008.

[112] Frisch, M. J.; Trucks, G. W.; Schlegel, H. B.; Scuseria, G. E.; Robb, M. A.; Cheeseman, J. R.; Scalmani, G.; Barone, V.; Mennucci, B; Petersson, G. A.; Nakatsuji, H.; Caricato, M.; Li, X.; Hratchian, H. P.; Izmaylov, A. F.; Bloino, J.; Zheng, G.; Sonnenberg, J. L.; Hada, M.; Ehara, M.; Toyota, K.; Fukuda, R.; Hasegawa, J.; Ishida, M.; Nakajima, T.; Honda, Y.; Kitao, O.; Nakai, H.; Vreven, T.; Montgomery, J. A. J.; Peralta, J. E.; Ogliaro, F.; Bearpark, M.; Heyd, J. J.; Brothers, E.; Kudin, K. N.; Staroverov, V. N.; Kobayashi, R.; Normand, J.; Raghavachari, K.; Rendell, A.; Burant, J. C.; Iyengar, S. S.; Tomasi, J.; Cossi, M.; Rega, N.; Millam, J. M.; Klene, M.; Knox, J. E.; Cross, J. B.; Bakken, V.; Adamo, C.; Jaramillo, J.; Gomperts, R.; Stratmann, R. E.; Yazyev, O.; Austin, A. J.; Cammi, R.; Pomelli, C.; Ochterski, J. W.; Martin, R. L.; Morokuma, K.; Zakrzewski, V. G.; Voth, G. A.; Salvador, P.; Dannenberg, J. J.; Dapprich, S.; Daniels, A. D.; Farkas, O.; Foresman, J. B.; Ortiz, J. V.; Cioslowski, J.; Fox, D. J.; Gaussian 09, Revision D.01, Gaussian, Inc.: Wallingford CT, **2013**.

[113] Perdew, J. P.; Burke, K.; Ernzerhof, M. *Phys. Rev. Lett.* **1996**, *77*, 3865.

[114] Chai, J.-D.; Head-Gordon, M. *Phys. Chem. Chem. Phys.* **2008**, *10*, 6615.

[115] Grimme, S.; Antony, J.; Ehrlich, S.; Krieg, H. *J. Chem. Phys.* **2010**, *132*, 154104.

[116] a) Hehre, W. J.; Ditchfield, R.; Pople, J. A. *J. Phys. Chem.* **1972**, *56*, 2257; b) Hariharan, P. C.; Pople, J. A. *Theor. Chim. Acta.* **1973**, *28*, 213; c) Francl, M. M.; Pietro, W. J.; Hehre, W. J.; Binkley, J. S.; Gordon, M. S.; Defrees, D. J.; Pople, J. A. *J. Chem. Phys.* **1982**, *77*, 3654.

[117] Andrae, D.; Haeussermann, U.; Dolg, M.; Stoll, H.; Preuss, H. *Theor. Chim. Acta* **1990**, *77*, 123.

[118] Marenich, A. V.; Cramer, C. J.; Truhlar, D. G. *J. Phys. Chem. B* **2009**, *113*, 6378.

[119] a) Ríos, P.; Rodríguez, A.; López-Serrano, J. *ACS Catal.* **2016**, *6*, 5715; b) Deubel, D. V. *J. Am. Chem. Soc.* **2008**, *130*, 665.

[120] Pipek, J.; Mezey, P.G. *J. Chem. Phys*. **1989**, *90*, 4916.

Chapter II

Hemilabile Behavior of Dialkyl Terphenyl Phosphines

II.1 INTRODUCTION

II.1.1 Ligand Hemilability in Organometallic Chemistry

Substrate coordination to the metal center of a complex is a fundamental step in transition metal-mediated homogeneous catalysis. This process requires a vacant site to be present in the first coordination sphere of the complex, highlighting the potential of unsaturated transition metal complexes as catalysts.[1] However, low coordinate species tend to be very reactive, leading to unforeseen reactions and catalyst deactivation.[2] Over the years, several strategies have emerged in order to hamper these undesired reactions, including the kinetic stabilization of the complex by the use of bulky ligands or employing hemilabile[3] ligands, which are hybrid, potentially polydentate ligands for which one of the coordinating functionalities can be displaced from the coordination sphere of the metal center while at least one group remains bound to the metal. These ligands can tame the exacerbated reactivity of unsaturated species while providing open coordination sites upon the reversible dissociation of the hemilabile group, permitting substrate coordination and, therefore, catalysis[4] (Scheme 1).

---

[1] Van Leeuwen, P. W. N. M. *Homogeneous Catalysis: Understanding the Art*; Kluwer Academic Publishers: Dordrecht, **2004**.
[2] Crabtree, R. H. *Chem. Rev.* **2015**, *115*, 127.
[3] Jeffrey, J. C.; Rauchfuss, T. B. *Inorg. Chem.* **1979**, *18*, 2658.
[4] a) Bader, A.; Lindner, E. *Coord. Chem. Rev.* **1991**, *108*, 27; b) Slone, C. S.; Weinberger, D. A.; Mirkin, C. A. *Prog. Inorg. Chem.* **1999**, *48*, 233; c) Braunstein, P.; Naud, F. *Angew. Chem. Int. Ed.* **2001**, *40*, 680; d) Bassetti, M. *Eur. J. Inorg. Chem.* **2006**, 4473; e) Zhang, W.-H.; Chien, S. W.; Hor, T. S. A. *Coord. Chem. Rev.* **2011**, *255*, 1991.

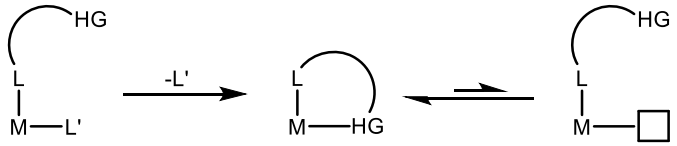

Scheme 1. Reversible coordination of an hemilabile group (HG) to a vacant site, represented as a square, generated upon dissociation of a ligand (L').

These strategies are not incompatible, and in fact the use of bulky, hemilabile ligands, such as the terphenyl radical was key to access exceptionally unsaturated species, being a paradigmatic example the isolation of the first dimetallic compound featuring a quintuple metal-metal bond[5] (Figure 1).

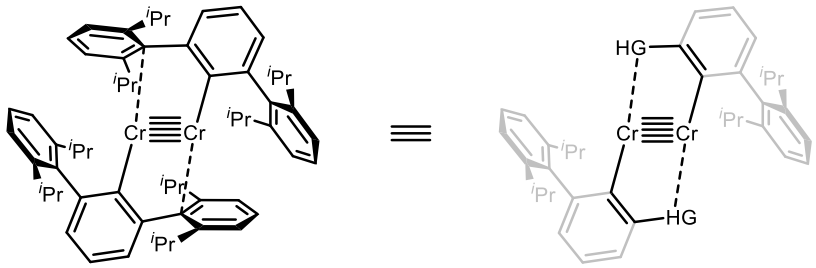

Figure 1. Power´s first quintuply bonded dimetallic compound, featuring weak metal-arene interactions with the hemilabile terphenyl ligand.

In 1968, Öfele[6] and Wanzlick[7] independently reported the first metal complexes bearing N-Heterocyclic carbenes (NHCs) as ligands. After the discovery of stable, free carbenes by Bertrand[8] and Arduengo,[9] these

[5] Nguyen, T.; Sutton, A. D.; Brynda, M.; Fettinger, J. C.; Long, G. J.; Power, P. P. *Science* **2005**, *310*, 844.
[6] Öfele, K. *J. Organomet. Chem.* **1968**, *12*, 42.
[7] Wanzlick, H. W.; Schönherr, H.-J. *Angew. Chem. Int. Ed. Engl.* **1968**, *7*, 141.
[8] a) Baceiredo, A.; Bertrand, G.; Sicard, G. *J. Am. Chem. Soc.* **1985**, *107*, 4781; b) Igau, A.; Grutzmacher, H.; Baceiredo, A.; Bertrand, G. *J. Am. Chem. Soc.* **1988**, *110*, 6463.

species have become the ligand of choice for many catalytic applications,[10] mainly due to the unique electronic properties of these ligands.[11] However, among the various approaches developed to improve the catalytic performance of carbene-containing transition metal complexes,[12] the use of hemilabile functionalities will be briefly discussed.

Although the widely used, arene-containing family of NHCs can take advantage of the hemilabile character of the flanking aryl group to stabilize unsaturated species[13] (Figure 2, Tamm), hemilabile carbene ligands usually bear a tethered functionality,[12] including heteroatom donor groups[14] or unsaturated C–C bonds[15] (Figure 2).

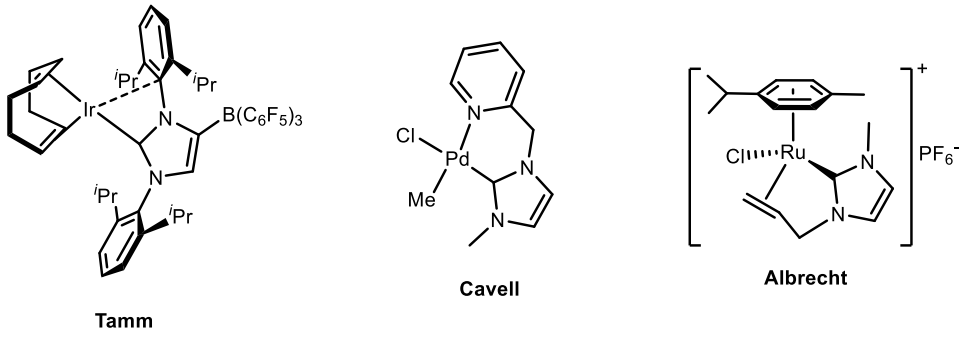

Figure 2. Selected examples of NHC ligand displaying hemilabile behavior.

---

[9] Arduengo, A. J.; Harlow, R. L.; Kline, M. *J. Am. Chem. Soc.* **1991**, *113*, 361.
[10] Hopkinson, M. N.; Richter, C.; Schedler, M.; Glorius, F. *Nature* **2014**, *510*, 485.
[11] a) Nelson, D. J.; Nolan, S. P. *Chem. Soc. Rev.* **2013**, *42*, 6723; b) Huynh, H. V. *Chem. Rev.* **2018**, *118*, 9457.
[12] Peris, E. *Chem. Rev.* **2018**, *118*, 9988.
[13] Kolychev, E. L.; Kronig, S.; Brandhorst, K.; Freytag, M.; Jones, P. G.; Tamm, M. *J. Am. Chem. Soc.* **2013**, *135*, 12448.
[14] McGuinness, D. S.; Cavell, K. J. *Organometallics*, **2000**, *19*, 741.
[15] Horn, S.; Albrecht, M. *Chem. Commun.* **2011**, *47*, 8802.

Cyclopentadienyl ligands, which have played a fundamental role in the development of organometallic chemistry and homogeneous catalysis, have also been functionalized with donor groups bound in a hemilabile fashion (Figure 3, left).[16] Focusing on C_5Me_4X complexes, where X is a pendant arm bearing an hemilabile group, particular interest has been devoted to cyclopentadienylphosphine ligands, due to their participation in homogeneous catalytic processes[17] (Figure 3, right).

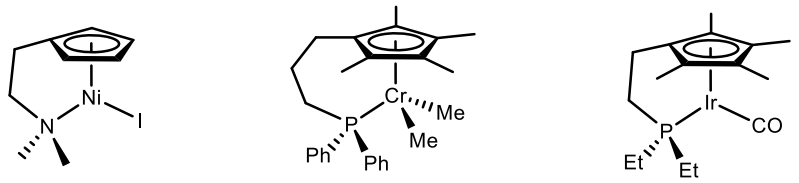

Fischer **Jensen & Jolly** **Cole-Hamilton**

Figure 3. Functionalized cyclopentadienyl ligands bearing amino- and phosphino functionalities.

[16] Jutzi, P.; Redeker, T. *Eur. J. Inorg. Chem.* **1998**, 663 and references therein.
[17] a) Butenschön, H. *Chem. Rev.* **2000**, *100*, 1527; b) Döhring, A.; Jensen, V. R.; Jolly, P. W.; Thiel, W.; Weber, J. C. *Organometallics* **2001**, *20*, 2234; c) McConnell, A. C.; Pogrozelec, P. J.; Slawin, A. M. Z.; Williams, G. L.; Elliott, P. I. P.; Haynes, A.; Marr, A. C.; Cole-Hamilton, D. J. *Dalton Trans.* **2006**, 91; d) Marr, A. C.; Nieuwenhuyzen, M.; Pollock, C. L.; Saunders, G. C. *Organometallics* **2007**, *26*, 2659; e) Bernechea, M.; Berenguer, J. R.; Lalinde, E.; Torroba, J. *Organometallics* **2009**, *28*, 312.

II.1.2 Hemilabile Phosphine Ligands

Tertiary phosphines (PR_3, where R represents an alkyl or aryl group) have got a fundamental relevance in the development of organometallic chemistry, particularly in catalysis, as they constitute one of the few types of ligands in which electronic and steric properties can be modified in a systematic and predictable manner using different R groups. So, by tuning the electronic influence and the size and shape of R it is possible to control the electron-richness of the metallic center and the steric hindrance in its environment. As a difference with respect to the analogous complexes with NR_3 ligands, metal-phosphine complexes use to have good solubility properties in common organic solvents and are also compatible with different oxidation states of the metal, properties that make them useful in homogeneous catalysis. Wilkinson´s catalyst,[18] $RhCl(PPh_3)_3$ (Scheme 2), constitutes a paradigmatic example of a phosphine-containing homogeneous catalysts. Although it is not an organometallic compound itself, organometallic Rh(III) intermediates participate in the catalytic hydrogenation of olefins.

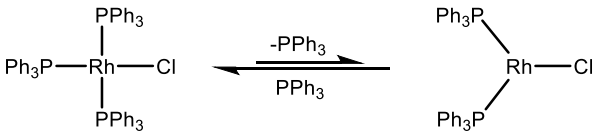

Precatalyst Active catalyst

Scheme 2. Wilkinson´s catalyst (left) and the true, unsaturated active specie, generated upon dissociation of one phosphine ligand.

[18] Young, J. F.; Osborn, J. A.; Jardine, F. H.; Wilkinson, G. *Chem. Commun.* **1965**, 131.

Diverse structural motifs have been developed to attach hemilabile functionalities to phosphine ligands. In order to facilitate the discussion, only three representative examples will be discussed: phosphino-borane, pincer type and dialkylbiaryl phosphine ligands.

II.1.2.1 Phosphine-Borane Ligands

The incorporation of Lewis acidic functionalities (Z-class ligands) to transition metal complexes is a promising strategy to achieve cooperative catalysis. Bound, σ-acceptor groups can display hemilabile-like behavior, for they can, upon reversible coordination of an X type ligand (e.g. hydride), break the M−Z bond and generate a vacant site at the metal center[19] (Scheme 3).

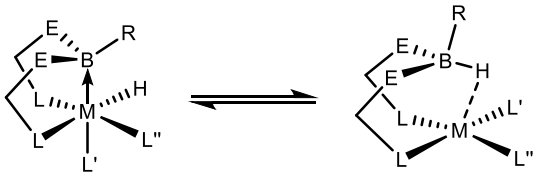

Scheme 3. Metal to boron hydrogen transfer.

Peters exploited this feature to achieve unprecedented efficiency in Ni-mediated styrene hydrogenation[20] (Scheme 4). Z-type ligands are not normally considered as hemilabile, however, in addition to a boron-nickel interaction Peters' complex also displays a short η^2 contact with the proximal aryl group, that vanishes upon incorporation of dihydrogen. Similar behavior was disclosed for a Pt compound containing a borane-appended analogue of bis(diphenylphosphino)ferrocene.[21] More recently, Peters' group disclosed that the Ni(0) complex is also an active hydrosilylation catalyst.[22]

[19] Owen, G. R. *Chem. Soc. Rev.* **2012**, *41*, 3535.
[20] Harman, W. H.; Peters, J. C. *J. Am. Chem. Soc.* **2012**, *134*, 5080.
[21] Cowie, B. E.; Emslie, D. J. H. *Chem. Eur. J.* **2014**, *20*, 16899.
[22] MacMillan, S. N.; Harman, W. H.; Peters, J. C. *Chem. Sci.* **2014**, *5*, 590.

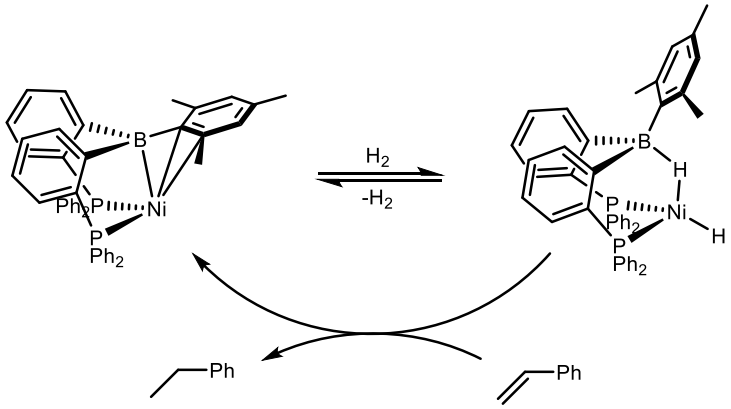

Scheme 4. Reversible hydrogen uptake and styrene hydrogenation by a Ni(0) complex bearing a diphosphine-borane ligand.

II.1.2.2 Phosphine-Containing Pincer-Type Ligands

The enhanced chemical and thermal stability that pincer-type ligands confer to transition metal centers, and the possibility of finely modulating their electronic and steric properties[23] were key features for their success in fundamental[24] and applied organometallic chemistry.[25] The importance of hemilability was known for classic, rigid and strongly coordinating tridentate pincer ligands,[26] prompting the design of more flexible ligands containing a less coordinating moiety. Due to the high diversity of reported scaffolds,[27] only the P-arene-P ligands developed by Agapie will be briefly discussed.

Several metal binding modes have been reported for *para*-terphenyl diphosphine ligands displaying an hemilabile arene. (Scheme 5) The variable hapticity of this tethered arene was found to be key in the discovery of new types of bimetallic reactivity, namely C−C coupling at a dinuclear Ni(I) complex[28]. This ligand was also instrumental in the development of several catalytic processes, comprising Mo-mediated

[23] Lawrence, M. A. W.; Green, K.-A.; Nelson, P. N.; Lorraine, S. C. *Polyhedron* **2018**, *143*, 11.
[24] a) Gozin, M.; Weisman, A.; Ben-David, Y.; Milstein, D. Nature 1993, 364, 699; b) Poverenov, E.; Efremenko, I.; Frenkel, A. I.; Ben-David, Y.; Shimon, L. J. W.; Leitus, G.; Konstantinovski, L.; Martin, J. M. L.; Milstein, D. *Nature* **2008**, *455*, 1093; c) Bernskoetter, W. H.; Schauer, C. K.; Goldberg, K. I.; Brookhart, M. *Science* **2009**, *326*, 553; d) Huang, Z.; White, P. S.; Brookhart, M. *Nature* **2010**, *465*, 598; e) Askevold, B.; Nieto, J. T.; Tussupbayev, S.; Diefenbach, M.; Herdtweck, E.; Holthausen, M. C.; Schneider, S. *Nat. Chem.* **2011**, *3*, 532.
[25] for a recent review see: Valdes, H.; García-Eleno, M. A.; Canseco-Gonzalez, D.; Morales-Morales, D. *ChemCatChem* **2018**, *10*, 1.
[26] van der Vlugt, J. I.; Pidko, E. A.; Vogt, D.; Lutz, M.; Spek, A. L.; Meetsma, A. *Inorg. Chem.* **2008**, *47*, 4442.
[27] a) Barrett, B. J.; Iluc, V. M. *Inorg. Chem.* **2014**, *53*, 7248; b) Miller, A. J. M. *Dalton Trans.* **2017**, *46*, 11987; c) Adams, G. M.; Weller, A. S. *Coord. Chem. Rev.* **2018**, *355*, 150.
[28] Velian, A.; Lin, S.; Miller, A. J. M.; Day, M. W.; Agapie, T. *J. Am. Chem. Soc.* **2010**, *132*, 6296.

ammonia-borane dehydrogenation[29] and Zr-catalyzed cotrimerization of alkynes and nitriles.[30] In addition, a plethora of fundamental advances[31] were achieved exploiting the unique properties of this hemilabile scaffold.

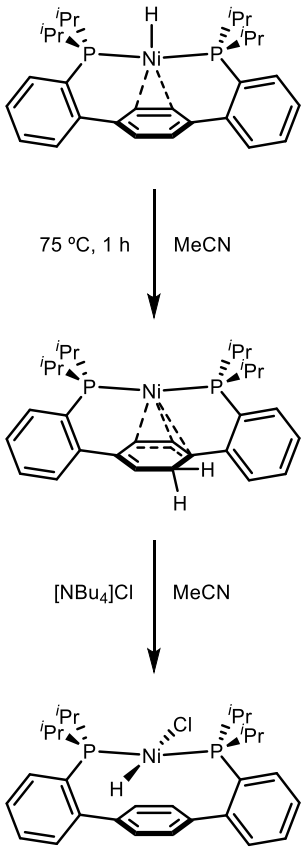

Scheme 5. Hemilabile behaviour of the P-arene-P ligand.

[29] Buss, J. A.; Edouard, G. A.; Cheng, C.; Shi, J.; Agapie, T. *J. Am. Chem. Soc.* **2014**, *136*, 11272.
[30] Low, C. H.; Rosenberg, J. N.; Lopez, M. A.; Agapie, T. *J. Am. Chem. Soc.* **2018**, *140*, 11906.
[31] a) Lin, S.; Day, M. W.; Agapie, T. *J. Am. Chem. Soc.* **2011**, *133*, 3828; b) Lin, S.; Herbert, D. E.; Velian, A.; Day, M. W.; Agapie, T. *J. Am. Chem. Soc.* **2013**, *135*, 15830; c) Buss, J. A.; Agapie, T. *Nature*, **2016**, *529*, 72; d) Horak, K. T.; Agapie, T. *J. Am. Chem. Soc.* **2016**, *138*, 3443; e) Buss, J. A.; Agapie, T. *J. Am. Chem. Soc.* **2016**, *138*, 16466; f) Buss, J. A.; Oyala, P. H.; Agapie, T. *Angew. Chem. Int. Ed.* **2017**, *56*, 14502; g) Buss, J. A.; Cheng, C.; Agapie, T. *Angew. Chem. Int. Ed.* **2018**, *57*, 9670; h) Buss, J. A.; VanderVelde, D. G.; Agapie, T. *J. Am. Chem. Soc.*, **2018**, *140*, 10121.

II.1.2.3 Dialkylbiaryl Phosphines

Although several tertiary phosphines with tethered hemilabile functionalities have been successfully applied in catalysis[32] this section is devoted to perhaps the most prominent example, the family of bulky, dialkylbiaryl phosphines developed by Buchwald, which are structurally related to the ligands employed in the present Thesis (Figure 4).

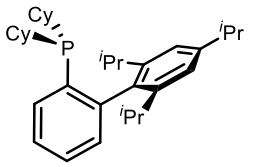

XPhos

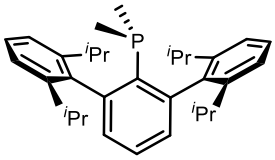

$PMe_2Ar^{Dipp}{}_2$

Figure 4. Representative examples of dialkylbiaryl and terphenyl phosphine ligands.

In the late 90s, Buchwald and coworkers discovered that palladium complexes bearing dialkylbiaryl phosphines were exceptional catalysts for C−C, C−N and C−O bond-forming reactions.[33] Over time, these bulky, hemilabile phosphine ligands became indispensable in organometallic chemistry and homogeneous catalysis (Figure 5).[34] In recent years,

---

[32] a) Kuriyama, M.; Nagai, K.; Yamada, K.; Miwa, Y.; Taga, T.; Tomioka, K. *J. Am. Chem. Soc.* **2002**, *124*, 8932; b) Lewis, J. C.; Berman, A. M.; Bergman, R. G.; Ellman, J. A. *J. Am. Chem. Soc.* **2008**, *130*, 2493; c) Jiménez, M. V.; Pérez-Torrente, J. J.; Bartolomé, M. I.; Vispe, E.; Lahoz, F. J.; Oro, L. A. *Macromolecules* **2009**, *42*, 8146.

[33] a) Old, D. W.; Wolfe, J. P.; Buchwald, S. L. *J. Am. Chem. Soc.* **1998**, *120*, 9722; b) Aranyos, A.; Old, D. W.; Kiyomori, A.; Wolfe, J. P.; Sadighi, J. P.; Buchwald, S. L. *J. Am. Chem. Soc.* **1999**, *121*, 4369; c) Wolfe, J. P.; Singer, R. A.; Yang, B. H.; Buchwald, S. L. *J. Am. Chem. Soc.* **1999**, *121*, 9550.

[34] a) Surry, D. S.; Buchwald, S. L. *Angew. Chem. Int. Ed*. **2008**, *47*, 6338; b) Martin, R.; Buchwald, S. L. *Acc. Chem. Res*. **2008**, *41*, 1461; c) Surry, D. S.; Buchwald, S. L. *Chem. Sci*. **2011**, *2*, 27; d) Liu, Z.; Yamamichi, H.; Madrahimov, S. T.; Hartwig, J. F; *J. Am. Chem. Soc.* **2011**, *133*, 2772; e) Nielsen, D. K.; Doyle, A. G. *Angew. Chem. Int. Ed.* **2011**, *50*, 6056.

dialkylbiaryl phosphines have been successfully employed in late-stage, palladium-mediated fluorination[35] and trifluoromethylation,[36] a challenging task of great importance due to the ample presence of fluorine in agrochemicals and pharmaceuticals.

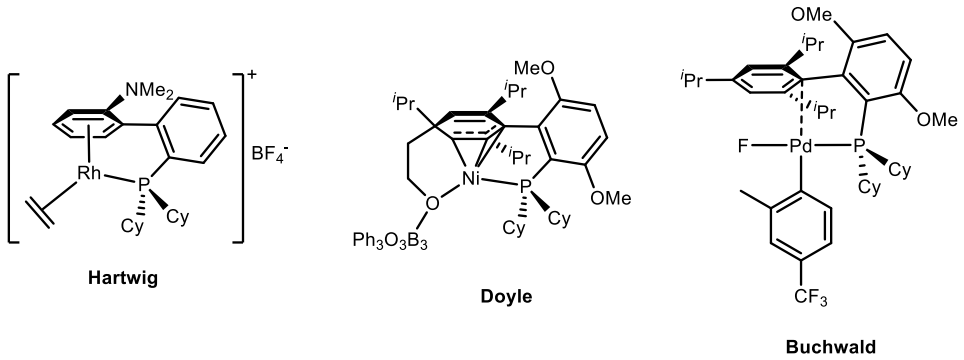

Figure 5. Hemilabile metal-arene interactions in catalytically active complexes bearing dialkylbiaryl phosphines.

The forthcoming *Results and Discussion* section of this Chapter describes our experimental and computational findings regarding the hemilabile character of terphenyl phosphine ligands in unsaturated, cationic iridium(I) complexes. The stereoelectronic properties of these ligands were evaluated by classic (Tolman´s) and alternative methods. Finally, the mechanism for the activation of a benzylic C−H bond at a neutral Ir(I) methyl complex is discussed.

[35] a) Watson, D. A.; Su, M.; Teverovskiy, G.; Zhang, Y.; García-Fortanet, J.; Kinzel, T.; Buchwald, S. L. *Science* **2009**, *325*, 1661; e) Sather, A. C.; Buchwald, S. L. *Acc. Chem. Res.* **2016**, *49*, 2146; f) Ye, Y.; Takada, T.; Buchwald, S. L. *Angew. Chem. Int. Ed.* **2016**, *55*, 15559.
[36] Cho, E. J.; Senecal, T. D.; Kinzel, T.; Zhang, Y.; Watson, D. A.; Buchwald, S. L. *Science* **2010**, *328*, 1679.

II.2 RESULTS AND DISCUSSION

II.2.1 Stereoelectronic properties of terphenyl phosphine ligands

The logical desire to enhance our comprehension of catalytic synthesis, reaching the power to predict selectivity, yield and other reaction parameters, has understandably led to increased emphasis in the investigation of ligand stereoelectronic properties. As stated in the introductory section of this Chapter, phosphine ligands occupy a prominent position in organometallic chemistry and homogeneous catalysis. Its ubiquity and usefulness has prompted a considerable amount of research to explore the effects of modifying phosphine substituents on the reactivity of the resulting metallic complexes and their catalytic performance. Subtle phosphine ligand effects have been uncovered in nickel, palladium and gold catalysis, as representative examples.[37] In a recent report, unique catalytic features, seemingly influenced by van der Waals dispersion forces,[38] were uncovered for tri(1-adamantyl)phosphine,[39] a molecule for which steric and electronic properties fall beyond conventional limits. In this Thesis, striking differences in reactivity were disclosed for two structurally related dimethyl terphenyl phosphines, $PMe_2Ar^{Xyl}{}_2$ and $PMe_2Ar^{Dipp}{}_2$ (Figure 6), prompting us to conduct studies to assess their stereoelectronic features.

[37] a) Wu, K.; Doyle, A. G. *Nat. Chem.* **2017**, *9*, 779; b) Niemeyer, Z. L.; Milo, A.; Hickey, D. P.; Sigman, M. S. *Nat. Chem.* **2016**, *8*, 610; c) Christian, A. H.; Niemeyer, Z. L.; Sigman, M. S.; Toste, F. D. *ACS Catal.* **2017**, *7*, 3973.
[38] a) Liptrot, D. J.; Power, P. P. *Nat. Rev. Chem*. **2017**, *1*, 0004; b) Wagner, J. P.; Schreiner, P. R. *Angew. Chem. Int. Ed*. **2015**, *54*, 12274; c) Guo, J.-D.; Liptrot, D. J.; Nagase, S.; Power, P. P. *Chem. Sci*. **2015**, *6*, 6235.
[39] Chen, L.; Ren, P.; Carrow, B. P. *J. Am. Chem. Soc*. **2016**, *138*, 6392.

$PMe_2Ar^{Xyl}_2$ $PMe_2Ar^{Dipp}_2$

Figure 6. Dimethyl terphenyl phosphine ligands.

From an electronic point of view, little differences were expected for these two phosphines, although $PMe_2Ar^{Dipp}_2$ should be a slightly better σ-donor, due to the superior inductive effect of the remote ^{i}Pr groups. To check this initial assumption, we decided to measure the Tolman Electronic Parameter, TEP, for these two phosphines. This parameter was introduced by Tolman in the 70s,[40] providing a broadly applicable method for assessing the donor capacity of a ligand based on infrared data of nickel carbonyl compounds ligated to the ligand under study. The room temperature reaction of $Ni(CO)_4$ and a P-donor ligand, L, generated the corresponding $Ni(CO)_3(L)$ species, from which the TEP of the ligand L was determined as the frequency of the symmetric A_1 carbonyl stretching mode. The greater the σ-donor capacity of a ligand in $Ni(CO)_3(L)$, the more enhanced back-donation it promotes from the metal center to orbitals with antibonding character relative to the C≡O bond, diminishing the magnitude of the wavenumber of the stretching vibration as the bond weakens. For $PMe_2Ar^{Xyl}_2$ and $PMe_2Ar^{Dipp}_2$, these nickel tricarbonyl species were independently prepared by another member of our group,[41] giving values of 2063.8 and 2062.9 cm^{-1}, respectively. Table 1 displays ν(CO) values for $Ni(CO)_3(L)$ complexes with archetypical phosphine ligands.

[40] Tolman, C. A. *J. Am. Chem. Soc.* **1970**, *92*, 2953.
[41] Marin, M.; Moreno, J. J.; Navarro-Gilabert, C.; Álvarez, E.; Maya, C.; Peloso, R.; Nicasio, M. C.; Carmona, E. *Chem. Eur. J.* **2018**, *in press.*

Phosphine	**$Ni(CO)_3(PR_3)$**
P^tBu_3	2056.1
XPhos	2059
$PMe_2Ar^{Dipp}{}_2$	2062.9
$PMe_2Ar^{Xyl}{}_2$	2063.8
PMe_3	2064.1
PPh_3	2068.9

Table 1. ν(CO) values (cm^{-1}) of selected alkyl, aryl and alkyl-aryl phosphine complexes.

However, this procedure presents a major drawback, since the starting material for the synthesis of $Ni(CO)_3(L)$ species is $Ni(CO)_4$, which is extremely toxic and volatile. In addition, bulky and potentially polydentate ligands, which importance in homogeneous catalysis cannot be overstated, usually lead to disubstitution, yielding the corresponding dicarbonyl complexes, $Ni(CO)_2(L)$ and avoiding the calculation of a reliable TEP. Over the years, several alternatives have been developed to overcome these issues,[42] and alternate carbonyl species, as $Cr(CO)_5(L)$,[43] $Rh(acac)(CO)(L)$[44] and $IrCl(CO)_2(L)$,[45] have been employed. The steric

[42] Kühl, O. *Coord. Chem. Rev.* **2005**, *249*, 693.
[43] Kendall, A. J.; Zakharov, L. N.; Tyler, D. R. *Inorg. Chem.* **2016**, *55*, 3079.
[44] Serron, S.; Huang, J.; Nolan, S. P. *Organometallics* **1998**, *17*, 534.
[45] a) Chianese, A. R.; Li, X.; Janzen, M. C.; Faller, J. W.; Crabtree, R. H. *Organometallics* **2003**, *22*, 1663; b) Diebolt, O.; Fortman, G. C.; Clavier, H.; Slawin, A. M. Z.; Escudero-Adán; E. C.; Benet-Buchholz, J.; Nolan, S. P. *Organometallics* **2011**, *30*, 1668.

clash between bulky, conical ligands as tertiary phosphines and crowded metal complexes can lead to significant front strain,[43] weakening the P−M bond and providing unreliable ν(CO) values. Therefore, we focused on square planar $IrCl(CO)_2(L)$ complexes, which based on the work of Nolan with related, bulky dialkyl biaryl phosphines, were expected to be well suited to accommodate a terphenyl phosphine ligand, and for which the average ν(CO) stretching values can be related to the TEP using the formula developed by Crabtree[45a] and later refined by Nolan. [45b]

$$\text{Crabtree: TEP} = 0.722 \times \nu(CO)_{average} + 593$$

$$\text{Nolan: TEP} = 0.847 \times \nu(CO)_{average} + 336$$

A large difference (7 cm^{-1}) was found for the average ν(CO) values gathered from the solid-state (Nujol) IR spectra of $IrCl(CO)_2PMe_2Ar^{Xyl}_2$ (2026 cm^{-1}) and $IrCl(CO)_2PMe_2Ar^{Dipp}_2$ (2019 cm^{-1}), whose experimental synthesis and full characterization is described in the next section of this Chapter. However, intra- and/or intermolecular interactions can affect vibrational modes, making solid-state IR measurements unreliable. The solution (CH_2Cl_2) IR spectra of these species gave average values of 2028 (Xyl) and 2027 (Dipp) cm^{-1}, in agreement with the Ni-based results and the expected trend. The use of Crabtree´s regression provided better results than Nolan´s, however, direct comparison between Ni and Ir TEP values was not possible.

Phosphine	**ν(CO) Ni (TEP)**	**$\nu(CO)_{average}$ Ir**	**TEP_{Ir} Crabtree**	**TEP_{Ir} Nolan**
$PMe_2Ar^{Xyl}_2$	2063.8	2028	2057	2054
$PMe_2Ar^{Dipp}_2$	2062.9	2027	2056	2053

Table 2. Average ν(CO) values (cm^{-1}) of $IrCl(CO)_2PMe_2Ar$' complexes and Ni and Ir-based TEP values.

The magnitude of the $^{31}P–^{77}Se$ scalar coupling constant ($^1J_{PSe}$) in the corresponding selenide provides an alternative procedure to measure the σ-donor capacity of a phosphorated ligand.[46] The scalar coupling, *J*, between two nuclei is a through-bond interaction. The spin of one nucleus polarizes the spins of the surrounding electrons, and this polarization can be transferred through chemical bonds, perturbing the energy levels of the neighboring magnetic nuclei. On these grounds, a greater *s*-character of the orbitals participating in the bond between two atoms is reflected in an augment in the magnitude of the scalar coupling, for the *s* is the only atomic orbital with a non-zero probability at the nucleus. The bonding in phosphine selenides[47] can be described by the resonance hybrids depicted in Figure 7. The analysis of the hybridization of the phosphorus and selenium atoms in these resonance hybrids reveals that the Se atom changes from sp^2 (**A**) to sp^3 (**B**). Hence, lower $^1J_{PSe}$ values are registered for more electron-donating phosphines, which comparatively favor the zwitterionic resonance hybrid **B**.

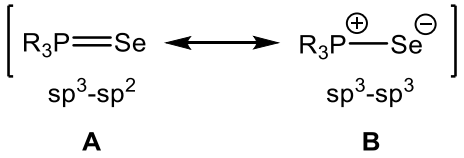

[46] a) Stec, W. J.; Okruszek, A.; Uznanski, B.; Michalski, J. *Phosphorus* **1972**, *2*, 97.
[47] Allen, D. W.; Nowell, I. W.; Taylor, B. F. *J. Chem. Soc. Dalton Trans.* **1985**, 2505.

Figure 7. Hybridization of the P and Se atoms in the resonance hybrids of phosphine selenides.

Despite their remarkable resistance towards oxidation under air ($t_{1/2} \approx 10$ days, 25 ºC in toluene),[48] $PMe_2Ar^{Xyl}_2$ and $PMe_2Ar^{Dipp}_2$ readily reacted with Se black in C_6D_6 in an NMR tube, quantitatively yielding the corresponding selenides. The $^1J_{PSe}$ was registered by means of $^{31}P\{^1H\}$ NMR (Figure 8), yielding values of 709 and 704 Hz for $PMe_2Ar^{Xyl}_2$ and $PMe_2Ar^{Dipp}_2$, respectively.

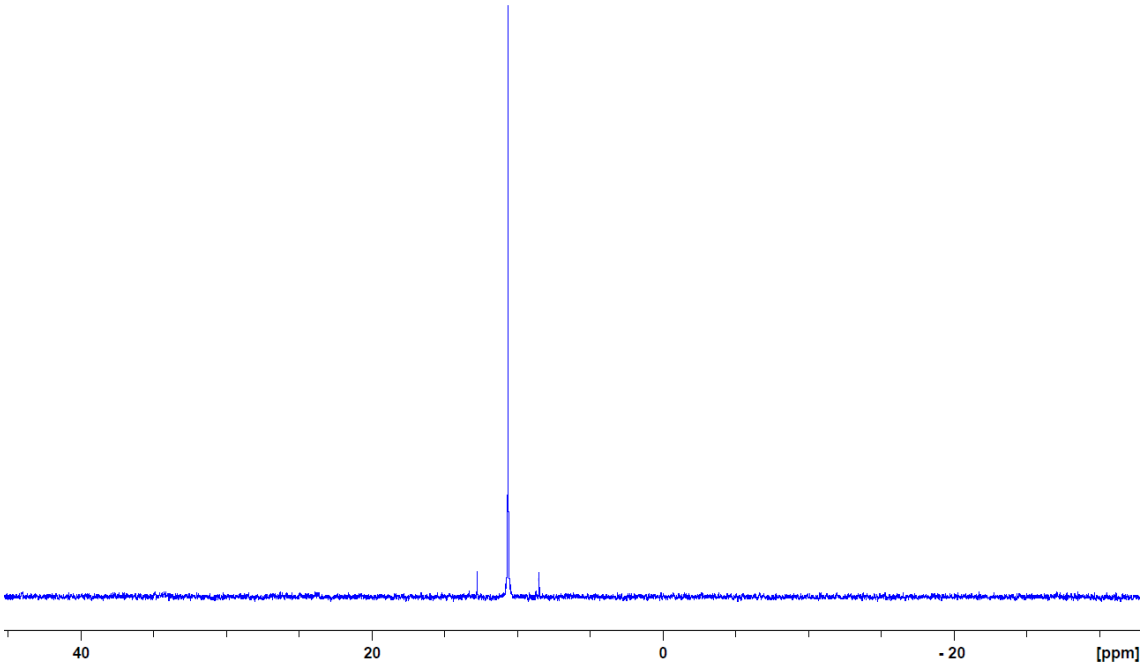

Figure 8. $^{31}P\{^1H\}$ NMR spectrum of $SePMe_2Ar^{Xyl}_2$ showing ^{77}Se satellites (7.6 % abundance).

[48] Ortega-Moreno, L.; Fernández-Espada, M.; Moreno, J. J.; Navarro-Gilabert, C.; Campos, J.; Conejero, S.; López-Serrano, J.; Maya, C.; Peloso, R.; Carmona, E. *Polyhedron* **2016**, *116*, 170.

In the absence of conformational mobility, for the vast majority of nuclei the scalar coupling (*J*) is independent of solvent and temperature. However, the magnitude of the $^{1}J_{PSe}$ depends on the solvent of choice,[49] which often makes comparing with literature data difficult. The polarity and/or specific solute−solvent interactions can favor one resonance hybrid over the other, and therefore C_6D_6 was the solvent of choice, for it is non-polar and has a boiling point (80.1 ºC) that permits the moderate heating that electron-poor and bulky phosphorated ligands require to react with elemental selenium. It is pertinent to recall that reliable $^{1}J_{PSe}$ comparisons should only be performed with structurally related ligands,[50] for the hybridization of the phosphorus atom is sensitive both to its degree of pyramidalization,[51] which depends on the bulk of the substituents, and to the electronegativity of the atoms connected to P, as *s*-character tends to concentrate in orbitals bonding to the more electropositive substituents, according to Bent´s rule.[52]

As a conclusion, the σ-donor capacity of $PMe_2Ar^{Xyl}_2$ and $PMe_2Ar^{Dipp}_2$ was found to be comparable or slightly superior to that of PMe_3. Alternative methodologies for the evaluation of this property have been studied, comprising neutral Ir carbonyl complexes and phosphine selenides. Whereas these alternative procedures confirmed that $PMe_2Ar^{Dipp}_2$ is a

[49] a) Dean, P. A. W. *Can. J. Chem.* **1979**, *57*, 754; b) Cogne, A.; Grand, A.; Laugier, J.; Robert, J. B.; Wiesenfeld, L. *J. Am. Chem. Soc.* **1980**, *102*, 2238; c) Carr, S. W.; Colton, R. *Aust. J. Chem.* **1981**, *34*, 35.
[50] Beckmann, U.; Süslüyan, D.; Kunz, P. C. *Phosphorus Sulfur Silicon Relat Elem.* **2011**, *186*, 2061.
[51] a) Pinnell, R. P.; Megerle, C. A.; Manatt, S. L.; Kroon, P. A. *J. Am. Chem. Soc.* **1973**, *95*, 977; b) Kroshefsky, R. D.; Weiss, R.; Verkade, J. G. *Inorg. Chem.* **1979**, *18*, 469.
[52] a) Bent, H. A. *Chem. Rev.* **1961**, *61*, 275; b) McFarlane, W.; Rycroft, D. S. *J. Chem. Soc., Dalton Trans.* **1973**, 2162; c) Alabugin, I. V.; Bresch, S.; Gomes, G. d. P. *J. Phys. Org. Chem.* **2015**, *28*, 147.

slightly better σ-donor than $PMe_2Ar^{Xyl}_2$, quantitative correlation with the Tolman Electronic Parameter (TEP) could not be achieved.

In addition to donor capacity, the pioneering work of Tolman also provided a simple and effective model for the determination of the steric properties of phosphine ligands, the Tolman Cone Angle (TCA).[40,53] Mingos' contribution[54] permitted the use of crystallographic data (cTCA) instead of space-filling (CPK) models. $Ni(CO)_3(L)$ complexes, for which monodentate coordination of the L ligand is almost guaranteed, could be a suitable model to measure cTCAs. However, the astonishing dearth of structurally characterized complexes of this type, combined with the aforementioned drawbacks of the preparation of $Ni(CO)_3(L)$ complexes, rule out these species as proper candidates for the general assessment of crystallographic TCAs. In turn, the molecular geometry of linear gold(I) chloride complexes, AuCl(L), has been extensively determined.[55] However, for dialkyl biaril and terphenyl phosphines, a flanking aryl ring is, in almost every case, placed nearby the gold atom (see Figure 9), achieving a disposition in the solid-state that might provide exceedingly high values for general, monodentate cone angle measurements.

[53] Tolman, C. A. *Chem. Rev.* **1977**, *77*, 313.
[54] Müller, T. E.; Mingos, D. M. P. *Transit. Metal Chem.* **1995**, *20*, 533.
[55] Clavier, H.; Nolan, S. P. *Chem. Commun.* **2010**, *46*, 841.

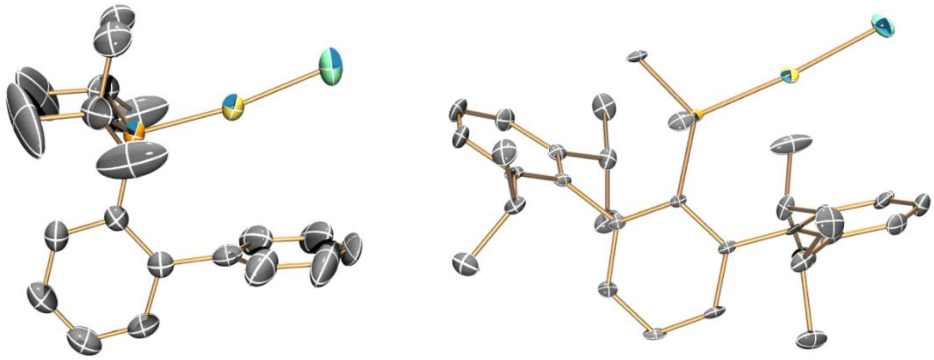

Figure 9. ORTEP diagrams of paradigmatic examples of neutral gold(I) phosphine complexes, from the Echavarren[56] (left) and our group[57] (right).

As a first approach, cTCA values were measured employing the geometries of the free ligands (Figure 10) following Mingos' procedure (Table 3), placing a metal atom at 2.28 Å from the P atom using the GaussView program.[58] The simplest dimethyl terphenyl phosphine, $PMe_2Ar^{Ph}_2$, was included for comparative purposes.

Phosphine	**Θ (cTCA 2.28)**	**θ_{Me1}**	**θ_{Me2}**	**$\theta_{Ar'}$**
$PMe_2Ar^{Ph}_2$	128.6	47.5	47.5	98.0
$PMe_2Ar^{Xyl}_2$	153.9	48.6	46.2	136.0
$PMe_2Ar^{Dipp}_2$	159.6	50.5	46.1	142.7

Table 3. Crystallographic Tolman Cone Angles (cTCA) measured for dimethyl terphenyl phosphines.

[56] Herrero-Gómez, E.; Nieto-Oberhuber, C.; López, S.; Benet-Buchholz, J.; Echavarren, A. *Angew. Chem. Int. Ed.* **2006**, *45*, 5455.
[57] Espada, M. F.; Campos, J.; López-Serrano, J.; Poveda, M. L.; Carmona, E. *Angew. Chem. Int. Ed.* **2015**, *54*, 15379.
[58] Dennington, R.; Keith, T.; Millam, J. M. GaussView, version 5; Semichem, Inc., Shawnee Mission, KS, USA, 2009.

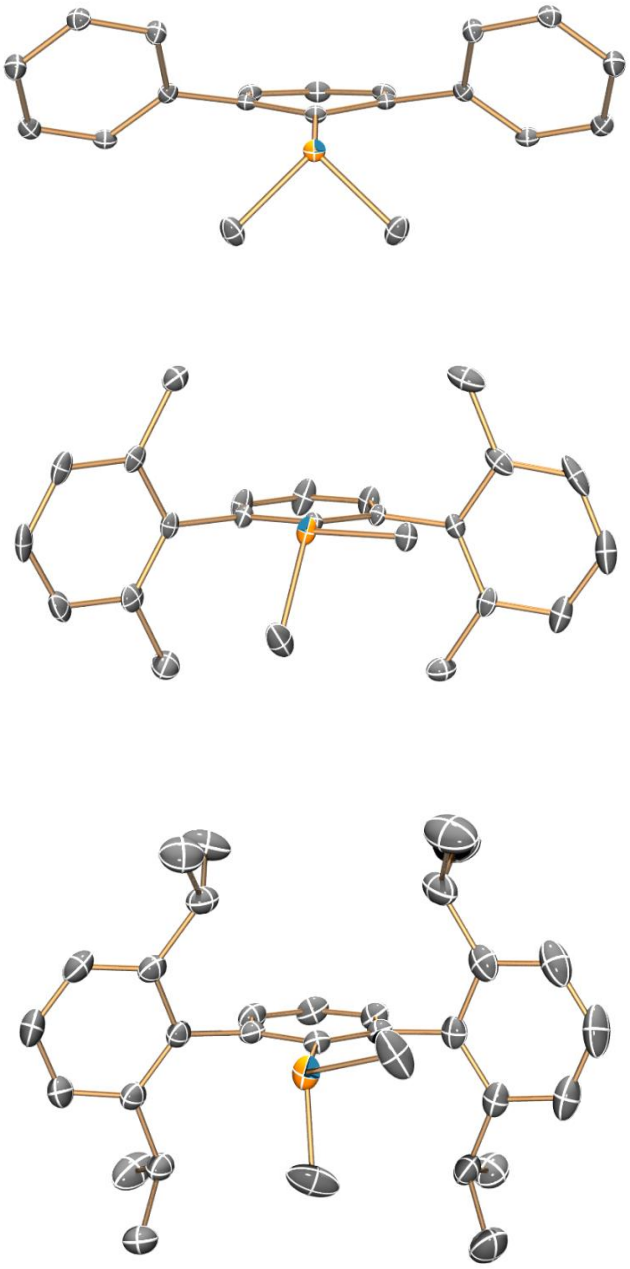

Figure 10. ORTEP diagrams of the dimethyl terphenyl phosphines $PMe_2Ar^{Ph}_2$, $PMe_2Ar^{Xyl}_2$ and $PMe_2Ar^{Dipp}_2$. Hydrogen atoms are excluded for clarity and thermal ellipsoids are set at 50 % probability.

However, it is well known that for bulky, elaborated ligands such a simple model may have a poor performance.[59] Several alternative methods have been developed to overcome this issue;[60] in the course of our investigations we decided to perform Solid Angle[61] and Buried Volume[62] (%V_{bur}) measurements. In these approaches the whole ligand is taken into consideration, not relying on the measurement of only three P-M-H angles (Figure 11). The Solid Angle is conceptually related to the Tolman procedure, giving the fraction of the internal surface of a sphere that encompasses the ligand that would be shadowed, considering the metal atom as the light source. In turn, the Buried Volume approach calculates the percentage of the volume of a sphere (3.5 Å radius, centered at the metal atom) that a certain ligand occupies, focusing in proximal steric effects.

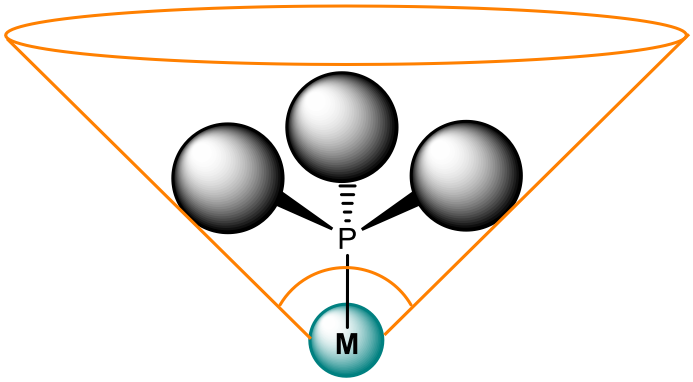

Tolman Cone Angle

[59] Bilbrey, J. A.; Kazez, A. H.; Locklin, J.; Allen, W. D. J. Comput. Chem. **2013**, *34*, 1189.
[60] Brown, T. L.; Lee, K. J. *Coord. Chem. Rev.* **1993**, *128*, 89.
[61] Immirzi, A.; Musco, A. *Inorg. Chim. Acta* **1977**, 25, L41.
[62] Poater, A.; Cosenza, B.; Correa, A.; Giudice, S.; Ragone, F.; Scarano, V.; Cavallo, L. *Eur. J. Inorg. Chem.* **2009**, *13*, 1759.

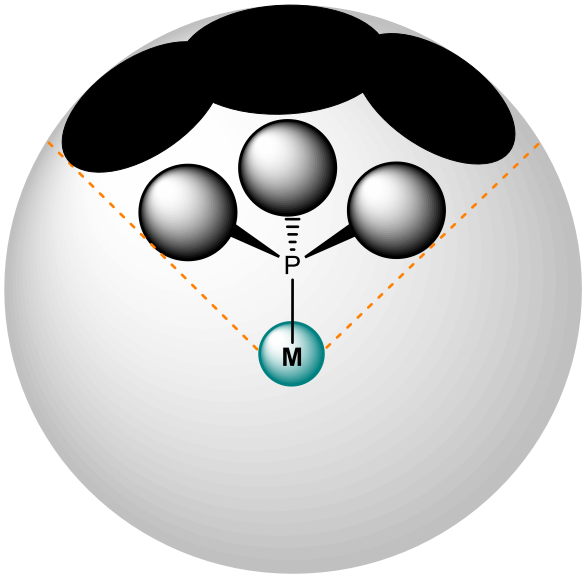

Solid Angle

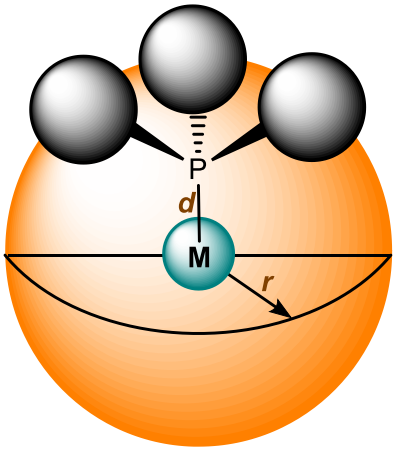

Buried Volume

Figure 11. Schematic representation of the Tolman Cone Angle (top), Solid Angle (mid) and Buried Volume (bottom).

Good correlation (R^2 = 0.959) between the Buried Volume and crystallographic Tolman Cone Angle was reported by Nolan for the geometries of free, symmetric alkyl and aryl phosphines.[55] However, Nolan does not extend this correlation to dialkylbiaryl phosphines. To assess the predictive power of this method, we measured the $\%V_{bur}$[62] values for the free-ligand geometries, (Table 4), and compared our experimental crystallographic cone angle values (153.9 (Xyl), 159.6 (Dipp)) with those calculated by regression analysis (212.8 (Xyl), 246.0 (Dipp)), revealing that that for non-symmetric, elaborated ligands, for which proximal steric effects play a decisive role, these essentially different methods ($\%V_{bur}$ and TCA) do not correlate well.

Phosphine	**$\%V_{bur}$**	**Regression TCA**	**cTCA**
$PMe_2Ar^{Ph}{}_2$	34.3	167.0	128.6
$PMe_2Ar^{Xyl}{}_2$	45.9	212.8	153.9
$PMe_2Ar^{Dipp}{}_2$	54.3	246.0	159.6

Table 4. Buried volume and Tolman Cone Angles (calculated according to Nolan´s regression formula and crystallographic data, respectively) for dimethyl terphenyl phosphines.

Solid angles (Ω) are measured in a dimensionless unit, the steradian, but for comparative purposes conversion to G (percentage of the metal coordination sphere shielded by the ligand) and Equivalent Cone Angle (Θ, ECA) is preferred. The ECA is computed as the apex angle of an equivalent single cone that would yield Ω.[59] ECA values of the free

phosphine ligand were computed using the same geometries as for cTCAs, employing the Solid-G program[63] (Table 5).

Phosphine	**ECA 2.28**	**G^X 2.28**
$PMe_2Ar^{Ph}{}_2$	140.0	32.9
$PMe_2Ar^{Xyl}{}_2$	170.0	45.6
$PMe_2Ar^{Dipp}{}_2$	190.0	54.4

Table 5. Equivalent Cone Angles (ECA) and normalized percentage of the sphere shielded by the ligand (G). The X superscript states that the values were calculated from crystallographic data.

Very weak correlation was found between cTCA and ECA, so further analysis will be solely focused on solid angle values, as the method is best suited to describe the molecular complexity of bulky, unsymmetrical ligands. Care needs to be taken prior to comparing values between different phosphines, as the conformation adopted by the phosphine is pivotal in these measurements.[41] Although free ligand values were evaluated in order to circumvent the fact that ECA values will greatly depend on the complex of choice, it is also evident that free phosphine geometries with an artificially added metal atom do not provide reliable results. The position of the metal is of paramount importance in these measurements, and some fragments of the ligand can be exceedingly close to it, providing unrealistically high solid and cone angle values. To overcome this issue, phosphine chalcogenides have been used as a reasonable alternative framework for measuring sterics, as these might

[63] Guzei, I. A.; Wendt, M. *Dalton Trans.* **2006**, 3991.

provide a more accurate description of the ligand in a coordination environment than the free phosphine.[37b,c;64] ECA values obtained for calculated, minimum-energy geometries of $Ni(CO)_3PMe_2Ar$' complexes were compared with those calculated for the free ligand and the corresponding phosphine chalcogenides[65] (Table 6).

ECA 2.28	**$Ni(CO)_3PR_3$**	**PR_3 (X-Ray)**	**$O=PR_3$**	**$Se=PR_3$**
$PMe_2Ar^{Ph}{}_2$	139.0	128.6	142.8	139.6
$PMe_2Ar^{Xyl}{}_2$	150.6	170.0	155.1	149.1
$PMe_2Ar^{Dipp}{}_2$	158.9	190.0	186.4	166.4

Table 6. Equivalent Cone Angle values for the most stable conformer of phosphine oxides, selenides and corresponding $Ni(CO)_3PMe_2Ar$' complexes, calculated at the ωB97XD/6-31G(d,p) level of theory, and the crystallographic ECAs for the free ligand.

All $Ni(CO)_3PMe_2Ar$' complexes attain the same conformation of the ligand, and therefore ECA values can be compared among them. Despite minimum energy conformers of $POMe_2Ar$' species have a conformation similar to that of the corresponding $Ni(CO)_3PMe_2Ar$' complexes, ECA values correlate very poorly, probably due to the P=O bond being short (*ca*. 1.50 Å) and the oxygen atom small when compared with the $Ni(CO)_3$

[64] a) Starosta, R.; Bażanów, B.; Barszczewski, W. *Dalton Trans.* **2010**, *39*, 7547; b) Tohmé, A.; Sahnoune, H.; Roisnle, T.; Dorcet, V.; Halet, J.-F.; Paul, F. *Organometallics*, **2014**, *33*, 3385.

[65] Calculations were performed with the Gaussian 09 program employing the Head-Gordon hybrid functional ωB97XD. Geometry optimizations were carried out in the gas phase without geometry constraints.

fragment. In turn, phosphine selenides have a typical P−Se bond length of ca. 2.10 Å, much closer to metal-phosphorus bond distances, and the bigger size of the Se atom might account to some extent for the bulkiness of the metal complex. This preliminary study suggests that selenides might be used as better descriptors of the sterics of phosphine ligands in a complex than oxides, especially for ligand parametrization studies.[37b]

To sum up, the stereoelectronic properties of bulky phosphine ligands have been studied through several approaches. To circumvent the disadvantages that the determination of the TEP presents, the donor capacity was evaluated by means of infrared spectroscopy of square planar, iridium(I) carbonyl complexes, providing qualitatively analogous results. However, a quantitative correlation with nickel measurements could not obtained by using the regression analysis previously reported in the literature. The donor capacity was also evaluated through the $^{1}J_{PSe}$ in the corresponding phosphine selenides, further confirming that $PMe_2Ar^{Dipp}_2$ is a slightly better σ-donor than $PMe_2Ar^{Xyl}_2$. However, only structurally similar ligands can be compared with this methodology, preventing a general use to classify phosphorated ligands. Regarding to the sterics, we confirmed that the Tolman Cone Angle is poorly suited to describe bulky, elaborated unsymmetrical ligands, favoring the use of Solid Angles and Buried Volumes. In addition, preliminary studies suggest that phosphine selenides can provide a more accurate description of a phosphine ligand in a coordination environment than phosphine oxides, which were recently used in ligand parametrization studies.

II.2.2 Synthesis and Reactivity of Ir(I) Neutral Complexes

The activation of small molecules in homogeneous catalysis is commonly achieved by means of oxidative addition to a low-coordinate transition metal complex, increasing the oxidation state and coordination number of the metal center in two units. Reductive elimination releases the functionalized molecule and regenerates the catalyst. Square planar, d^8 complexes play a key role in industrially relevant processes, as palladium mediated cross coupling[66] or the Monsanto and Cativa processes for the manufacture of acetic acid by carbonylation of methanol,[67] to name a few paradigmatic examples (Figure 12).

[66] a) Miyaura, N.; Suzuki, A. *Chem. Rev.* **1995**, *95*, 2457; b) Beletskaya, I. P.; Cheprakov, A. V. *Chem. Rev.* **2000**, *100*, 3009; c) King, A. O.; Okukado, N.; Negishi, E. *J. Chem. Soc., Chem. Commun.* **1977**, 683; d) Stille, J. K. *Angew. Chem. Int. Ed.* **1986**, *25*, 508; e) Sonogashira, K. *J. Organomet. Chem.* **2002**, *653*, 46; f) Wolfe, J. P.; Tomori, J.; Sadighi, J. P.; Yin, J.; Buchwald, S. L. *J. Org. Chem.* **2000**, *65*, 1158; g) Hartwig, J. F.; Kawatsura, M.; Hauck, S. I.; Shaughnessy, K. H.; Alcazar-Roman, L. M. *J. Org. Chem.* **1999**, *64*, 5575; h) Tamao, K.; Koji, S.; Kumada, M. *J. Am. Chem. Soc.* **1972**, *94*, 4374.

[67] a) Haynes, A.; Mann, B. E.; Gulliver, D. J.; Morris, G. E.; Maitlis, P. M. *J. Am. Chem. Soc.* **1991**, *113*, 8567; b) Haynes, A.; Mann, B. E.; Morris, G. E.; Maitlis, P. M. *J. Am. Chem. Soc.* **1993**, *115*, 4093; c) Jones, J. H. *Platinum Metals Rev.* **2000**, *44*, 94; d) Sunley, G. J.; Watson, D. J. *Catal. Today* **2000**, *58*, 293.

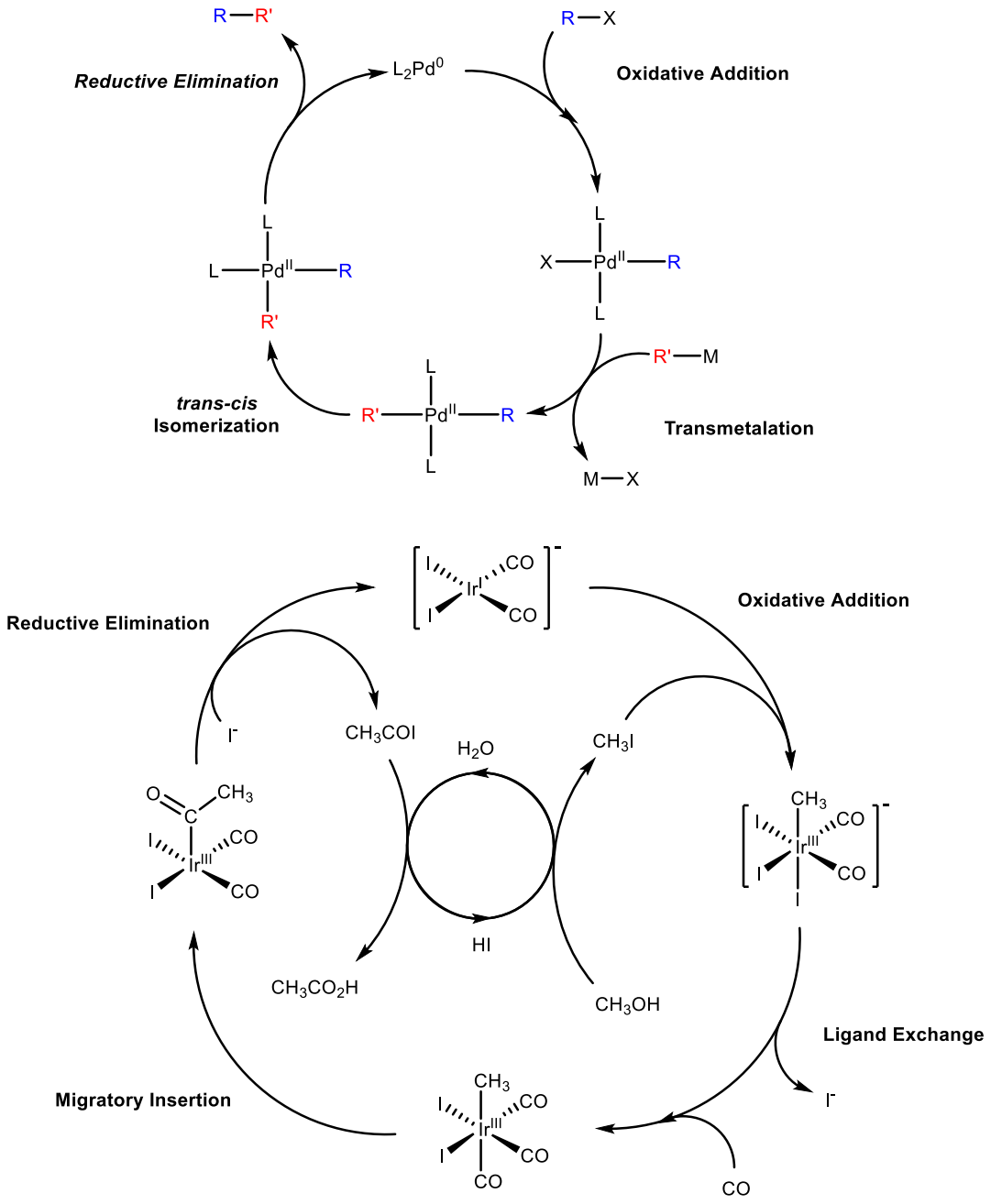

Figure 12. Palladium cross-coupling (top) and Cativa process (bottom) mechanisms.

Fundamental breakthroughs in this field were achieved by the study of iridium(I) complexes, especially Vaska´s complex,[68] $IrCl(CO)(PPh_3)_2$, a neutral bis phosphine species that displays a rich reactivity (Figure 13). This 16-electron complex can reversibly add several covalent molecules,[69] including dihydrogen,[70] Lewis acidic molecules, as sulphur dioxide or boron trifluoride,[71] alkenes,[72] alkyl halides[73] and, more importantly, dioxygen[74] and carbon monoxide,[75] being the first synthetic system to mimic the behaviour of hemoglobin.

[68] Vaska, L.; DiLuzio, J. W. *J. Am. Chem. Soc.* **1961**, *83*, 2784.
[69] Vaska, L. *Acc. Chem. Res.* **1968**, *1*, 335.
[70] Vaska, L.; DiLuzio, J. W. *J. Am. Chem. Soc*. **1962**, *84*, 679.
[71] La Placa, S. J.; Ibers, J. A. *Inorg. Chem.* **1966**, *5*, 405.
[72] Vaska, L.; Rhodes, R. E. *J. Am. Chem. Soc.* **1965**, *87*, 4970.
[73] Chock, P. B.; Halpern, J. *J. Am. Chem. Soc.* **1966**, *88*, 3511.
[74] a) Vaska, L. *Science* **1963**, *140*, 809; b) La Placa, S. J.; Ibers, J. A. *J. Am. Chem. Soc.* **1965**, *87*, 2581.
[75] a) Vaska, L. *Science* **1966**, *152*, 769; b) Abu-Hasanayn, F.; Emge, T. J.; Maguire, J. A.; Krogh-Jespersen, K.; Goldman, A. S. *Organometallics* **1994**, *13*, 5177.

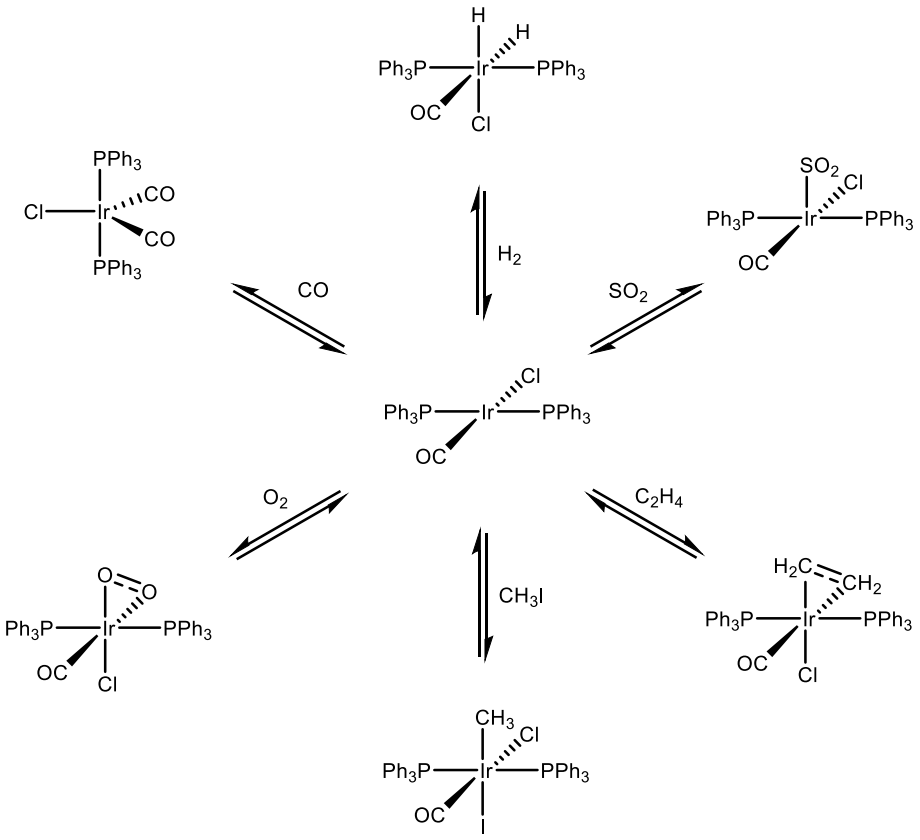

Figure 13. Vaska´s complex (center) and selected examples of its reactivity towards covalent molecules.

This Chapter encompasses our results on the reactivity of Ir(I) complexes built around two selected terphenyl phosphines, $PMe_2Ar^{Xyl}_2$ and $PMe_2Ar^{Dipp}_2$. Using $[IrCl(COD)]_2$ (COD = 1,5-cyclooctadiene) as a precursor (Scheme 6), coordination of the phosphine ligand was first suggested by color change of the solution from orange-red to yellow, and further confirmed by NMR spectroscopy, which gave comparable data for $IrCl(COD)PMe_2Ar^{Xyl}_2$, **1(Xyl)**, and $IrCl(COD)PMe_2Ar^{Dipp}_2$, **1(Dipp)**, and therefore only the former will be discussed.

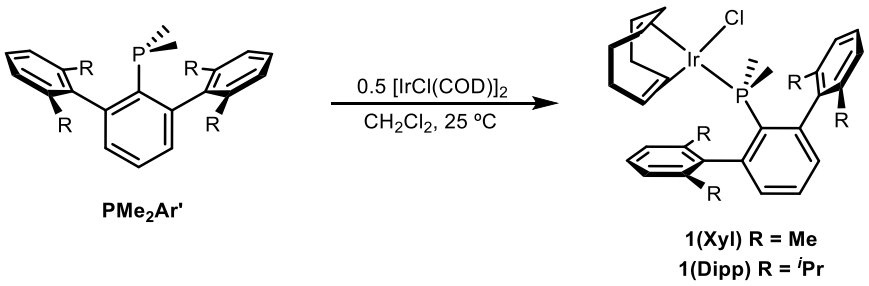

Scheme 6. Synthesis of type **1** complexes. R stands for Me (Xyl) and ^{i}Pr (Dipp) groups.

A singlet at −9.3 ppm, recorded in the $^{31}P\{^{1}H\}$ spectrum of **1(Xyl)**, was indicative of phosphine coordination to the metal center (*cf.* −41.8 ppm for the free phosphine). The ^{1}H NMR spectra corroborated the monodentate coordination of the phosphine ligand in these species, as the equivalence of the flanking aryl rings gave rise to only four aromatic signals, belonging to the *p*-C_6H_3 (1H), *p*-Xyl (2H), *m*-Xyl (4H) and *m*-C_6H_3 (2H), and a single resonance for the methyl groups of the xylyl rings (12H). Two sets of alkenic protons were recorded for the COD ligand at 4.57 and 2.27 ppm, assigned to the *trans* and *cis* (relative to the phosphine), respectively. The corresponding $^{13}C\{^{1}H\}$ resonances were found at 88.8 (d, $^{2}J_{CP}$ = 16 Hz, *trans*) and 52.1 (*cis*) ppm.

II.2.2.1 Iridium(I) Methyl Complexes

Several breakthroughs were achieved by the study of the reactivity of transition metal methyl complexes, as briefly detailed in Section **I.2.4.1** of the first chapter of this Thesis. On this basis, we found of interest to access complexes containing an Ir−CH_3 functionality. In doing so, type **1** complexes were reacted with $ZnMe_2$, yielding IrMe(COD)PMe_2Ar' species, **2**, as orange solids (Scheme 7).

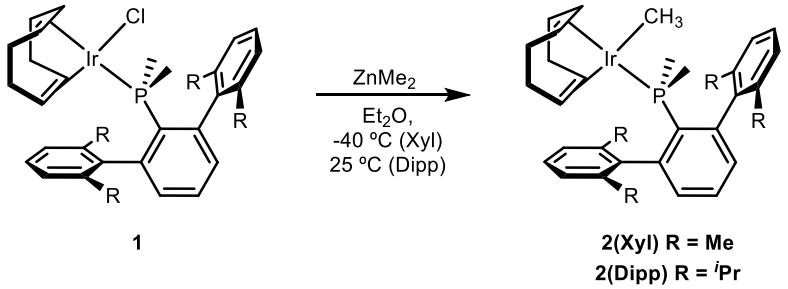

1 **2(Xyl) R = Me**
2(Dipp) R = ^{i}Pr

Scheme 7. Synthesis of type **2** complexes. R stands for Me (Xyl) and ^{i}Pr (Dipp) groups.

Despite the structural similarity of complexes **2(Xyl)** and **2(Dipp)**, the former presented limited thermal stability in solution and its spectroscopical characterization had to be done below −20 ºC. A slight (1.9 ppm) downfield chemical shift difference in the $^{31}P\{^{1}H\}$ NMR spectra was recorded for **2(Xyl)** (−7.4 ppm) relative to **1(Xyl)**, in agreement with the structural resemblance of these species. The ^{1}H NMR data is also very similar, except for a doublet ($^{3}J_{HP}$ = 6.5 Hz, 3H) at 0.22 ppm, that was assigned to the Ir−CH_3 moiety. A doublet ($^{2}J_{CP}$ = 7 Hz) corresponding to this group was also registered in the $^{13}C\{^{1}H\}$ NMR spectrum at 8.8 ppm. **2(Dipp)** presented analogous NMR features which will not be discussed.

A new greenish species, **3(Xyl)**, characterized by a $^{31}P\{^{1}H\}$ resonance at −1.9 ppm, formed when a solution of complex **2(Xyl)** was allowed to stand

above −20 ºC. A few broad signals were registered in the room temperature ^{1}H spectrum, revealing that a dynamic process was taking place in solution. Upon lowering the temperature to −10 ºC these peaks sharpened, permitting an accurate NMR assignment. The presence of only three out of the four original benzylic methyl groups, along with the inequivalence of the 9 aromatic protons and the disappearance of the high-field peak belonging to the Ir−CH_3 moiety suggested that metalation of one the flanking xylyl rings, accompanied by methane release, had taken place (Scheme 8).

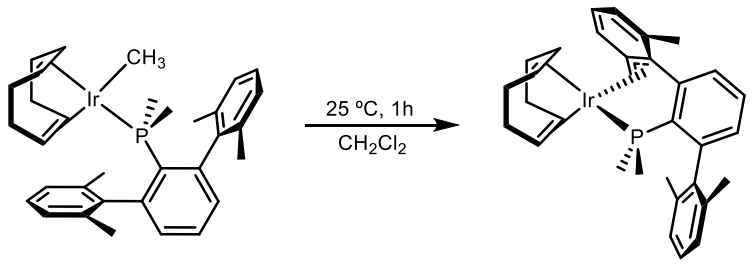

2(Xyl) **3(Xyl)**

Scheme 8. Conversion of **2(Xyl)** into **3(Xyl)**.

Consistent with this hypothesis, a doublet of doublets ($^{3}J_{HP}$ = 15.0 Hz, $^{2}J_{HH}$ = 5.2 Hz, 1H) was located at 1.17 ppm, assigned as one of the Ir−CH_2 protons. The second Ir−CH_2 proton could be located at 2.01 by means of two-dimensional NMR experiments (COSY and HSQC), as it was overlapped by a neighboring signal. Upon complete assignment of the ^{1}H NMR spectrum, it was clear that the observed fluxional behavior was exclusive of the cyclooctadiene ligand. Two sets of exchange cross peaks were recorded in the EXSY experiment for the four alkenic protons of the COD ligand (Figure 14), along with the corresponding exchange signals for the CH_{2COD} protons. Possible explanations for the fluxionality of the COD ligand are disclosed in the forthcoming paragraphs and in Scheme 9.

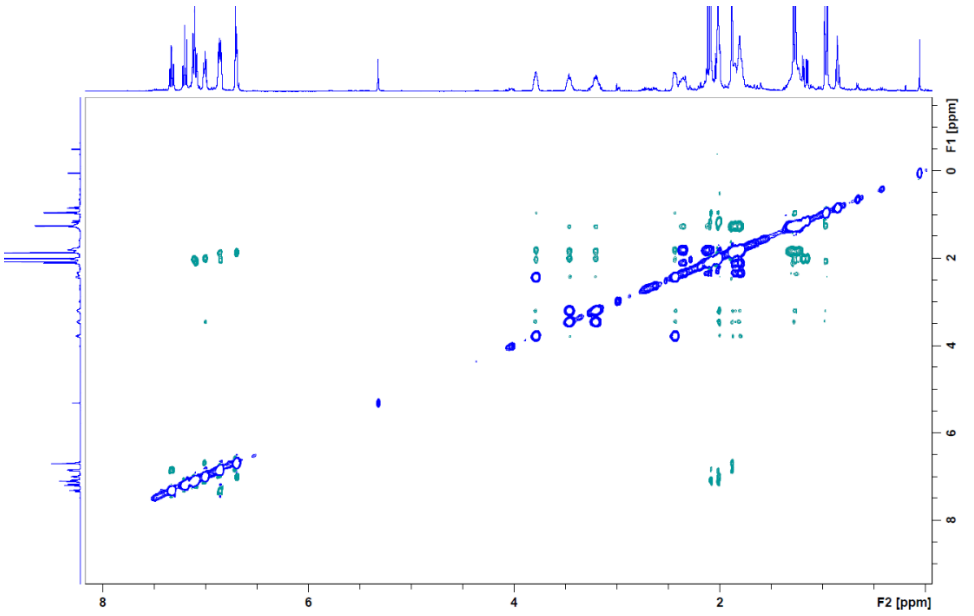

Figure 14. NOESY spectrum of **3(Xyl)** recorded at −10 ºC. Exchange cross-peaks were only detected for signals belonging to the COD ligand, located between 1.5 and 4 ppm.

Analysis of the $^{13}C\{^{1}H\}$ spectrum of **3(Xyl)** was consistent with the metalation of one flanking xylyl ring. The methylenic carbon bound to the metal center was recorded at 30.0 ppm as a doublet ($^{2}J_{CP}$ = 5 Hz), slightly downfield relative to the free Me_{Xyl} groups, which resonate around 22 ppm. In addition, a multiplet at 111.6 ppm was assigned to the *ipso* and one of the *ortho* carbon atoms of the metalated ring, significantly upfield compared to the values of the free xylyl ring (141.1 ppm (*ipso*), 137.4 and 136.3 ppm (*ortho*)) and the other *ortho* carbon of the same arene (137.9 ppm). This finding supported κ^{1}-P,η^{3}-C coordination of the metalated phosphine, establishing a pseudoallylic interaction to yield an 18-electron complex. This hypothesis was further confirmed by X-Ray crystallography (Figure 15).

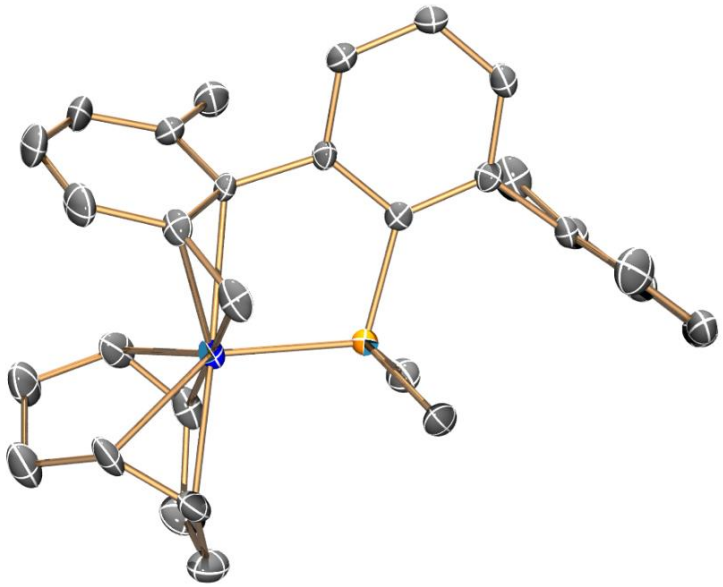

Figure 15. ORTEP diagram of complex **3(Xyl)**. Hydrogen atoms are excluded for clarity and thermal ellipsoids are set at 50 % probability.

Complex **3(Xyl)** displays a distorted square pyramid geometry, with the phosphorus atom in the apical position. The pseudoallylic interaction is characterized by Ir−C bond distances of 2.138(4), 2.177(3) and 2.287(4) Å, corresponding to the benzylic, *ortho* and *ipso* positions, respectively. The pyramidalization of the bound ipso carbon diminished the angle between the *o*-C_6H_3, *ipso*-Xyl and *p*-Xyl carbon atoms to 148.20 º, whereas for the free xylyl this value was 177.85 º.

II.2.2.2 C−H Activation at Iridium(I): Computational Studies

Although iridium(I) species have been extensively studied in the context of C−H bond activation processes, many of these transformations comprised the generation of reactive, 14-electron species upon ligand dissociation.[76] In fact, the first example of an additive-free oxidative addition of a C−H bond to a d^8, square planar iridium complex was recently reported by Milstein, which required the participation of a non-innocent pincer ligand.[77] We considered of interest to computationally investigate the mechanism of the C−H bond activation that forms complex **3(Xyl)** from **2(Xyl)**.[78] The most accessible pathway (Figure 16) involves oxidative addition (Figure 17) of a benzylic C−H bond to afford an iridium (III) hydride (Figure 18), which is trans to the P atom (**H-*trans***, Figure 19); this process entails a barrier of 26.3 kcal/mol and gives a species 13.2 kcal/mol above **2(Xyl)**. The reductive elimination of methane (26.5 kcal/mol, Figure 20) gives a square planar complex at −12.5 kcal/mol, **A**. A transition state connecting this intermediate with the observed product, **3(Xyl)** (−10.9 kcal/mol), could not be found, however, the η^1 to η^3 allyl isomerization is expected to be facile. It is pertinent to recall that both NMR and X-Ray diffraction studies support the existence of a pseudoallylic interaction, and therefore the **3(Xyl)** should be thermodynamically favored over **A**.

---

[76] a) Janowicz, A.H.; Bergman, R. G. *J. Am. Chem. Soc.* **1982**, *104*, 352; b) Hoyano, J. K.; Graham, W.A.G. *J. Am. Chem. Soc.* **1982**, *104*, 3723.

[77] Kumar, A.; Feller, M.; Ben-David, Y.; Diskin-Posner, Y.; Milstein, D. *Chem. Commun.* **2018**, *54*, 5365.

[78] Calculations were performed with the Gaussian 09 program employing the hybrid functional M06. Geometry optimizations were carried out in the gas phase without geometry constraints.

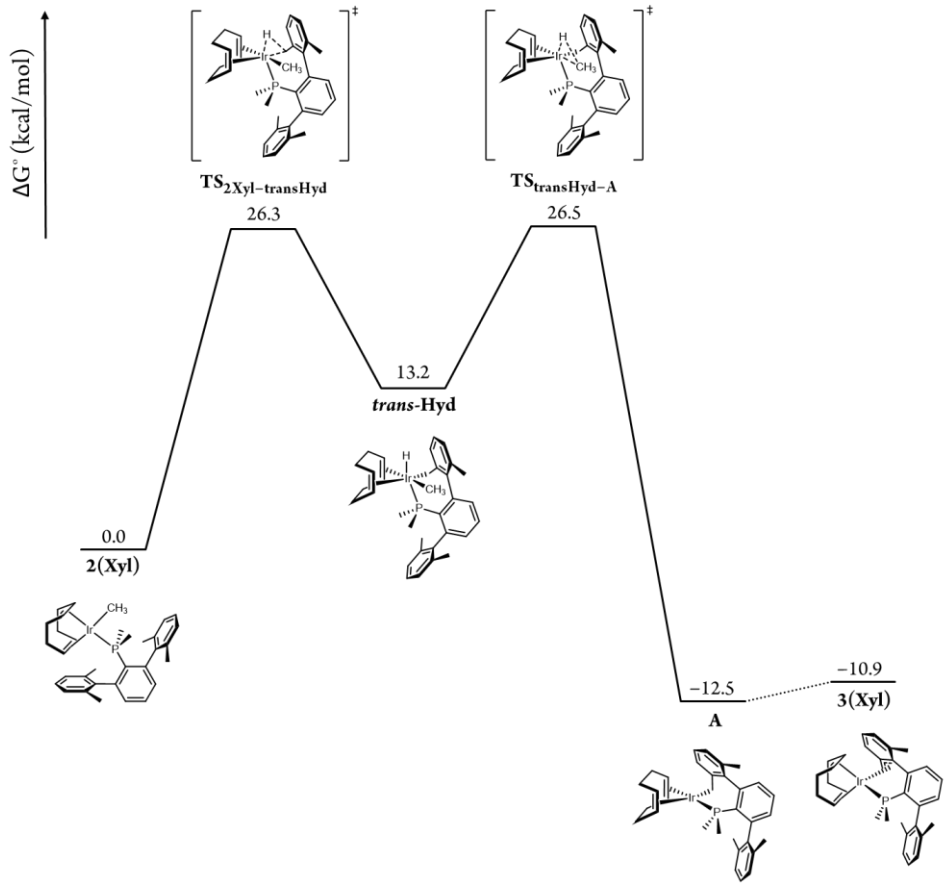

Figure 16. ΔGº profile for the conversion of **2(Xyl)** into **3(Xyl)** via a *trans* iridium(III) hydride.

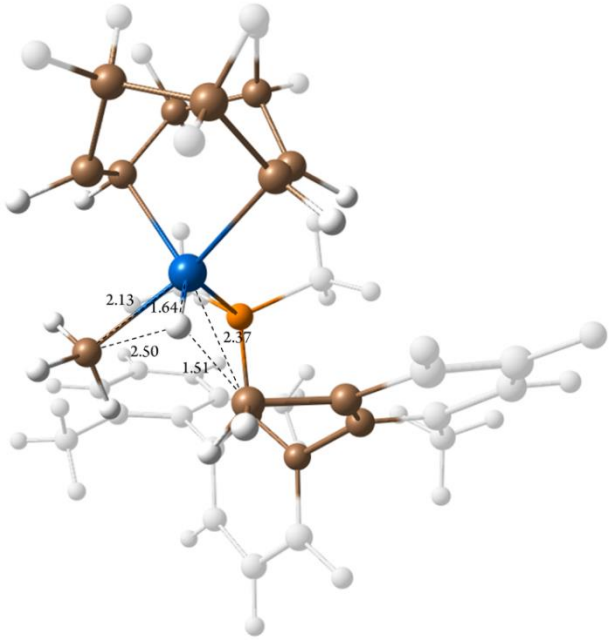

Figure 17. Molecular geometry of the transition state associated with the oxidative addition that yields the *trans* hydride, **TS$_{2Xyl-transHyd}$.**

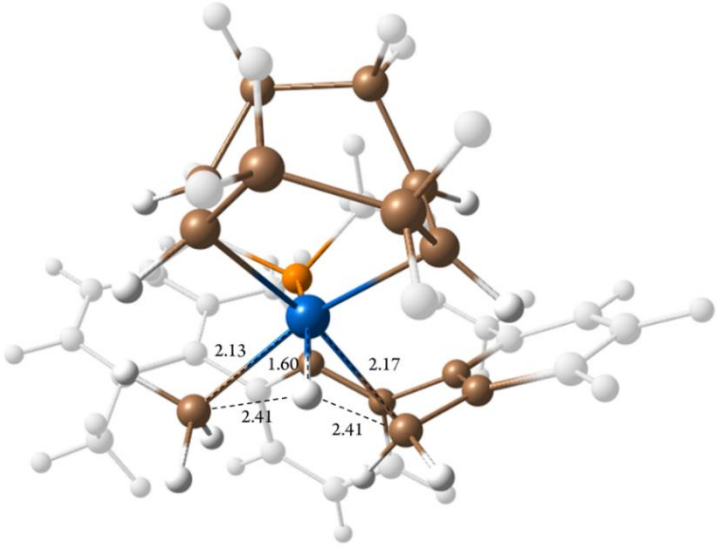

Figure 18. Molecular geometry of the *trans* hydride, ***trans*-Hyd**.

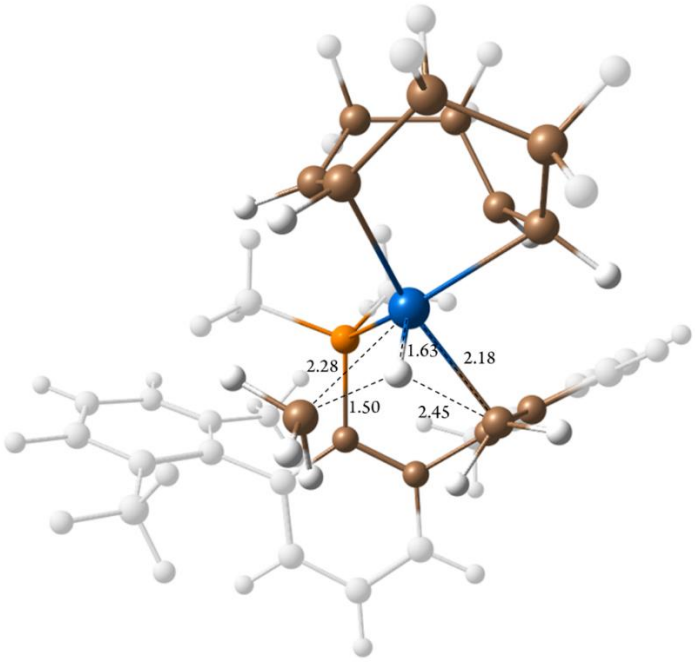

Figure 19. Molecular geometry of the transition state associated with the reductive elimination from the *trans* hydride, $\mathbf{TS_{transHyd-A}}$.

The dynamic behavior of the COD ligand in complex **3(Xyl)** can be explained through the participation of intermediate **A**, for which calculations suggest being close in energy to **3(Xyl)** and thus accessible under working conditions. To attain the square planar geometry of **A**, the COD ligand must rotate *ca*. 90 degrees from the distorted square pyramid geometry in **3(Xyl)**, giving access to the observed site exchange upon regeneration of **3(Xyl)** (Scheme 9).

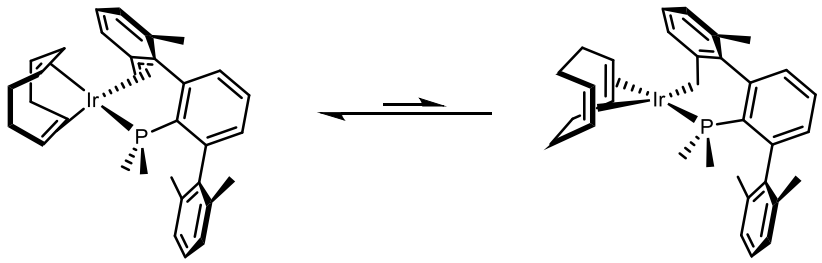

3(Xyl) **A**

Scheme 9. Proposed participation of the square planar intermediate **A** in the dynamic behavior of the COD ligand in **3(Xyl)**.

II.2.2.3 Alternative mechanisms

The barriers depicted in Figure 16 are somewhat high to be in precise agreement with experimental conditions. Therefore, several alternative pathways were considered.

The oxidative addition of a benzylic C−H bond at complex **2(Xyl)** can give an octahedral iridium(III) hydride in *cis* to the phosphine, **H-*cis***, at 18.6 kcal/mol (Figure 20). However, the oxidative addition and reductive elimination steps for this pathway entail energy barriers of 38.6 and 36.4 kcal/mol, respectively (Figure 21), ruling this pathway out.

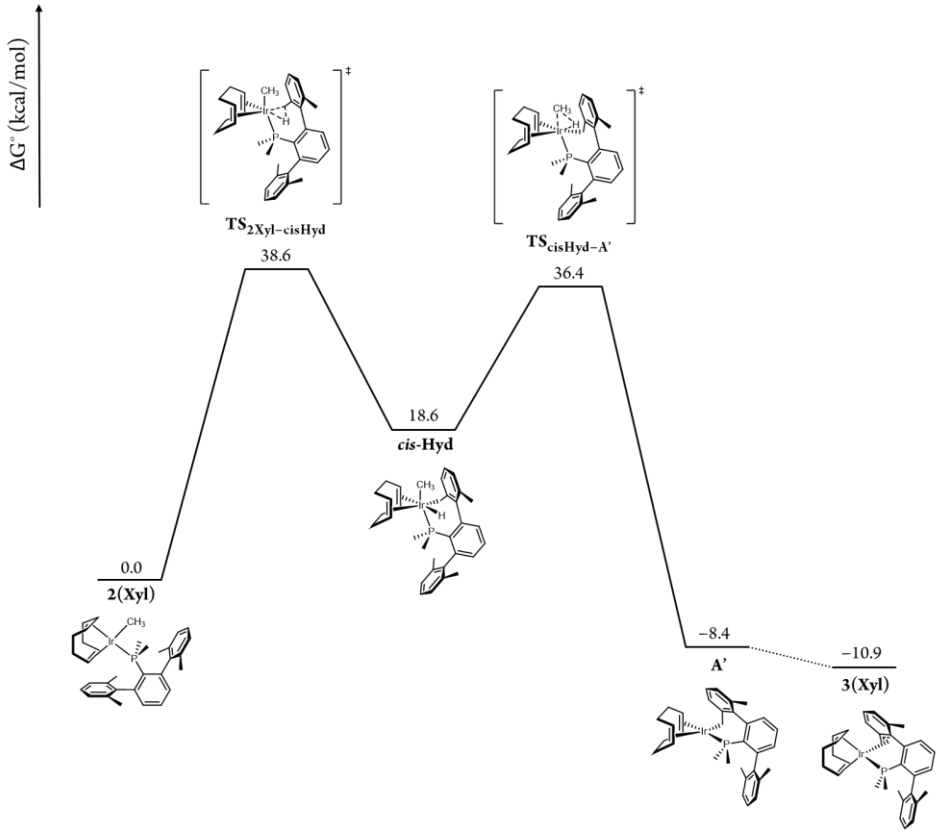

Figure 20. ΔGº profile for the conversion of **2(Xyl)** into **3(Xyl)** via a *cis* iridium(III) hydride.

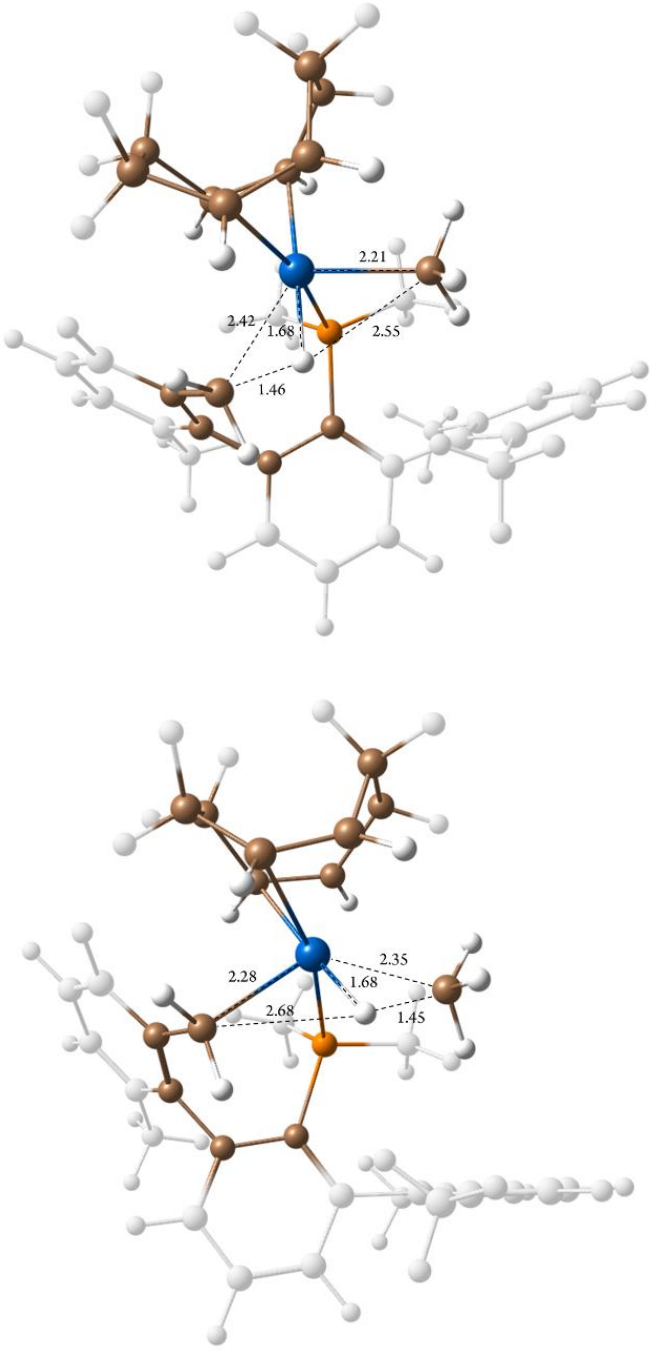

Figure 21. Molecular geometries of the transition states associated with the oxidative addition (**TS$_{2Xyl-cisHid}$**, top) and reductive elimination (**TS$_{cisHid-A'}$**, bottom) involving the *cis* hydride.

A concerted pathway involving σ-bond metathesis (σ-BM) was also evaluated. A relaxed scan of the H_{MeXyl}−$C_{Ir–CH3}$ bond distance at **2(Xyl)** gave the proper geometry to obtain a transition state for the concerted hydrogen migration to the metal alkyl (Figure 22). However, this transition state, located at 50.6 kcal/mol, was not representative of σ-BM, being more related to the direct H atom transfer reported in the first chapter of this Thesis.

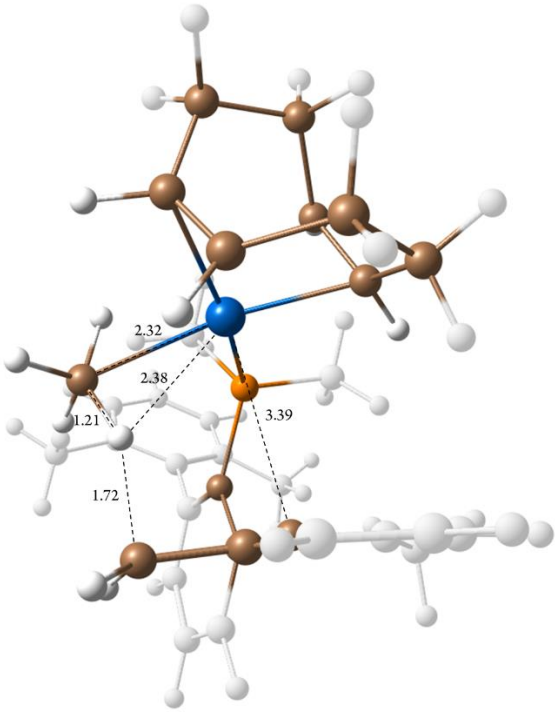

Figure 22. Molecular geometry of the transition state associated with the direct H atom transfer from the benzylic position to the metal alkyl group.

In order to find a true σ-BM transition state, the reaction coordinate for the reductive elimination of methane was analyzed. The molecular geometry found for a H_{Ir}−$C_{Ir–CH3}$ bond distance of 1.75 Å was used as the starting point for a subsequent relaxed scan, shortening the H_{Ir}−$C_{Ir–CH2}$ bond distance while keeping H_{Ir}−$C_{Ir–CH3}$ constant at 1.75 Å. A transition state

search, launched keeping this constraint, converged to give two imaginary frequencies (Figure 23): −813 cm^{-1}, corresponding to the H transfer, and −160 cm^{-1}, associated to the imposed constraint. This TS, best described as a metal-assisted σ-bond metathesis (MAσ-BM), was located at 44.7 kcal/mol relative to **2(Xyl)**.

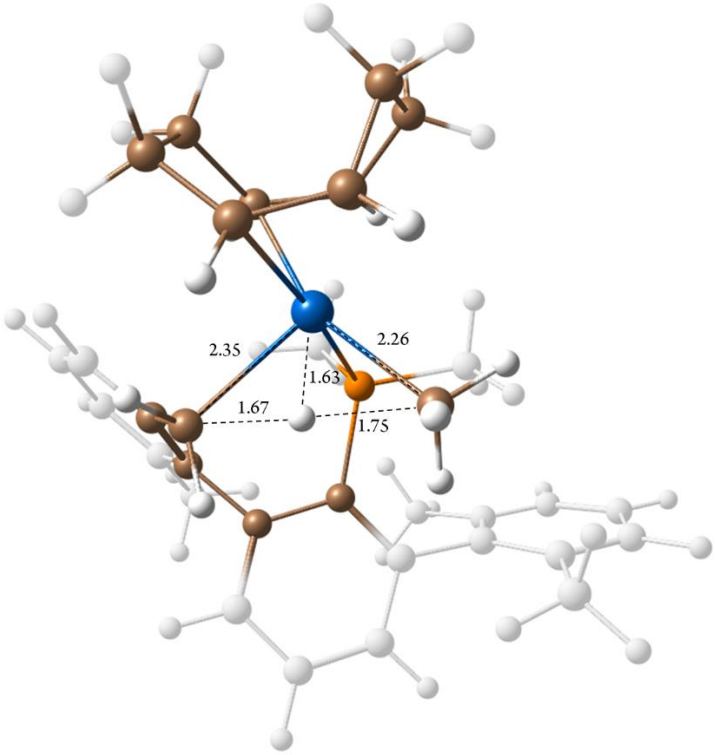

Figure 23. Molecular geometry of the transition state associated with the MAσ-BM. The H_{Ir}–C_{Ir-CH3} bond distance was fixed at 1.75 Å.

A constraint-free TS search was carried out starting from the geometry of the aforementioned TS, converging to a classic oxidative addition TS at 39.7 kcal/mol after the separation of the two participating carbon atoms (3.93 Å, *cf*. the 3.41 Å for the constraint-including TS), being very close energy and geometry-wise to **$TS_{2Xyl-cisHid}$**.

Finally, the C−H activation occurring at a formally 14-electron species, generated upon dissociation of one of the COD alkene groups, was evaluated (Figure 24). Exceedingly high barriers were found for the corresponding oxidative addition (Figure 25) and reductive elimination processes (36.6 and 32.6 kcal/mol, respectively), making this pathway a non-competitive one.

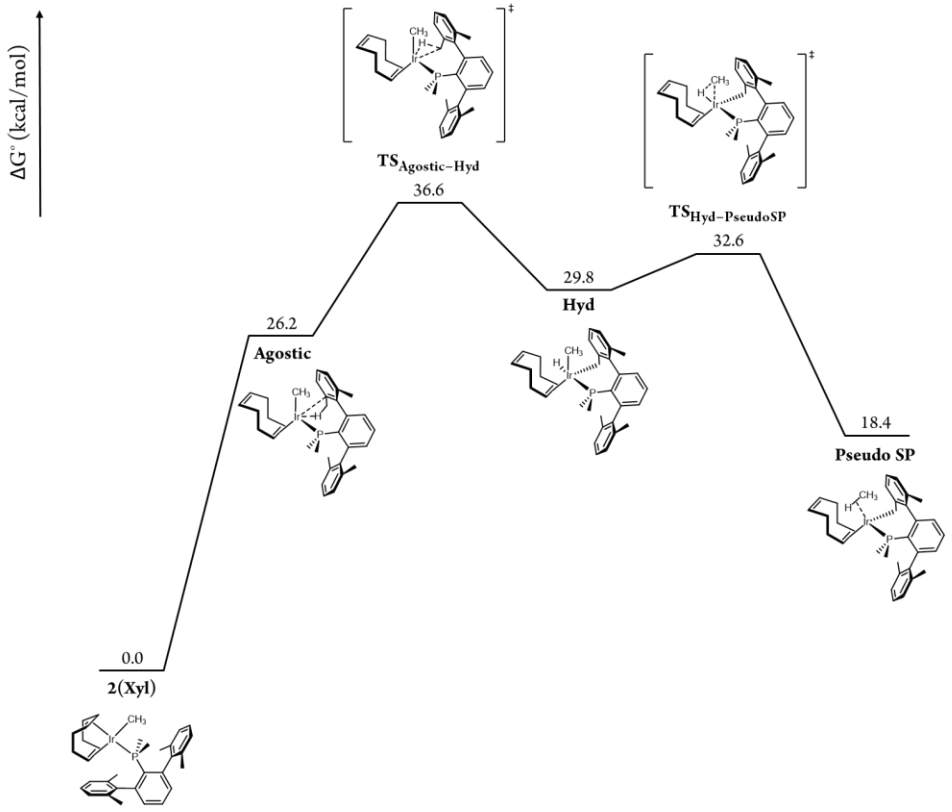

Figure 24. ΔGº profile for the C−H activation of the benzylic position at a formally 14-electron complex.

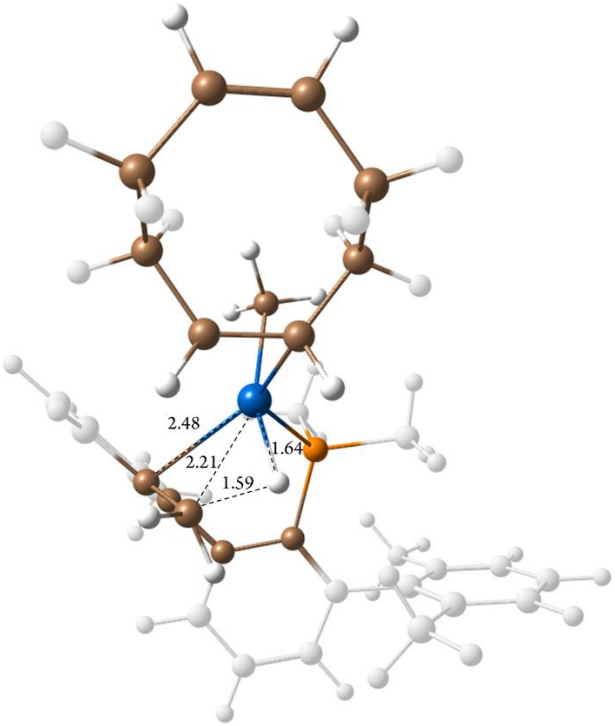

Figure 25. Molecular geometry of the transition state associated with the oxidative addition at a formally 14-electron complex.

On these grounds, our computational results suggest that the C−H bond activation that conduces to the formation of **3(Xyl)** starting from **2(Xyl)** occurs through oxidative addition to give an octahedral iridium(III) hydride, in trans relative to the phosphine, which undergoes reductive elimination to form a 16-electron, square planar isomer of **3(Xyl)** (**A**). As mentioned at the beginning of this section, the related complex **2(Dipp)** based on a bulkier phosphine was stable towards cyclometalation and CH_4 release at room temperature over prolonged periods of time. The reasons behind the enhanced stability of complex **2(Dipp)** will be studied in due course.

II.2.2.4 Neutral Carbonyl Complexes

In the previous section of this Chapter, the average stretching frequency of the carbonyl groups in $IrCl(CO)_2PMe_2Ar$' complexes were used to assess the donor capacity of the studied phosphines. These neutral dicarbonyl phosphine complexes, **4**, were prepared by exposing a dichloromethane solution of the corresponding cyclooctadiene complex (**1**) to a carbon monoxide atmosphere (1 bar, Scheme 10).

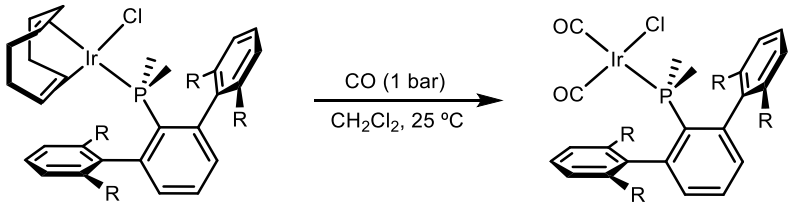

1 **4(Xyl) R = Me**
4(Dipp) R = ^{i}Pr

Scheme 10. Synthesis of type **4** complexes. R stands for Me (Xyl) and ^{i}Pr (Dipp) groups.

The yellow solution turned significantly paler upon exposure to CO, and further chemical changes were detected by means of NMR spectroscopy. The $^{31}P\{^{1}H\}$ spectrum of **4(Xyl)** showed a single peak at −10.9 ppm, reflecting little chemical shift change (−1.6 ppm) relative to **1(Xyl)**. The apparent symmetry observed in the ^{1}H NMR spectrum was in accordance with the monodentate coordination of the phosphine ligand. The carbonyl groups resonated as doublets at 177.7 ($^{2}J_{CP}$ = 126 Hz, *trans*) and 168.3 ($^{2}J_{CP}$ = 13 Hz, *cis*) ppm. Unequivocal confirmation regarding the molecular structure of these species was obtained by means of X-Ray crystallography (Figure 26). In the solid state, **4(Xyl)** presented an Ir−*trans*-CO bond distance of 1.896(3) Å, significantly larger than for the *cis* carbonyl group (1.827(4) Å) in agreement with the greater *trans* influence of the phosphine

ligand. The metal center is not located on top of a flanking aryl ring, the Ir−P−*ipso*-C_6H_3−*o*-C_6H_3 torsion being close to 45 º. Comparable results were registered for **4(Dipp).**

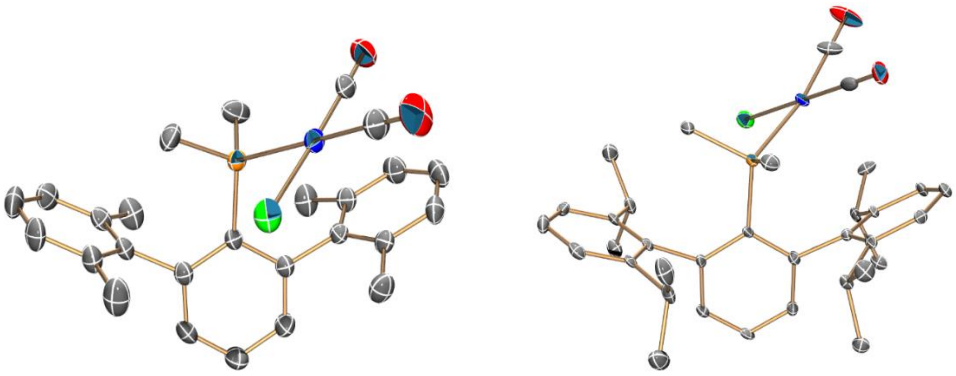

Figure 26. ORTEP diagrams of complexes **4(Xyl)** (left) and **4(Dipp)** (right). Hydrogen atoms are excluded for clarity and thermal ellipsoids are set at 50 % probability.

II.2.3 Synthesis and Reactivity of Ir(I) Cationic Complexes

In homogeneous catalysis, ligand dissociation is often required to form unsaturated, reactive complexes, which are the active species in the subsequent catalytic cycle. Wilkinson´s catalyst,[18] $RhCl(PPh_3)_3$, constitutes a signature example of this behavior, as the active species in the catalytic hydrogenation of olefins is the trigonal, 14-electron complex $RhCl(PPh_3)_2$. In many cases ligand dissociation is indeed the rate-limiting-step of the overall reaction, being the extreme case the complete inactivity of a precatalyst in the absence of additives that promote ligand dissociation. A classic strategy to generate a permanent vacant coordination site on a metal center to boost up its reactivity consists in forcing the irreversible substitution of an X type ligand with a weakly coordinating anion (ej. BF_4^-, PF_6^-) by using alkaline or silver salts. In addition, the cationic character of the resulting unsaturated metal complexes typically leads to a significant enhancement of its reactivity. On a negative note, an uncontrolled increase in reactivity is often accompanied by unforeseen molecular pathways, including decomposition; the use of bulky and/or hemilabile ligands is an effective strategy to prevent these undesired events from occurring.

II.2.3.1 Cationic Carbonyl Complexes

The reactivity of the aforementioned Vaska´s complex has been enhanced by replacement of the bound chloride ligand with a weakly coordinating carborane anion.[79] However, the structural characterization of the formally 14-electron species remained elusive for the authors. In this section, our results englobing the reactivity of several cationic iridium(I) complexes related to Vaska´s system are presented, disclosing the importance of the hemilabile character of the terphenyl phosphine ligands employed to stabilize this type of unsaturated species.

Salt metathesis of chloride complexes **4** with the sodium salt of the weakly coordinating BAr_F anion (BAr_F = [{3,5-$(CF_3)_2$-$C_6H_3)_4$}B]$^-$) afforded the desired cationic dicarbonyl complexes, $[Ir(CO)_2(PMe_2Ar')]BAr_F$ (**5(CO)$_2$BAr$_F$**) (Scheme 11).

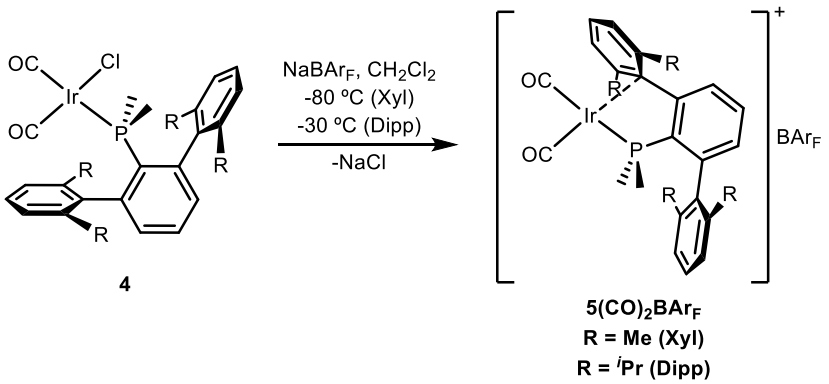

Scheme 11. Synthesis of cationic, dicarbonylic complexes, **5$^+$(CO)$_2$**.

These unsaturated species presented limited solution stability and were therefore characterized at low temperatures (−60 ºC (Xyl) and 0 ºC (Dipp)). The CH_2Cl_2 IR spectrum of (**5(Xyl)$^+$(CO)$_2$**) displayed two strong

[79] Douvris, C.; Reed, C. A. *Organometallics* **2008**, *27*, 807.

bands at 2094 and 2027 cm^{-1} (similar values were obtained for the Dipp analog), significantly blueshifted relative to the corresponding values recorded for **4(Xyl)** (2068 and 1987 cm^{-1}), in agreement with the cationic character of the complex. A substantial chemical shift displacement of the $^{31}P\{^{1}H\}$ resonance gave rise to a singlet at 16.2 ppm (*cf*. the –10.9 ppm for **4(Xyl)**), suggesting that in these unsaturated species, chloride elimination could be compensated by the coordination of a flanking aryl substituent. The side rings of the terphenyl group were found to be inequivalent in the ^{1}H NMR spectrum, further supporting this hypothesis. Two singlets were recorded for the benzylic methyl groups (Me_{Xyl}) of **5(Xyl)$^{+}$(CO)$_2$** at 2.05 and 1.94 ppm, pointing to the existence of an apparent symmetry plane containing the central ring of the terphenyl moiety. Two distinctive doublets were detected in the carbonyl region of the $^{13}C\{^{1}H\}$ spectrum, at 183.0 ($^{2}J_{CP}$ = 102 Hz) and 162.4 ($^{2}J_{CP}$ = 14 Hz) ppm. The magnitude of these scalar couplings, which is heavily reliant on the geometrical disposition relative to the P atom, correlates well with those measured for **4(Xyl)**, supporting that the square planar geometry around the metal center was retained. Whereas the *ipso* carbon of the coordinated xylyl ring resonates at a relative high field, 117.4 ppm, relative to its counterpart at the free ring (136.2 ppm), no variation was observed for the neighboring *ortho* carbons, (139.1, *o*-Xyl'; 136.2, *o*-Xyl), consistent with η^{1}-C_{ipso} coordination of the arene.

X-Ray crystallography provided unambiguous confirmation of the structural features advanced by solution NMR studies (Figure 27). The greater *trans* influence of the phosphine ligand was reflected in a large Ir−*trans*-CO bond distance of 1.94(1) Å, whereas the Ir−*cis*-CO bond distance was 1.85(1) Å), resemblant of the behaviour of type **4** species. The *ipso* carbon of the coordinated xylyl ring was located at 2.297(9) Å

from the metal center, while the *ortho* carbon atoms could be found at 2.571(8) and 2.74(1) Å. The marked pyramidalization of the *ipso* carbon was responsible of an *ortho*-C_6H_3–*ipso*-Xyl'–*p*-Xyl' angle of 155.3(6) º.

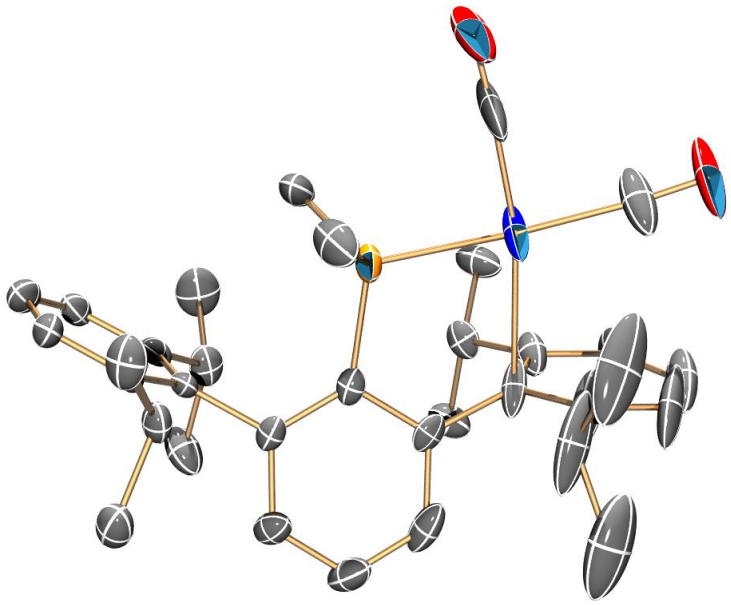

Figure 27. ORTEP diagram of the cation of complex **5(Dipp)$^+$(CO)$_2$**. Hydrogen atoms are excluded for clarity and thermal ellipsoids are set at 50 % probability.

Even at −60 ºC, chemical exchange peaks were detected in the aromatic and aliphatic regions of the EXSY spectrum due to interchange between the coordinated and free xylyl rings of compound **5(Xyl)$^+$(CO)$_2$**, exposing the lability of the metal-arene interaction (Figure 28). Introducing *iso*-propyl groups at the 2 and 6 positions of the flaking arenes provided kinetic stabilization, as no exchange was observed for the side rings of the terphenyl moiety of complex **5(Dipp)$^+$(CO)$_2$** at 0 ºC.

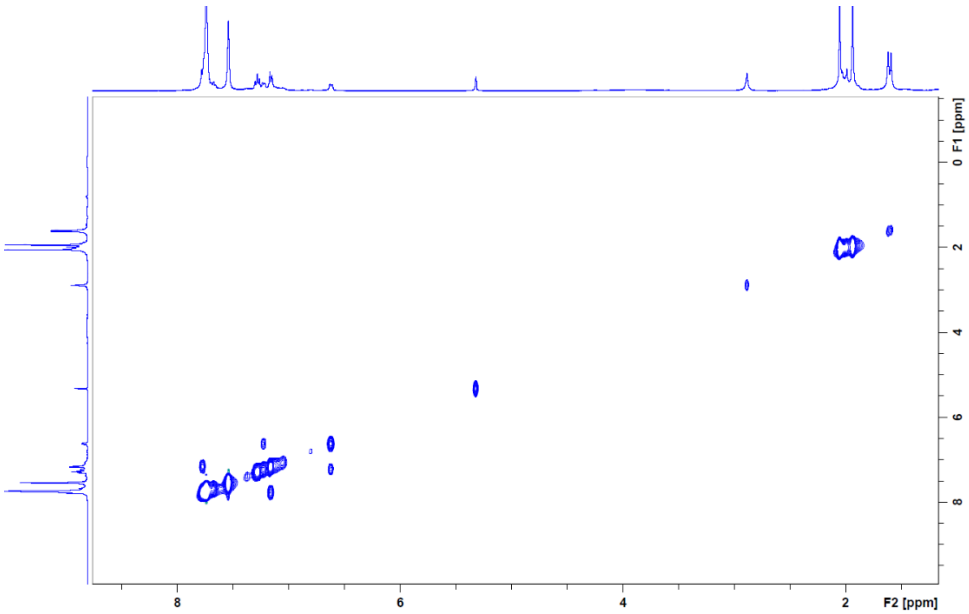

Figure 28. NOESY spectrum recorded at −60 ºC showing chemical exchange peaks of the coordinated and free xylyl rings of compound **5(Xyl)$^{+}$(CO)$_2$**.

II.2.3.2 Topological analysis of $5^{+}(CO)_2$

The extent of bonding interaction between the iridium atom and the flanking ring in complexes $\mathbf{5^{+}(CO)_2}$ was investigated by means of the quantum theory of atoms in molecules (QTAIM).[80] Analysis of the calculated electron densities of $\mathbf{5^{+}(CO)_2}$ with the Multiwfn program[81] reveals bond critical points (bcps) and unique bond paths (bp) between the iridium and the corresponding *ipso* carbon of complexes $\mathbf{5^{+}(CO)_2}$ supporting non-covalent interactions indicated by their solid state (X-Ray Diffraction) and calculated[82] geometries (Figure 29).

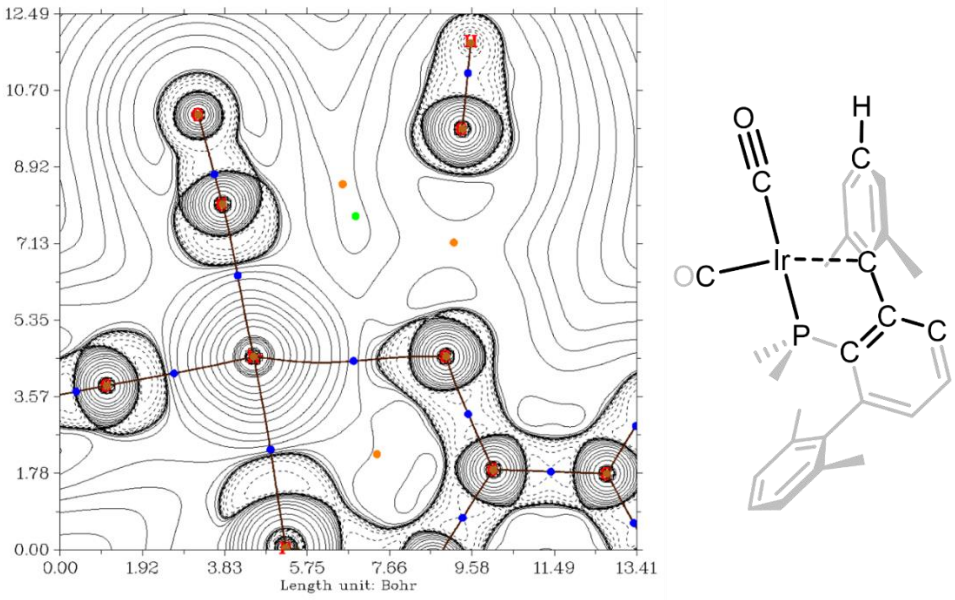

Figure 29. Plot of the laplacian of the electron density, $\nabla^2\rho$, of complex $\mathbf{5(Xyl)^{+}(CO)_2}$ in the Ir–P–*ipso*-Xyl' plane calculated with the ωB97X-D

[80] Bader, R. F. W. *Atom in Molecules: A Quantum Theory*; Oxford University Press: Oxford, U.K. **1995**.
[81] Lu, T.; Chen, F. *J. Comput. Chem.* **2012**, *33*, 580.
[82] Calculations were performed with the Gaussian 09 program employing the Head-Gordon hybrid functional ωB97XD. Geometry optimizations were carried out without geometry constraints and included solvent (dichloromethane).

functional. The solid and dashed lines correspond to positive and negative values of $\nabla^2\rho$, respectively. In plane bcps and bps of the electron density are superimposed.

The topological properties of the electron density at bcps have been associated to the nature of the interaction between atoms.[83] QTAIM analysis of the electron density ($\boldsymbol{\rho_b}$) at relevant bcps of type **5$^+$(CO)$_2$** complexes (Table 7) indicates that the strength of the Ir-C_{arene} interaction is similar for **5(Xyl)$^+$(CO)$_2$** and **5(Dipp)$^+$(CO)$_2$**, as indicated from the magnitude of the electron density ($\boldsymbol{\rho_b}$) at the corresponding bcp. This finding supports that the lack of lability of the metal arene interaction in **5(Dipp)$^+$(CO)$_2$** does not arise from a thermodynamic effect.

Complex[a]	**Bond**	$\boldsymbol{\rho_b}$[b]	$\boldsymbol{G_b}$[c]	$\boldsymbol{V_b}$[c]	$\boldsymbol{H_b}$[c]	$\lvert \boldsymbol{V_b} \rvert / \boldsymbol{G_b}$	$\boldsymbol{\nabla^2\rho}$[d]
5(Xyl)$^+$(CO)$_2$	Ir−C_{ipso}	0.063	0.047	−0.064	−0.017	1.357	0.122
5(Dipp)$^+$(CO)$_2$	Ir−C_{ipso}	0.064	0.048	−0.066	−0.018	1.367	0.122

Table 7. Electronic parameters derived from the topological analysis of the Ir−C_{ipso} interaction in **5$^+$(CO)$_2$** complexes. [a]Calculations with the ωB97X-D functional, [b]e·bohr^{-3}, [c]hartree, [d]e·bohr^{-5}.

In addition, positive values of the Laplacian of the electron density ($\nabla^2\rho$), values of the total energy density (H) close to zero, and ratios of the potential energy density to the kinetic energy density between 1 and 2 ($1 < \lvert V \rvert / G < 2$) at the relevant bcps are characteristic of metal ligand interactions.[83]

[83] a) Varadwaj, P. R.; Cukrowski, I.; Marques, H. M. *J. Phys. Chem. A* **2008**, *112*, 10657; b) Varadwaj, P. R.; Varadwaj, A.; Marques, H. M. *J. Phys. Chem. A* **2011**, *115*, 5592.

II.2.3.3 Reactivity of $5^{+}(CO)_2$ Complexes

Dichloromethane solutions of **$5^{+}(CO)_2$** complexes underwent further chemical changes, although the reaction outcome was dependent on the phosphine employed. **$5(Dipp)^{+}(CO)_2$** was slowly ($t_{1/2}$ = 15 h, 25 ºC) converted into a new species presenting a $^{31}P\{^{1}H\}$ resonance at 6.1 ppm. The analysis of the ^{1}H NMR spectrum confirmed that the flanking aryl rings remained inequivalent, and the apparent symmetry plane containing the central ring of the terphenyl moiety also persisted, pointing to the existence of a metal-arene interaction. Further supporting this hypothesis, the *meta* and *para* protons of one flanking ring resonated at 7.04 and 6.24 ppm, respectively, significantly high-fielded relative to its counterparts (7.30 and 7.50 ppm) while displaying a $^{3}J_{HH}$ of just 6.6 Hz (*cf.* the 7.8 Hz value for the non-coordinated ring) and a $^{3}J_{HP}$ of 0.9 Hz for the *meta* protons. The η^6 coordination of the Dipp ring was confirmed by $^{13}C\{^{1}H\}$ NMR spectroscopy, disclosing several doublets at 127.7 (2 Hz, *o*-Dipp'), 108.4 (5 Hz, *ipso*-Dipp'), 98.4 (3 Hz, *m*-Dipp') and 90.0 (7 Hz, *p*-Dipp') ppm. In addition, only one carbonyl group could be detected at 167.7 ppm (d, $^{2}J_{CP}$ = 14 Hz), suggesting that CO dissociation triggered κ^1-P,η^6-arene coordination of the phosphine ligand (Scheme 12). In agreement with this proposal, a single band in the IR spectrum was ascribed to a metal carbonyl (1997 cm^{-1}).

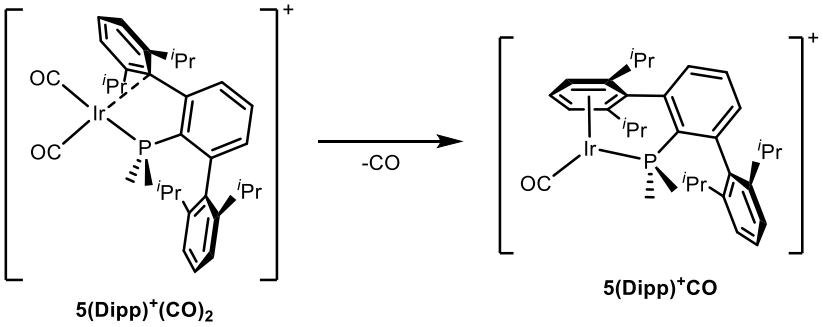

Scheme 12. Formation of **5(Dipp)$^+$CO** upon carbon monoxide dissociation from **5(Dipp)$^+$(CO)$_2$**.

X-Ray crystallography provided unequivocal confirmation of the two-legged piano stool structure of **5(Dipp)$^+$CO** (Figure 30). An Ir–CO bond distance of 1.841(5) Å was registered, whereas all the Ir–C_{arene} bond distances fell in the range of 2.187(6) and 2.342(5) Å.

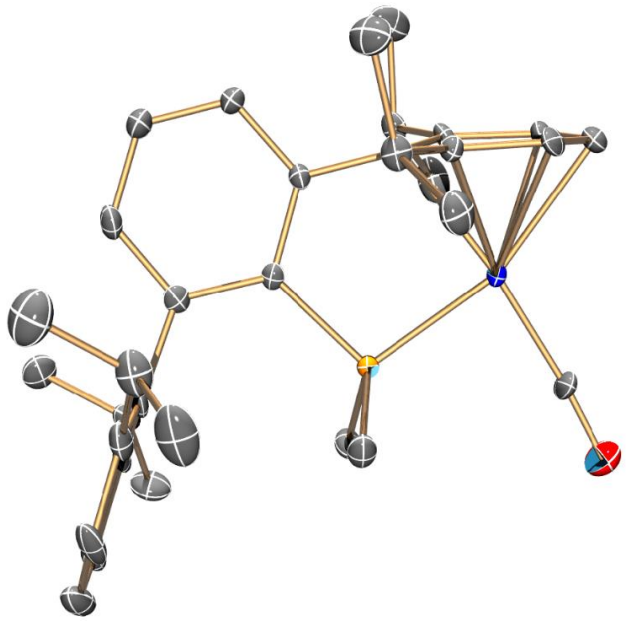

Figure 30. ORTEP diagram of the cation of complex **5(Dipp)$^+$CO**. Hydrogen atoms are excluded for clarity and thermal ellipsoids are set at 50 % probability.

In contrast, **5(Xyl)$^+$(CO)$_2$** evolved faster ($t_{1/2}$ = 3.5 h, 25 ºC) to produce an equimolar mixture of two species, characterized by $^{31}P\{^1H\}$ resonances with δ of 6.7 and −20.2 ppm, the former being assigned to **5(Xyl)$^+$CO** after comparison of its IR and NMR features with those identified for **5(Dipp)$^+$CO**. The observed 1:1 ratio of the products, along with the identification of two ν(CO) bands in the IR spectrum associated to the

unidentified product (2126 and 2027 cm^{-1}), prompted us to explore a disproportionation-like scenario, where two molecules of **5(Xyl)$^+$(CO)$_2$** would yield the mono- and tricarbonyl species, **5(Xyl)$^+$CO** and **5(Xyl)$^+$(CO)$_3$**, respectively (Scheme 13).

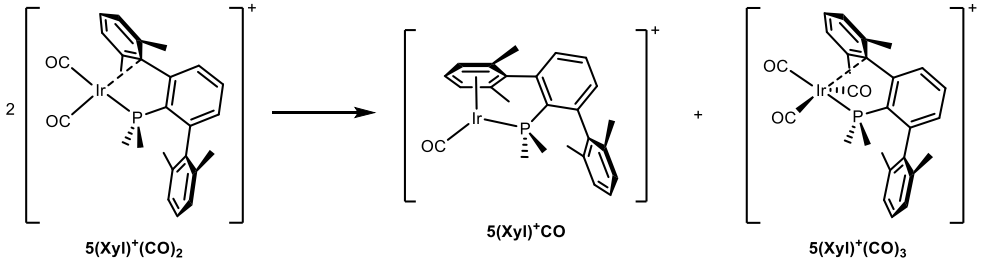

Scheme 13. Disproportionation of **5(Xyl)$^+$(CO)$_2$** into **5(Xyl)$^+$CO** and **5(Xyl)$^+$(CO)$_3$**.

To confirm this hypothesis, a Young NMR tube containing a CD_2Cl_2 solution of complex **5(Xyl)$^+$(CO)$_2$** was stirred under a CO atmosphere (1 bar), yielding a single product detected at −20.2 ppm in the $^{31}P\{^1H\}$ spectrum. The room temperature ^1H and $^{13}C\{^1H\}$ NMR spectra disclosed that coordination of a third carbon monoxide molecule restored the equivalence of the flanking xylyl rings, congruent with greater saturation of the metal center in the tricarbonylic species. Two doublets in a 2:1 ratio were detected in the $^{13}C\{^1H\}$ spectrum of complex **5(Xyl)$^+$(CO)$_3$**, at 173.1 ($^2J_{CP}$ = 15 Hz, *cis*-CO) and 168.2 ($^2J_{CP}$ = 88 Hz, *trans*-CO) ppm. However, the unusual breadth presented by several signals, particularly the $^{13}C\{^1H\}$ resonance associated to the *ipso* carbon of the flanking xylyl rings (132.3 ppm) suggested that a dynamic process might be taking place in solution. Variable temperature ^1H NMR studies (Figure 31) confirmed this hypothesis; upon lowering the temperature, all the signals, apart from the ones corresponding to the PMe_2 and *p*-C_6H_3 protons, were splitted,

indicating the inequivalence of the flanking rings of the terphenyl moiety. The exchange of these rings had a $\Delta G^{\ddagger}$ of 10.7 kcal/mol, as derived from line shape analysis.

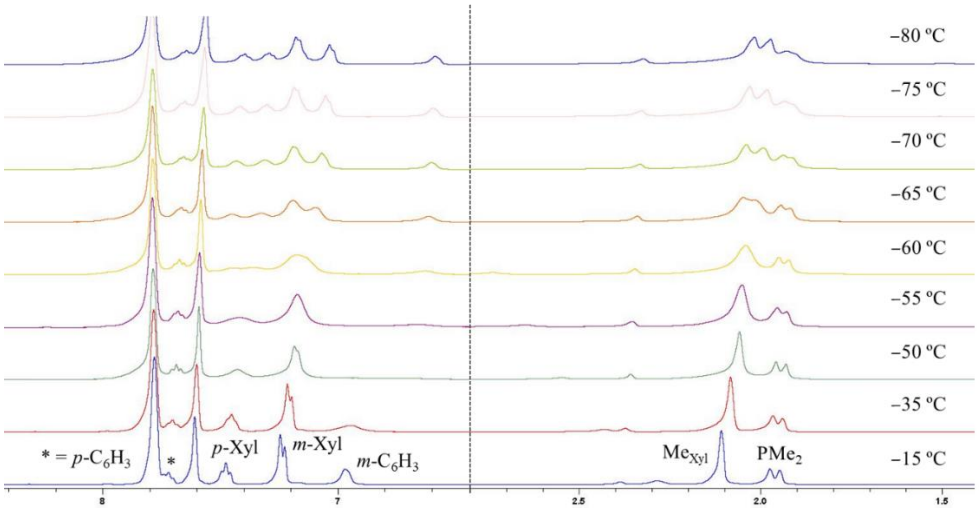

Figure 31. Aromatic and aliphatic regions of the ^{1}H NMR spectra of **5(Xyl)$^{+}$(CO)$_3$** from −15 ºC (bottom) to −80 ºC (top).

The molecular geometry of complex **5(Xyl)$^{+}$(CO)$_3$**, which could also be prepared by exposing complex **5(Xyl)$^{+}$CO** to CO atmosphere (1.2 bar), was determined by means of single crystal X-Ray Diffraction studies (Figure 32), confirming the tricarbonylic formulation and disclosing a weak interaction between the iridium center and an *ipso* carbon atom of a flanking xylyl ring placed at 2.523(4) Å (*cf.* the 2.297(9) Å reported for **5(Dipp)$^{+}$(CO)$_2$**). The pyramidalization of the bound *ipso* carbon was measured through the *o*-C$_6$H$_3$−*ipso*-Xyl'−*p*-Xyl' angle. A value of 159.6(3) º was recorded, larger than the corresponding value for **5(Dipp)$^{+}$(CO)$_2$**, 155.3(6) º and hence consistent with the lesser degree of metal unsaturation of the tricarbonylic compound. Taking the metal-arene interaction into account, the geometry around the metal center is best described as a distorted trigonal bipyramid featuring a wide angle (149.2(2) º) between

the Ir–*cis*-CO bonds, which displayed bond distances of 1.920(5) and 1.904(7) Å. A larger bond distance (1.954(5) Å) was recorded for the *trans*-CO.

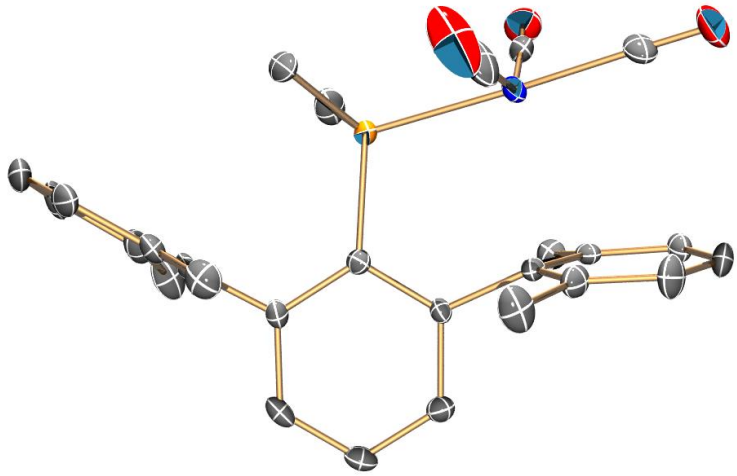

Figure 32. ORTEP diagram of the cation of complex **5(Xyl)$^{+}$(CO)$_3$**. Hydrogen atoms are excluded for clarity and thermal ellipsoids are set at 50 % probability.

As anticipated, exposing a dichloromethane solution of **5(Dipp)$^{+}$(CO)$_n$** (n = 1, 2) to a carbon monoxide atmosphere led to the formation of **5(Dipp)$^{+}$(CO)$_3$**, which presented similar spectroscopic features to those reported for **5(Xyl)$^{+}$(CO)$_3$**. However, while the solid-state structure of **5(Dipp)$^{+}$(CO)$_3$** has not yet been determined, its DFT-optimized geometry discloses shorter Ir-C_{arene} contact to the *ortho* carbon (Figure 33) than to the *ipso* carbon, probably due to steric hindrance between the *iso*-propyl substituents of the flanking aryl and the carbonyl ligands *cis* to the phosphine.

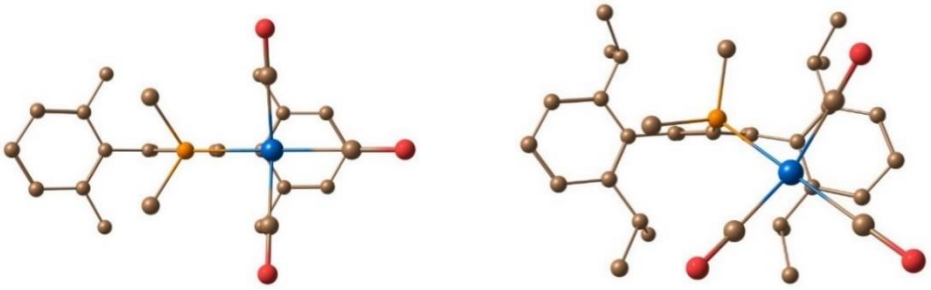

Figure 33. Upper view of the DFT-optimized structures of complexes **5(Xyl)$^+$(CO)$_3$** (right) and **5(Dipp)$^+$(CO)$_3$** (left).

The weak metal-arene interaction in these tricarbonylic complexes, **5$^+$(CO)$_3$**, was further studied by topological analysis. Analysis of the calculated electron densities of **5(Xyl)$^+$(CO)$_3$** revealed a bond critical point (bcp) and a unique bond path (bp) between the iridium and the *ipso*-Xyl' carbon atoms, supporting the existence of the non-covalent interaction indicated by the solid state (X-Ray Diffraction) and calculated (DFT) geometries (Figure 34).

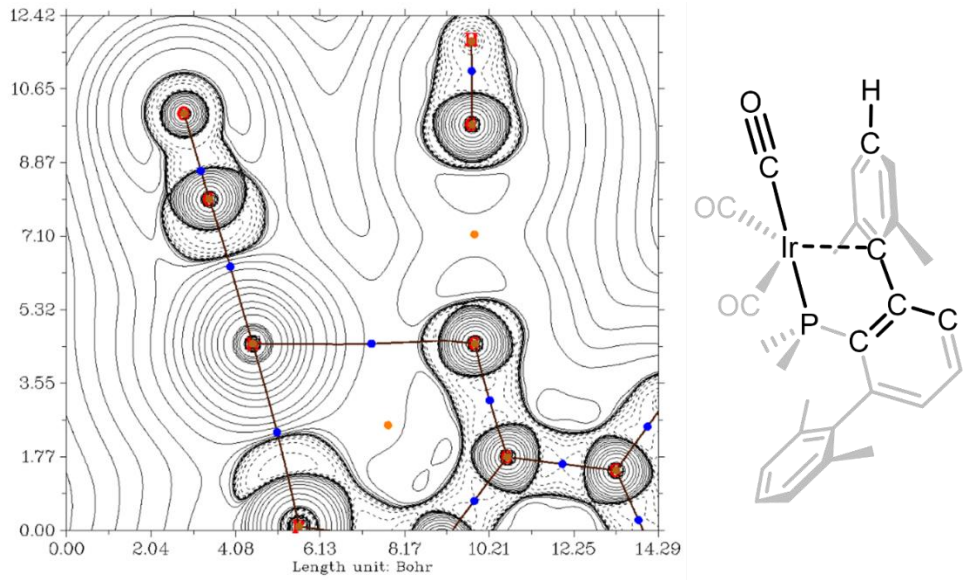

Figure 34. Plot of the laplacian of the electron density, $\nabla^2\rho$, of complex **5(Xyl)$^+$(CO)$_3$** in the Ir–P–*ipso*-Xyl' plane calculated with the ωB97X-D functional. The solid and dashed lines correspond to positive and negative values of $\nabla^2\rho$, respectively. In plane bcps and bps of the electron density are superimposed.

For **5(Dipp)$^+$(CO)$_3$** a bcp and a unique bp was found connecting the iridium and one *ortho*-Xyl' carbon atoms, supporting the existence of a weak interaction between these two centers (Figure 35).

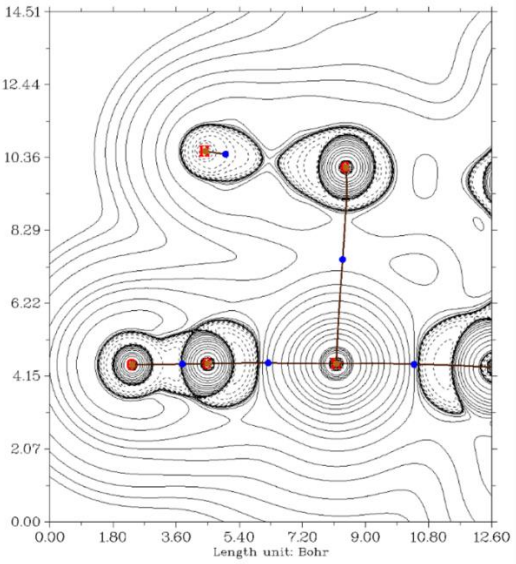

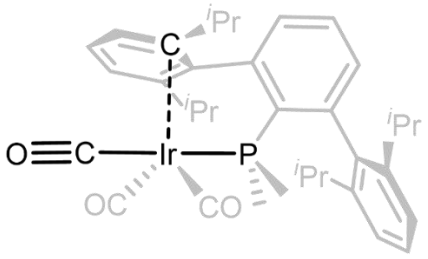

Figure 35. Plot of the laplacian of the electron density, $\nabla^2\rho$, of complex **5(Dipp)$^+$(CO)$_3$** in the Ir–P–*ortho*-Xyl' plane calculated with the ωB97X-D functional. The solid and dashed lines correspond to positive and negative values of $\nabla^2\rho$, respectively. In plane bcps and bps of the electron density are superimposed.

The results of the topological analysis performed for type **5$^+$(CO)$_2$** and **5$^+$(CO)$_3$** complexes are summarized in Table 8. In agreement with experimental and calculated bond distances, the magnitude of the electron

density (ρ_b) at the corresponding bcps indicate that the metal arene interaction is stronger for the dicarbonylic species. In addition, the change in molecular geometry due to steric hindrance (see Figure 33) is reflected in a weaker metal-arene interaction for **5(Dipp)$^+$(CO)$_3$**.

Complex[a]	Bond	ρ_b[b]	G_b[c]	V_b[c]	H_b[c]	$\lvert V_b \rvert / G_b$	$\nabla^2\rho$[d]
5(Xyl)$^+$(CO)$_2$	**Ir−C$_{ipso}$**	0.063	0.047	−0.064	−0.017	1.357	0.122
5(Dipp)$^+$(CO)$_2$	**Ir−C$_{ipso}$**	0.064	0.048	−0.066	−0.018	1.367	0.122
5(Xyl)$^+$(CO)$_3$	**Ir−C$_{ipso}$**	0.026	0.018	−0.019	−0.001	1.053	0.068
5(Dipp)$^+$(CO)$_3$	**Ir−C$_{ortho}$**	0.020	0.014	−0.013	0.000	0.974	0.056

Table 8. Electronic parameters derived from the topological analysis of the metal-arene interaction in **5$^+$(CO)$_n$** complexes (n = 2, 3). [a]Calculations with the ωB97X-D functional, [b]e·bohr^{-3}, [c]hartree, [d]e·bohr^{-5}.

The CO capture by type **5$^+$** complexes was found to be reversible. Heating under reflux a solution containing **5(Xyl)$^+$(CO)$_3$** permitted the isolation and characterization of complex **5(Xyl)$^+$CO** (Figure 36) after several vacuum cycles. This species presented IR, NMR and X-Ray Diffraction data comparable to those discussed for **5(Dipp)$^+$CO**.

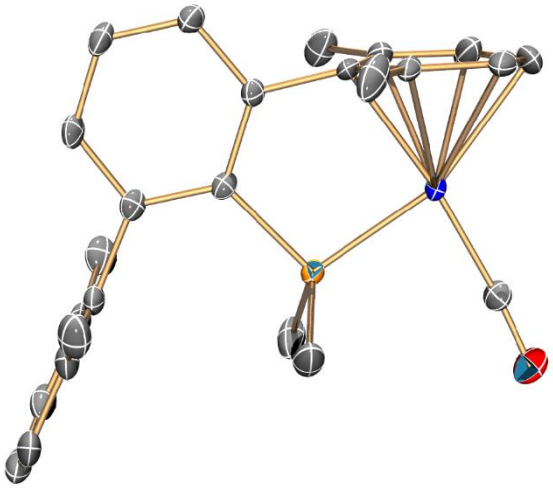

Figure 36. ORTEP diagram of the cation of complex **5(Xyl)$^{+}$CO**. Hydrogen atoms are excluded for clarity and thermal ellipsoids are set at 50 % probability.

II.2.3.4 Kinetic and Computational Studies

With the aim of gaining insight into the observed phosphine-dependent CO rearrangement, kinetic and computational studies were carried out. The linear expression of Eyring´s equation has the following form, where *k* stands for the reaction rate constant, T is the absolute temperature, R is the gas constant, k_B is Boltzmann´s constant and *h* is Planck´s constant:

$$\ln\frac{k}{T} = \frac{-\Delta H^{\ddagger}}{R}\cdot\frac{1}{T} + ln\frac{k_B}{h} + \frac{\Delta S^{\ddagger}}{R}$$

Hence, a plot of ln *k*/T against 1/T is a straight line with a slope of $-\Delta H^{\ddagger}/R$ that intersects the ordinate axis at ln $k_B/h + \Delta S^{\ddagger}/R$. On these grounds, we conducted $^{31}P\{^{1}H\}$ NMR kinetic experiments at four different temperatures to obtain the thermodynamic activation parameters for the dissociation of carbon monoxide at dicarbonylic **5⁺CO** complexes. The corresponding Eyring diagrams are displayed at Figures 37 and 38, whereas the activation parameters are summarized at Table 9. The errors in these activation parameters were computed from the error propagation formulas derived by Girolami and coworkers.[84] The total uncertainty in the determination of the rate constants, *k*, was assumed to be 5 %, whereas the estimated uncertainty in the temperature measurements was 1 K.[85]

[84] Morse, P. M.; Spencer, M. D.; Wilson, S. R.; Girolami, G. S. *Organometallics* **1994**, *13*, 1646.
[85] a) Abbott, J. K. C.; Li, L.; Xue, Z.-L. *J. Am. Chem. Soc.* **2009**, *131*, 8246; b) Jiménez, M. V.; Fernández-Tornos, J.; Pérez-Torrente, J. J.; Modrego, F. J.; García-Orduña, P.; Oro, L. A. *Organometallics* **2015**, *34*, 926.

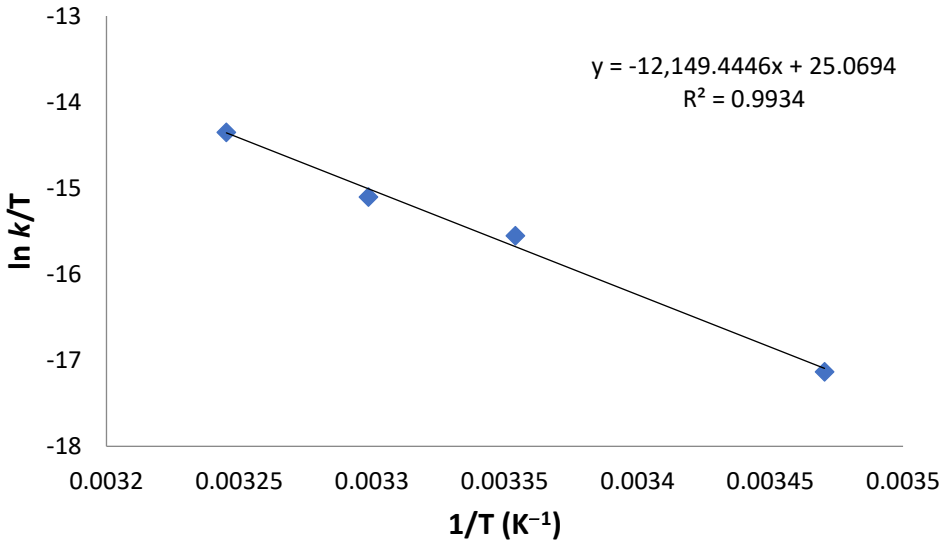

Figure 37. Eyring diagram for the carbon monoxide dissociation at **5(Xyl)$^{+}$(CO)$_2$**, obtained from kinetic experiments performed at 288.15, 298.15, 303.15 and 308.15 K.

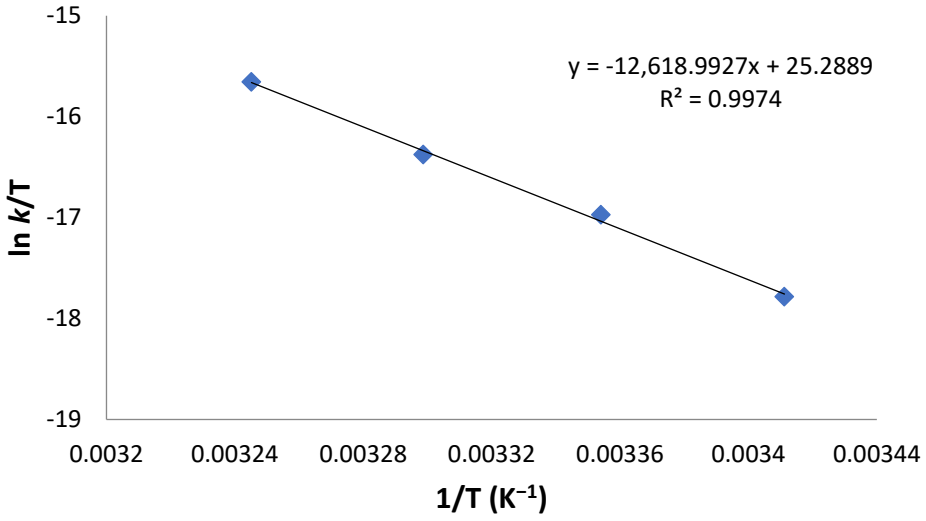

Figure 38. Eyring diagram for the carbon monoxide dissociation at **5(Dipp)$^{+}$(CO)$_2$**, obtained from kinetic experiments performed at 293.15, 298.15, 303.15 and 308.15 K.

	ΔH‡ (kcal/mol)	**ΔS‡** (cal/mol·K)	**ΔG$^{‡}_{298.15}$** (kcal/mol)
5(Xyl)$^{+}$(CO)$_2$	24.1±1.9	2.6±6.3	23.4±3.8
5(Dipp)$^{+}$(CO)$_2$	25.2±2.6	3.4±8.6	24.2±5.2

Table 9. Experimental activation parameters for the dissociation of a CO ligand at **5^{+}(CO)$_2$** species.

According to DFT studies[86] (Figure 39), the tricarbonylic species, **5^{+}(CO)$_3$**, are predicted to be thermodynamically more stable than the mono and dicarbonylic compounds, especially the xylyl-containing one, located at −9.5 kcal/mol relative to the dicarbonyl plus CO. The steric clash between the *iso*-propyl groups of the terphenyl moiety and the *cis*-CO ligands prevents the formation of a stronger metal-arene interaction in this species, significantly destabilizing the tricarbonyl bearing the Dipp-derived phosphine (−2.6 kcal/mol).

On the other hand, the monocarbonylic complexes are the least stable species considering both phosphines, situated at 8.3 (Xyl) and 11.7 (Dipp)

[86] Calculations were performed with the Gaussian 09 program employing the Head-Gordon hybrid functional ωB97XD. Geometry optimizations were carried out without geometry constraints including solvent effects (dichloromethane) for minima, whereas transition states were optimized in the gas phase to ensure convergence and the solvent effects were included in subsequent single point calculations. The energies reported were obtained from single point calculations on the geometries previously optimized at the 6-31G(d,p) level using the Dunning's triple-ζ basis set cc-pVTZ for C, H, P and O.

kcal/mol higher than the corresponding dicarbonyl complex. On these grounds, the spontaneous formation of **5(Dipp)$^+$CO** from **5(Dipp)$^+$(CO)$_2$** is ascribed to the irreversible loss of carbon monoxide from the solution, whereas the carbonyl disproportionation is only thermodynamically favored for **5(Xyl)$^+$(CO)$_2$** (–1.2 kcal/mol (Xyl), 9.1 kcal/mol (Dipp)), in good agreement with experimental observations. The calculated barrier for the CO capture by **5(Xyl)$^+$(CO)$_2$** is low enough (7.8 kcal/mol, Figure 40) for this process to occur, preventing the irreversible departure of CO from the solution; for the Dipp system this barrier raises to 14.0 kcal/mol.

On a final note, the calculated barriers for the dissociation of the *trans*-carbon monoxide (Figure 41) from the dicarbonylic species (18.3 kcal/mol (Xyl), 22.1 kcal/mol (Dipp)) qualitatively concord with those obtained by kinetic NMR experiments (23.4 and 24.2 kcal/mol, respectively).

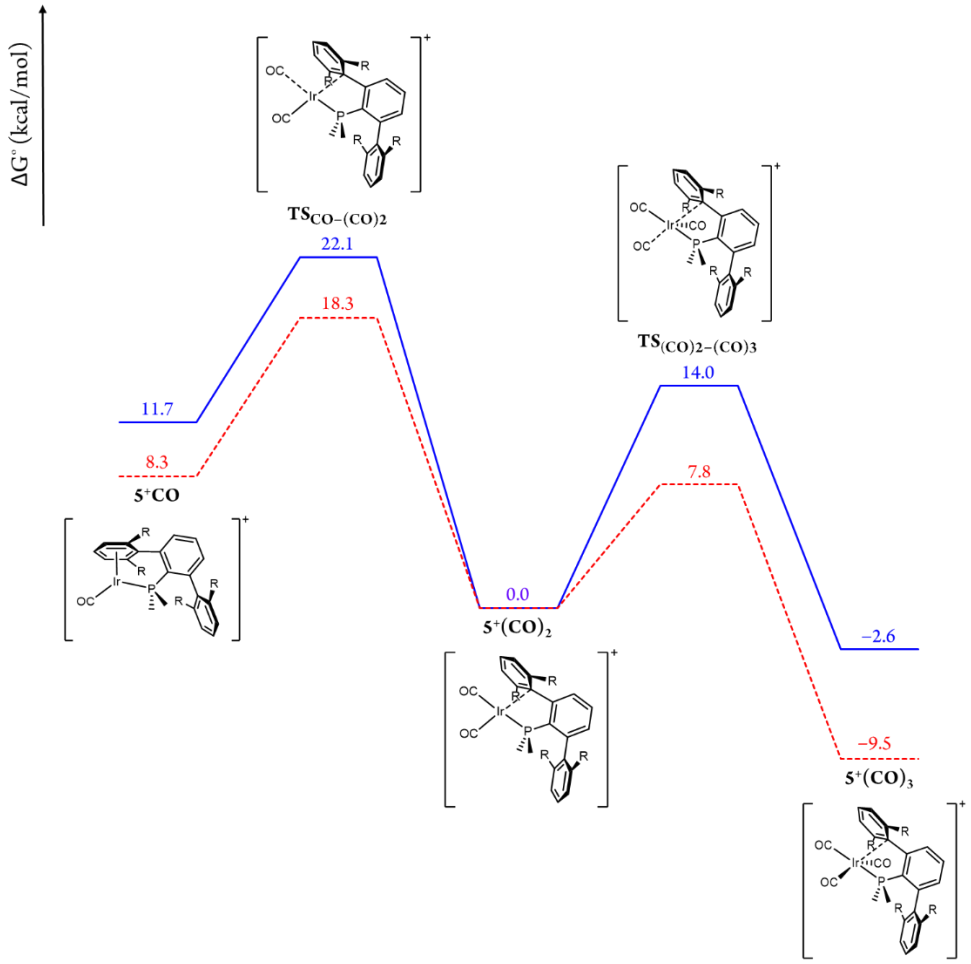

Figure 39. ΔGº profile for CO dissociation and capture in type **5$^+$(CO)$_n$** complexes (n = 1−3). The dashed, red line corresponds to the xylyl system, whereas the blue, solid line represents the one containing the bulkier, dipp-containing phosphine.

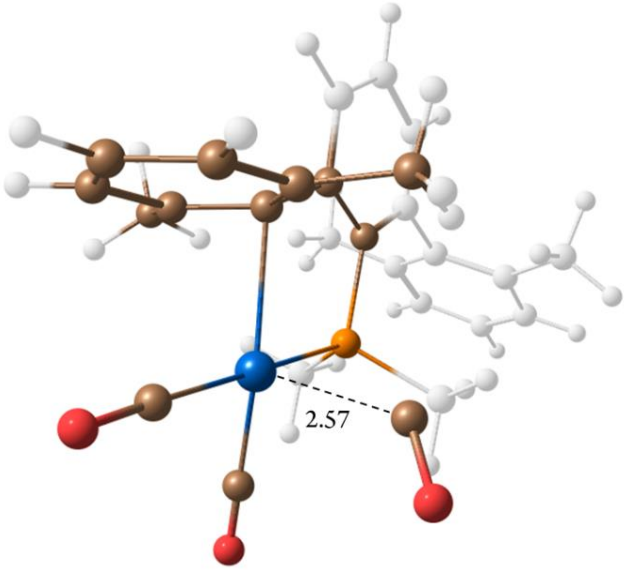

Figure 40. Molecular geometry of the transition state associated with the capture of CO at **5(Xyl)$^{+}$(CO)$_2$**.

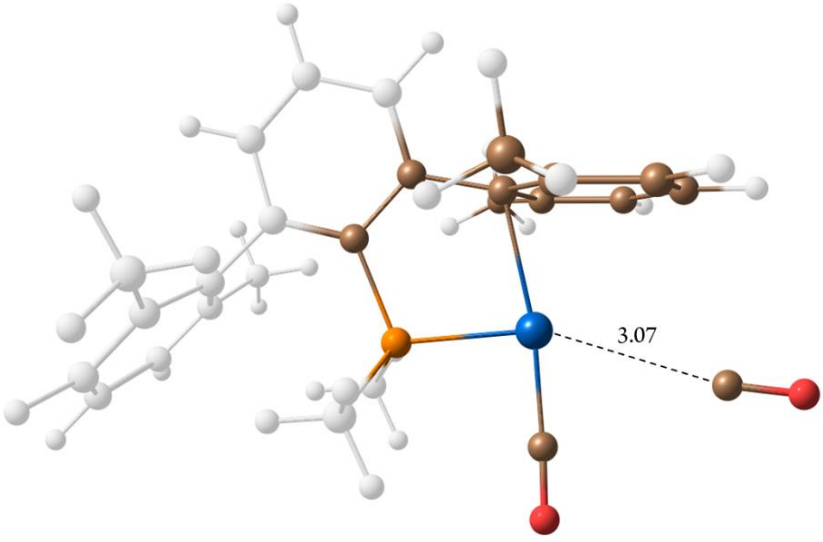

Figure 41. Molecular geometry of the transition state associated with the dissociation of CO at **5(Xyl)$^{+}$(CO)$_2$**.

Studies on the reactivity of analogous rhodium complexes, $RhCl(CO)_2PMe_2Ar'$, upon chloride abstraction were simultaneously conducted by another member of our research group.[87] In that case, the dicarbonylic complexes, $[Rh(CO)_2PMe_2Ar']BAr_F$, were not detected, even when the reactions were carried out and monitored at −80 ºC. Lower barriers (14.9 kcal/mol, Xyl, 16.8 kcal/mol, Dipp) were calculated for the dissociation of a CO molecule from the corresponding Rh dicarbonyls, in agreement with the observed decreased stability of the rhodium counterparts, which directly lead to the monocarbonyl compounds $[Rh(CO)PMe_2Ar']BAr_F$ upon chloride abstraction from the neutral species.

[87] Moreno, J. J.; Espada, M. F.; Krüger, E.; López-Serrano, J.; Campos, J.; Carmona, E. *Eur. J. Inorg. Chem.* **2018**, 2309.

II.2.3.5 Cationic Alkene Complexes

One of the seminal reports of Crabtree disclosed a remarkable activity of a cationic iridium(I) phosphine complex, $[Ir(COD)(py)(PCy_3)][PF_6]$, as a hydrogenation catalyst.[88] Over the years, several modifications were made to improve diverse catalytic features of the so-called Crabtree catalyst, including its activity, stability and solubility, and enantioselective versions of the system were also developed (Figure 42). Many of these advances involved the use of phosphine or hemilabile phosphine-containing ligands,[89] with notable exceptions,[13,90] and the influence of weakly coordinating anions in the process was examined.[91]

[88] a) Crabtree, R. H.; Morris, G. E. *J. Organomet. Chem.* **1977**, *135*, 395; b) Crabtree, R. H.; Felkin, H.; Morris, G. E. *J. Organomet. Chem.* **1977**, *141*, 205; c) Crabtree, R. *Acc. Chem. Res.* **1979**, *12*, 331.

[89] a) Lightfoot, A.; Schnider, P.; Pfaltz, A. *Angew. Chem. Int. Ed.* **1998**, *37*, 2897; b) Vazquez-Serrano, L. D.; Owens, B. T.; Buriak, J. M. Chem. Commun. 2002, 2518; c) Cipot, J.; McDonald, R.; Stradiotto, M. *Chem. Commun.* **2005**, 4932; d) Cipot, J.; McDonald, R.; Ferguson, M. J.; Schatte, G.; Stradiotto, M. *Organometallics* **2007**, *26*, 594; e) Franzke, A.; Pfaltz, A. *Chem. Eur. J.* **2011**, *17*, 4131; f) Bennie, L. S.; Fraser, C. J.; Irvine, S.; Kerr, W. J.; Andersson, S.; Nilsson, G. N. *Chem. Commun.* **2011**, *47*, 11653.

[90] a) Lee, H. M.; Jiang, T.; Stevens, E. D.; Nolan, S. P. *Organometallics* **2001**, *20*, 1255; b) Perry, M. C.; Cui, X.; Powell, M. T.; Hou, D.-R.; Reibenspies, J. H.; Burgess, K. *J. Am. Chem. Soc.* **2003**, *125*, 113; c) Cui, X.; Burgess, K. *J. Am. Chem. Soc.* **2003**, *125*, 14212; d) Schumacher, A.; Bernasconi, M.; Pfaltz, A. *Angew. Chem. Int. Ed.* **2013**, *52*, 7422.

[91] a) Smidt, S. P.; Zimmermann, N.; Studer, M.; Pfaltz, A. *Chem. Eur. J.* **2004**, *10*, 4685; c) Wüstenberg, B.; Pfaltz, A. *Adv. Synth. Catal.* **2008**, *350*, 174.

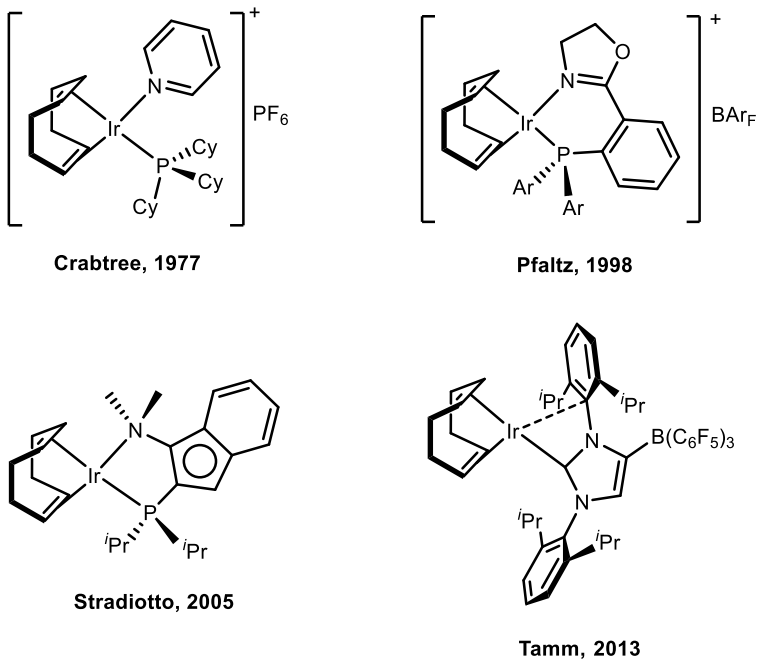

Figure 42. Representative examples of the evolution of Crabtree type catalysts, including zwitterionic complexes reported by Stradiotto and Tamm.

Salt metathesis of chloride complexes **1** with $NaBAr_F$ in dichloromethane afforded a mixture of cationic alkene complexes of formula $[Ir(COD)(PMe_2Ar')]BAr_F$ (**6**$^+$ and **7**$^+$), in a variable ratio depending on the phosphine employed. Whereas η^1-coordination of a flanking arene had been reported in the literature for related iridium species bearing bulky N-Heterocyclic carbenes,[13] the use of these bulky phosphines allows hapticity changes to occur within both the side ring of the terphenyl substituent and the COD ligand, stablishing an observable equilibrium with the isomeric, 18-electron species featuring η^6-coordination of the flanking arene and η^2-coordination of the cyclooctadiene ligand (Scheme 14).

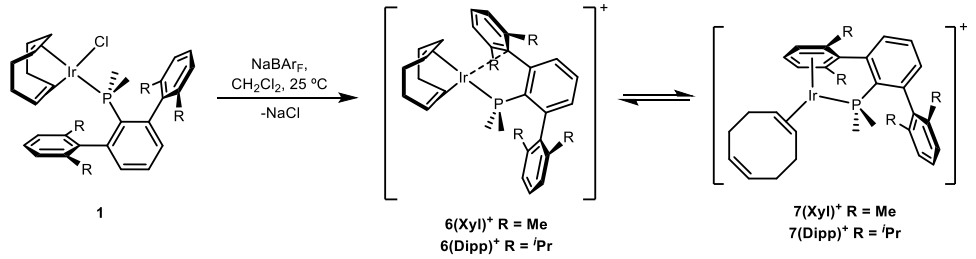

Scheme 14. Synthesis and solution equilibrium of complexes **6**$^+$ and **7**$^+$.

$^{31}P\{^1H\}$ NMR analysis of the reaction crudes disclosed two singlets, at *ca*. 16 (**6**$^+$) and 2.0 (**7**$^+$) ppm; these chemical shifts are close to those found for other complexes with similar coordination of the phosphine ligand, for instance **5(Xyl)$^+$(CO)$_2$** (16.2 ppm) and **5(Xyl)$^+$CO** (6.7 ppm). For the xylyl system, a **6**$^+$:**7**$^+$ ratio of 59:41 was found, whereas the use of the bulkier phosphine, $PMe_2Ar^{Dipp}{}_2$, favored η^2-coordination of the COD ligand, yielding a **6**$^+$:**7**$^+$ ratio of 14:86. The η^2:η^2 coordination of the COD ligand in complex **6(Xyl)**$^+$ was confirmed by two ^1H resonances located at 3.24 and 3.18 ppm, belonging to the alkenic CH_{COD} protons. The corresponding carbon atoms resonate at 103.7 (d, $^2J_{CP}$ = 11 Hz, *trans*-CH_{COD}) and 62.3 (*cis*-CH_{COD}) ppm. In turn, the analogous CH_{COD} resonances of complex **7(Xyl)**$^+$ were found at 5.60 and 2.93 ppm, the former being attributed to the non-coordinated alkene. In addition, the *m*- and *p*-Xyl' protons resonated at 6.63 and 5.60 ppm, respectively, displaying a $^3J_{HH}$ of only 6.2 Hz, indicative of η^6-arene coordination. $^{13}C\{^1H\}$ data corroborated this proposal: the alkenic carbon atoms of the COD ligand resonated at 129.9 (free) and 52.9 (bound) ppm, while the signals corresponding to the coordinated arene were found at 108.7 (*o*-Xyl'), 107.1 (d, $^2J_{CP}$ = 5 Hz, *ipso*-Xyl'), 105.0 (d, $^2J_{CP}$ = 3 Hz, *m*-Xyl') and 86.2 (d, $^2J_{CP}$ = 10 Hz, *p*-Xyl'). The molecular structure of complex **6(Xyl)**$^+$ was confirmed by means of X-Ray diffraction studies (Figure 43), revealing the existence of

an Ir−C_{ipso} bond distance of 2.308(4) Å. The pyramidalization of the bound *ipso* carbon atom was responsible of a reduced *o*-C_6H_3−*ipso*-Xyl'−*p*-Xyl' angle of 147.5(3) º. Finally, larger Ir−CH_{COD} average bond distances (2.242(4) versus 2.129(4) Å) were measured in *trans* to the phosphorus atom, concordant with the larger *trans* influence of the phosphine.

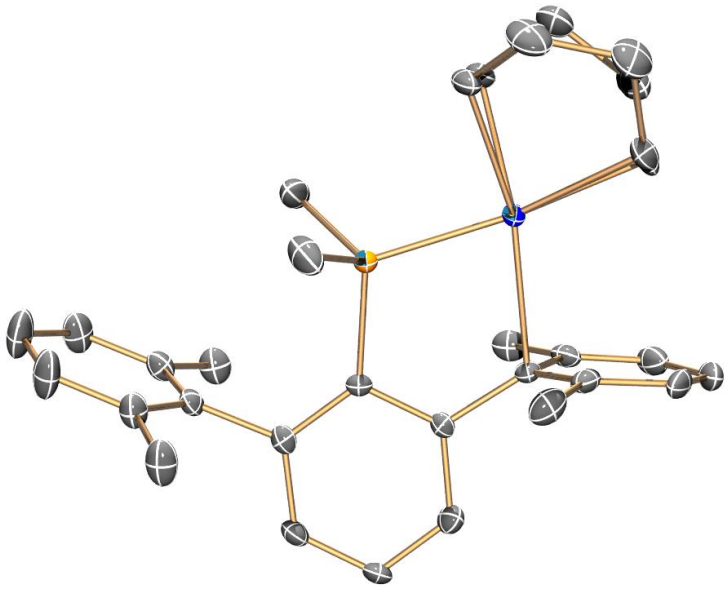

Figure 43. ORTEP diagram of the cation of complex **6(Xyl)**$^+$. Hydrogen atoms are excluded for clarity and thermal ellipsoids are set at 50 % probability.

The structural characterization of type **7**$^+$ complexes was not achieved for iridium. However, our group[87] unambiguously disclosed this coordination mode for a related rhodium complex, [Rh(COD)($PMe_2Ar^{Xyl}_2$)]BAr_F (Figure 44).

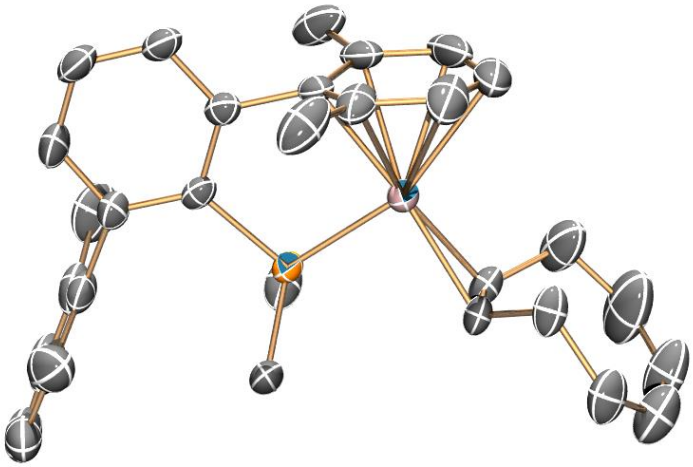

Figure 44. ORTEP diagram of the cation of complex [Rh(COD)($PMe_2Ar^{Xyl}_2$)]BAr_F. Hydrogen atoms are excluded for clarity and thermal ellipsoids are set at 50 % probability.

The addition of pyridine to the equilibrium mixture of complexes **6**$^+$ and **7**$^+$ results in quantitative formation of [Ir(COD)(py)($PMe_2Ar^{Xyl}_2$)]$^+$, **8(Xyl)**$^+$, a sterically encumbered version of the widely used Crabtree catalyst[92] (Scheme 15). As mentioned before, the latter, as well as many other COD Ir(I) compounds bearing phosphine ligands, have found ample use in catalysis,[93] highlighting the potential of compounds like **8(Xyl)**$^+$ for these purposes.

[92] Crabtree, R. H. *Acc. Chem. Res.* **1979**, *12*, 331.
[93] Andersson, P. G. *Iridium Catalysis. Top. Organomet. Chem.*, Springer, Berlin, **2011.**

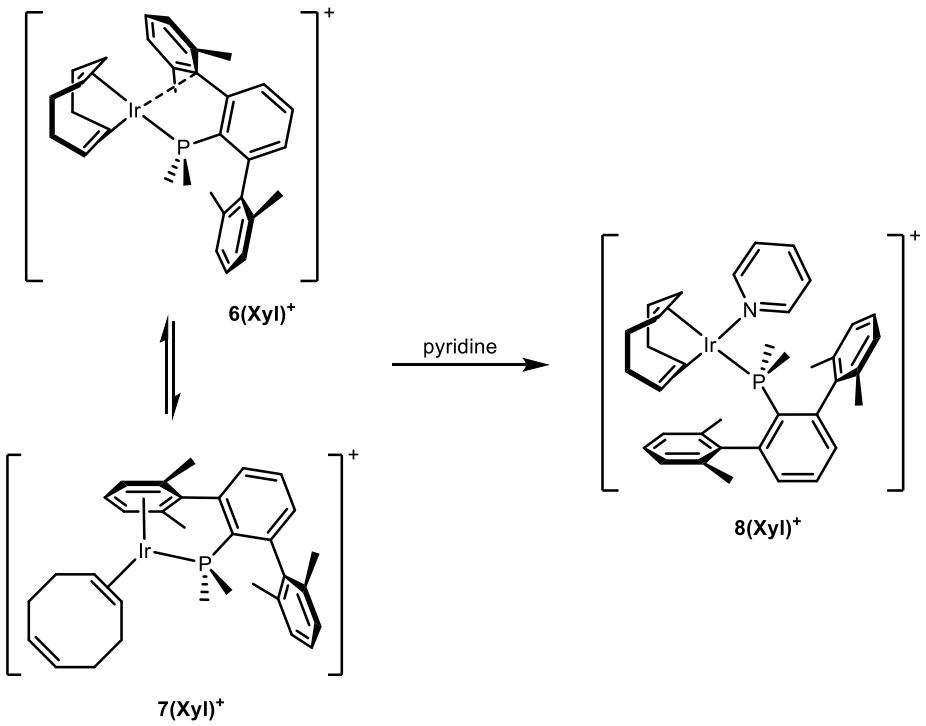

Scheme 15. Synthesis of the pyridine adduct **8(Xyl)**$^+$.

The $^{31}P\{^1H\}$ NMR peak of **8(Xyl)**$^+$ appears at lower frequency (–12.1 ppm) than those of **6(Xyl)**$^+$ (δ = 16.9 ppm) and **7(Xyl)**$^+$ (δ = 2.0 ppm), that is, shifted to higher frequency by only about 30 ppm relative to free phosphine. This region is characteristic of κ^1-P monodentate coordination of the phosphine ligand in square planar complexes, as denoted by **1(Xyl)**, **2(Xyl)** and **4(Xyl)** (δ = –9.3, –7.4 and –10.9 ppm, respectively). The κ^1-P coordination of the phosphine in **8(Xyl)**$^+$ was confirmed by the symmetrical pattern observed for its deshielded (7.1–7.6 ppm) aromatic ^1H NMR resonances and by the presence of two signals, each corresponding to two protons, at δ = 3.49 and 3.98 ppm, denoting η^2:η^2-coordination of COD. The corresponding alkenic carbon atoms resonate at 89.7 and 66.4 ppm, in agreement with the proposed formulation.

To extend the series of iridium and rhodium olefin compounds, ethylene complexes, analogous to Hartwig's key intermediate in hydroamination reactions,[34d] were targeted (Figure 45, right). Accordingly, the ethylene rhodium[87] and iridium (**9**$^{+}$) adducts were cleanly obtained from the reactions of the corresponding dimers $[MCl(C_2H_4)_2]_2$ (M = Rh, Ir) with $NaBAr_F$ in the presence of the phosphine (Figure 45).

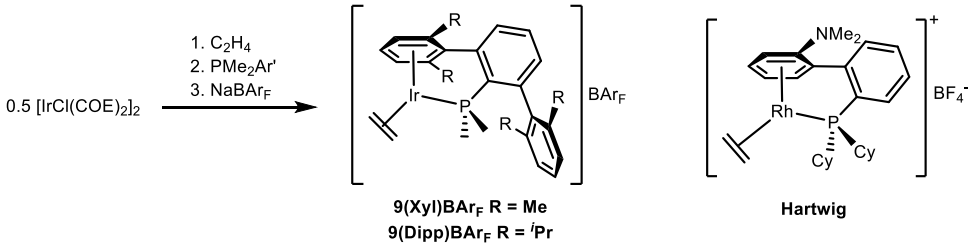

Figure 45. Synthesis of iridium ethylene complexes **9BAr$_F$** and Hartwig´s hydroamination catalyst.

Addition of $NaBAr_F$ proved essential to favor quantitative formation of the desired iridium ethylene adducts, as in its absence cationic compounds **9** with chloride as counteranion formed along with various other species containing a metal-bound chloride ligand. The $^{31}P\{^1H\}$ chemical shift of complexes **9** (2.1 ppm), and the ^1H and $^{13}C\{^1H\}$ NMR spectra are in accord with the proposed η^6 coordination of one of the phosphine aryl substituents. Whereas in the rhodium compounds the ethylene ligand undergoes fast rotation on the NMR timescale at 25 °C, such that the four hydrogen atoms give rise to broad ^1H NMR resonances around 2.9 ppm, while the ^{13}C nuclei resonate as a doublet in the proximity of 46 ppm ($^1J_{CRh}$ = 13 Hz). Hindered ethylene rotation in their iridium analogues reflects the stronger Ir–η^2-C_2H_4 bond compared to the Rh–η^2-C_2H_4 bond due to the higher basicity of iridium. This fact is evidenced by two distinctive signals at around 1.7 and 3.0 ppm due to the ethylene ligand in the ^1H NMR

spectra of compounds $\mathbf{9}^{+}$ (Figure 46). The rotation is only partially hindered at 25 ºC, as chemical exchange cross peaks were detected in the EXSY experiment of $\mathbf{9}^{+}$ complexes.

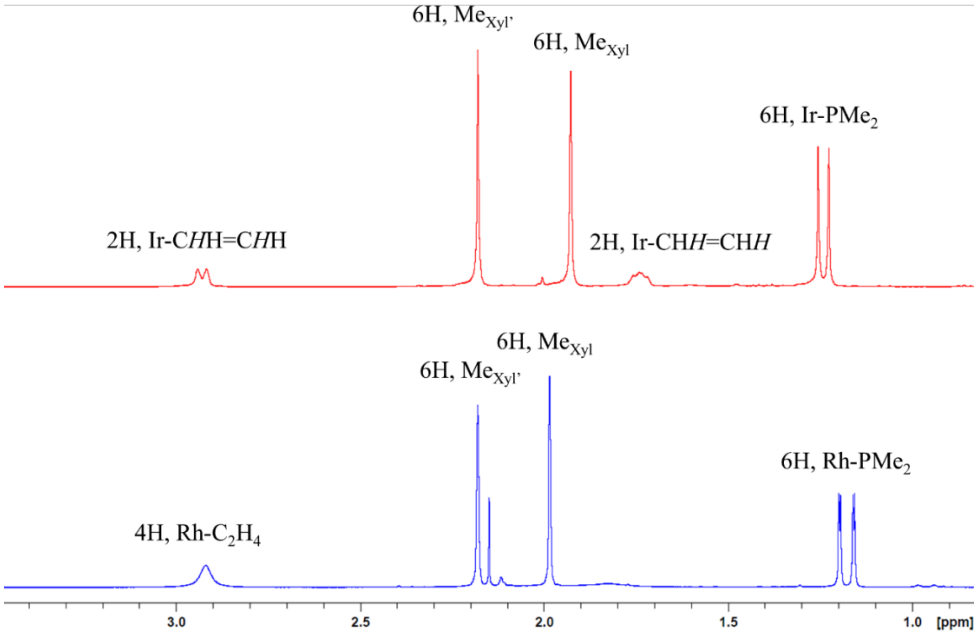

Figure 46. High-field region of the ^{1}H NMR spectra of $\mathbf{9(Xyl)}^{+}$ (red, top) and its corresponding Rh analog, $[Rh(C_2H_4)(PMe_2Ar^{Xyl}_2)]^{+}$ (blue, bottom).

The corresponding $^{13}C\{^{1}H\}$ NMR resonance appears at about 24 ppm, and therefore the ^{13}C signals of the C_2H_4 ligand in complexes $\mathbf{9}^{+}$ are shielded by more than 20 ppm with respect to those in the rhodium analogues, owing to the greater sp^3 character of the carbon atoms as a consequence of increased π back-donation from the Ir(I) center. It is widely accepted that the low-frequency shift of the olefin carbon atoms relative to free ethylene (δ = 122.8 ppm) increases with π back-bonding.[94]

[94] Cavallo, L.; Macchioni, A.; Zuccaccia, C.; Zuccaccia, D.; Orabona, I.; Ruffo, F. *Organometallics* **2004**, *23*, 2137.

The spectroscopic differences in metal-alkene bonding were computationally studied by means of molecular orbital localization.[95] For the Rh system, the bonding follows the classic Dewar-Chatt-Duncanson[96] model: a filled ethylene pi-orbital donates its electron density to an empty d-orbital of the metal center to stablish a σ bond (Figure 47, left), whereas back-donation involves a filled d orbital of the metal and a π*-orbital of the alkene (Figure 47, right).

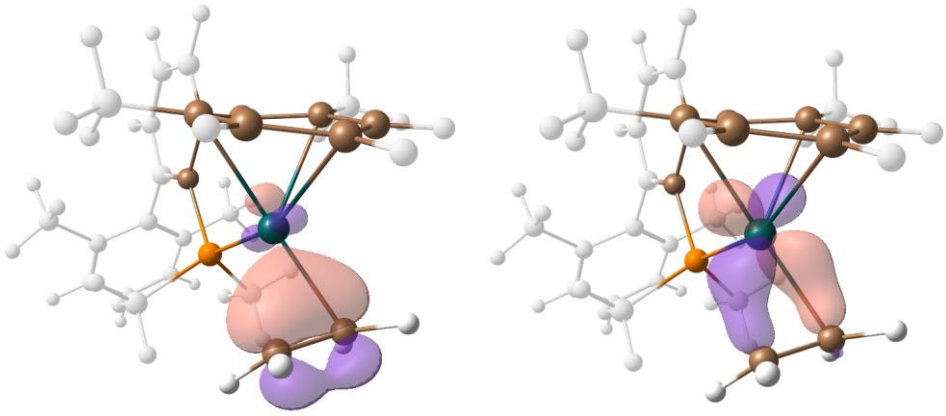

Figure 47. Localized molecular orbitals participating in metal-alkene bonding in the Rh ethylene complex $[Rh(C_2H_4)(PMe_2Ar^{Xyl}_2)]BAr_F$.

In agreement with NMR data, the metal-ethylene bonding in type $\mathbf{9}^+$ complexes is described by two symmetric, localized molecular orbitals that form two Ir−C σ bonds (Figure 48), thus favoring a metallacyclopropane, Ir(III) formulation as the ground state for complexes $\mathbf{9}^+$. The calculated C–C bond distance for $\mathbf{9(Xyl)}^+$ was 1.424 Å, slightly larger than that of its Rh counterpart (1.402 Å).

[95] a) Vidossich, P.; Lledós, A. *Dalton Trans.* **2014**, *43*, 11145; b) Calculations were performed with the Gaussian 09 program employing the M06 hybrid functional. Geometry optimizations were carried out in the gas phase without geometry constraints.

[96] a) Dewar, J. S. *Bull. Soc. Chim. Fr.* **1951**, *18*, C71; b) Chatt, J.; Duncanson, L. A. *J. Chem. Soc.* **1953**, 2939.

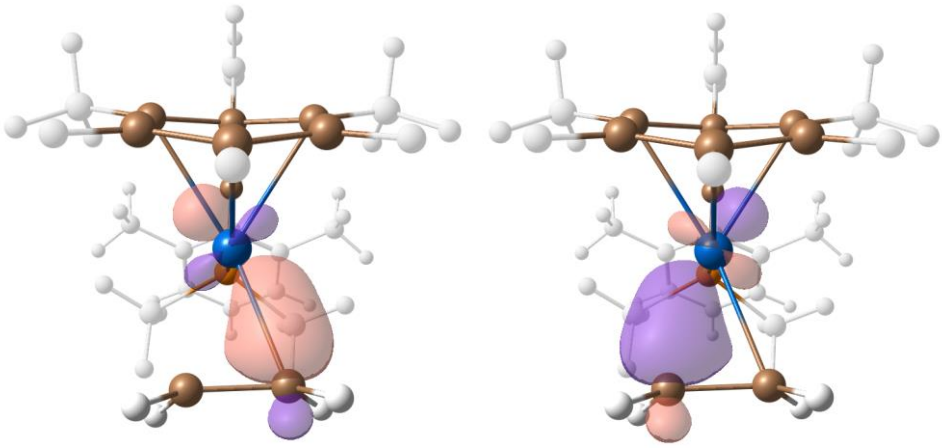

Figure 48. Localized molecular orbitals participating in metal-alkene bonding in the Ir ethylene complex **9(Xyl)**$^{+}$.

Summary and Conclusions

Las propiedades estereoelectrónicas de los ligandos dimetilterfenil fosfina se evaluaron mediante diversas estrategias. El Parámetro Electrónico de Tolman, TEP, se comparó con la frecuencia media de tensión de CO en complejos $IrCl(CO)_2(PMe_2Ar')$ y con la constante de acoplamiento $^1J_{PSe}$ de los correspondientes seleniuros de fosfina, mientras que el Ángulo Cónico de Tolman, TCA, se estudió junto con Ángulos Sólidos y Volúmenes Ocupados. Se descubrió y estudió computacionalmente una reacción de activación C−H que tiene lugar en un complejo neutro de metilo de iridio(I). El carácter hemilabil de los ligandos fosfina de terfenilo fue clave para la estabilización de especies catiónicas e insaturadas de iridio(I), para los cuales se han descubierto diversos procesos de reorganización de ligandos CO y ciclooctadieno. El enlace en complejos catiónicos de etileno de Rh e Ir fue también estudiado por medio de espectroscopía de RMN y cálculos DFT.

The stereoelectronic properties of dimethylterphenyl phosphine ligands were evaluated by several strategies. The Tolman Electronic Parameter, TEP, was compared with the average CO stretching frequencies at $IrCl(CO)_2(PMe_2Ar')$ complexes and with the $^1J_{PSe}$ coupling constant of the corresponding phosphine selenides, whereas the Tolman Cone Angle, TCA, was studied along with Solid Angles and Buried Volumes. A C−H activation reaction taking place at a neutral, iridium(I) methyl complex was disclosed and computationally studied. The hemilabile character of

terphenyl phosphine ligands was key for the stabilization of unsaturated, cationic iridium(I) species, for which several ligand rearrangement processes, comprising CO and cyclooctadiene, were disclosed. The bonding of cationic ethylene complexes of Rh and Ir was also studied by means of NMR spectroscopy and DFT calculations.

II.3 EXPERIMENTAL SECTION

II.3.1 General Considerations

All manipulations were carried out using standard Schlenk techniques, under high purity nitrogen. All solvents were dried and distilled under nitrogen prior to use. *n*-Pentane (C_5H_{12}) and *n*-hexane (C_6H_{14}) were distilled over sodium. Diethyl ether was distilled over sodium/benzophenone. CH_2Cl_2 and CD_2Cl_2 were dried over CaH_2. $[IrCl(COD)]_2$, $[IrCl(COE)_2]_2$,[97] $NaBAr_F$[98] and PMe_2Ar'[99] were prepared according to literature methods. All cationic complexes were isolated as salts of the BAr_F anion. Solution NMR spectra were recorded on Bruker AMX-300, DRX-400 and DRX-500 spectrometers. Spectra were referenced to external $SiMe_4$ (δ: 0 ppm) using the residual proton solvent peaks as internal standards (^1H NMR experiments), or the characteristic resonances of the solvent nuclei (^{13}C NMR experiments), while ^{31}P was referenced to H_3PO_4. Spectral assignments were made by routine one- and two-dimensional NMR experiments (^1H, $^1H\{^{31}P\}$, $^{13}C\{^1H\}$, $^{31}P\{^1H\}$, COSY, NOESY, HSQC and HMBC) where appropriate. For elemental analyses a LECO TruSpec CHN elementary analyzer was utilized.

Calculations were performed at the DFT level with the Gaussian 09 (Revision D.01) program.[100] The hybrid functionals M06[101] and

---

[97] Giordano, G.; Crabtree, R. H. *Inorg. Synth.* **1990**, *28*, 91.
[98] Yakelis, N. A.; Bergman, R. G. *Organometallics* **2005**, *24*, 3579.
[99] a) Campos, J.; Ortega-Moreno, L.; Conejero, S.; Peloso, R.; López-Serrano, J.; Maya, C.; Carmona, E. *Chem. Eur. J.* **2015**, *21*, 8883; b) Ortega-Moreno, L.; Peloso, R.; Maya, C.; Suárez, A.; Carmona, E. *Chem. Commun.* **2015**, *51*, 17008.
[100] Frisch, M. J.; Trucks, G. W.; Schlegel, H. B.; Scuseria, G. E.; Robb, M. A.; Cheeseman, J. R.; Scalmani, G.; Barone, V.; Mennucci, B; Petersson, G. A.; Nakatsuji, H.; Caricato, M.; Li, X.; Hratchian, H. P.; Izmaylov, A. F.; Bloino, J.; Zheng, G.; Sonnenberg, J. L.; Hada, M.; Ehara, M.; Toyota, K.; Fukuda, R.; Hasegawa, J.; Ishida, M.; Nakajima, T.; Honda, Y.; Kitao, O.; Nakai, H.; Vreven,

ωB97XD[102] were used throughout the computational study. Geometry optimizations were carried out without geometry constraints, using the 6-31G(d,p)[103] basis set to represent the C, H, P, O and Se atoms and the Stuttgart/Dresden Effective Core Potential and its associated basis set (SDD)[104] to describe the Ir, and Ni atoms. Bulk solvent effects (dichloromethane, diethylether, benzene) were included with the SMD continuum model.[105] The stationary points and their nature as minima or saddle points (TS) were characterized by vibrational analysis, which also produced enthalpy (H), entropy (S) and Gibbs energy (G) data at 298.15 K. The minima connected by a given transition state were determined by Intrinsic Reaction Coordinate (IRC) calculations or by perturbing the transition states along the TS coordinate and optimizing to the nearest minimum. Localized molecular orbital studies were carried out following the Pipek-Mezey criterion.[106]

T.; Montgomery, J. A. J.; Peralta, J. E.; Ogliaro, F.; Bearpark, M.; Heyd, J. J.; Brothers, E.; Kudin, K. N.; Staroverov, V. N.; Kobayashi, R.; Normand, J.; Raghavachari, K.; Rendell, A.; Burant, J. C.; Iyengar, S. S.; Tomasi, J.; Cossi, M.; Rega, N.; Millam, J. M.; Klene, M.; Knox, J. E.; Cross, J. B.; Bakken, V.; Adamo, C.; Jaramillo, J.; Gomperts, R.; Stratmann, R. E.; Yazyev, O.; Austin, A. J.; Cammi, R.; Pomelli, C.; Ochterski, J. W.; Martin, R. L.; Morokuma, K.; Zakrzewski, V. G.; Voth, G. A.; Salvador, P.; Dannenberg, J. J.; Dapprich, S.; Daniels, A. D.; Farkas, O.; Foresman, J. B.; Ortiz, J. V.; Cioslowski, J.; Fox, D. J.; Gaussian 09, Revision D.01, Gaussian, Inc.: Wallingford CT, **2013**.

[101] Zhao, Y.; Truhlar, D. G. *Theor. Chem. Acc.* **2006**, *120*, 215.

[102] Chai, J.-D.; Head-Gordon, M. *Phys. Chem. Chem. Phys.* **2008**, *10*, 6615.

[103] a) Hehre, W. J.; Ditchfield, R.; Pople, J. A. *J. Phys. Chem.* **1972**, *56*, 2257; b) Hariharan, P. C.; Pople, J. A. *Theor. Chim. Acta.* **1973**, *28*, 213; c) Francl, M. M.; Pietro, W. J.; Hehre, W. J.; Binkley, J. S.; Gordon, M. S.; Defrees, D. J.; Pople, J. A. *J. Chem. Phys.* **1982**, *77*, 3654.

[104] Andrae, D.; Haeussermann, U.; Dolg, M.; Stoll, H.; Preuss, H. *Theor. Chim. Acta* **1990**, *77*, 123.

[105] Marenich, A. V.; Cramer, C. J.; Truhlar, D. G. *J. Phys. Chem. B* **2009**, *113*, 6378.

[106] Pipek, J.; Mezey, P.G. *J. Chem. Phys*. **1989**, *90*, 4916.

II.3.1 Synthesis and Characterization of New Complexes

Complex 1(Xyl)

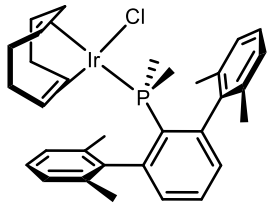

A solid mixture of $[IrCl(COD)]_2$ (75.0 mg, 0.112 mmol) and $PMe_2Ar^{Xyl}{}_2$ (77.9 mg, 0.225 mmol) was dissolved in dry CH_2Cl_2 (7 mL) in a Schlenk flask provided with a stir bar. The reaction mixture was stirred for 1 h, yielding a yellow solution. The solvent was then removed *in vacuo* and the product washed with 3 mL of cold pentane, providing a bright yellow, air-stable solid (141 mg, 92 %).

Anal. Calcd. for $C_{32}H_{39}ClIrP$: C, 56.33; H, 5.76. **Found**: C, 56.6; H, 5.8.

^{1}H NMR (400 MHz, CD_2Cl_2, 25 ºC): δ 7.48 (td, $^3J_{HH}$ = 7.6 Hz, $^5J_{HP}$ = 1.7 Hz, 1H, *p*-C_6H_3), 7.22 (m, 2H, *p*-Xyl), 7.13 (d, $^3J_{HH}$ = 7.8 Hz, 4H, *m*-Xyl), 6.99 (dd, $^3J_{HH}$ = 7.6 Hz, $^4J_{HP}$ = 2.8 Hz, 2H, *m*-C_6H_3), 4.57 (m, 2H, CH_{COD}), 2.27 (m, 2H, CH_{COD}), 2.22 (s, 12H, Me_{Xyl}), 2.12 (m, 2H, CH_{2COD}), 1.96 (m, 2H, CH_{2COD}), 1.54 (m, 2H, CH_{2COD}), 1.37 (m, 2H, CH_{2COD}), 1.07 (d, 6H, $^2J_{HP}$ = 8.4 Hz, PMe_2).

^{13}C{^{1}H} NMR (100 MHz, CD_2Cl_2, 25 ºC): δ 146.6 (d, $^2J_{CP}$ = 9 Hz, *o*-C_6H_3), 142.2 (d, $^3J_{CP}$ = 4 Hz, *ipso*-Xyl), 137.5 (*o*-Xyl), 131.1 (d, $^3J_{CP}$ = 8 Hz, *m*-C_6H_3), 130.5 (d, $^4J_{CP}$ = 2 Hz, *p*-C_6H_3), 130.2 (d, $^1J_{CP}$ = 42 Hz, *ipso*-C_6H_3), 128.3 (*p*-Xyl), 127.9 (*m*-Xyl), 88.8 (d, $^2J_{CP}$ = 16 Hz, CH_{COD}), 52.1 (CH_{COD}), 34.1 (d, $^3J_{CP}$ = 3 Hz, CH_{2COD}), 29.2 (d, $^3J_{CP}$ = 2 Hz, CH_{2COD}), 22.6 (Me_{Xyl}), 12.7 (d, $^1J_{CP}$ = 31 Hz, PMe_2).

^{31}P{^{1}H} NMR (160 MHz, CD_2Cl_2, 25 ºC) δ: −9.3.

Complex 1(Dipp)

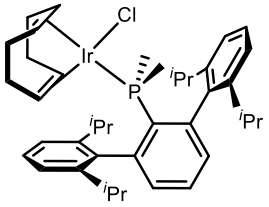

A solid mixture of $[IrCl(cod)]_2$ (112.0 mg, 0.166 mmol) and $PMe_2Ar^{Dipp}{}_2$ (153.7 mg, 0.335 mmol) was dissolved in dry CH_2Cl_2 (10 mL) in a Schlenk flask provided with a stir bar. The reaction mixture was stirred for 1 h, yielding a yellow solution. The solvent was removed in vacuo and the product washed with 5 mL of cold pentane, providing a bright yellow, air-stable solid (248.9 mg, 94 %).

Anal. Calcd. for $C_{40}H_{55}ClIrP$: C, 60.47; H, 6.98. **Found**: C, 60.15; H, 7.01.

^{1}H NMR (400 MHz, CD_2Cl_2, 25 ºC) δ: 7.41 (t, $^3J_{HH}$ = 7.7 Hz, 2H, *p*-Dipp), 7.39 (td, $^3J_{HH}$ = 7.5 Hz, $^5J_{HP}$ = 1.6 Hz, 1H, *p*-C_6H_3), 7.28 (d, $^3J_{HH}$ = 7.7 Hz, 4H, *m*-Dipp), 7.16 (dd, $^3J_{HH}$ = 7.5 Hz, $^4J_{HP}$ = 2.7 Hz, *m*-C_6H_3), 4.50 (br, 2H, CH_{COD}), 2.87 (br, 4H, ($CHMe_2$)$_{Dipp}$), 2.33 (br, 2H, CH_{COD}), 2.00 (br, 4H, CH_{2COD}), 1.52 (m, 2H, CH_{2COD}), 1.40 (d, $^3J_{HH}$ = 6.7 Hz, 12H, Me_{Dipp}), 1.29 (m, 2H, CH_{2COD}), 1.12 (d, $^2J_{HP}$ = 8.6 Hz, 6H, PMe_2), 1.01 (d, $^3J_{HH}$ = 6.7 Hz, 12H, Me_{Dipp}).

^{13}C{^{1}H} NMR (100 MHz, CD_2Cl_2, 25 ºC) δ: 147.9 (*o*-Dipp), 144.8 (d, $^2J_{CP}$ = 9 Hz, *o*-C_6H_3), 140.1 (d, $^3J_{CP}$ = 4 Hz, *ipso*-Dipp), 133.1 (d, $^3J_{CP}$ = 7 Hz, *m*-C_6H_3), 131.3 (d, $^1J_{CP}$ = 39 Hz, *ipso*-C_6H_3), 129.2 (*p*-Dipp), 127.5 (d, $^4J_{CP}$ = 2 Hz, *p*-C_6H_3), 123.2 (*m*-Dipp), 86.6 (d, $^2J_{CP}$ = 16 Hz, CH_{COD}), 53.0 (CH_{COD}), 33.6 (d, $^3J_{CP}$ = 4 Hz, CH_{2COD}), 31.3 (($CHMe_2$)$_{Dipp}$), 29.8 (d, $^3J_{CP}$

= 2 Hz, CH_{2COD}), 26.3 (Me_{Dipp}), 23.4 (Me_{Dipp}), 14.4 (d, $^{1}J_{CP}$ = 31 Hz, PMe_2).

$^{31}P\{^{1}H\}$ NMR (160 MHz, CD_2Cl_2, 25 ºC) δ: −9.0.

Complex 2(Xyl)

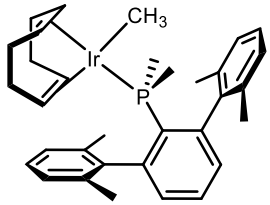

A Et_2O solution of complex **1(Xyl)** (25 mg, 0.037 mmol) was placed in a thick-wall ampoule provided with a stir bar and cooled to −70 ºC. $ZnMe_2$ (1.2 eq) was added and the solution was stirred for 1 h, turning red at −55 ºC. Stirring continued for additional 1.5 h, allowing the solution to reach −40 ºC. At this temperature, the solvent and excess $ZnMe_2$ were removed under reduced pressure. The residue was extracted with cold (−40 ºC) CH_2Cl_2, affording complex **2(Xyl)** as an orange solid. The yield is estimated to be quantitative based on spectroscopic methods.

^{1}H NMR (400 MHz, CD_2Cl_2, −20 ºC) δ: 7.43 (td, $^3J_{HH}$ = 7.6 Hz, $^5J_{HP}$ = 1.5 Hz, 1H, *p*-C_6H_3), 7.17 (m, 2H, *p*-Xyl), 7.07 (d, $^3J_{HH}$ = 7.5 Hz, 4H, *m*-Xyl), 6.96 (dd, $^3J_{HH}$ = 7.6 Hz, $^4J_{HP}$ = 2.6 Hz, 2H, *m*-C_6H_3), 3.86 (m, 2H, CH_{COD}), 2.32 (m, 2H, CH_{COD}), 2.11 (s, 12H, Me_{Xyl}), 1.99 (m, 2H, CH_{2COD}), 1.81 (m, 2H, CH_{2COD}), 1.52 (m, 2H, CH_{2COD}), 1.38 (m, 2H, CH_{2COD}), 0.99 (d, $^2J_{HP}$ = 7.6 Hz, 6H, PMe_2), 0.22 (d, $^3J_{HP}$ = 6.5 Hz, 3H, Ir−CH_3).

^{13}C{^{1}H} NMR (100 MHz, CD_2Cl_2, −35 ºC) δ: 145.5 (d, $^2J_{CP}$ = 9 Hz, *o*-C_6H_3), 141.7 (d, $^3J_{CP}$ = 4 Hz, *ipso*-Xyl), 136.9 (*o*-Xyl), 131.0 (d, $^1J_{CP}$ = 36 Hz, *ipso*-C_6H_3), 130.4 (d, $^3J_{CP}$ = 7 Hz, *m*-C_6H_3), 129.6 (d, $^4J_{CP}$ = 2 Hz, *p*-C_6H_3), 127.5 (*p*-Xyl), 127.2 (*m*-Xyl), 79.6 (d, $^2J_{CP}$ = 16 Hz, CH_{COD}), 61.2 (CH_{COD}), 32.1 (d, $^3J_{CP}$ = 3 Hz, CH_{2COD}), 30.7 (d, $^3J_{CP}$ = 1 Hz, CH_{2COD}), 21.9 (Me_{Xyl}), 12.4 (d, $^1J_{CP}$ = 30 Hz, PMe_2), 8.8 (d, $^2J_{CP}$ = 7 Hz, Ir−CH_3).

^{31}P{^{1}H} NMR (160 MHz, CD_2Cl_2, −20 ºC) δ: −7.4.

Complex 2(Dipp)

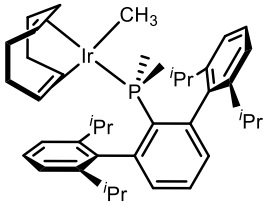

A Et_2O solution of complex **1(Dipp)** (30 mg, 0.037 mmol) was placed in a thick-wall ampoule provided with a stir bar. $ZnMe_2$ (1.2 eq) was added and the solution was stirred for 1 h, turning orange. The solvent and excess $ZnMe_2$ were removed under reduced pressure. The residue was extracted with CH_2Cl_2, affording complex **2(Dipp)** as an orange solid. The yield is estimated to be quantitative based on spectroscopic methods.

^{1}H NMR (500 MHz, CD_2Cl_2, 25 ºC) δ: 7.36 (t, $^3J_{HH}$ = 7.7 Hz, 2H, *p*-Dipp), 7.33 (td, $^3J_{HH}$ = 7.7 Hz, $^5J_{HP}$ = 1.4 Hz, 1H, *p*-C_6H_3), 7.23 (d, $^3J_{HH}$ = 7.7 Hz, 4H, *m*-Dipp), 7.13 (dd, $^3J_{HH}$ = 7.6 Hz, $^4J_{HP}$ = 2.4 Hz, 2H, *m*-C_6H_3), 3.76 (m, 2H, CH_{COD}), 2.74 (sept, $^3J_{HH}$ = 6.7 Hz, 4H, (C*H*Me_2)$_{Dipp}$), 2.42 (m, 2H, CH_{COD}), 1.86 (m, 4H, CH_{2COD}), 1.49 (m, 2H, CH_{2COD}), 1.37 (m, 2H, CH_{2COD}), 1.35 (d, $^3J_{HH}$ = 6.7 Hz, 12H, Me_{Dipp}), 1.05 (d, $^2J_{HP}$ = 7.9 Hz, 6H, PMe_2), 0.98 (d, $^3J_{HH}$ = 6.6 Hz, 12H, Me_{Dipp}), 0.32 (d, $^3J_{HP}$ = 6.5 Hz, 3H, Ir−CH_3).

^{13}C{^{1}H} NMR (100 MHz, CD_2Cl_2, 25 ºC) δ: 147.8 (*o*-Dipp), 144.6 (d, $^2J_{CP}$ = 9 Hz, *o*-C_6H_3), 140.4 (d, $^3J_{CP}$ = 3 Hz, *ipso*-Dipp), 133.6 (d, $^1J_{CP}$ = 31 Hz, *ipso*-C_6H_3), 132.8 (d, $^3J_{CP}$ = 7 Hz, *m*-C_6H_3), 129.0 (*p*-Dipp), 127.0 (d, $^4J_{CP}$ = 2 Hz, *p*-C_6H_3), 123.0 (*m*-Dipp), 77.2 (d, $^2J_{CP}$ = 16 Hz, CH_{COD}), 63.2 (CH_{COD}), 32.2 (d, $^3J_{CP}$ = 3 Hz, CH_{2COD}), 31.8 (d, $^3J_{CP}$ = 2 Hz, CH_{2COD}), 31.4 ((*C*HMe_2)$_{Dipp}$), 26.2 (Me_{Dipp}), 23.3 (Me_{Dipp}), 15.1 (d, $^1J_{CP}$ = 30 Hz, PMe_2), 6.1 (d, $^2J_{CP}$ = 7 Hz, Ir−CH_3),

^{31}P{^{1}H} NMR (160 MHz, CD_2Cl_2, 25 ºC) δ: −7.3.

Complex 3(Xyl)

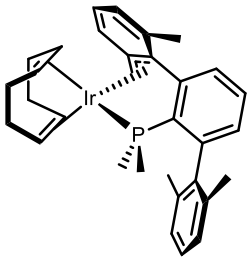

A Et_2O solution of complex **1(Xyl)** (105 mg, 0.154 mmol) was placed in a thick-wall ampoule provided with a stir bar. $ZnMe_2$ (1.2 eq) was added and the solution was stirred for 1 h. The solvent and excess $ZnMe_2$ were removed under reduced pressure and residue was extracted with CH_2Cl_2, affording complex **3(Xyl)** as a yellow greenish solid. The yield is estimated to be quantitative based on spectroscopic methods. Single crystals were grown from a saturated pentane solution at −32 ºC.

^{1}H NMR (400 MHz, CD_2Cl_2, −10 ºC) δ: 7.33 (td, $^3J_{HH}$ = 7.6 Hz, $^5J_{HP}$ = 1.9 Hz, 1H, *p*-C_6H_3), 7.20 (t, $^3J_{HH}$ = 7.5 Hz, 1H, *p*-Xyl), 7.10 (m, 2H, *m*-Xyl), 7.00 (m, 1H, *m*'-Xyl'), 6.86 (m, 2H, *m*-C_6H_3, *m*'-C_6H_3), 6.70 (m, 2H, *m*-Xyl', *p*-Xyl'), 3.79 (m, 1H, CH_{COD}), 3.46 (m, 1H, CH_{COD}), 3.20 (m, 1H, CH_{COD}), 2.44 (m, 1H, CH_{COD}), 2.36 (m, 1H, CH_{2COD}), 2.10 (br m, 1H, CH_{2COD}), 2.09 (s, 3H, Me_{Xyl}), 2.02 (s, 3H, Me_{Xyl}), 2.01 (m, 1H, IrC*H*H), 1.88 ($Me_{Xyl'}$), 1.87 to 1.76 (br m, 4H, CH_{2COD}), 1.27 (d, $^2J_{HP}$ = 8.1 Hz, 3H, P*Me*Me), 1.35 to 1.21 (br m, 2H, CH_{2COD}), 1.17 (dd, $^3J_{HP}$ = 15.0 Hz, $^2J_{HH}$ = 5.2 Hz, 1H, IrCH*H*), 0.97 (d, $^2J_{HP}$ = 8.4 Hz, 3H, PMe*Me*).

^{13}C{^{1}H} NMR (100 MHz, CD_2Cl_2, −10 ºC) δ: 148.0 (d, $^2J_{CP}$ = 31 Hz, *o*-C_6H_3), 144.1 (*o*-C_6H_3), 141.1 (*ipso*-Xyl), 137.9 (*o*-Xyl'), 137.4 (*o*-Xyl), 136.3 (*o*-Xyl), 134.0 (d, $^1J_{CP}$ = 39 Hz, *ipso*-C_6H_3), 132.0 (d, $^3J_{CP}$ = 11 Hz, *m*'-C_6H_3), 130.2 (*p*-C_6H_3), 129.6 (d, $^3J_{CP}$ = 5 Hz, *m*-C_6H_3), 127.8 (*p*-Xyl),

127.6 (d, $^{3}J_{CP}$ = 2 Hz, *m*'-Xyl'), 127.3 (*m*-Xyl), 127.1 (*m*-Xyl), 124.0 (*p*-Xyl'), 121.0 (*m*-Xyl'), 111.6 (m, *ipso*-Xyl', *o*'-Xyl'), 71.6 (d, $^{2}J_{CP}$ = 3 Hz, CH_{COD}), 66.5 (d, $^{2}J_{CP}$ = 22 Hz, CH_{COD}), 64.6 (CH_{COD}), 61.3 (CH_{COD}), 36.3 (CH_{2COD}), 34.3 (m, CH_{2COD}), 30.6 (CH_{2COD}), 30.0 (d, $^{2}J_{CP}$ = 5 Hz, $IrCH_2$), 29.9 (CH_{2COD}), 22.1 (Me_{Xyl}), 21.8 ($Me_{Xyl'}$), 21.3 (Me_{Xyl}), 17.5 (d, $^{1}J_{CP}$ = 28 Hz, P*Me*Me), 13.2 (d, $^{1}J_{CP}$ = 30 Hz, PMe*Me*).

$^{31}P\{^{1}H\}$ NMR (120 MHz, CD_2Cl_2, 25 ºC) δ: −1.9.

Complex 4(Xyl)

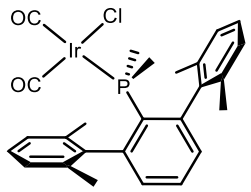

A thick-wall ampoule (volume *ca*. 50 mL) provided with a stir bar was charged with **1(Xyl)** (52.1 mg, 0.076 mmol), CH_2Cl_2 (4 mL) and CO (1 bar). The solution turned pale yellow and was stirred for 30 min. The solvent was removed under vacuum, yielding **4(Xyl)** as an air-stable, pale-yellow powder (44.8 mg, 94%). Cyclooctadiene traces were removed coevaporating with pentane. Single crystals were grown from a saturated hexane solution of the complex at −32 ºC.

Anal. Calcd. for $C_{26}H_{27}ClIrO_2P$: C, 49.56; H, 4.32. **Found**: C, 49.61; H, 4.25.

IR (Nujol): υ(Ir-CO) 2067, 1985 cm^{-1}.

IR(CH_2Cl_2): υ(Ir-CO) 2068, 1987 cm^{-1}.

^{1}H NMR (400 MHz, CD_2Cl_2, 25 ºC) δ: 7.59 (t, $^3J_{HH}$ = 7.6 Hz, 1H, *p*-C_6H_3), 7.26 (m, 2H, *p*-Xyl), 7.17 (d, $^3J_{HH}$ = 7.5 Hz, 4H, *m*-Xyl) 7.10 (dd, $^3J_{HH}$ = 7.6 Hz, $^4J_{HP}$ = 3.1 Hz, 2H, *m*-C_6H_3), 2.13 (s, 12H, Me_{Xyl}), 1.36 (d, $^2J_{HP}$ = 9.7 Hz, 6H, PMe_2).

^{13}C{^{1}H} NMR (100 MHz, CD_2Cl_2, 25 ºC) δ: 177.7 (d, $^2J_{CP}$ = 126 Hz, *trans*-CO), 168.3 (d, $^2J_{CP}$ = 13 Hz, *cis*-CO), 147.3 (d, $^2J_{CP}$ = 10 Hz, *o*-C_6H_3), 141.6 (d, $^3J_{CP}$ = 4 Hz, *ipso*-Xyl), 136.9 (*o*-Xyl), 132.0 (d, $^4J_{CP}$ = 2 Hz, *p*-C_6H_3), 131.4 (d, $^3J_{CP}$ = 8 Hz, *m*-C_6H_3), 128.6 (*p*-Xyl), 128.5 (*m*-Xyl), 127.3 (d, $^1J_{CP}$ = 48 Hz, *ipso*-C_6H_3), 22.3 (Me_{Xyl}), 16.3 (d, $^1J_{CP}$ = 38 Hz, PMe_2).

^{31}P{^{1}H} NMR (160 MHz, CD_2Cl_2, 25 ºC) δ: −10.9.

Complex 4(Dipp)

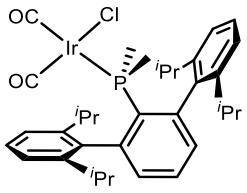

A thick-wall ampoule (volume *ca*. 50 mL) provided with a stir bar was charged with **1(Dipp)** (96.0 mg, 0.120 mmol), CH_2Cl_2 (4 mL) and CO (1 bar). The solution turned pale yellow and was stirred for 30 min. The solvent was removed under vacuum, yielding **4(Dipp)** as an air-stable, pale-yellow powder (71.2 mg, 80%). Cyclooctadiene traces were removed coevaporating with pentane. Single crystals were grown by slow diffusion of pentane into a dichloromethane solution of the complex at −32 ºC.

Anal. Calcd. for $C_{34}H_{43}ClIrO_2P$: C, 55.01; H, 5.84. **Found**: C, 55.24; H, 6.19.

IR (Nujol): υ(Ir-CO) 2059, 1978 cm^{-1}.

IR (CH_2Cl_2): υ(Ir-CO) 2067, 1987 cm^{-1}.

^{1}H NMR (500 MHz, CD_2Cl_2, 25 ºC) δ: 7.48 (td, $^3J_{HH}$ = 7.6 Hz, $^5J_{HP}$ = 1.7 Hz, 1H, *p*-C_6H_3), 7.41 (t, $^3J_{HH}$ = 7.8 Hz, 2H, *p*-Dipp), 7.28 (d, $^3J_{HH}$ = 7.8 Hz, 4H, *m*-Dipp), 7.25 (dd, $^3J_{HH}$ = 7.7 Hz, $^4J_{HP}$ = 3.3 Hz, 2H, *m*-C_6H_3), 2.71 (sept, $^3J_{HH}$ = 6.7 Hz, 4H, (C*H*Me_2)$_{Dipp}$), 1.40 (d, $^3J_{HH}$ = 6.7 Hz, 12H, Me_{Dipp}), 1.28 (d, $^2J_{HP}$ = 9.9 Hz, 6H, PMe_2), 1.00 (d, $^3J_{HH}$ = 6.7 Hz, 12H, Me_{Dipp}).

^{13}C{^{1}H} NMR (125 MHz, CD_2Cl_2, 25 ºC) δ: 178.1 (d, $^2J_{CP}$ = 126 Hz, *trans*-CO), 168.6 (d, $^2J_{CP}$ = 13 Hz, *cis*-CO), 147.6 (*o*-Dipp), 145.1 (d, $^2J_{CP}$ = 10 Hz, *o*-C_6H_3), 139.3 (d, $^3J_{CP}$ = 3 Hz, *ipso*-Dipp), 133.5 (d, $^3J_{CP}$ = 8 Hz, *m*-C_6H_3), 129.5 (*p*-Dipp), 128.9 (d, $^1J_{CP}$ = 48 Hz, *ipso*-C_6H_3), 128.8 (*p*-

C_6H_3), 123.7 (*m*-Dipp), 31.5 (($CHMe_2$)$_{Dipp}$), 26.1 (Me_{Dipp}), 23.4 (Me_{Dipp}), 16.5 (d, $^1J_{CP}$ = 38 Hz, PMe_2).

$^{31}P\{^1H\}$ NMR (200 MHz, CD_2Cl_2, 25 ºC) δ: −7.8.

Complex 5(Xyl)$^{+}$(CO)$_2$

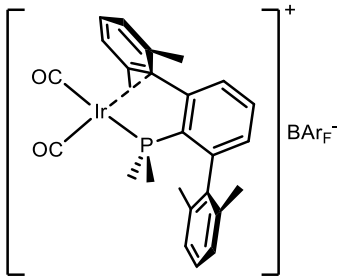

To a solid mixture of complex **4(Xyl)** (0.02 mmol) and NaBAr$_F$ (0.02 mmol), placed in a thick-wall ampoule provided with a stir bar, was added 0.7 mL of cold (–78 ºC) CD_2Cl_2 and the resulting solution kept cold and stirred for 30 min. The solution was filtered with cannula over an NMR tube placed in a dry ice/acetone bath. The spectroscopic data for this compound were collected at low temperature (−60 ºC) for preventing CO liberation. The yield is estimated to be quantitative based on spectroscopic data. Analytically pure samples of the BAr$_F$ salt of the complex were obtained evaporating the solvent and washing with pentane at low temperature. IR data was collected from freshly prepared, cold CH_2Cl_2 solutions.

IR (CH_2Cl_2): υ(Ir-CO) 2094, 2027 cm^{-1}.

Anal. Calcd. for $C_{58}H_{39}BF_{24}IrO_2P$: C, 47.78; H, 2.70. **Found**: C, 47.70; H, 2.26.

^{1}H NMR (400 MHz, CD_2Cl_2, −60 ºC) δ: 7.77 (d, $^3J_{HH}$ ≈ 7.6 Hz, 2H, *m*-Xyl'), 7.74 (s, 8H, *o*-Ar), 7.68 (t, $^3J_{HH}$ = 7.5 Hz, 1H, *p*-C_6H_3), 7.54 (s, 4H, *p*-Ar), 7.28 (t, $^3J_{HH}$ = 7.6 Hz, 2H, *p*-Xyl, *p*-Xyl'), 7.22 (dd, $^3J_{HH}$ = 7.0 Hz, $^4J_{HP}$ = 2.4 Hz, 1H, *m*-C_6H_3), 7.16 (d, $^3J_{HH}$ = 7.5 Hz, 2H, *m*-Xyl), 6.62 (d, $^3J_{HH}$ = 6.8 Hz, 1H, *m*'-C_6H_3), 2.05 (s, 6H, $Me_{Xyl'}$), 1.94 (s, 6H, Me_{Xyl}), 1.60 (d, $^2J_{HP}$ = 10.6 Hz, 6H, PMe_2).

$^{13}C\{^{1}H\}$ NMR (100 MHz, CD_2Cl_2, −60 ºC) δ: 183.0 (d, $^{2}J_{CP}$ = 102 Hz, *trans*-CO), 162.4 (d, $^{2}J_{CP}$ = 14 Hz, *cis*-CO), 161.4 (q, $^{1}J_{CB}$ = 49 Hz, *ipso*-Ar), 147.2 (*o*-C_6H_3), 143.9 (d, $^{2}J_{CP}$ = 27 Hz, *o*-C_6H_3), 139.1 (*o*-Xyl'), 136.2 (*ipso*-Xyl, *o*-Xyl), 135.6 (*p*-C_6H_3), 134.3 (*o*-Ar), 134.2 (*m*-Xyl'), 133.2 (*p*-Xyl or *p*-Xyl'), 132.1 (d, $^{3}J_{CP}$ = 6 Hz, *m*-C_6H_3), 130.7 (d, $^{3}J_{CP}$ = 15 Hz, *m*'-C_6H_3), 129.7 (d, $^{1}J_{CP}$ = 56 Hz, *ipso*-C_6H_3), 129.1 (*p*-Xyl or *p*-Xyl'), 128.3 (q, $^{2}J_{CF}$ = 31 Hz, *m*-Ar), 127.5 (*m*-Xyl), 124.1 (q, $^{1}J_{CF}$ = 272 Hz, CF_3), 117.4 (d, $^{2}J_{CP}$ = 3 Hz, *ipso*-Xyl'), 117.2 (m, *p*-Ar), 23.6 ($Me_{Xyl'}$), 21.0 (Me_{Xyl}), 14.4 (d, $^{1}J_{CP}$ = 40 Hz, PMe_2).

$^{31}P\{^{1}H\}$ NMR (160 MHz, CD_2Cl_2, −60 ºC) δ: 16.2.

Complex 5(Dipp)$^{+}$(CO)$_2$

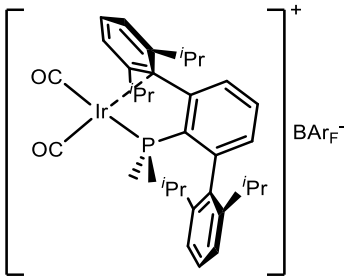

To a solid mixture of complex **4(Dipp)** (0.02 mmol) and $NaBAr_F$ (0.02 mmol), placed in a thick-wall ampoule provided with a stir bar, was added 0.7 mL of cold (–30 ºC) CD_2Cl_2 and the resulting solution kept cold and stirred for 30 min. The solution was filtered with cannula over an NMR tube placed in a dry ice/acetone bath. The spectroscopic data for this compound were collected at low temperature (0 ºC) for preventing CO liberation. The yield is estimated to be quantitative based on spectroscopic data. Analytically pure samples of this compound were obtained evaporating the solvent and washing with pentane at low temperature. IR data was collected from freshly prepared, cold CH_2Cl_2 solutions. Single crystals were grown by slow diffusion of pentane into a dichloromethane solution of the complex at −32 ºC.

IR (CH_2Cl_2): υ(Ir-CO) 2093, 2027 cm^{-1}.

Anal. Calcd. for $C_{66}H_{55}BF_{24}IrO_2P$: C, 50.49; H, 3.53. **Found**: C, 50.57; H, 3.47.

^{1}H NMR (500 MHz, CD_2Cl_2, 25 ºC) δ: 7.99 (d, $^3J_{HH}$ = 7.8 Hz, 2H, *m*-Dipp'),7.72 (s, 8H, *o*-Ar), 7.69 (m, 1H, *p*-C_6H_3), 7.59 (t, $^3J_{HH}$ = 7.7 Hz, 1H, *p*-Dipp'), 7.56 (s, 4H, *p*-Ar), 7.54 (t, $^3J_{HH}$ = 8.0 Hz, 1H, *p*-Dipp), 7.43 (dd, $^3J_{HH}$ = 7.4 Hz, $^4J_{HP}$ = 3.1 Hz, 1H, *m*-C_6H_3), 7.35 (d, $^3J_{HH}$ = 7.8 Hz, 2H, *m*-Dipp), 6.79 (d, $^3J_{HH}$ = 7.6 Hz, 1H, *m*'-C_6H_3), 2.28 (sept, $^3J_{HH}$ = 6.8 Hz, 4H,

(C*H*Me$_2$)$_{Dipp}$, (C*H*Me$_2$)$_{Dipp'}$), 1.64 (d, $^2J_{HP}$ = 10.7 Hz, 6H, PMe$_2$), 1.56 (d, $^3J_{HH}$ = 6.9 Hz, 6H, Me$_{Dipp'}$), 1.31 (d, $^3J_{HH}$ = 6.8, 6H, Me$_{Dipp}$), 1.05 (d, $^3J_{HH}$ = 6.6 Hz, 6H, Me$_{Dipp'}$), 1.03 (d, $^3J_{HH}$ = 6.8 Hz, 6H, Me$_{Dipp}$).

^{13}C{^{1}H} NMR (100 MHz, CD_2Cl_2, 0 ºC) δ: 183.0 (d, $^2J_{CP}$ = 102 Hz, *trans*-CO), 163.4 (d, $^2J_{CP}$ = 14 Hz, *cis*-CO), 162.0 (q, $^1J_{CB}$ = 50 Hz, *ipso*-Ar), 150.6 (*o*-Dipp'), 147.1 (*o*-Dipp), 146.5 (d, $^2J_{CP}$ = 2 Hz, *o*-C_6H_3), 142.5 (d, $^2J_{CP}$ = 26 Hz, *o*-C_6H_3), 135.0 (*o*-Ar), 134.6 (*p*-Dipp'), 134.24 (d, $^3J_{CP}$ = 9 Hz, *m*-C_6H_3), 134.22 (*p*-C_6H_3), 133.8 (d, $^3J_{CP}$ = 2 Hz, *ipso*-Dipp), 132.4 (d, $^3J_{CP}$ = 15 Hz, *m*'-C_6H_3), 132.1 (d, $^1J_{CP}$ = 57 Hz, *ipso*-C_6H_3), 131.3 (*m*-Dipp'), 130.8 (*p*-Dipp), 129.0 (q, $^2J_{CF}$ = 31 Hz, *m*-Ar), 124.8 (q, $^1J_{CF}$ = 272 Hz, CF_3), 123.6 (*m*-Dipp), 118.1 (d, $^2J_{CP}$ = 3 Hz, *ipso*-Dipp'), 117.7 (m, *p*-Ar), 34.6 ((*C*HMe$_2$)$_{Dipp'}$), 31.6 ((*C*HMe$_2$)$_{Dipp}$), 26.5 (Me$_{Dipp'}$), 26.2 (Me$_{Dipp}$), 24.2 (Me$_{Dipp'}$), 21.3 (Me$_{Dipp}$), 16.0 (d, $^1J_{CP}$ = 40 Hz, PMe$_2$).

^{31}P{^{1}H} NMR (160 MHz, CD_2Cl_2, 25 ºC) δ: 15.2.

Complex 5(Xyl)$^{+}$CO

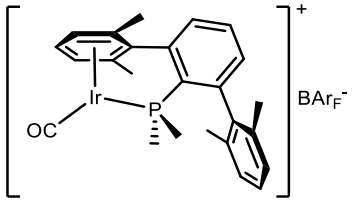

To a solid mixture of complex **4(Xyl)** (0.04 mmol) and $NaBAr_F$ (0.04 mmol), placed in a thick-wall ampoule provided with a stir bar, was added 5 mL of CH_2Cl_2 and the resulting solution stirred for 10 min. The solution was filtered, kept under reflux and periodically opened to vacuum until CO liberation was complete. Solvent was removed under reduced pressure and the product washed with pentane to yield an air-stable, analytically pure yellow powder in *ca.* 85% yield. Single crystals suitable for X-Ray diffraction were grown by means of slow pentane diffusion in a dichloromethane solution of the complex at –32 ºC. **[5(Xyl)CO]BAr$_F$** was also obtained pure allowing a dichloromethane solution of [**5(Xyl)(CO)$_2$]BAr$_F$** to stand in an open-to-air NMR tube for several days.

IR (Nujol): υ(Ir-CO) 2000 cm^{-1}.

Anal. Calcd. for $C_{57}H_{39}BF_{24}IrOP$: C, 47.88; H, 2.75. **Found**: C, 47.89; H, 2.40.

^{1}H NMR (400 MHz, CD_2Cl_2, 25 ºC) δ: 7.83 (m, 1H, *p*-C_6H_3), 7.73 (s, 8H, *o*-Ar), 7.60 (m, 1H, *m*'-C_6H_3), 7.57 (s, 4H, *p*-Ar), 7.34 (t, $^3J_{HH}$ = 7.7 Hz, 1H, *p*-Xyl), 7.31 (m, 1H, *m*-C_6H_3), 7.20 (d, $^3J_{HH}$ = 7.6 Hz, 2H, *m*-Xyl), 7.04 (d, $^3J_{HH}$ = 6.4 Hz, 2H, *m*-Xyl'), 6.09 (t, $^3J_{HH}$ = 6.5 Hz, 1H, *p*-Xyl'), 2.26 (s, 6H, $Me_{Xyl'}$), 1.97 (s, 6H, Me_{Xyl}), 1.70 (d, $^2J_{HP}$ = 12.1 Hz, 6H, PMe_2).

$^{13}C\{^{1}H\}$ NMR (100 MHz, CD_2Cl_2, 25 ºC) δ: 167.2 (d, $^{2}J_{CP}$ = 14 Hz, CO), 162.2 (q, $^{1}J_{CB}$ = 50 Hz, *ipso*-Ar), 148.9 (d, $^{2}J_{CP}$ = 3 Hz, *o*-C_6H_3), 141.3 (d, $^{2}J_{CP}$ = 18 Hz, *o*-C_6H_3), 139.2 (d, $^{1}J_{CP}$ = 58 Hz, *ipso*-C_6H_3), 136.9 (d, $^{3}J_{CP}$ = 3 Hz, *ipso*-Xyl), 136.7 (*o*-Xyl), 135.2 (*o*-Ar), 134.7 (d, $^{4}J_{CP}$ = 2 Hz, *p*-C_6H_3), 133.6 (d, $^{3}J_{CP}$ = 8 Hz, *m*-C_6H_3), 130.0 (*p*-Xyl), 129.3 (q, $^{2}J_{CF}$ = 32 Hz, *m*-Ar), 128.5 (*m*-Xyl), 128.4 (d, $^{3}J_{CP}$ = 14 Hz, *m*'-C_6H_3), 125.0 (q, $^{1}J_{CF}$ = 272 Hz, CF_3), 117.9 (m, *p*-Ar), 116.9 (d, $^{2}J_{CP}$ = 2 Hz, *o*-Xyl'), 109.7 (d, $^{2}J_{CP}$ = 5 Hz, *ipso*-Xyl'), 103.0 (d, $^{2}J_{CP}$ = 3 Hz, *m*-Xyl'), 89.1 (d, $^{2}J_{CP}$ = 7 Hz, *p*-Xyl'), 21.4 (Me_{Xyl}), 19.4 ($Me_{Xyl'}$), 19.3 (d, $^{1}J_{CP}$ = 43 Hz, PMe_2).

$^{31}P\{^{1}H\}$ NMR (160 MHz, CD_2Cl_2, 25 ºC) δ: 6.7.

Complex 5(Dipp)$^{+}$CO

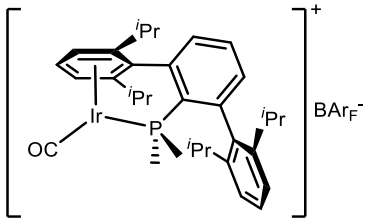

To a solid mixture of complex **4(Dipp)** (0.04 mmol) and $NaBAr_F$ (0.04 mmol), placed in a thick-wall ampoule provided with a stir bar, was added 5 mL of CH_2Cl_2 and the resulting solution stirred for 10 min. The solution was filtered, kept under reflux and periodically opened to vacuum until CO liberation was complete. Solvent was removed under reduced pressure and the product washed with pentane to yield an air-stable, analytically pure yellow powder in *ca.* 85% yield. Single crystals suitable for X-Ray diffraction were grown by means of slow pentane diffusion in a dichloromethane solution of the complex at −32 ºC. **[5(Dipp)(CO)]BAr$_F$** was also obtained pure allowing a dichloromethane solution of **[5(Dipp)(CO)$_2$]BAr$_F$** to stand in an open-air NMR tube for several days.

IR (Nujol): υ(Ir-CO) 1997 cm^{-1}.

Anal. Calcd. for $C_{65}H_{55}BF_{24}IrOP$: C, 50.63; H, 3.60. **Found**: C, 50.35; H, 3.47.

^{1}H NMR (400 MHz, CD_2Cl_2, 25 ºC) δ: 7.77 (td, $^3J_{HH}$ = 7.6 Hz, $^5J_{HP}$ = 2.4 Hz, 1H, *p*-C_6H_3), 7.72 (s, 8H, *o*-Ar), 7.69 (ddd, $^3J_{HH}$ = 7.6 Hz, $^4J_{HP}$ = 2-.3 Hz, $^4J_{HH}$ = 1.2 Hz, 1H, *m*'-C_6H_3), 7.56 (s, 4H, *p*-Ar), 7.50 (t, $^3J_{HH}$ = 7.8 Hz, 1H, *p*-Dipp), 7.44 (ddd, $^3J_{HH}$ = 7.5 Hz, $^4J_{HP}$ = 3.8 Hz, $^4J_{HH}$ = 1.1 Hz, 1H, *m*-C_6H_3), 7.30 (d, $^3J_{HH}$ = 7.8 Hz, 2H, *m*-Dipp), 7.04 (dd, $^3J_{HH}$ = 6.6 Hz, $^3J_{HP}$ = 0.9 Hz, 2H, *m*-Dipp'), 6.24 (t, $^3J_{HH}$ = 6.6 Hz, 1H, *p*-Dipp'), 2.19 (sept, $^3J_{HH}$ = 6.6 Hz, 4H, (C*H*Me$_2$)$_{Dipp}$, (C*H*Me$_2$)$_{Dipp'}$), 1.67 (d, $^2J_{HP}$ = 12.1

Hz, 6H, PMe_2), 1.33 (d, $^3J_{HH}$ = 6.9 Hz, 6H, $Me_{Dipp'}$), 1.26 (d, $^3J_{HH}$ = 6.7 Hz, 6H, $Me_{Dipp'}$), 1.25 (d, $^3J_{HH}$ = 6.7 Hz, 6H, Me_{Dipp}), 1.02 (d, $^3J_{HH}$ = 6.6 Hz, 6H, Me_{Dipp}).

$^{13}C\{^1H\}$ NMR (100 MHz, CD_2Cl_2, 25 ºC) δ: 167.7 (d, $^2J_{CP}$ = 14 Hz, CO), 162.2 (q, $^1J_{CB}$ = 50 Hz, *ipso*-Ar), 147.3 (*o*-Dipp), 147.2 (d, $^2J_{CP}$ = 3 Hz, *o*-C_6H_3), 140.6 (d, $^1J_{CP}$ = 58 Hz, *ipso*-C_6H_3), 140.4 (d, $^2J_{CP}$ = 18 Hz, *o*-C_6H_3), 135.3 (*o*-Ar), 134.9 (d, $^3J_{CP}$ = 8 Hz, *m*-C_6H_3), 134.4 (d, $^3J_{CP}$ = 3 Hz, *ipso*-Dipp), 132.7 (d, $^4J_{CP}$ = 2 Hz, *p*-C_6H_3), 131.0 (*p*-Dipp), 129.3 (q, $^2J_{CF}$ = 31 Hz, *m*-Ar), 128.9 (d, $^3J_{CP}$ = 14 Hz, *m*'-C_6H_3), 127.7 (d, $^2J_{CP}$ = 2 Hz, *o*-Dipp'), 125.1 (q, $^1J_{CF}$ = 272 Hz, CF_3), 123.7 (*m*-Dipp), 117.9 (m, *p*-Ar), 108.4 (d, $^2J_{CP}$ = 5 Hz, *ipso*-Dipp'), 98.4 (d, $^2J_{CP}$ = 3 Hz, *m*-Dipp'), 90.0 (d, $^2J_{CP}$ = 7 Hz, *p*-Dipp'), 31.8 ($(CHMe_2)_{Dipp}$), 29.9 ($(CHMe_2)_{Dipp'}$), 26.4 (Me_{Dipp}), 24.8 ($Me_{Dipp'}$), 23.7 ($Me_{Dipp'}$), 21. 5 (Me_{Dipp}), 21.3 (d, $^1J_{CP}$ = 44 Hz, PMe_2).

$^{31}P\{^1H\}$ NMR (160 MHz, CD_2Cl_2, 25 ºC) δ: 6.1.

Complex 5(Xyl)$^{+}$(CO)$_3$

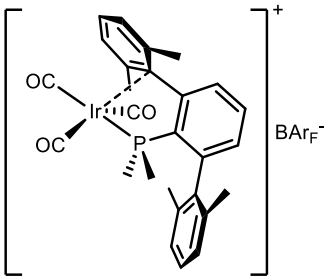

A CH_2Cl_2 solution of complex **[5(Xyl)(CO)$_2$]BAr$_F$** (0.02 mmol) was placed in a thick-wall ampoule, charged with 1.2 bar of CO and stirred for 10 min. The solvent was removed under reduced pressure and the product washed with pentane to yield the desired compound as an analytically pure yellow powder in *ca.* 85% yield. Single crystals suitable for X-Ray diffraction were grown through slow pentane diffusion in a dichloromethane solution of the complex at –32 ºC. The product can also be obtained starting from complex [**5(Xyl)CO]BAr$_F$** under similar conditions.

IR (CH_2Cl_2): υ(Ir-CO) 2126, 2027 cm^{-1}.

Anal. Calcd. for $C_{59}H_{39}BF_{24}IrO_3P$: C, 47.69; H, 2.65. **Found**: C, 47.66; H, 2.19.

^{1}H NMR (400 MHz, CD_2Cl_2, 25 ºC) δ: 7.74 (s, 8H, *o*-Ar), 7.71 (t, $^3J_{HH}$ = 7.2 Hz, 1H, *p*-C_6H_3), 7.58 (s, 4H, *p*-Ar), 7.47 (t, $^3J_{HH}$ = 7.6 Hz, 2H, *p*-Xyl), 7.24 (d, $^3J_{HH}$ = 7.5 Hz, 4H, *m*-Xyl), 6.97 (br, 2H, *m*-C_6H_3), 2.11 (s, 12H, Me_{Xyl}), 1.93 (d, $^2J_{HP}$ = 10.9 Hz, 6H, PMe_2).

^{13}C{^{1}H} NMR (100 MHz, CD_2Cl_2, 25 ºC) δ: 173.1 (d, $^2J_{CP}$ = 15 Hz, *cis*-CO), 168.2 (d, $^2J_{CP}$ = 88 Hz, *trans*-CO), 162.2 (q, $^1J_{CB}$ = 50 Hz, *ipso*-Ar), 147.4 (d, $^2J_{CP}$ = 12 Hz, *o*-C_6H_3), 140.1 (*o*-Xyl), 135.6 (d, $^4J_{CP}$ = 2 Hz, *p*-

C_6H_3), 135.2 (*o*-Ar), 132.3 (br, *ipso*-Xyl), 132.1 (d, $^3J_{CP}$ = 10 Hz, *m*-C_6H_3), 131.0 (*p*-Xyl), 130.4 (d, $^1J_{CP}$ = 58 Hz, *ipso*-C_6H_3), 129.3 (q, $^2J_{CF}$ = 31 Hz, *m*-Ar), 128.7 (*m*-Xyl), 125.0 (q, $^1J_{CF}$ = 272 Hz, CF_3), 117.9 (m, *p*-Ar), 21.9 (Me_{Xyl}), 18.1 (d, $^1J_{CP}$ = 43 Hz, PMe_2).

$^{31}P\{^1H\}$ NMR (160 MHz, CD_2Cl_2, 25 ºC) δ: –20.2.

Complex 5(Dipp)$^{+}$(CO)$_3$

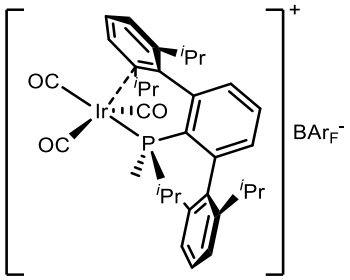

A CH_2Cl_2 solution of complex **[5(Dipp)(CO)$_2$]BAr$_F$** (0.02 mmol) was placed in a thick-wall ampoule, charged with 1.2 bar of CO and stirred for 10 min. The solvent was removed under reduced pressure and the product washed with pentane to yield the desired compound as an analytically pure yellow powder in *ca.* 85% yield. The product can also be obtained starting from complex **[5(Dipp)(CO)]BAr$_F$** under similar conditions.

IR (CH_2Cl_2): υ(Ir-CO) 2125, 2025 cm^{-1}.

Anal. Calcd. for $C_{67}H_{55}BF_{24}IrO_3P$: C, 50.35; H, 3.47. **Found**: C, 50.47; H, 3.04.

^{1}H NMR (400 MHz, CD_2Cl_2, 0 ºC) δ: 7.71 (s, 8H, *o*-Ar), 7.64 (td, $^3J_{HH}$ = 7.7 Hz, $^5J_{HP}$ = 2.2 Hz, 1H, *p*-C_6H_3), 7.60 (t, $^3J_{HH}$ = 7.8 Hz, 2H, *p*-Dipp), 7.56 (s, 4H, *p*-Ar), 7.38 (d, $^3J_{HH}$ = 7.9 Hz, 4H, *m*-Dipp), 7.19 (dd, $^3J_{HH}$ = 7.7 Hz, $^4J_{HP}$ = 3.5 Hz, 2H, *m*-C_6H_3), 2.41 (sept, $^3J_{HH}$ = 6.7 Hz, 4H, (C*H*Me$_2$)$_{Dipp}$), 1.83 (d, $^2J_{HP}$ = 11.0 Hz, 6H, PMe$_2$), 1.38 (d, $^3J_{HH}$ = 6.8 Hz, 12H, Me$_{Dipp}$), 0.97 (d, $^3J_{HH}$ = 6.6 Hz, 12H, Me$_{Dipp}$).

^{13}C{^{1}H} NMR (100 MHz, CD_2Cl_2, 0 ºC) δ: 173.2 (d, $^2J_{CP}$ = 14 Hz, *cis*-CO), 168.7 (d, $^2J_{CP}$ = 91 Hz, *cis*-CO), 161.9 (q, $^1J_{CB}$ = 50 Hz, *ipso*-Ar), 149.9 (br, *o*-Dipp), 144.4 (d, $^2J_{CP}$ = 11 Hz, *o*-C_6H_3), 135.0 (*o*-Ar), 134.0 (d, $^3J_{CP}$ = 10 Hz, *m*-C_6H_3), 132.0 (d, $^4J_{CP}$ = 2 Hz, *p*-C_6H_3), 131.9 (*p*-Dipp),

130.9 (d, $^{1}J_{CP}$ = 59 Hz, *ipso*-C_6H_3), 130.5 (br, *ipso*-Dipp), 129.0 (q, $^{2}J_{CF}$ = 31 Hz, *m*-Ar), 124.8 (q, $^{1}J_{CF}$ = 272 Hz, CF_3), 124.5 (*m*-Dipp), 117.7 (m, *p*-Ar), 32.4 (CHMe$_2$)$_{Dipp}$), 25.8 (Me$_{Dipp}$), 22.6 (Me$_{Dipp}$), 18.5 (d, $^{1}J_{CP}$ = 43 Hz, PMe_2).

^{31}P{^{1}H} NMR (160 MHz, CD_2Cl_2, 25 ºC) δ: –21.0.

Complexes 6(Xyl)$^+$ and 7(Xyl)$^+$

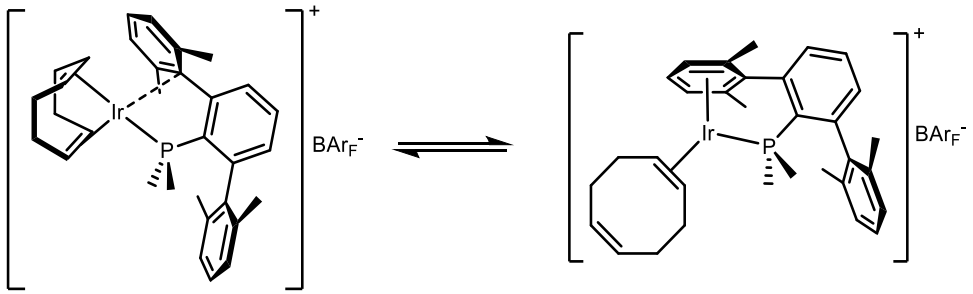

[6(Xyl)]BAr$_F$ **[7(Xyl)]BAr$_F$**

To a solid mixture of complex **1(Xyl)** (0.07 mmol) and NaBAr$_F$ (0.07 mmol), placed in a thick-wall ampoule provided with a stir bar, was added 5 mL of CH_2Cl_2. The resulting solution was stirred for 10 min at room temperature, filtered and the volatiles evaporated under reduced pressure to obtain a mixture of complexes **[6(Xyl)]BAr$_F$** and **[7(Xyl)]BAr$_F$** as a red powder in *ca*. 85% yield. Single crystals of **[6(Xyl)]BAr$_F$** were grown from a saturated hexane-dichloromethane solution.

Anal. Calcd. for $C_{64}H_{51}BF_{24}IrP$: C, 50.91; H, 3.40. Found: C, 50.61; H, 3.70.

[6(Xyl)]BAr$_F$: **^{1}H NMR** (400 MHz, CD_2Cl_2, −15 ºC) δ: 7.60 (td, $^3J_{HH}$ = 7.6 Hz, $^5J_{HP}$ = 2.3 Hz, 1H, *p*-C_6H_3), 7.41 to 7.16 (br and overlapped, 6H, *m*-Xyl, *p*-Xyl), 7.15 (*m*-C_6H_3(COSY)), 6.68 (br, 1H, *m*-C_6H_3), 3.24 (br, 2H, CH_{COD}), 3.18 (br, 2H, CH_{COD}), 1.97 (s, 6H, Me_{Xyl}), 1.96 (br, 6H, CH_{2COD}), 1.82 (s, 6H, Me_{Xyl}), 1.57 (m, 2H, CH_{2COD}), 1.37 (d, $^1J_{CP}$ = 9.8 Hz, 6H, PMe_2).

^{13}C{^{1}H} NMR (100 MHz, CD_2Cl_2, −15 ºC) δ: 134.5 (overlapped, *p*-C_6H_3), 130.6 (d, $^3J_{CP}$ = 15 Hz, *m*-C_6H_3), 103.7 (d, $^2J_{CP}$ = 11 Hz, CH_{COD}), 62.3 (CH_{COD}), 33.6 (CH_{2COD}), 28.7 (CH_{2COD}), 22.7 (Me_{Xyl}), 21.2 (Me_{Xyl}), 12.0 (d, $^1J_{CP}$ = 37 Hz, PMe_2).

$^{31}P\{^{1}H\}$ NMR (160 MHz, CD_2Cl_2, 25 ºC) δ: 16.9 (59%).

[7(Xyl)]BAr$_F$: ^{1}H NMR (500 MHz, CD_2Cl_2, 25 ºC) δ: 7.76 (td, $^{3}J_{HH}$ = 7.6 Hz, $^{5}J_{HP}$ = 2.1 Hz, 1H, *p*-C_6H_3), 7.63 (*m*'-C_6H_3(COSY)), 7.30 (t, $^{3}J_{HH}$ = 7.6 Hz, 1H, *p*-Xyl), 7.26 (ddd, $^{3}J_{HH}$ = 7.6 Hz, $^{4}J_{HP}$ = 3.5 Hz, $^{4}J_{HH}$ = 1.2 Hz, 1H, *m*-C_6H_3), 7.17 (d, $^{3}J_{HH}$ = 7.6 Hz, 2H, *m*-Xyl), 6.63 (d, $^{3}J_{HH}$ = 6.2 Hz, 2H, *m*-Xyl'), 5.60 (m, 3H, *p*-Xyl', CH_{COD}), 2.93 (m, 2H, $IrCH_{COD}$), 2.41 to 2.26 (m, 4H, CH_{2COD}), 2.17 (s, 6H, $Me_{Xyl'}$), 1.98 (m, 2H, CH_{2COD}), 1.95 (s, 6H, Me_{Xyl}), 1.76 (m, 2H, CH_{2COD}), 1.28 (d, $^{1}J_{CP}$ = 11.3 Hz, 6H, PMe_2).

$^{13}C\{^{1}H\}$ NMR (100 MHz, CD_2Cl_2, –15 ºC) δ: 140.1 (d, $^{1}J_{CP}$ = 59 Hz, *ipso*-C_6H_3), 129.9 (CH_{COD}), 127.8 (overlapped, *m*'-C_6H_3), 108.7 (*o*-Xyl'), 107.1 (d, $^{2}J_{CP}$ = 5 Hz, *ipso*-Xyl'), 105.0 (d, $^{2}J_{CP}$ = 3 Hz, *m*-Xyl'), 86.2 (d, $^{2}J_{CP}$ = 10 Hz, *p*-Xyl'), 52.9 ($IrCH_{COD}$), 36.1 (CH_{2COD}), 32.6 (CH_{2COD}), 21.2 (Me_{Xyl}), 19.1 ($Me_{Xyl'}$), 13.0 (d, $^{1}J_{CP}$ = 40 Hz, PMe_2).

$^{31}P\{^{1}H\}$ NMR (160 MHz, CD_2Cl_2, 25 ºC) δ: 2.0 (41%).

Complexes 6(Dipp)$^+$ and 7(Dipp)+

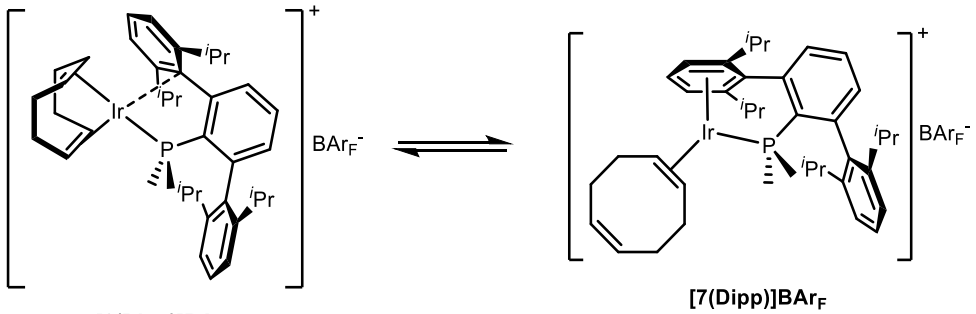

[6(Dipp)]BAr$_F$ **[7(Dipp)]BAr$_F$**

To a solid mixture of complex **1(Dipp)** (0.07 mmol) and $NaBAr_F$ (0.07 mmol), placed in a thick-wall ampoule provided with a stir bar, was added 5 mL of CH_2Cl_2. The resulting solution was stirred for 10 min at room temperature, filtered and the volatiles evaporated under reduced pressure to obtain a mixture of complexes **[6(Dipp)]BAr$_F$** and **[7(Dipp)BAr$_F$]** as an orange powder in *ca*. 85% yield.

Anal. Calcd. for $C_{72}H_{67}BF_{24}IrP$: C, 53.31; H, 4.16. **Found**: C, 53.28; H, 4.50.

[6(Dipp)]BAr$_F$: **^{1}H NMR** (500 MHz, CD_2Cl_2, 25 ºC) δ: 3.43 (m, 2H, CH_{COD}), 3.18 (m, 2H, CH_{COD}), 2.55 (m, 2H, ($CHMe_2$)$_{Dipp}$), 2.38 (($CHMe_2$)$_{Dipp}$(COSY)), 2.33 (CH_{2COD}(COSY)), 2.28 (CH_{2COD}(COSY)), 2.12 (CH_{2COD}(COSY)), 2.05 (CH_{2COD}(COSY)), 1.37 (d, $^2J_{HP}$ = 9.8 Hz, 6H, PMe_2), 1.34 (Me_{Dipp}(COSY)), 1.29 (Me_{Dipp}(COSY)), 1.11 (Me_{Dipp}(COSY)), 1.07 (Me_{Dipp}(COSY)).

^{13}C{^{1}H} NMR (100 MHz, CD_2Cl_2, 25 ºC) δ: 105.4 (d, $^2J_{CP}$ = 11 Hz, CH_{COD}), 61.0 (CH_{COD}), 13.6 (d, $^1J_{CP}$ = 37 Hz, PMe_2).

^{31}P{^{1}H} NMR (200 MHz, CD_2Cl_2, 25 ºC) δ: 14.8 (14%).

[7(Dipp)]BAr$_F$: ^{1}H NMR (500 MHz, CD_2Cl_2, 25 ºC) δ: 7.74 (overlapped m, 1H, *m*'-C_6H_3), 7.71 (td, $^3J_{HH}$ = 7.3 Hz, $^5J_{HP}$ = 1.8 Hz, 1H, *p*-C_6H_3), 7.46 (t, $^3J_{HH}$ = 7.7 Hz, 1H, *p*-Dipp), 7.37 (overlapped m, 1H, *m*-C_6H_3), 7.28 (d, $^3J_{HH}$ = 7.7 Hz, 2H, *m*-Dipp), 6.64 (d, $^3J_{HH}$ = 6.3 Hz, 2H, *m*-Dipp'), 5.77 (t, $^3J_{HH}$ = 6.3 Hz, 1H, *p*-Dipp'), 5.62 (m, 2H, CH_{COD}), 2.96 (m, 2H, $IrCH_{COD}$), 2.40 (m, 4H, CH_{2COD}), 2.25 (sept, $^3J_{HH}$ = 6.7 Hz, 2H, $(CHMe_2)_{Dipp}$), 2.13 (sept, $^3J_{HH}$ = 6.8 Hz, 2H, $(CHMe_2)_{Dipp'}$), 2.06 (m, 2H, CH_{2COD}), 1.85 (m, 2H, CH_{2COD}), 1.32 (d, $^3J_{HH}$ = 6.9 Hz, 6H, $Me_{Dipp'}$), 1.28 (d, $^2J_{HP}$ = 11.4 Hz, 6H, PMe_2), 1.24 (m, 12H, $Me_{Dipp'}$, Me_{Dipp}), 1.00 (d, $^3J_{HH}$ = 6.6 Hz, 6H, Me_{Dipp}).

^{13}C{^{1}H} NMR (100 MHz, CD_2Cl_2, 25 ºC) δ: 147.2 (*o*-Dipp), 146.3 (*o*-C_6H_3), 142.3 (d, $^1J_{CP}$ = 59 Hz, *ipso*-C_6H_3), 141.2 (d, $^2J_{CP}$ = 18 Hz, *o*-C_6H_3), 135.5 (*ipso*-Dipp), 134.7 (d, $^3J_{CP}$ = 7 Hz, *m*-C_6H_3), 132.0 (*p*-C_6H_3), 130.7 (*p*-Dipp), 130.4 (CH_{COD}), 128.8 (d, $^3J_{CP}$ = 7 Hz, *m*'-C_6H_3), 123.7 (*m*-Dipp), 120.1 (*o*-Dipp'), 106.9 (d, $^2J_{CP}$ = 5 Hz, *ipso*-Dipp'), 101.7 (d, $^2J_{CP}$ = 4 Hz, *m*-Dipp'), 88.3 (d, $^2J_{CP}$ = 11 Hz, *p*-Dipp'), 53.5 ($IrCH_{COD}$), 36.7 (CH_{2COD}), 32.8 (CH_{2COD}), 31.7 ($(CHMe_2)_{Dipp}$), 29.7 ($(CHMe_2)_{Dipp'}$), 26.3 (Me_{Dipp}), 24.7 ($Me_{Dipp'}$), 23.7 ($Me_{Dipp'}$), 21.6 (Me_{Dipp}), 15.3 (d, $^1J_{CP}$ = 40 Hz, PMe_2).

^{31}P{^{1}H} NMR (200 MHz, 25 ºC, CD_2Cl_2) δ: 1.9 (86%).

Complex 8(Xyl)$^+$

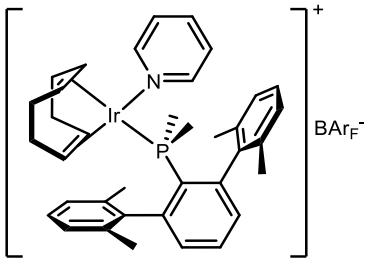

Pyridine (0.020 mmol) was added to a dichloromethane solution of complexes **[6(Xyl)]BAr$_F$** and [**7(Xyl)]BAr$_F$** (0.018 mmol), which immediately turned from red to light orange. The solution was stirred for 5 min at room temperature and the solvent was removed under reduced pressure. Excess pyridine was evaporated together with pentane (2x5 mL). The finely divided orange solid was washed with pentane (5 mL) and dried under reduced pressure, affording the desired compound in 82% yield.

Anal. Calcd. for $C_{69}H_{56}BF_{24}IrNP$: C, 52.15; H, 3.55; N, 0.88. **Found**: C, 52.46; H, 3.43; N, 0.69.

^{1}H NMR (400 MHz, CD_2Cl_2, 25 ºC) δ: 8.06 (m, 2H, 2,6-py), 7.72 (m, 9H, *o*-Ar, 4-py), 7.57 (td, $^3J_{HH}$ = 7.7 Hz, $^5J_{HP}$ = 1.7 Hz, 1H, *p*-C_6H_3), 7.56 (s, 4H, *p*-Ar), 7.31 (m, 4H, 3,5-py, *p*-Xyl), 7.18 (d, $^3J_{HH}$ = 7.5 Hz, 4H, *m*-Xyl), 7.09 (dd, $^3J_{HH}$ = 7.6 Hz, $^4J_{HP}$ = 3.1 Hz, 2H, *m*-C_6H_3), 3.98 (m, 2H, CH_{COD}), 3.49 (br, 2H, CH_{COD}), 2.28 to 2.18 (m, 4H, CH_{2COD}), 2.15 (s, 12H, Me_{Xyl}), 1.87 to 1.72 (m, 4H, CH_{2COD}), 0.82 (d, $^2J_{HP}$ = 8.3 Hz, 6H, PMe_2).

^{13}C{^{1}H} NMR (100 MHz, CD_2Cl_2, 25 ºC) δ: 162.2 (q, $^1J_{CB}$ = 50 Hz, *ipso*-Ar), 150.6 (2,6-py), 145.9 (d, $^2J_{CP}$ = 10 Hz, *o*-C_6H_3), 141.2 (d, $^3J_{CP}$ = 3 Hz, *ipso*-Xyl), 139.0 (4-py), 137.4 (*o*-Xyl), 135.2 (*o*-Ar), 132.3 (d, $^3J_{CP}$ = 8 Hz, *m*-C_6H_3), 131.8 (d, $^4J_{CP}$ = 2 Hz, *p*-C_6H_3), 129.3 (q, $^2J_{CF}$ = 31 Hz, *m*-Ar), 129.0 (*p*-Xyl), 128.4 (*m*-Xyl), 127.4 (3,5-py), 126.8 (d, $^1J_{CP}$ = 41 Hz, *ipso*-

C_6H_3), 125.0 (q, $^1J_{CF}$ = 272 Hz, CF_3), 117.9 (m, *p*-Ar), 89.7 (d, $^2J_{CP}$ = 13 Hz, CH_{COD}), 66.4 (br, CH_{COD}), 32.7 (br, CH_{2COD}), 29.4 (br, CH_{2COD}), 22.4 (Me_{Xyl}), 14.3 (d, $^1J_{CP}$ = 34 Hz, PMe_2).

$^{31}P\{^1H\}$ NMR (160 MHz, CD_2Cl_2, 25 ºC) δ: −12.1.

Complex 9(Xyl)$^+$

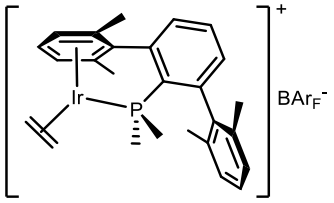

Ethylene was bubbled through a deoxygenated pentane solution of $[IrCl(COE)_2]_2$ (0.11 mmol, 15 mL, −20 ºC) in an ampoule, until the yellow coloration fades. A red precipitate formed upon addition of the phosphine (0.22 mmol) dissolved in pentane (8 mL). $NaBAr_F$ (0.22 mmol) was suspended in CH_2Cl_2 (8 mL) and added to the reaction mixture, which gradually turned pale yellow. The solution was allowed to reach room temperature and the solvent was removed under reduced pressure. The complex was extracted with CH_2Cl_2 (8 mL), the solvent evaporated under reduced pressure and the solid washed with pentane (10 mL), yielding complex **[9(Xyl)]BAr$_F$** as a pure, pale solid in *ca.* 80% yield.

Anal. Calc. for $C_{58}H_{43}BF_{24}IrP$: C, 48.72; H, 3.03. **Found**: C, 48.92; H, 3.09.

^{1}H NMR (400 MHz, CD_2Cl_2, 25 ºC) δ: 7.74 (s, 8H, *o*-Ar), 7.73 (overlapped m, 1H, *p*-C_6H_3), 7.64 (ddd, $^3J_{HH}$ = 7.6 Hz, $^4J_{HP}$ = 2.1 Hz, $^4J_{HH}$ = 1.1 Hz, 1H, *m*'-C_6H_3), 7.56 (s, 4H, *p*-Ar), 7.25 (t, $^3J_{HH}$ = 7.7 Hz, 1H, *p*-Xyl), 7.21 (ddd, $^3J_{HH}$ = 7.5 Hz, $^4J_{HP}$ = 3.4 Hz, $^4J_{HH}$ = 1.1 Hz, 1H, *m*-C_6H_3), 7.13 (d, $^3J_{HH}$ = 7.6 Hz, 2H, *m*-Xyl), 6.78 (d, $^3J_{HH}$ = 6.2 Hz, 2H, *m*-Xyl'), 5.30 (td, $^3J_{HH}$ = 6.2 Hz, $^3J_{HP}$ = 1.7 Hz, 1H, *p*-Xyl'), 2.93 (m, 2H, C*H*H=C*H*H), 2.18 (s, 6H, $Me_{Xyl'}$), 1.93 (s, 6H, Me_{Xyl}), 1.74 (m, 2H, CH*H*=CH*H*), 1.24 (d, $^2J_{HP}$ = 11.4 Hz, 6H, PMe_2).

$^{13}C\{^1H\}$ NMR (100 MHz, CD_2Cl_2, 25 ºC) δ: 162.3 (q, $^1J_{CB}$ = 50 Hz, *ipso*-Ar), 148.4 (*o*-C_6H_3), 142.2 (d, $^2J_{CP}$ = 18 Hz, *o*-C_6H_3), 141.3 (d, $^1J_{CP}$ = 59 Hz, *ipso*-C_6H_3), 137.9 (d, $^3J_{CP}$ = 2 Hz, *ipso*-Xyl), 136.7 (*o*-Xyl), 135.3 (*o*-Ar), 134.0 (*p*-C_6H_3), 133.3 (d, $^3J_{CP}$ = 7 Hz, *m*-C_6H_3), 129.7 (*p*-Xyl), 129.4 (q, $^2J_{CF}$ = 31 Hz, *m*-Ar), 128.3 (m, *m*'-C_6H_3, *m*-Xyl), 125.1 (q, $^1J_{CF}$ = 272 Hz, CF_3), 118.0 (m, *p*-Ar), 110.6 (*o*-Xyl'), 109.5 (d, $^2J_{CP}$ = 5 Hz, *ipso*-Xyl'), 102.6 (d, $^2J_{CP}$ = 4 Hz, *m*-Xyl'), 84.7 (d, $^2J_{CP}$ = 11 Hz, *p*-Xyl'), 24.5 (C_2H_4), 21.4 (Me_{Xyl}), 19.1 ($Me_{Xyl'}$), 13.4 (d, $^1J_{CP}$ = 40 Hz, PMe_2).

$^{31}P\{^1H\}$ NMR (160 MHz, CD_2Cl_2, 25 ºC) δ: 2.1.

Complex 9(Dipp)$^+$

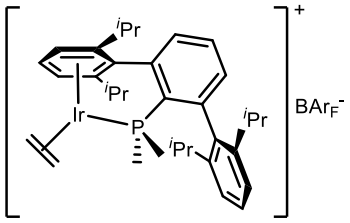

Ethylene was bubbled through a deoxygenated pentane solution of $[IrCl(COE)_2]_2$ (0.11 mmol, 15 mL, −20 ºC) in an ampoule, until the yellow coloration fades. A red precipitate formed upon addition of the phosphine (0.22 mmol) dissolved in pentane (8 mL). $NaBAr_F$ (0.22 mmol) was suspended in CH_2Cl_2 (8 mL) and added to the reaction mixture, which gradually turned pale yellow. The solution was allowed to reach room temperature and the solvent was removed under reduced pressure. The complex was extracted with CH_2Cl_2 (8 mL), the solvent evaporated under reduced pressure and the solid washed with pentane (10 mL), yielding complex **[9(Dipp)]BAr$_F$** as a pure, pale solid in *ca*. 80% yield.

Anal. Calc. for $C_{66}H_{60}BF_{24}IrP$: C, 51.37; H, 3.92. **Found**: C, 51.40; H, 4.07.

^{1}H NMR (500 MHz, CD_2Cl_2, 25 ºC) δ: 7.77 (ddd, $^3J_{HH}$ = 7.6 Hz, $^4J_{HP}$ = 2.2 Hz, $^4J_{HH}$ = 1.4 Hz, 1H, *m*'-C_6H_3), 7.73 (td overlapped, $^3J_{HH}$ = 7.5 Hz, $^5J_{HP}$ = 2.2 Hz, 1H, *p*-C_6H_3), 7.72 (s, 8H, *o*-Ar), 7.56 (s, 4H, *p*-Ar), 7.46 (t, $^3J_{HH}$ = 7.8 Hz, 1H, *p*-Dipp), 7.38 (ddd, $^3J_{HH}$ = 7.3 Hz, $^4J_{HP}$ = 3.6 Hz, $^4J_{HH}$ = 1.3 Hz, 1H, *m*-C_6H_3), 7.27 (d, $^3J_{HH}$ = 7.8 Hz, 2H, *m*-Dipp), 6.88 (dd, $^3J_{HH}$ = 6.4 Hz, $^3J_{HP}$ = 0.7 Hz, 2H, *m*-Dipp'), 5.57 (td, $^3J_{HH}$ = 6.4 Hz, $^3J_{HP}$ = 1.7 Hz, 1H, *p*-Dipp'), 2.97 (m, 2H, C*H*H=C*H*H), 2.22 (sept, $^3J_{HH}$ = 6.7 Hz, 2H, (C*H*Me$_2$)$_{Dipp}$), 2.16 (sept, $^3J_{HH}$ = 6.9 Hz, 2H, (C*H*Me$_2$)$_{Dipp'}$), 1.79 (m, 2H, CH*H*=CH*H*), 1.30 (d, $^3J_{HH}$ = 6.9 Hz, 6H, Me$_{Dipp'}$), 1.28 (d, $^3J_{HH}$ = 6.8 Hz,

6H, $Me_{Dipp'}$), 1.24 (d, $^{2}J_{HP}$ = 11.4 Hz, 6H, PMe_2), 1.23 (d, $^{3}J_{HH}$ = 6.7 Hz, 6H, Me_{Dipp}), 1.00 (d, $^{3}J_{HH}$ = 6.7 Hz, 6H, Me_{Dipp}).

$^{13}C\{^{1}H\}$ NMR (100 MHz, CD_2Cl_2, 25 ºC) δ: 162.3 (q, $^{1}J_{CB}$ = 50 Hz, *ipso*-Ar), 147.2 (*o*-Dipp), 146.5 (*o*-C_6H_3), 142.7 (d, $^{1}J_{CP}$ = 59 Hz, *ipso*-C_6H_3), 141.2 (d, $^{2}J_{CP}$ = 18 Hz, *o*-C_6H_3), 135.3 (*o*-Ar, *ipso*-Dipp (overlapped)), 134.7 (d, $^{3}J_{CP}$ = 7 Hz, *m*-C_6H_3), 132.1 (*p*-C_6H_3), 130.7 (*p*-Dipp), 129.3 (q, $^{2}J_{CF}$ = 31 Hz, *m*-Ar), 128.8 (d, $^{3}J_{CP}$ = 13 Hz, *m*'-C_6H_3), 125.1 (q, $^{1}J_{CF}$ = 272 Hz, CF_3), 123.6 (*m*-Dipp), 121.5 (*o*-Dipp'), 117.9 (m, *p*-Ar), 108.7 (d, $^{2}J_{CP}$ = 5 Hz, *ipso*-Dipp'), 98.3 (d, $^{2}J_{CP}$ = 4 Hz, *m*-Dipp'), 86.0 (d, $^{2}J_{CP}$ = 11 Hz, *p*-Dipp'), 31.7 ((CHMe$_2$)$_{Dipp}$), 29.8 ((CHMe$_2$)$_{Dipp'}$), 26.3 (Me_{Dipp}), 24.9 ($Me_{Dipp'}$), 23.9 (C_2H_4), 23.7 ($Me_{Dipp'}$), 21.5 (Me_{Dipp}), 15.3 (d, $^{1}J_{CP}$ = 40 Hz, PMe_2).

$^{31}P\{^{1}H\}$ NMR (160 MHz, CD_2Cl_2, 25 ºC) δ: 2.1.

REFERENCES

[1] Van Leeuwen, P. W. N. M. *Homogeneous Catalysis: Understanding the Art*; Kluwer Academic Publishers: Dordrecht, **2004**.

[2] Crabtree, R. H. *Chem. Rev.* **2015**, *115*, 127.

[3] Jeffrey, J. C.; Rauchfuss, T. B. *Inorg. Chem.* **1979**, *18*, 2658.

[4] a) Bader, A.; Lindner, E. *Coord. Chem. Rev.* **1991**, *108*, 27; b) Slone, C. S.; Weinberger, D. A.; Mirkin, C. A. *Prog. Inorg. Chem.* **1999**, *48*, 233; c) Braunstein, P.; Naud, F. *Angew. Chem. Int. Ed.* **2001**, *40*, 680; d) Bassetti, M. *Eur. J. Inorg. Chem.* **2006**, 4473; e) Zhang, W.-H.; Chien, S. W.; Hor, T. S. A. *Coord. Chem. Rev.* **2011**, *255*, 1991.

[5] Nguyen, T.; Sutton, A. D.; Brynda, M.; Fettinger, J. C.; Long, G. J.; Power, P. P. *Science* **2005**, *310*, 844.

[6] Öfele, K. *J. Organomet. Chem.* **1968**, *12*, 42.

[7] Wanzlick, H. W.; Schönherr, H.-J. *Angew. Chem. Int. Ed. Engl.* **1968**, *7*, 141.

[8] a) Baceiredo, A.; Bertrand, G.; Sicard, G. *J. Am. Chem. Soc.* **1985**, *107*, 4781; b) Igau, A.; Grutzmacher, H.; Baceiredo, A.; Bertrand, G. *J. Am. Chem. Soc.* **1988**, *110*, 6463.

[9] Arduengo, A. J.; Harlow, R. L.; Kline, M. *J. Am. Chem. Soc.* **1991**, *113*, 361.

[10] Hopkinson, M. N.; Richter, C.; Schedler, M.; Glorius, F. *Nature* **2014**, *510*, 485.

[11] a) Nelson, D. J.; Nolan, S. P. *Chem. Soc. Rev.* **2013**, *42*, 6723; b) Huynh, H. V. *Chem. Rev.* **2018**, *118*, 9457.

[12] Peris, E. *Chem. Rev.* **2018**, *118*, 9988.

[13] Kolychev, E. L.; Kronig, S.; Brandhorst, K.; Freytag, M.; Jones, P. G.; Tamm, M. *J. Am. Chem. Soc.* **2013**, *135*, 12448.

[14] McGuinness, D. S.; Cavell, K. J. *Organometallics*, **2000**, *19*, 741.

[15] Horn, S.; Albrecht, M. *Chem. Commun.* **2011**, *47*, 8802.

[16] Jutzi, P.; Redeker, T. *Eur. J. Inorg. Chem.* **1998**, 663 and references therein.

[17] a) Butenschön, H. *Chem. Rev.* **2000**, *100*, 1527; b) Döhring, A.; Jensen, V. R.; Jolly, P. W.; Thiel, W.; Weber, J. C. *Organometallics* **2001**, *20*, 2234; c) McConnell, A. C.; Pogrozelec, P. J.; Slawin, A. M. Z.; Williams, G. L.; Elliott, P. I. P.; Haynes, A.; Marr, A. C.; Cole-Hamilton, D. J. *Dalton Trans.* **2006**, 91; d) Marr, A. C.; Nieuwenhuyzen, M.; Pollock, C. L.; Saunders, G. C. *Organometallics* **2007**, *26*, 2659; e) Bernechea, M.; Berenguer, J. R.; Lalinde, E.; Torroba, J. *Organometallics* **2009**, *28*, 312.

[18] Young, J. F.; Osborn, J. A.; Jardine, F. H.; Wilkinson, G. *Chem. Commun.* **1965**, 131.

[19] Owen, G. R. *Chem. Soc. Rev.* **2012**, *41*, 3535.

[20] Harman, W. H.; Peters, J. C. *J. Am. Chem. Soc.* **2012**, *134*, 5080.

[21] Cowie, B. E.; Emslie, D. J. H. *Chem. Eur. J.* **2014**, *20*, 16899.

[22] MacMillan, S. N.; Harman, W. H.; Peters, J. C. *Chem. Sci.* **2014**, *5*, 590.

[23] Lawrence, M. A. W.; Green, K.-A.; Nelson, P. N.; Lorraine, S. C. *Polyhedron* **2018**, *143*, 11.

[24] a) Gozin, M.; Weisman, A.; Ben-David, Y.; Milstein, D. Nature 1993, 364, 699; b) Poverenov, E.; Efremenko, I.; Frenkel, A. I.; Ben-David, Y.; Shimon, L. J. W.; Leitus, G.; Konstantinovski, L.; Martin, J. M. L.; Milstein, D. *Nature* **2008**, *455*, 1093; c) Bernskoetter, W. H.; Schauer, C. K.; Goldberg, K. I.; Brookhart, M. *Science* **2009**, *326*, 553; d) Huang, Z.; White, P. S.; Brookhart, M. *Nature* **2010**, *465*, 598; e) Askevold, B.; Nieto, J. T.; Tussupbayev, S.; Diefenbach, M.; Herdtweck, E.; Holthausen, M. C.; Schneider, S. *Nat. Chem.* **2011**, *3*, 532.

[25] for a recent review see: Valdes, H.; García-Eleno, M. A.; Canseco-Gonzalez, D.; Morales-Morales, D. *ChemCatChem* **2018**, *10*, 1.

[26] van der Vlugt, J. I.; Pidko, E. A.; Vogt, D.; Lutz, M.; Spek, A. L.; Meetsma, A. *Inorg. Chem.* **2008**, *47*, 4442.

[27] a) Barrett, B. J.; Iluc, V. M. *Inorg. Chem.* **2014**, *53*, 7248; b) Miller, A. J. M. *Dalton Trans.* **2017**, *46*, 11987; c) Adams, G. M.; Weller, A. S. *Coord. Chem. Rev.* **2018**, *355*, 150.

[28] Velian, A.; Lin, S.; Miller, A. J. M.; Day, M. W.; Agapie, T. *J. Am. Chem. Soc.* **2010**, *132*, 6296.

[29] Buss, J. A.; Edouard, G. A.; Cheng, C.; Shi, J.; Agapie, T. *J. Am. Chem. Soc.* **2014**, *136*, 11272.

[30] Low, C. H.; Rosenberg, J. N.; Lopez, M. A.; Agapie, T. *J. Am. Chem. Soc.* **2018**, *140*, 11906.

[31] a) Lin, S.; Day, M. W.; Agapie, T. *J. Am. Chem. Soc.* **2011**, *133*, 3828; b) Lin, S.; Herbert, D. E.; Velian, A.; Day, M. W.; Agapie, T. *J. Am. Chem. Soc.* **2013**, *135*, 15830; c) Buss, J. A.; Agapie, T. *Nature*, **2016**, *529*, 72; d) Horak, K. T.; Agapie, T. *J. Am. Chem. Soc.* **2016**, *138*, 3443; e) Buss, J. A.; Agapie, T. *J. Am. Chem. Soc.* **2016**, *138*, 16466; f) Buss, J. A.; Oyala, P. H.; Agapie, T. *Angew. Chem. Int. Ed.* **2017**, *56*, 14502; g) Buss, J. A.; Cheng, C.; Agapie, T. *Angew. Chem. Int. Ed.* **2018**, *57*, 9670; h) Buss, J. A.; VanderVelde, D. G.; Agapie, T. *J. Am. Chem. Soc.*, **2018**, *140*, 10121.

[32] a) Kuriyama, M.; Nagai, K.; Yamada, K.; Miwa, Y.; Taga, T.; Tomioka, K. *J. Am. Chem. Soc.* **2002**, *124*, 8932; b) Lewis, J. C.; Berman, A. M.; Bergman, R. G.; Ellman, J. A. *J. Am. Chem. Soc.* **2008**, *130*, 2493; c) Jiménez, M. V.; Pérez-Torrente, J. J.; Bartolomé, M. I.; Vispe, E.; Lahoz, F. J.; Oro, L. A. *Macromolecules* **2009**, *42*, 8146.

[33] a) Old, D. W.; Wolfe, J. P.; Buchwald, S. L. *J. Am. Chem. Soc.* **1998**, *120*, 9722; b) Aranyos, A.; Old, D. W.; Kiyomori, A.; Wolfe, J. P.; Sadighi, J. P.; Buchwald, S. L. *J. Am. Chem. Soc.* **1999**, *121*, 4369; c) Wolfe, J. P.; Singer, R. A.; Yang, B. H.; Buchwald, S. L. *J. Am. Chem. Soc.* **1999**, *121*, 9550.

[34] a) Surry, D. S.; Buchwald, S. L. *Angew. Chem. Int. Ed*. **2008**, *47*, 6338; b) Martin, R.; Buchwald, S. L. *Acc. Chem. Res*. **2008**, *41*, 1461; c) Surry, D. S.; Buchwald, S. L. *Chem. Sci*. **2011**, *2*, 27; d) Liu, Z.; Yamamichi, H.; Madrahimov, S. T.; Hartwig, J. F; *J. Am. Chem. Soc.* **2011**, *133*, 2772; e) Nielsen, D. K.; Doyle, A. G. *Angew. Chem. Int. Ed.* **2011**, *50*, 6056.

[35] a) Watson, D. A.; Su, M.; Teverovskiy, G.; Zhang, Y.; García-Fortanet, J.; Kinzel, T.; Buchwald, S. L. *Science* **2009**, *325*, 1661; e) Sather, A. C.; Buchwald, S. L. *Acc. Chem. Res.* **2016**, *49*, 2146; f) Ye, Y.; Takada, T.; Buchwald, S. L. *Angew. Chem. Int. Ed.* **2016**, *55*, 15559.

[36] Cho, E. J.; Senecal, T. D.; Kinzel, T.; Zhang, Y.; Watson, D. A.; Buchwald, S. L. *Science* **2010**, *328*, 1679.

[37] a) Wu, K.; Doyle, A. G. *Nat. Chem.* **2017**, *9*, 779; b) Niemeyer, Z. L.; Milo, A.; Hickey, D. P.; Sigman, M. S. *Nat. Chem.* **2016**, *8*, 610; c) Christian, A. H.; Niemeyer, Z. L.; Sigman, M. S.; Toste, F. D. *ACS Catal.* **2017**, *7*, 3973.

[38] a) Liptrot, D. J.; Power, P. P. *Nat. Rev. Chem*. **2017**, *1*, 0004; b) Wagner, J. P.; Schreiner, P. R. *Angew. Chem. Int. Ed*. **2015**, *54*, 12274; c) Guo, J.-D.; Liptrot, D. J.; Nagase, S.; Power, P. P. *Chem. Sci*. **2015**, *6*, 6235.

[39] Chen, L.; Ren, P.; Carrow, B. P. *J. Am. Chem. Soc*. **2016**, *138*, 6392.

[40] Tolman, C. A. *J. Am. Chem. Soc.* **1970**, *92*, 2953.

[41] Marin, M.; Moreno, J. J.; Navarro-Gilabert, C.; Álvarez, E.; Maya, C.; Peloso, R.; Nicasio, M. C.; Carmona, E. *Chem. Eur. J.* **2018**, *in press.*

[42] Kühl, O. *Coord. Chem. Rev.* **2005**, *249*, 693.

[43] Kendall, A. J.; Zakharov, L. N.; Tyler, D. R. *Inorg. Chem.* **2016**, *55*, 3079.

[44] Serron, S.; Huang, J.; Nolan, S. P. *Organometallics* **1998**, *17*, 534.

[45] a) Chianese, A. R.; Li, X.; Janzen, M. C.; Faller, J. W.; Crabtree, R. H. *Organometallics* **2003**, *22*, 1663; b) Diebolt, O.; Fortman, G. C.; Clavier, H.; Slawin, A. M. Z.; Escudero-Adán; E. C.; Benet-Buchholz, J.; Nolan, S. P. *Organometallics* **2011**, *30*, 1668.

[46] a) Stec, W. J.; Okruszek, A.; Uznanski, B.; Michalski, J. *Phosphorus* **1972**, *2*, 97.

[47] Allen, D. W.; Nowell, I. W.; Taylor, B. F. *J. Chem. Soc. Dalton Trans.* **1985**, 2505.

[48] Ortega-Moreno, L.; Fernández-Espada, M.; Moreno, J. J.; Navarro-Gilabert, C.; Campos, J.; Conejero, S.; López-Serrano, J.; Maya, C.; Peloso, R.; Carmona, E. *Polyhedron* **2016**, *116*, 170.

[49] a) Dean, P. A. W. *Can. J. Chem.* **1979**, *57*, 754; b) Cogne, A.; Grand, A.; Laugier, J.; Robert, J. B.; Wiesenfeld, L. *J. Am. Chem. Soc.* **1980**, *102*, 2238; c) Carr, S. W.; Colton, R. *Aust. J. Chem.* **1981**, *34*, 35.

[50] Beckmann, U.; Süslüyan, D.; Kunz, P. C. *Phosphorus Sulfur Silicon Relat Elem.* **2011**, *186*, 2061.

[51] a) Pinnell, R. P.; Megerle, C. A.; Manatt, S. L.; Kroon, P. A. *J. Am. Chem. Soc.* **1973**, *95*, 977; b) Kroshefsky, R. D.; Weiss, R.; Verkade, J. G. *Inorg. Chem.* **1979**, *18*, 469.

[52] a) Bent, H. A. *Chem. Rev.* **1961**, *61*, 275; b) McFarlane, W.; Rycroft, D. S. *J. Chem. Soc., Dalton Trans.* **1973**, 2162; c) Alabugin, I. V.; Bresch, S.; Gomes, G. d. P. *J. Phys. Org. Chem.* **2015**, *28*, 147.

[53] Tolman, C. A. *Chem. Rev.* **1977**, *77*, 313.

[54] Müller, T. E.; Mingos, D. M. P. *Transit. Metal Chem.* **1995**, *20*, 533.

[55] Clavier, H.; Nolan, S. P. *Chem. Commun.* **2010**, *46*, 841.

[56] Herrero-Gómez, E.; Nieto-Oberhuber, C.; López, S.; Benet-Buchholz, J.; Echavarren, A. *Angew. Chem. Int. Ed.* **2006**, *45*, 5455.

[57] Espada, M. F.; Campos, J.; López-Serrano, J.; Poveda, M. L.; Carmona, E. *Angew. Chem. Int. Ed.* **2015**, *54*, 15379.

[58] Dennington, R.; Keith, T.; Millam, J. M. GaussView, version 5; Semichem, Inc., Shawnee Mission, KS, USA, 2009.

[59] Bilbrey, J. A.; Kazez, A. H.; Locklin, J.; Allen, W. D. J. Comput. Chem. **2013**, *34*, 1189.

[60] Brown, T. L.; Lee, K. J. *Coord. Chem. Rev.* **1993**, *128*, 89.

[61] Immirzi, A.; Musco, A. *Inorg. Chim. Acta* **1977**, 25, L41.

[62] Poater, A.; Cosenza, B.; Correa, A.; Giudice, S.; Ragone, F.; Scarano, V.; Cavallo, L. *Eur. J. Inorg. Chem.* **2009**, *13*, 1759.

[63] Guzei, I. A.; Wendt, M. *Dalton Trans.* **2006**, 3991.

[64] a) Starosta, R.; Bażanów, B.; Barszczewski, W. *Dalton Trans.* **2010**, *39*, 7547; b) Tohmé, A.; Sahnoune, H.; Roisnle, T.; Dorcet, V.; Halet, J.-F.; Paul, F. *Organometallics*, **2014**, *33*, 3385.

[66] a) Miyaura, N.; Suzuki, A. *Chem. Rev.* **1995**, *95*, 2457; b) Beletskaya, I. P.; Cheprakov, A. V. *Chem. Rev.* **2000**, *100*, 3009; c) King, A. O.; Okukado, N.; Negishi, E. *J. Chem. Soc., Chem. Commun.* **1977**, 683; d) Stille, J. K. *Angew. Chem. Int. Ed.* **1986**, *25*, 508; e) Sonogashira, K. *J. Organomet. Chem.* **2002**, *653*, 46; f) Wolfe, J. P.; Tomori, J.; Sadighi, J. P.; Yin, J.; Buchwald, S. L. *J. Org. Chem.* **2000**, *65*, 1158; g) Hartwig, J. F.; Kawatsura, M.; Hauck, S. I.; Shaughnessy, K. H.; Alcazar-Roman, L. M. *J. Org. Chem.* **1999**, *64*, 5575; h) Tamao, K.; Koji, S.; Kumada, M. *J. Am. Chem. Soc.* **1972**, *94*, 4374.

[67] a) Haynes, A.; Mann, B. E.; Gulliver, D. J.; Morris, G. E.; Maitlis, P. M. *J. Am. Chem. Soc.* **1991**, *113*, 8567; b) Haynes, A.; Mann, B. E.; Morris, G. E.; Maitlis, P. M. *J. Am. Chem. Soc.* **1993**, *115*, 4093; c) Jones, J. H. *Platinum Metals Rev.* **2000**, *44*, 94; d) Sunley, G. J.; Watson, D. J. *Catal. Today* **2000**, *58*, 293.

[68] Vaska, L.; DiLuzio, J. W. *J. Am. Chem. Soc.* **1961**, *83*, 2784.

[69] Vaska, L. *Acc. Chem. Res.* **1968**, *1*, 335.

[70] Vaska, L.; DiLuzio, J. W. *J. Am. Chem. Soc*. **1962**, *84*, 679.

[71] La Placa, S. J.; Ibers, J. A. *Inorg. Chem.* **1966**, *5*, 405.

[72] Vaska, L.; Rhodes, R. E. *J. Am. Chem. Soc.* **1965**, *87*, 4970.

[73] Chock, P. B.; Halpern, J. *J. Am. Chem. Soc.* **1966**, *88*, 3511.

[74] a) Vaska, L. *Science* **1963**, *140*, 809; b) La Placa, S. J.; Ibers, J. A. *J. Am. Chem. Soc.* **1965**, *87*, 2581.

[75] a) Vaska, L. *Science* **1966**, *152*, 769; b) Abu-Hasanayn, F.; Emge, T. J.; Maguire, J. A.; Krogh-Jespersen, K.; Goldman, A. S. *Organometallics* **1994**, *13*, 5177.

[76] a) Janowicz, A.H.; Bergman, R. G. *J. Am. Chem. Soc.* **1982**, *104*, 352; b) Hoyano, J. K.; Graham, W.A.G. *J. Am. Chem. Soc.* **1982**, *104*, 3723.

[77] Kumar, A.; Feller, M.; Ben-David, Y.; Diskin-Posner, Y.; Milstein, D. *Chem. Commun.* **2018**, *54*, 5365.

[79] Douvris, C.; Reed, C. A. *Organometallics* **2008**, *27*, 807.

[80] Bader, R. F. W. *Atom in Molecules: A Quantum Theory*; Oxford University Press: Oxford, U.K. **1995**.

[81] Lu, T.; Chen, F. *J. Comput. Chem.* **2012**, *33*, 580.

[83] a) Varadwaj, P. R.; Cukrowski, I.; Marques, H. M. *J. Phys. Chem. A* **2008**, *112*, 10657; b) Varadwaj, P. R.; Varadwaj, A.; Marques, H. M. *J. Phys. Chem. A* **2011**, *115*, 5592.

[84] Morse, P. M.; Spencer, M. D.; Wilson, S. R.; Girolami, G. S. *Organometallics* **1994**, *13*, 1646.

[85] a) Abbott, J. K. C.; Li, L.; Xue, Z.-L. *J. Am. Chem. Soc.* **2009**, *131*, 8246; b) Jiménez, M. V.; Fernández-Tornos, J.; Pérez-Torrente, J. J.; Modrego, F. J.; García-Orduña, P.; Oro, L. A. *Organometallics* **2015**, *34*, 926.

[87] Moreno, J. J.; Espada, M. F.; Krüger, E.; López-Serrano, J.; Campos, J.; Carmona, E. *Eur. J. Inorg. Chem.* **2018**, 2309.

[88] a) Crabtree, R. H.; Morris, G. E. *J. Organomet. Chem.* **1977**, *135*, 395; b) Crabtree, R. H.; Felkin, H.; Morris, G. E. *J. Organomet. Chem.* **1977**, *141*, 205; c) Crabtree, R. *Acc. Chem. Res.* **1979**, *12*, 331.

[89] a) Lightfoot, A.; Schnider, P.; Pfaltz, A. *Angew. Chem. Int. Ed.* **1998**, *37*, 2897; b) Vazquez-Serrano, L. D.; Owens, B. T.; Buriak, J. M. Chem. Commun. 2002, 2518; c) Cipot, J.; McDonald, R.; Stradiotto, M. *Chem. Commun.* **2005**, 4932; d) Cipot, J.; McDonald, R.; Ferguson, M. J.; Schatte, G.; Stradiotto, M. *Organometallics* **2007**, *26*, 594; e) Franzke, A.; Pfaltz, A. *Chem. Eur. J.* **2011**, *17*, 4131; f) Bennie, L. S.; Fraser, C. J.; Irvine, S.; Kerr, W. J.; Andersson, S.; Nilsson, G. N. *Chem. Commun.* **2011**, *47*, 11653.

[90] a) Lee, H. M.; Jiang, T.; Stevens, E. D.; Nolan, S. P. *Organometallics* **2001**, *20*, 1255; b) Perry, M. C.; Cui, X.; Powell, M. T.; Hou, D.-R.; Reibenspies, J. H.; Burgess, K. *J. Am. Chem. Soc.* **2003**, *125*, 113; c) Cui, X.; Burgess, K. *J. Am. Chem. Soc.* **2003**, *125*, 14212; d) Schumacher, A.; Bernasconi, M.; Pfaltz, A. *Angew. Chem. Int. Ed.* **2013**, *52*, 7422.

[91] a) Smidt, S. P.; Zimmermann, N.; Studer, M.; Pfaltz, A. *Chem. Eur. J.* **2004**, *10*, 4685; c) Wüstenberg, B.; Pfaltz, A. *Adv. Synth. Catal.* **2008**, *350*, 174.

[92] Crabtree, R. H. *Acc. Chem. Res.* **1979**, *12*, 331.

[93] Andersson, P. G. *Iridium Catalysis. Top. Organomet. Chem.*, Springer, Berlin, **2011.**

[94] Cavallo, L.; Macchioni, A.; Zuccaccia, C.; Zuccaccia, D.; Orabona, I.; Ruffo, F. *Organometallics* **2004**, *23*, 2137.

[95] a) Vidossich, P.; Lledós, A. *Dalton Trans.* **2014**, *43*, 11145.

[96] a) Dewar, J. S. *Bull. Soc. Chim. Fr.* **1951**, *18*, C71; b) Chatt, J.; Duncanson, L. A. *J. Chem. Soc.* **1953**, 2939.

[97] Giordano, G.; Crabtree, R. H. *Inorg. Synth.* **1990**, *28*, 91.

[98] Yakelis, N. A.; Bergman, R. G. *Organometallics* **2005**, *24*, 3579.

[99] a) Campos, J.; Ortega-Moreno, L.; Conejero, S.; Peloso, R.; López-Serrano, J.; Maya, C.; Carmona, E. *Chem. Eur. J.* **2015**, *21*, 8883; b) Ortega-Moreno, L.; Peloso, R.; Maya, C.; Suárez, A.; Carmona, E. *Chem. Commun.* **2015**, *51*, 17008.

[100] Frisch, M. J.; Trucks, G. W.; Schlegel, H. B.; Scuseria, G. E.; Robb, M. A.; Cheeseman, J. R.; Scalmani, G.; Barone, V.; Mennucci, B; Petersson, G. A.; Nakatsuji, H.; Caricato, M.; Li, X.; Hratchian, H. P.; Izmaylov, A. F.; Bloino, J.; Zheng, G.; Sonnenberg, J. L.; Hada, M.; Ehara, M.; Toyota, K.; Fukuda, R.;

Hasegawa, J.; Ishida, M.; Nakajima, T.; Honda, Y.; Kitao, O.; Nakai, H.; Vreven, T.; Montgomery, J. A. J.; Peralta, J. E.; Ogliaro, F.; Bearpark, M.; Heyd, J. J.; Brothers, E.; Kudin, K. N.; Staroverov, V. N.; Kobayashi, R.; Normand, J.; Raghavachari, K.; Rendell, A.; Burant, J. C.; Iyengar, S. S.; Tomasi, J.; Cossi, M.; Rega, N.; Millam, J. M.; Klene, M.; Knox, J. E.; Cross, J. B.; Bakken, V.; Adamo, C.; Jaramillo, J.; Gomperts, R.; Stratmann, R. E.; Yazyev, O.; Austin, A. J.; Cammi, R.; Pomelli, C.; Ochterski, J. W.; Martin, R. L.; Morokuma, K.; Zakrzewski, V. G.; Voth, G. A.; Salvador, P.; Dannenberg, J. J.; Dapprich, S.; Daniels, A. D.; Farkas, O.; Foresman, J. B.; Ortiz, J. V.; Cioslowski, J.; Fox, D. J.; Gaussian 09, Revision D.01, Gaussian, Inc.: Wallingford CT, **2013**.

[101] Zhao, Y.; Truhlar, D. G. *Theor. Chem. Acc.* **2006**, *120*, 215.

[102] Chai, J.-D.; Head-Gordon, M. *Phys. Chem. Chem. Phys.* **2008**, *10*, 6615.

[103] a) Hehre, W. J.; Ditchfield, R.; Pople, J. A. *J. Phys. Chem.* **1972**, *56*, 2257; b) Hariharan, P. C.; Pople, J. A. *Theor. Chim. Acta.* **1973**, *28*, 213; c) Francl, M. M.; Pietro, W. J.; Hehre, W. J.; Binkley, J. S.; Gordon, M. S.; Defrees, D. J.; Pople, J. A. *J. Chem. Phys.* **1982**, *77*, 3654.

[104] Andrae, D.; Haeussermann, U.; Dolg, M.; Stoll, H.; Preuss, H. *Theor. Chim. Acta* **1990**, *77*, 123.

[105] Marenich, A. V.; Cramer, C. J.; Truhlar, D. G. *J. Phys. Chem. B* **2009**, *113*, 6378.

[106] Pipek, J.; Mezey, P.G. *J. Chem. Phys*. **1989**, *90*, 4916.